



The Synthesis and Evaluation of Nitrile-Containing Ferroelectric Chiral Liquid Crystal Dopants

Thesis submitted for Degree of Doctor of Philosophy by

Viswanath Reddy

(Under the supervision of Dr. Rob Lewis)

November 2014

*This thesis is dedicated to the memory of my mother,
Smt. Laxmidevi Arakeri and mother-in-law,
Smt. Shivalingamma Kolur. I miss them every
day, but their support and encouragement are always
with me.*

Abstract

Ferroelectric Liquid Crystal Displays offer fast switching times in the sub millisecond region and a high contrast ratio. There is a need for faster refresh rates to cope with fast moving images and the possibility of sequential red-green-blue illumination that will enable higher definition quality. This has led to a renewed interest in the ferroelectric liquid crystal display mode which employs a smectic C* material generated *via* addition of a chiral dopant to an achiral SmC host.

This thesis first reviews liquid crystals and their properties, the smectic C* phase in particular and previous work on chiral dopants. Ferroelectricity and its use in an LCD display mode is explained.

The aim is to prepare a stable chiral dopant that is compatible with a difluoroterphenyl based host FLC mixture and to provide a moderate spontaneous polarisation, a long N* pitch length and maintain the broad temperature range of the achiral host.

This report first describes the synthesis of (S)-2-((3'-fluoro-4'-(octyloxy)-[1,1'-biphenyl]-4-yl)oxy)propanenitrile as a chiral dopant. The compound has a similar structure to a standard biphenyl ester dopant BE8OF2N, but replaces an ester link to the stereogenic centre with an ether link, with the main aim of increasing chemical stability. The key part of the synthesis involves an S_N2 reaction between lactamide tosylate and a hydroxybiphenyl. The non-mesogenic dopant was formulated as 5, 7 and 10% w/w mixtures with an FLC host mixture (KCHM211) that contains only dialkyldifluoroterphenyls. Liquid crystal phase transitions and N* pitch lengths are reported and the phase transitions are compared with that from the BE8OF2N with KCHM211 host mixture. The spontaneous polarisation at room temperature was found to be 20 nC cm^{-2} and the tilt angle of the SmC* phase temperature range is reported.

This result lead to the synthesis of three mesogenic dopants and the synthesis is described, employing the same chiral 2-cyanoethyl group linked by oxygen to the difluoroterphenyl core used in the FLC host mixture. The derivatives with an *ortho* difluorophenyl group in the middle ring or the end ring remote from the chiral centre have blue phases, but those with the fluoro-substituents adjacent to the chiral group possess an N* phase. All

the mesogenic dopants were formulated in a 7% w/w mixture with KCH-M211. LC phase behaviour, and electrooptic data is reported. The results are compared with those from the non-mesogenic dopant. Dopant reduce the SmC*-SmA* by only 3 °C from that of the host mixture, but has a low P_s (maximum 6 nC cm⁻²).

The P_s of the terphenyl dopants is lower than expected, and molecular modelling and single crystal X-ray diffraction studies were used in an attempt to rationalise this observation. The electron distribution and dipole moments were calculated, but they follow a different trend to that of the P_s data. The single crystal structure also shows a different conformation of the chiral nitrile relative to the aromatic fluoro-substituents than that obtained by modelling. These results indicate the complexity in predicting or explaining the magnitude of P_s in ferroelectric liquid crystals.

Acknowledgments

First and foremost I wish to express my sincere gratitude to my supervisor Dr. Rob Lewis. I would like to thank him for his continuous support of my PhD study, for his patience, motivation, enthusiasm, and immense knowledge. It has been an honour to be his first Ph.D. student. I will always remember his calm and relaxed nature, and the way he asks “YES! How can I help you?” whenever I enter his office. I am thankful to the Almighty for giving me a mentor like him. His guidance helped me in all the time of research and writing of this thesis. I could not have imagined having a better advisor and mentor for my PhD study. I express my deepest gratitude to my second supervisor Dr. Mike Hird for boosting my morale throughout the course of research. He has always been caring, a source of wisdom and motivation. He is a great teacher. I gratefully acknowledge Prof. Georg Mehl and Dr. Tim Prior for their expertise in X-ray diffraction and Dr. David Benoit for the molecular modelling studies.

One person who has always been ready to help me was Dave Allan. He was very helpful as a co-researcher in the same lab. Thank you Dave for all your support especially LaTeX! It is my pleasure to acknowledge all my current and previous colleagues, especially Dr. Andy, Dr. Rob, Dr. Ben, Dr. Thamba, Dr. Chris, Dr. Ana, Srinivas, Zia, Rami, Tony, Amos and Murali for their enormous support and providing a good atmosphere in the lab. I will always be grateful to them for helping me to develop the scientific approach and attitude. I would like to thank Kingston Chemicals and the University of Hull for funding my research.

I can't imagine my current position without the love and support from my family. I thank my father, Sri. Devappa Arakeri and mother, Smt. Laxmidevi Arakeri for striving hard to provide a good education for me and my siblings. It feels impossible to describe their support in words. If I have to mention one thing about them, among many, then I would proudly mention that my parents are very humble and they taught me how to lead a simple life. I would like to thank my sisters Pushpa, Suma and Jaya for their support and encouragement.

Last but not least, I would like to pay high regards to my wife, Hemalatha and son, Chinmaya for their sincere encouragement and inspiration throughout my research work and lifting me uphill in this phase of life.

Contents

List of Tables	15
1 Introduction	18
1.1 Introduction to Liquid Crystals	18
1.1.1 Introduction to Liquid Crystals	18
1.1.2 Historical Development	19
1.1.3 Classification of Liquid Crystals	21
1.2 Liquid Crystal Phases	22
1.2.1 Introduction to Liquid Crystal Phases	22
1.3 Phases, Structures and Textures of Liquid Crystals	25
1.3.1 The Nematic Phase	25
1.3.2 The Cholesteric or Chiral Nematic Phase (N*)	28
1.3.3 The SmA and SmA* phases	28
1.3.4 The SmC Phase	29
1.3.5 The Blue Phase	32
1.4 Ferroelectric Liquid Crystals	34
1.4.1 Molecular Description of Spontaneous Polarisation	37
1.4.2 Liquid Crystal Hosts	38
1.4.3 Liquid Crystal Chiral Dopants	42
1.4.4 Amplification of Chirality in Liquid Crystals	46
1.5 Fluorinated Liquid Crystals	48
1.5.1 Effect of the Location of Fluoro Substituents	48
1.5.2 Fluoro Substitution at a Lateral Position	49
2 Research Aim	51
2.1 Current FLC Mixtures	51
2.2 Project Outline	55
2.3 Schemes and Mechanisms	57
2.4 Mechanistic Discussion of the Synthetic Routes	75
2.5 Second Generation Dopants	80
3 Evaluation of Liquid Crystals	84
3.1 Polarized Optical Microscopy	84
3.2 Differential Scanning Calorimetry	85
3.3 Electro-Optical Studies	85

4	Results and Discussion	88
4.1	Characterisation Of Ferroelectric Liquid Crystal Dopants	88
4.1.1	NMR Shift Experiment	88
4.1.2	Optical Rotation	90
4.1.3	The Phase Transition Temperatures	92
4.1.4	Phase Characterisation of Host Mixture KCHM211 Doped with Compounds 35 , 67 , 77 and 87	94
4.1.5	Pitch Length and Helical Twisting Power	99
4.1.6	Pitch Length and Helical Twisting Power of Dopant 67	103
4.1.7	Tilt Angle	105
4.1.8	Spontaneous Polarisation (<i>P_s</i>)	108
4.2	The Study of Alkoxyterphenyl Mesogenic Dopant 94	113
4.3	Characterisation of Second Generation FLC Dopants	115
4.3.1	Optical Rotation	115
4.3.2	The Phase Transition Temperatures	116
4.3.3	Characterisation of 110 Doped with KCHM211	117
4.4	X-Ray Analysis	118
4.4.1	Bragg's Law	118
4.4.2	Single Crystal X-Ray Diffraction	121
4.5	X-Ray Diffraction Experiments (XRD)	126
5	Molecular Modeling	129
5.1	Advanced Molecular Modeling	132
5.1.1	Calculating Dipole Moments	132
5.1.2	B3LYP_G Method	137
5.1.3	Temperature Calculations	137
5.1.4	Molecular Dynamics Results	138
5.1.5	Visual Comparison of Conformations from 0 K and 300 K Random Snapshots	139
6	Conclusion	142
7	Experimental	147
7.1	General Instrumentation and Techniques	147
7.1.1	¹ H, ¹³ C and ¹⁹ F Nuclear Magnetic Resonance(NMR)	147
7.1.2	Infrared Spectrometry	147
7.1.3	Mass Spectrometry	147
7.1.4	Chromatography	147

7.1.5	Purity of Intermediates and Final Compounds	148
7.1.6	Melting Points and Transition Temperatures	148
7.2	Reagents and Reaction Solvents	148
7.3	Experimental Procedures	150
7.3.1	(<i>S</i>)-1-Amino-1-oxopropan-2-yl 4-methylbenzenesulfonate — 33 . .	150
7.3.2	4-Bromo-2-fluoro-1-(octyloxy)benzene — 40	150
7.3.3	3-Fluoro-4-((octyloxy)phenyl)boronic acid — 41	151
7.3.4	1-(Benzyloxy)-4-bromobenzene — 44	152
7.3.5	4'-(Benzyloxy)-3-fluoro-4-(octyloxy)-1,1'-biphenyl — 45	153
7.3.6	3'-Fluoro-4'-(octyloxy)-[1,1'-biphenyl]-4-ol — 46	154
7.3.7	(<i>R</i>)-2-((3'-Fluoro-4'-(octyloxy)-[1,1'-biphenyl]-4-yl)oxy)propanamide — 47	155
7.3.8	(<i>R</i>)-2-((3'-Fluoro-4'-(octyloxy)-[1,1'-biphenyl]-4-yl)oxy)propanenitrile — 48	156
7.3.9	(<i>R</i>)-2-((3'-Fluoro-4'-(octyloxy)-[1,1'-biphenyl]-4-yl)oxy)propanamide — 49	157
7.3.10	(<i>R</i>)-2-((3'-Fluoro-4'-(octyloxy)-[1,1'-biphenyl]-4-yl)oxy)propanenitrile — 36	158
7.3.11	(<i>R</i>)-1-Amino-1-oxopropan-2-yl 4-methylbenzenesulfonate — 34 . .	159
7.3.12	2-(4-Bromophenoxy)tetrahydro-2H-pyran — 53	160
7.3.13	2-((3'-Fluoro-4'-(octyloxy)-[1,1'-biphenyl]-4-yl)oxy)tetrahydro-2H-pyran — 54	160
7.3.14	3'-Fluoro-4'-(octyloxy)-[1,1'-biphenyl]-4-ol — 55	161
7.3.15	(<i>S</i>)-2-((3'-Fluoro-4'-(octyloxy)-[1,1'-biphenyl]-4-yl)oxy)propanamide — 56	162
7.3.16	(<i>S</i>)-2-((3'-Fluoro-4'-(octyloxy)-[1,1'-biphenyl]-4-yl)oxy)propanenitrile — 35	163
7.3.17	1-(4-Bromophenyl)pentan-1-one — 58	164
7.3.18	1-Bromo-4-pentylbenzene — 59	165
7.3.19	(2,3-Difluorophenyl)boronic acid — 61	166
7.3.20	2,3-Difluoro-4'-pentyl-1,1'-biphenyl — 62	166
7.3.21	(2,3-Difluoro-4'-pentyl-[1,1'-biphenyl]-4-yl)boronic acid — 63 . . .	167
7.3.22	4-(Benzyloxy)-2',3'-difluoro-4''-pentyl-1,1':4',1''-terphenyl — 64 . .	168
7.3.23	2',3'-Difluoro-4''-pentyl-[1,1':4',1''-terphenyl]-4-ol — 65	169
7.3.24	(<i>R</i>)-2-((2',3'-Difluoro-4''-pentyl-[1,1':4',1''-terphenyl]-4-yl)oxy)propan- amide — 66	170

7.3.25	(<i>R</i>)-2-((2',3'-Difluoro-4"-pentyl-[1,1':4',1"-terphenyl]-4-yl)oxy)propane-nitrile — 67	171
7.3.26	1-(2,3-Difluorophenyl)pentan-1-ol — 68	172
7.3.27	<i>E</i> -1,2-Difluoro-3-(pent-1-en-1-yl)benzene — 69	173
7.3.28	1,2-Difluoro-3-pentylbenzene — 70	173
7.3.29	(2,3-Difluoro-4-pentylphenyl)boronic acid — 71	174
7.3.30	(4-Bromo-4'-(octyloxy)-1,1'-biphenyl — 71	174
7.3.31	2,3-Difluoro-4"--(octyloxy)-4-pentyl-1,1':4',1"-terphenyl — 74	175
7.3.32	2",3"-Difluoro-4"-pentyl-[1,1':4',1"-terphenyl]-4-ol — 75	176
7.3.33	(<i>R</i>)-2-((2",3"-Difluoro-4"-pentyl-[1,1':4',1"-terphenyl]-4-yl)oxy)propanamide — 76	177
7.3.34	(<i>R</i>)-2-((2",3"-Difluoro-4"-pentyl-[1,1':4',1"-terphenyl]-4-yl)oxy)propanenitrile — 77	178
7.3.35	1-(4'-Bromo-[1,1'-biphenyl]-4-yl)pentan-1-one — 79	179
7.3.36	4-Bromo-4'-pentyl-1,1'-biphenyl — 80	180
7.3.37	1,2-Difluoro-3-(nonyloxy)benzene — 82	181
7.3.38	(2,3-Difluoro-4-(nonyloxy)phenyl)boronic acid — 83	181
7.3.39	2,3-Difluoro-4-(nonyloxy)-4"-pentyl-1,1':4',1"-terphenyl — 84	182
7.3.40	2,3-Difluoro-4"-pentyl-[1,1':4',1"-terphenyl]-4-ol — 85	183
7.3.41	(<i>R</i>)-2-((2,3-Difluoro-4"-pentyl-[1,1':4',1"-terphenyl]-4-yl)oxy)propanamide — 86	184
7.3.42	(<i>R</i>)-2-((2,3-Difluoro-4"-pentyl-[1,1':4',1"-terphenyl]-4-yl)oxy)propane-nitrile — 87	185
7.3.43	4'-(Benzyloxy)-2,3-difluoro-1,1'-biphenyl — 88	186
7.3.44	4'-(Benzyloxy)-2,3-difluoro-[1,1'-biphenyl]-4-yl)boronic acid — 89	187
7.3.45	4-(Benzyloxy)-2',3'-difluoro-4"--(hexyloxy)-1,1':4',1"-terphenyl — 91	188
7.3.46	(2',3'-Difluoro-4"--(hexyloxy)-[1,1':4',1"-terphenyl]-4-ol — 92	189
7.3.47	(<i>R</i>)-2-((2',3'-Difluoro-4"--(hexyloxy)-[1,1':4',1"-terphenyl]-4-yl)oxy)propanamide — 93	190
7.3.48	(<i>R</i>)-2-((2',3'-Difluoro-4"--(hexyloxy)-[1,1':4',1"-terphenyl]-4-yl)oxy)propanenitrile 94	191
7.3.49	(<i>S</i>)-2-(Ethoxycarbonyl)hexanoic acid	192
7.3.50	(±)-2-butyl-3-hydroxypropionic acid	193
7.3.51	(<i>R</i>)-2-(Hydroxymethyl)hexanoic acid phenylethanammonium salt	194
7.3.52	(<i>R</i>)-2-(Hydroxymethyl)hexanoic acid	195
7.3.53	Benzyl (<i>R</i>)-2-(hydroxymethyl)hexanoate	195
7.3.54	(<i>S</i>)-2-Hydroxy-4-methylpentanoic acid — 102	196

7.3.55 Benzyl (<i>S</i>)-2-hydroxy-4-methylpentanoate — 103	197
7.3.56 (2 <i>S</i> ,3 <i>S</i>)-2-Hydroxy-3-methylpentanoic acid — 105	198
7.3.57 Benzyl (2 <i>S</i> ,3 <i>S</i>)-2-hydroxy-3-methylpentanoate — 106	198
7.3.58 Benzyl (2 <i>R</i> ,3 <i>S</i>)-2-((2,3-difluoro-4''-pentyl-[1,1':4', 1''-terphenyl]-4-yl)oxy)-3-methylpentanoate — 107	200
7.3.59 (2 <i>R</i> ,3 <i>S</i>)-2-((2,3-Difluoro-4''-pentyl-[1,1':4',1''-terphenyl]-4-yl)oxy) - 3-methylpentanoic acid — 108	201
7.3.60 (2 <i>R</i> ,3 <i>S</i>)-2-((2,3-Difluoro-4''-pentyl-[1,1':4',1''-terphenyl]-4-yl)oxy)-3-methylpentanamide — 109	202
7.3.61 (2 <i>R</i> ,3 <i>S</i>)-2-((2,3-Difluoro-4''-pentyl-[1,1':4',1''-terphenyl]-4-yl)oxy)-3-methylpentanenitrile — 110	203
7.3.62 Benzyl (<i>R</i>)-2-((2,3-difluoro-4''-pentyl-[1,1':4',1''-terphenyl]-4-yl)oxy)-4-methylpentanoate — 111	204
7.3.63 (<i>R</i>)-2-((2,3-Difluoro-4''-pentyl-[1,1':4',1''-terphenyl]-4-yl)oxy)-4-methylpentanoic acid — 112	205
7.3.64 (<i>R</i>)-2-((2,3-Difluoro-4''-pentyl-[1,1':4',1''-terphenyl]-4-yl)oxy)-4-methylpentanamide — 113	206
7.3.65 (<i>R</i>)-2-((2,3-Difluoro-4''-pentyl-[1,1':4',1''-terphenyl]-4-yl)oxy)-4-methylpentanenitrile — 114	207

8 Bibliography

209

List of Figures

1	States of Matter	18
2	First practical liquid crystal display	19
3	Twisted liquid crystal nematic (TN) effect	20
4	Classification of thermotropic liquid crystalline mesophases	21
5	Structural template for a calamitic liquid crystal.	22
6	Phase transitions between crystal, liquid crystal, and isotropic liquid phases for a calamitic material as a function of temperature.	23
7	Structure of the chiral nematic phase showing the helical twist of n along z over $\frac{1}{2}$ of the helical pitch, P	24
8	Molecular order in the nematic phase	26
9	Schlieren texture of the nematic phase	26
10	Examples of mesogenic core units.	27
11	Photomicrographs of the cholesteric phase	28
12	Photomicrograph of the SmA phase	29
13	Schematic representation of molecular order in the SmC phase.	30
14	Transition from nematic schlieren (right) texture to a SmC schlieren texture (left) on cooling	31
15	Mosaic texture in a BPII phase	32
16	Phase diagram for the 3 blue phases as a function of chirality and temperature.	33
17	Molecular symmetry in achiral SmC, SmC* phase with resulting.	34
18	(a) Helical structure in the SmC* phase without external constraints constraints; (b) SmC* phase with external constraints leads to SSFLC state.	35
19	Switching between the opposite applied field in an SSFLC system.	36
20	The bent-cylinder binding site with a guest molecule in the SmC* phase, according to the Boulder model.	37
21	Liquid crystal hosts 5CB and 8OCB with their transition temperatures.	38
22	Phase diagram similar to that for the binary mixture of 5BC and 8OCB.	39
23	Achiral fluorinated terphenyl host compounds.	40
24	The structure of chiral dopants.	43
25	A typical examples of axial chiral dopants.	44
26	The structure of MBBA	46
27	The structure where cyano group close to the molecular core	47
28	A typical structural template for a calamitic liquid crystal.	49
29	Effect of transition temperatures on fluoro substitution.	50

30	The structures and transition temperature of host mixture KCHM211.	52
31	The structure of BE8OF2N.	53
32	The general structure of cyanohydrin ether linked FLC.	54
33	(<i>R</i>) and (<i>S</i>)-1-amino-1-oxopropan-2-yl 4-methylbenzenesulfonate	55
34	The targeted non-mesogenic liquid crystal dopant	56
35	Mimic of targeted mesogenic liquid crystal dopants.	56
36	Proposed mechanism for the racemisation.	75
37	Proposed mechanism for the transformation of a 4-bromophenol to 2-(4 bromophenoxy)tetrahydro-2H-pyran.	76
38	Catalytic cycle for Suzuki coupling reaction.	77
39	The S _N 2 mechanism for tosylation of phenol to form lactamide ethers.	78
40	Proposed mechanism for conversion of amide to nitrile using the Vilsmeier reagent.	79
41	The structures of second generation dopants.	80
42	Proposed mechanism for Mitsunobu Reaction.	82
43	The molecular tilt by applying applied field in SmC* phase.	86
44	Current versus time for a ferroelectric liquid crystal, using the ALCT sys- tem and software.	87
45	The NMR shift reagent experimental signals of compound 36	89
46	The blue phases of the compound 77 are shown in the following pictures taken from camera fitted POM; (1) BP I, (2) BP II, (3) BP II (mosaic) and (4) BPIII (fog phase)	93
47	The comparison of phase transitions of FLC chiral dopants with KCH- M211 mixture (7% w/w).	95
48	Photograph of dopant 35 with KCHM211 (7 % w/w) shows (1) focal conic and homeotropic texture of SmA* and (2) finger print textures of the N* phase	96
49	Photograph of dopant 77 with KCHM211 (7 % w/w)	97
50	Photograph of dopant 67 with KCHM211 (7 % w/w)	97
51	Photograph of dopant 87 with KCHM211 (7 % w/w)	98
52	The schematic diagram of Cano wedge	99
53	Microphotograph of a stripe – wedge Grandjean – Cano cell filled with dopant 35 with KCHM211 (7 % w/w)	100
54	Comparison of pitch length of dopant 35 with 5, 7 and 10% mixture of KCHM211 (w/w)	102
55	Comparison of helical twisting power 35 with 5, 7 and 10 % mixture of KCHM211 (w/w)	103

56	Pitch length of dopant 67 with KCHM211 mixture (7% w/w).	104
57	Helical twisting power of dopant 67 with KCHM211 mixture (7% w/w). . .	104
58	Tilt angles <i>vs</i> temperatures of dopants 35 and 67 with KCHM211 mixture (7% w/w).	107
59	Spontaneous polarisation of dopant 35 with KCHM211 mixture (7% w/w). . .	110
60	Spontaneous polarisation of dopant 67 with KCHM211 mixture (7% w/w) . . .	111
61	The alkoxyterphenyl mesogenic dopant 94	113
62	The N* pitch unwinding at transition to SmA* phase for compound 94 at 115.4 °C.	114
63	The fingerprint texture of N* phase for compound 94 at 138.3 °C.	114
64	description of a) Bragg's Diffraction Law b) 2-D X-ray diffraction pattern. . .	119
65	2-D X-ray diffraction pattern of oriented samples.	120
66	ORTEP diagram of (S)-2-((3'-fluoro-4'-(octyloxy)-[1,1'-biphenyl]-4-yl)oxy)- propanenitrile 35 with atom numbering.	121
67	The powder pattern of the dopant 35	124
68	Molecular packing of dopant 35 in the crystal	124
69	Molecular packing of dopant 35 in the crystal, projected along the crystal- lographic direction.	125
70	XRD of dopant 35 with KCHM211 (7% w/w) N* at 114.5 °C.	127
71	DSC thermograph of dopant 35 with KCHM211 (7% w/w).	128
72	Schematic of a molecule with a pair of off-centre dipoles μ^{\pm}	130
73	The colour-coded Mulliken Charge distribution of dopant 35	131
74	The total dipole moment from the two methods.	134
75	The dopant 67 showing different conformations obtained from minimisation and dynamics simulations at 300 K	139
76	The dopant 87 showing different conformations obtained minimisation and dynamics simulations at 300 K	139
77	The dipole moment using x,y components.	140
78	The dipole projection in chiral dopants a. 35 , b. 67 , c. 77 , d. 87 , e. 117 and f. 118	141
79	The biphenyl dopant 35	142
80	Difluoro terphenyl mesogenic liquid crystal dopants where X=F= 77 , Y=F= 67 and Z=F= 87	143
81	The new chiral units 100 , 103 and 106	145
82	The targeted new chiral dopants.	146

List of Schemes

1	Synthesis of (<i>S</i>)-lactamide tosylate, 33	57
2	Synthesis of boronic acid 41	57
3	Synthesis of 1-(benzyloxy)-4-bromobenzene 44	57
4	Synthesis of (<i>R</i>)-2-((3'-fluoro-4'-(octyloxy)-[1,1'-biphenyl]-4-yl)oxy)-propane- nitrile 48	58
5	Synthesis of (<i>R</i>)-2-((3'-fluoro-4'-(octyloxy)-[1,1'-biphenyl]-4-yl)oxy)-propane- nitrile 36 without KI	59
6	Synthesis of (<i>R</i>)-lactamide tosylate, 34	59
7	Synthesis of (<i>S</i>)-2-((3'-fluoro-4'-(octyloxy)-[1,1'-biphenyl]-4-yl)oxy)-propane- nitrile 35	60
8	Synthesis of (2,3-difluoro-4'-pentyl-[1,1'-biphenyl]-4-yl)boronic acid 63	61
9	Synthesis of (<i>R</i>)-2-((2',3'-difluoro-4"-pentyl-[1,1':4',1"-terphenyl]-4-yl)oxy)- -propanenitrile 67	62
10	Synthesis of (2,3-difluoro-4-pentylphenyl)boronic acid 71	63
11	Synthesis of 4-bromo-4'-(octyloxy)-1,1'-biphenyl 73	64
12	Synthesis of (<i>R</i>)-2-((2",3"-difluoro-4"-pentyl-[1,1':4',1"-terphenyl]-4-yl)oxy)- -propanenitrile 77	65
13	Synthesis of 4-bromo-4'-pentylbiphenyl 80	66
14	Synthesis of (2,3-difluoro-4-(nonyloxy)phenyl)boronic acid 83	66
15	Synthesis of (<i>R</i>)-2-((2,3-difluoro-4"-pentyl-[1,1':4',1"-terphenyl]-4-yl)oxy)- propanenitrile 87	67
16	Synthesis of 2',3'-difluoro-4'-(hexyloxy)-[1,1':4',1"-terphenyl]-4-ol 92	68
17	Synthesis of (<i>R</i>)-2-((2',3'-difluoro-4'-(hexyloxy)-[1,1':4',1"-terphenyl]-4-yl)- oxy)propanenitrile 94	69
18	Synthesis of (<i>R</i>)-benzyl 2-(hydroxymethyl)hexanoate	70
19	Synthesis of (<i>S</i>)-benzyl 2-hydroxy-4-methylpentanoate 103	71
20	Synthesis of (2 <i>S</i> ,3 <i>S</i>)-benzyl 2-hydroxy-3-methylpentanoate 106	72
21	Synthesis of (2 <i>R</i> ,3 <i>S</i>)-2-((2,3-difluoro-4"-pentyl-[1,1':4',1"-terphenyl]-4-yl)- oxy)-3-methylpentanenitrile 110	73
22	Synthesis of (<i>R</i>)-2-((2,3-difluoro-4"-pentyl-[1,1':4',1"-terphenyl]-4-yl)-oxy)-4- methylpentanenitrile 114	74

List of Tables

1	The examples of dopants with transition temperatures.	45
2	The optical rotation of non-mesogenic dopants	90
3	The optical rotation of mesogenic dopants	91
4	The phase transition temperatures of targeted chiral dopants	92
5	Phase transitions (°C) from POM of FLC chiral dopants with KCHM211 mixture (7% w/w)	95
6	Pitch length of dopant 35 with 5,7 and 10% mixture of KCHM211.(w/w) .	101
7	The helical twisting power 35 with 5,7 and 10% mixture of KCHM211.(w/w)	103
8	Determination of pitch length and helical twisting power of dopant 67 with KCHM211 mixture (7% w/w).	103
9	Tilt angles of dopant 35 with KCHM211 mixture (7% w/w).	106
10	Tilt angles of dopant 67 with KCHM211 mixture (7% w/w).	106
11	Spontaneous polarisation of dopant 35 with KCHM211 mixture (7% w/w). .	109
12	Spontaneous polarisation of dopant 67 with KCHM211 mixture (7% w/w). .	111
13	The optical rotation of second generation FLC dopants	115
14	The phase transition temperatures of second generation FLC dopants . .	116
15	Phase transitions of dopant 110 with KCHM211 mixture (7% w/w)	117
16	Crystal data and structure refinement for compounds 35	123
17	SAXS data of dopant 35 with 5,7 and 10% mixture of KCHM211.(w/w) . .	126
18	Repeat conformational search and energy minimisation to show reproducibility.	133
19	Total dipole difference between results of the two methods	134
20	The lowest conformation energy values	135
21	Total dipole coordinates from optimisation in XYZ vectors using PBE RT Magnitude	136
22	Total dipole co-ordinates from optimisation in XYZ vectors using B3LYP_G Magnitude	137
23	Total dipole difference between results of CP2K and B3LYP_G methods .	138

List of Symbols & Abbreviations

$[\phi]$	Optical rotation
Δn	Birefringence
η	Refractive index
θ	Angle
P	Pitch length
S_N2	Second order nucleophilic substitution
(n)	Orientation of molecular long axes
3D	Three dimension
Å	Angstrom
°	Degree
P_S	Spontaneous Polarisation
BP	Blue phase
C*	Chiral smectic C
CD	Circular dichroism
Crys	Crystallisation
DCM	dichloromethane
DEG	diethylene glycol
DERA	Defence Evaluation Research Agency
DFT	Density functional theory
dm	Decimeter
DMAP	4-(Dimethylamino)pyridine
FLC	Ferroelectric liquid crystal
HCl	hydrogen chloride / hydrochloric acid
I	Isotopic
LC	Liquid crystal
LCD	liquid crystal display
m.p	Melting point
MBBA	N-(4-Methoxybenzylidene)-4-butylaniline

mg	milligram
N	Nematic liquid crystal phase
N*	Chiral nematic phase
NMR	Nuclear Magnetic Resonance
SmA	Smectic A
SmC	Smectic C
SSFLC	Surface-stabilized ferroelectric liquid crystal
TGBA	twist grain boundary phase
TN	Twisted nematic
TNLCD	Twisted nematic liquid crystal display
TV	Television
VAN	Vertical align nematic
z	The layer normal

1 Introduction

1.1 Introduction to Liquid Crystals

1.1.1 Introduction to Liquid Crystals

The common states of matter are solid, liquid and gas, which differ mainly by the types and degree of order present in the phase. When substances are heated, they go from a crystalline solid (possessing high order) to an isotropic liquid (highly disordered). Some substances, however, exhibit intermediate states lacking some of the order found in solids, but possessing more order than in liquids (Figure 1). These ordered fluids are called liquid crystals. Sometimes this phase is also referred as the fourth state of matter. The liquid crystalline phases are more commonly called as the mesophase. The mesophase exists due to anisotropy within the phase. Crystalline solids have typically both positional and orientational order where conventional liquids have neither of them; all molecular directions are non-equivalent as opposed to a conventional liquid where isotropic distribution is observed. In the mesophase, molecules possess a degree of orientational and rarely positional order due to weak anisotropic interactions, though the order is only a fraction of that observed in a crystalline solid, resulting in the observed fluidity. The unique properties of the mesophase have led to a vast interest in the fields of chemistry and physics.

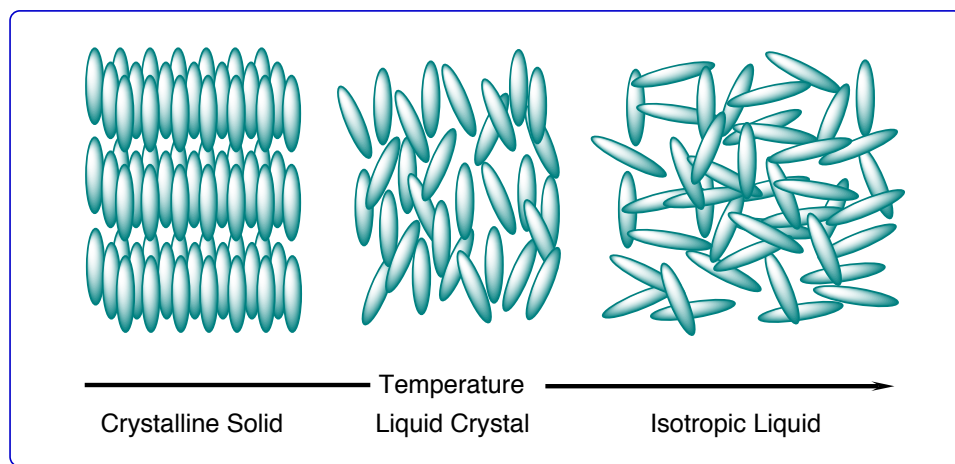


Figure 1. States of Matter

1.1.2 Historical Development

In 1888 an Austrian botanist Friedrich Reinitzer found in a manner similar to different previous reports, such as those from Heintz and Duffy on stearic acid, a phase of cloudy liquid between the crystalline state and the liquid state of cholesteryl benzoate. However, Reinitzer is considered as the first scientist to recognize that the cloudy liquid was a new kind of state of matter.^{1,2} Samples of the cholesteryl benzoate prepared by Reinitzer were sent by him to the physicist Otto Lehmann, who studied them using a polarizing microscope. Lehmann initially postulated that the structure of the liquid crystalline phase was attributable to the coexistence of phases in various states of aggregation due to an imperfect phase transition. However, his observations of only one homogeneous phase using the polarisation microscope contradicted his own theory. Later on Lehmann describes this strange material as a "soft crystal".³ The first successful study of a completely synthetic liquid crystal was carried out by Gatterman and Ritschke with the production of p-azoxyanisole in 1890.⁴ Later in 1922 Georges Friedel identified three different types of liquid phase, *i.e.*, nematic, cholesteric (chiral nematic) and smectic phases in his publication "Les Etats Mesomorphes de la Matière" and introduced this terminology into the literature.⁵ In addition he observed the effects on liquid crystalline phases of electric and magnetic fields.⁶ In the 1960s the first display application was proposed by Richard Williams and George Heilmeyer based on the dynamic scattering mode (DSM) effect.^{7,8} This led to the first practical liquid crystal display (LCD) application which, compared to display devices of the time, offered lower voltage and power consumption (Figure 2). However, the requirement for continuous current flow limited their application in battery operated devices.

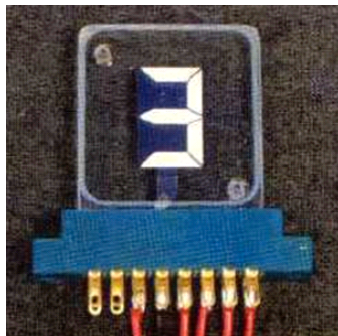


Figure 2. First practical liquid crystal display⁹

Revolutionary work by George Gray and co-workers at the University of Hull led to the discovery of the cyanobiphenyl a class of nematic liquid crystals, which exhibited electrochemically stable nematic phases at room temperatures.⁵ This enabled the successful functioning of a new type of liquid crystal display. Independently devised by James Ferguson and co-workers, and Wolfgang Heilfrich and Martin Schadt,¹⁰ the new display was based on the twisted LC nematic (TN) effect discovered by Charles-Victor Mauguin (Figure 3). Twisted Nematic liquid crystal displays offered significant advantages over other display technologies of the time, including low power consumption and small size, making them ideal for battery operated, hand-held devices. These early reports of flat-panel displays encouraged a new and continuous research effort into liquid crystal in general and synthesis of new liquid crystals materials for use in LCDs in particular.^{11,9}

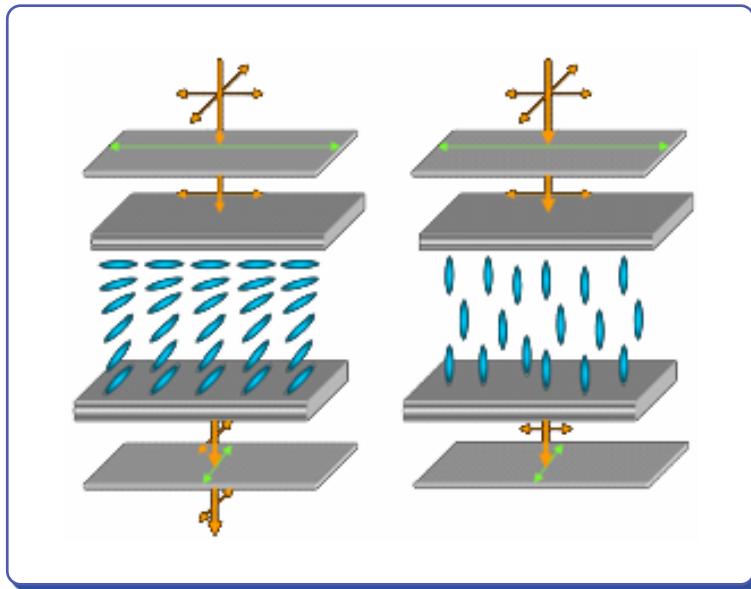


Figure 3. Twisted liquid crystal nematic (TN) effect^{12,13}

1.1.3 Classification of Liquid Crystals

Liquid crystals can be classified into lyotropic and thermotropic. Thermotropic liquid crystals are formed by a change in temperature, whereas lyotropic liquid crystals are formed by the addition of solvent. Thermotropic liquid crystals are the most common type of synthetic liquid crystals due to their use as nematic liquid crystalline mixtures in commercial Liquid Crystal Displays (LCDs). Thermotropic liquid crystals can be further divided by molecular structure into calamitic, discotic and polymeric liquid crystals. Calamitic liquid crystals possess a lathe-like or rigid-rod-like shape, where one molecular axis is much longer than the other two axes. There are many phases; nematic, smectic, cubic, columnar and TGB. This is summarised in Figure 4.¹⁴

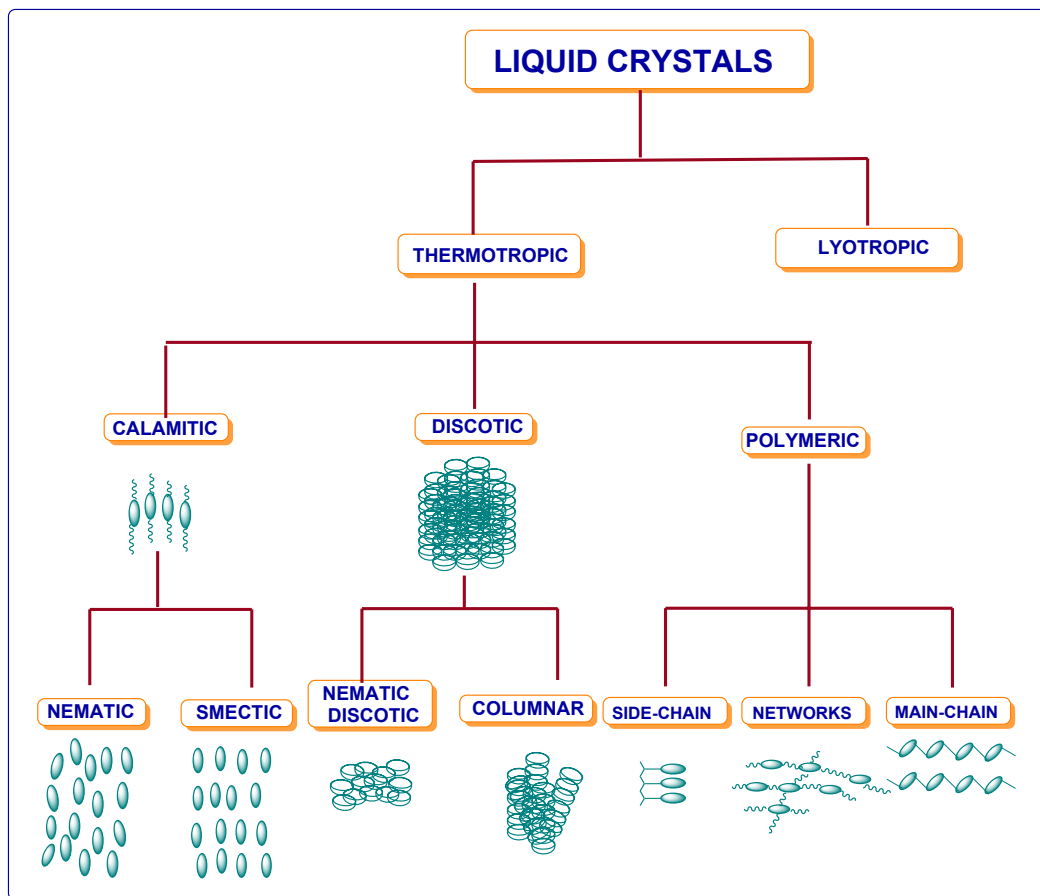


Figure 4. Classification of thermotropic liquid crystalline mesophases

1.2 Liquid Crystal Phases

1.2.1 Introduction to Liquid Crystal Phases

There are two types of mesogens, namely lyotropic and thermotropic mesogens. Lyotropic mesogens form phases as a function of their concentration in a solvent and temperature; thermotropic mesogens form liquid crystalline phases as a function of temperature, and are the main focus of our research. The most economically important type of thermotropic materials are calamitic liquid crystals, which are formed by rod-like molecules consisting of a rigid core and flexible alkyl side-chains, as shown in Figure 5, where A and B are core units which are linked by linking group Y, but normally most of the compound are directly linked without any linking group. R and R' are the terminal chains connected through X and Z or sometimes directly linked through the core units. M and N are the lateral substitution mainly to the obtain the required mesogenic properties. In my work the lateral substitution is F.¹⁵

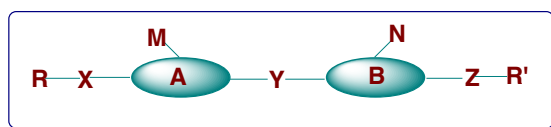


Figure 5. Structural template for a calamitic liquid crystal.

Calamitic mesogens can form economically two most important classes of liquid crystal phases: nematic and smectic. The nematic phase has orientational order along the molecular long axis, but no other level of order. Molecules in the smectic phase have both orientational and lamellar order. There exists many types of smectic mesophases, but the smectic A (SmA) and smectic C (SmC) phases are the most usually observed as shown in Figure 6.

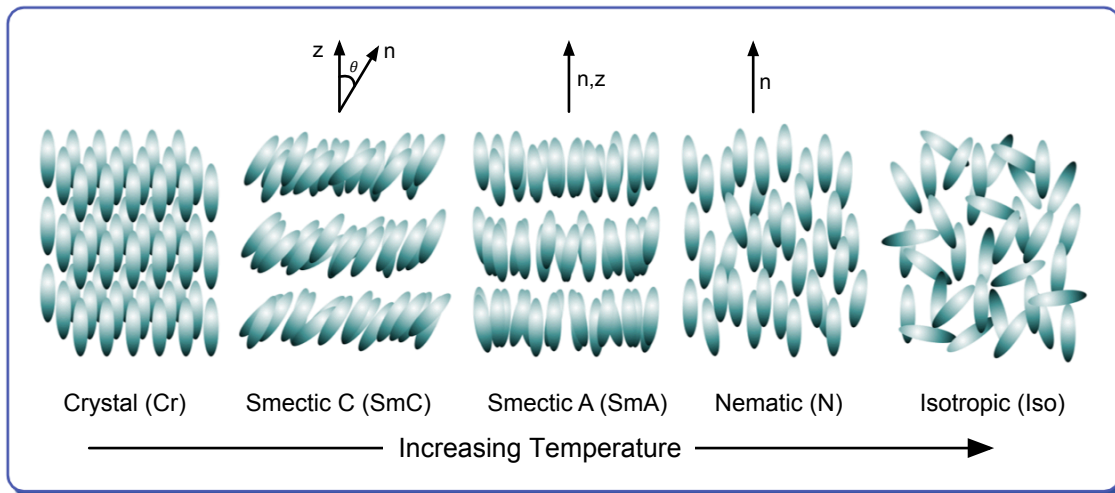


Figure 6. Phase transitions between crystal, liquid crystal, and isotropic liquid phases for a calamitic material as a function of temperature.

The main difference between the two phases is that the orientation of molecular long axes (n) is parallel to the layer normal z in the SmA phase, whereas n is tilted by an angle θ with respect to z in the SmC phase. For mesogens forming both the SmA and SmC phases, the SmC phase always forms at lower temperatures. The liquid crystal phases described up to now are achiral phases formed by achiral molecules. However, chiral mesophases are of particular interest because of their potential use in a wide range of technological applications, including a variety of electro optical ON/OFF light shutters. Presently, most liquid crystal display applications are based on ON/OFF light shutters formed by chiral nematic liquid crystals. The chiral nematic phase (N^*) is also known as cholesteric phase, By virtue of chirality, molecules in the N^* phase are not uniformly organized along one direction, but instead twist along an axis z perpendicular to n to give a helical structure in the bulk that minimizes free energy, as shown in Figure 7. The length corresponding to a full rotation (360°) of n about z is defined as the helical pitch (p), which is temperature dependent and reflects the degree of twisting. In spite of the many virtues of the N^* liquid crystal, chiral smectic (SmC^*) liquid crystals have been investigated as an alternative to twisted nematic liquid crystal display (TNLCD) due to their low power requirement and fast switching time.^{4,16–18}

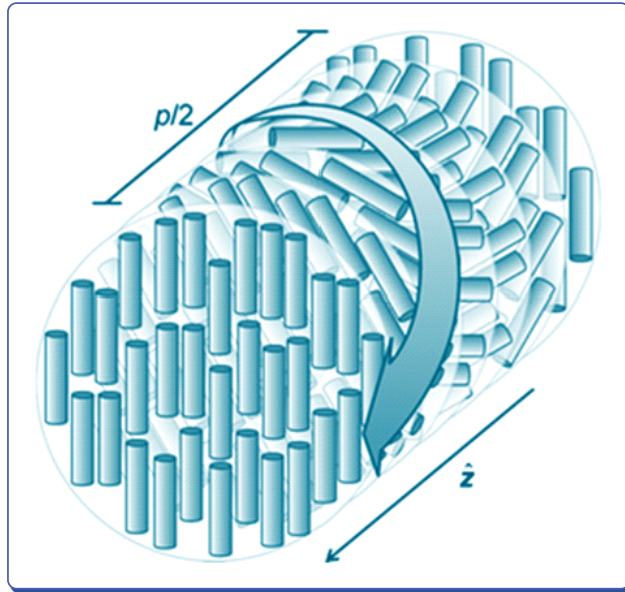


Figure 7. Structure of the chiral nematic phase showing the helical twist of n along z over $\frac{1}{2}$ of the helical pitch, p .¹⁹

1.3 Phases, Structures and Textures of Liquid Crystals

The liquid crystalline phases and properties are a outcome of the self organising actions of the mesogens, and in addition, the orientation of the director with respect to the surface of an electro-optic cell or device. It is essential to control the type of orientation of the liquid crystalline layer aligned on surfaces or in cells. The liquid crystal optical properties in different phases often directly reflect the symmetry of their structures. Anisotropy of the refractive index, or birefringence, is one of the typical physical properties of liquid crystals, and it allows for the visualisation of the macroscopic molecular orientation. In thin liquid crystal sample, cells placed between two crossed polarisers under an optical microscope, a range of textures and birefringence colours will be observed. These textures not only look beautiful but also provide a lot of information about the macroscopic structure of the liquid crystal phases. Although there are many investigation techniques available to study the structure and physical properties of liquid crystal phases, microscope observations often give sufficient information to determine the structure even if a well aligned domains are not obtained.

1.3.1 The Nematic Phase

The nematic liquid crystal phase (N) is the simplest liquid crystal phase. It is characterised by a high degree of long range orientational order but no translational order. The molecules in the nematic phase uniformly align with their longest axis orientated in a preferred direction often described in terms of a unit vector called the director (n), as shown in Figure 8

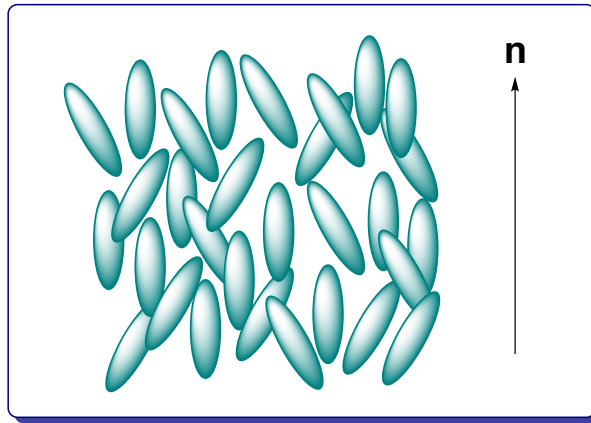


Figure 8. Molecular order in the nematic phase

The lack of positional order results in the promotion of free molecular diffusion throughout the sample, and a high degree of fluidity. Generally nematic phase will contain domains. The orientation of the director is constant in each domain but is different in different domains. When these defect regions are viewed under a polarizing microscope as shown in Figure 9, they appear as dark threads (Nematic word comes from the Greek which means thread.²⁰

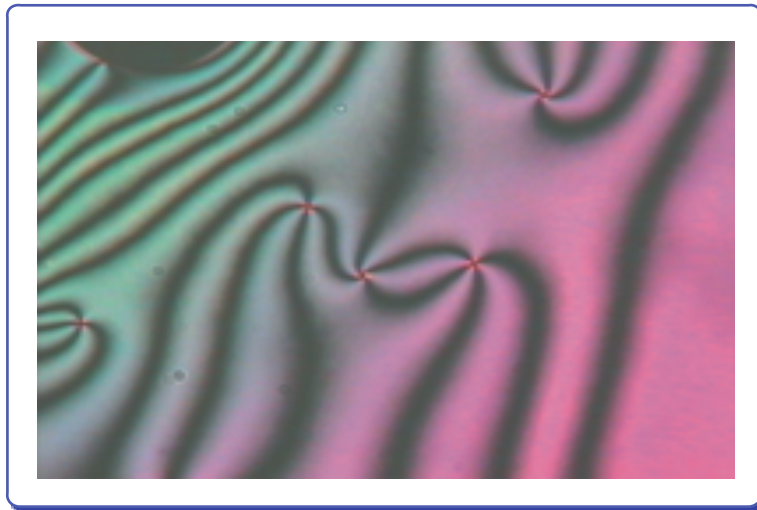


Figure 9. Schlieren texture of the nematic phase.²¹

The structural properties of liquid crystal play a significant role in the exhibition of the nematic phase. The design of specific structural features allows for modification of the liquid crystal physical properties. The rigid core unit is the most

critical part of liquid crystal and maintains shape anisotropy. Generally the core unit is aromatic in nature (*i.e.* phenyl **1**, biphenyl **2**, terphenyl **3**, naphthyl **4**), even non-aromatic (*i.e.* cyclohexyl **5**) and heterocyclic structures (*i.e.* pyrimidyl **6**) can also be used. Figure 10.²² Molecular axes can be extended through by using the terminal functionalities, which also alter the physical properties of the nematic phase. The n-alkyl and n-alkyloxy groups can increase mesophase stability and lower the melting point of the materials, which is crucial for ambient temperature applications. The strategic positioning of lateral substituents, either polar (*i.e.* F, CN, CF₃) or non-polar (*i.e.* CH₃), located on the core unit or the terminal chains, can be used to alter the physical properties.²³

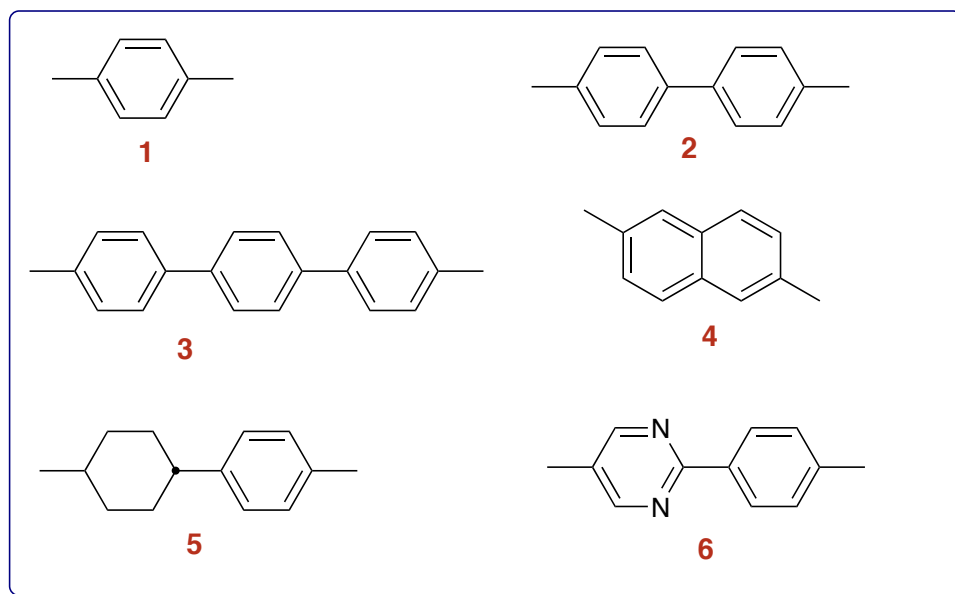


Figure 10. Examples of mesogenic core units.

1.3.2 The Cholesteric or Chiral Nematic Phase (N*)

Cholesteric or chiral nematic phase textures observed in planar and homeotropic cells are shown in Figure 11 (a). The observed colour is not the birefringence but the selective reflection colour originates from the helical structure of short pitch. Lines observed in Grandjean-Cano cells come into view because of the thickness gradient of cell. Grandjean-Cano lines are defect lines which form in between the two regions of various numbers of helical pitches. Material with long pitch helix, Figure 11 (b) is not a selective reflection colour but a colour due to birefringence and optical rotation is observed. Network-like defect lines are oily-streak lines. In the homeotropic cell or a planar cell of material with short pitch helix, the focal conic texture in Figure 11 (c) is frequently observed. The helical pitch is longer than the resolution limit of the microscope, then, finger-print textures or helical pitch lines are observed in such focal conic textures Figure 11 (d).

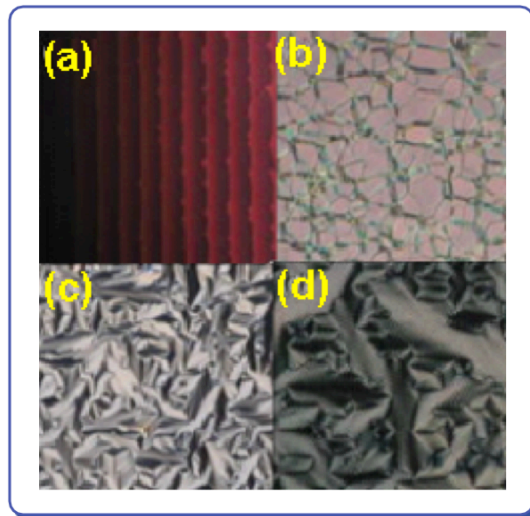


Figure 11. Photomicrographs of the cholesteric phase.²⁴

1.3.3 The SmA and SmA* phases

SmA phase focal conic texture in a planar cell with no rubbing action, and the uniaxial texture in a homeotropic cell are shown in Figure 12. The obvious optic axis *i.e.* fast axis and slow axis of the media is parallel to the layer normal to the SmA phase. To obtain the layer normal direction in focal conic textures, attention

should be paid to details of the texture, like the shape of focal conics and layer wrinkle lines. The SmA* phase exhibits a little electroclinic response under application of an electric field, *i.e.* the major optic axis tilts by a small angle under a high electric field. This is a polar effect, the sign of the tilt changing when the applied field is reversed.²²



Figure 12. Photomicrograph of the SmA phase.²¹

1.3.4 The SmC Phase

Another smectic phase with one dimensional positional order and looks similar to SmA is SmC phase. Here the molecules are not on average orthogonal to the layer plane, and hence the molecular directors, lie at an average angle θ to the layer plane as shown in Figure 13.

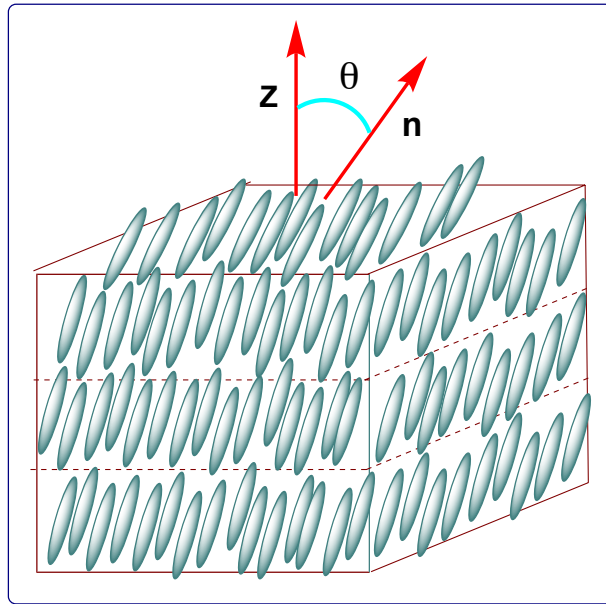


Figure 13. Schematic representation of molecular order in the SmC phase.

The angle θ is temperature dependent and the SmC phase is the tilted analogue of a SmA phase. The tilt is usually caused by dipole-induced intermolecular interactions. The formation of SmC is influenced mainly by the molecular structure, particularly symmetrical molecules with two terminal alkyl or alkoxy chains. In some cases, branching in the terminal chain can increase the chances for a material to exhibit the SmC phase. There may be influence of the dipole moment of the molecule to enhance the SmC transition as well. The zig-zag molecular shapes produce the necessary tilting within the layers to form the SmC phase. The usual microscopic textures exhibited by the SmC phase are the schlieren and the broken focal-conic fan textures as shown in Figure 14. The SmC can be obtained either by cooling the isotropic, the nematic or the SmA phases. Cooling the focal-conic fan texture of SmA shows the focal-conic fan texture of the SmC phase Figure 14.^{21,25-27}

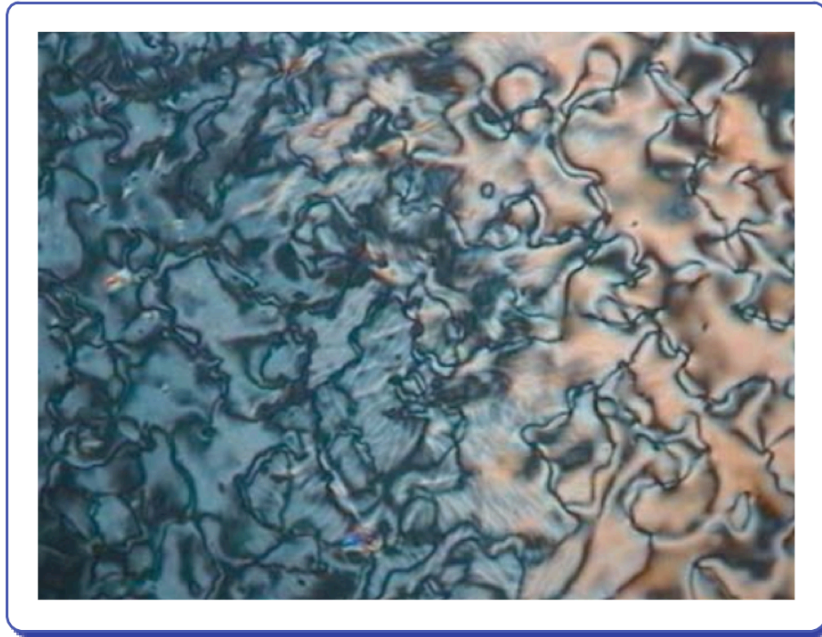


Figure 14. Transition from nematic schlieren (right) texture to a SmC schlieren texture (left) on cooling.²¹

1.3.5 The Blue Phase

The blue phase was first noticed by Reinitzer in 1888 while cooling cholesterol benzoate and named as “bright blue-violet colour phenomenon” which can be noticed by small change in temperature. In 1975 Armitage and Price studied in detail the stability, different types and thermodynamic properties of cholesteric liquid crystals.²⁸

After the initial observations, such as Reinitzer’s, the blue phases were observed to reflect blue light, for this reason they were named as the “blue phases”. The usual thermal order in mesophase of chiral liquid crystal materials follow the sequence, smectic to helical nematic to isotropic with increase in temperature. The blue phase is observed between the boundary of chiral nematic (N^*) phase and isotropic in highly chiral liquid crystal materials. There are three known phases BPI, BP II and BP III that can be observed. These phases are separated by first order transitions. The BP III has a similar symmetry to that of the isotropic phase, where as BPI has body centred cubic and BP II has simple cubic symmetry. The colourful textures of BPI and BP II appear as mosaic phases, Figure 15 and BP III appears as a misty blue or fog texture during slow heating.

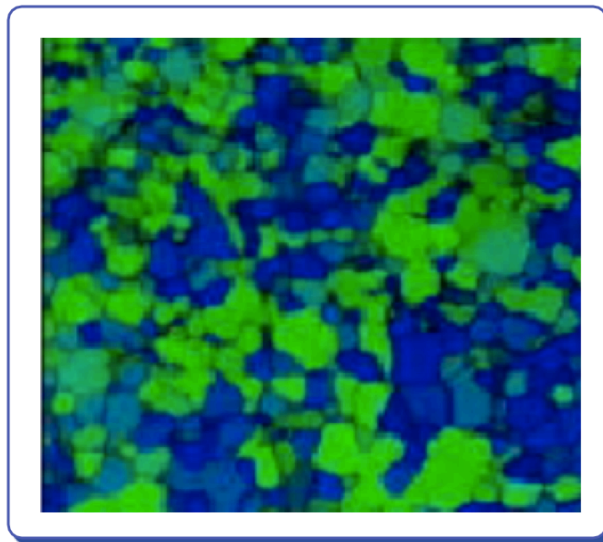


Figure 15. Mosaic texture in a BP II phase.²⁴

The smectic blue phase similar to normal blue phase has been studied which has smectic like transitional symmetry of the molecular mean position, in which

the smectic sheets are not perfect planes but are rotated about an axis as in grooves in a screw.

A schematic phase diagram Figure 16 based on the function of temperature and chirality is shown below. Low chirality liquid crystal molecules do not show any blue phase because of longer pitch length and weaker helical twisting power. As chirality increases or the pitch becomes tighter, BPI, BP II and BP III mesophases appear. In highly chiral molecules the BP II phase disappears as pitch length becomes exceptionally tight. The critical point between BP III and the isotropic phase shows the same symmetry.^{29,30 31,32}

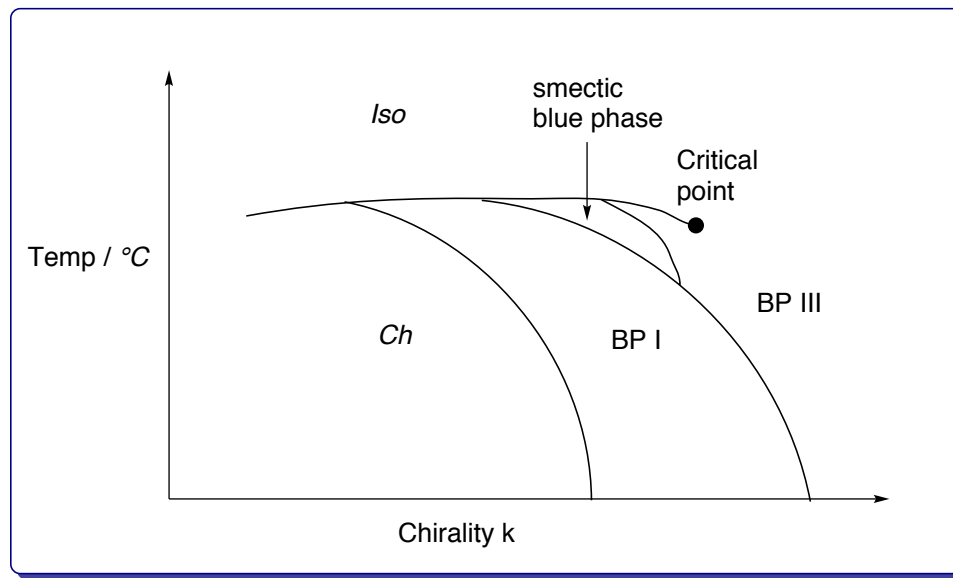


Figure 16. Phase diagram for the 3 blue phases as a function of chirality and temperature.³³

The appearance of the blue phases under POM is very different to those of usual calamitic liquid crystal phases which show birefringence. The array of defects are the main reason for the blue phase appearance. An achiral host material doped with a chiral dopant results in a chiral mixture possessing a single helical axis *i.e* N to N* and SmC to SmC*. The presence of double twist cylinders in the blue phase is critical in stabilising the phase compared to conventional liquid crystal phases. There must be a different driving force in the formation of the blue phase versus the nematic and smectic phases.^{34 35}

1.4 Ferroelectric Liquid Crystals

If a material possesses a spontaneous electric polarisation whose orientation can be reversed by applying different electric field polarity, it is termed ferroelectric. The SmC^* phase possesses this property but only when it is aligned in a planar geometry and the natural helical pitch is completely suppressed. It was Meyer who predicted the possibility of ferroelectricity in SmC^* liquid crystals by considering the symmetry elements of the phase. The achiral SmC phase has on average C_{2h} symmetry, the individual elements of which are a C_2 axis of rotation perpendicular to the layer normal, a reflection σ plane in the same plane as the layers and an inversion centre. When the σ reflection and centre of symmetry are not present it results in a macroscopic electric polarisation parallel to the C_2 axis, which is the sum of contributions of transverse dipole moments of the constituent mesogens along the C_2 axis (Figure 17). Application of the C_2 operation on the polarisation vectors along the other two orthogonal axes causes them to be reversed. Hence, there is no net polarisation other than along the C_2 axis. This permanent electric polarisation is known as the spontaneous polarisation, (P_S), and such SmC^* phases are ferroelectric in nature.³⁶

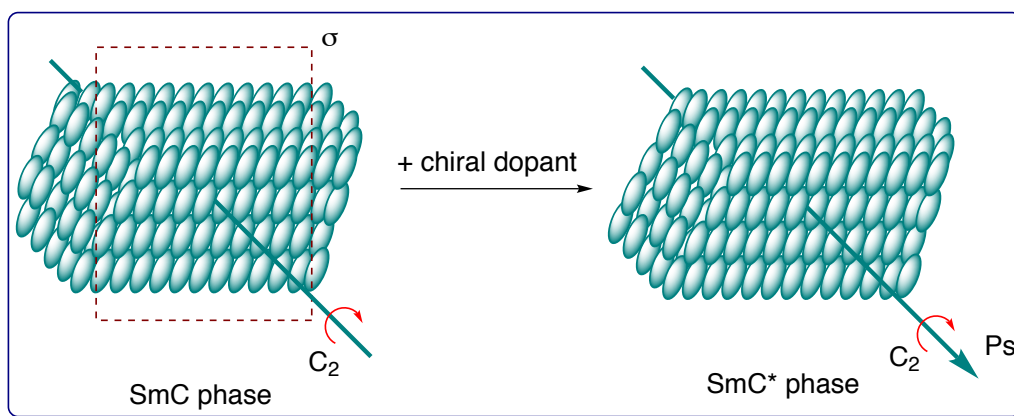


Figure 17. Molecular symmetry in achiral SmC , SmC^* phase with resulting P_S ³⁷.

In absence of alignment constraints, the SmC^* phase forms a helical structure as shown in Figure 18 (a), in which the P_S vector rotates from one layer to the next resulting in zero P_S . In 1980, Clark and Lagerwall showed that the SmC^* helix can be suppressed if an SmC^* material is planar aligned between rubbed polyimide-coated glass slides. The cell gap must be of the same size as the

helical pitch, p for this to occur. Figure 18 (b).³⁷ This arrangement of the SmC^* phase is termed a surface-stabilized ferroelectric liquid crystal (SSFLC).

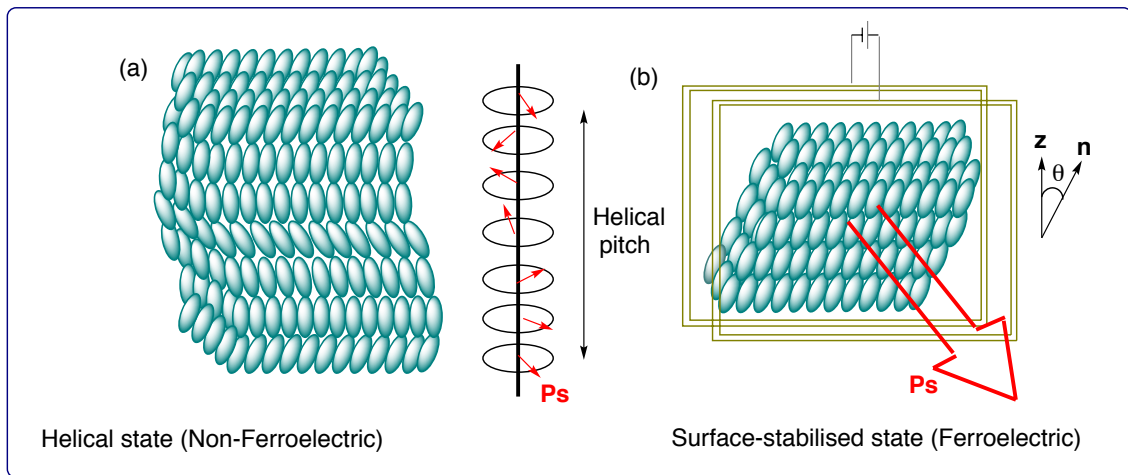


Figure 18. (a) Helical structure in the SmC^* phase without external constraints; (b) SmC^* phase with external constraints leads to SSFLC state.³⁷

An external field applied parallel to the $[C_2]$ axis, causes the tilted mesogens of a SSFLC to switch from one tilt orientation to another by precession of about z . Mesogens go from $+\theta$ tilt orientation to $-\theta$ tilt as the electric field is reversed. If the birefringence is matched with the cell thickness, the device acts a quarter wave plate retarding the polarisation by 90° . This enables the SSFLC film to act as a light shutter if it is placed between crossed polarisers as shown in Figure 19.

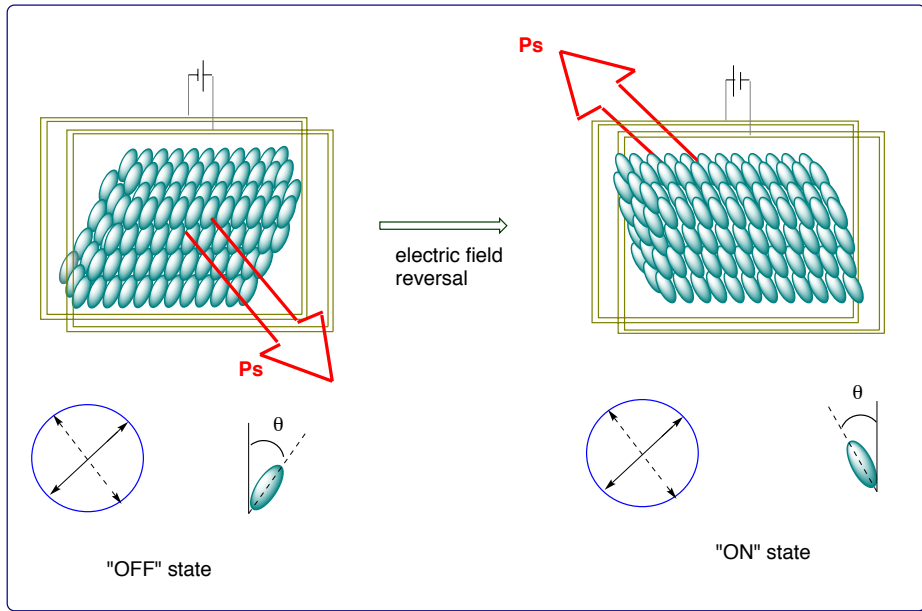


Figure 19. Switching between the opposite applied field in an SSFLC system.³⁷

1.4.1 Molecular Description of Spontaneous Polarisation

An understanding of spontaneous polarisation at the molecular level is generally based on the so called Boulder Model which was developed by Walba and Clark in 1986.³⁸ The zigzag conformation in the SmC phase has been adopted from optical and X-ray experiments.³⁶ The model is based on a bent-cylinder with a zigzag C_2 symmetric shape. The mesogens are more tilted than the side chains which all adopt an anti-conformation. Steric coupling between polar groups and the chiral centre leads to an orientational bias of the corresponding molecular dipole along the C_2 axis and it is this which creates spontaneous polarisation, (P_S).^{36, 39,40}

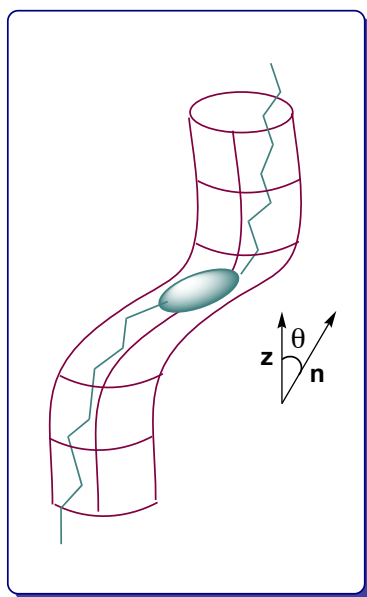


Figure 20. The bent-cylinder binding site with a guest molecule in the SmC* phase, according to the Boulder model.³⁶

1.4.2 Liquid Crystal Hosts

The materials used in the liquid crystal display are generally a mixture of several components. The usage of a mixture will enable the desired mesophase sequences to have the optimum temperature range and particularly, is the simplest way to obtain the minimum crystallisation temperature. The FLC mixture compositions also helps to tune the required physical and electro-optical properties. A good demonstration of this comes from the early research on cyanobiphenyls. The nematic binary mixture of 5CB and 8OCB is a commercially available material. 5CB has a low melting point with a narrow nematic phase temperature range whereas the mainly SmA 8OCB has a much higher clearing point but has a high melting point. The mixture of approximately 35 % 5CB and 65 % 8OCB gives the eutectic composition and considerably reduces the melting point with a phase transition: Crys 5 N 50 °C I as shown in Figure 22

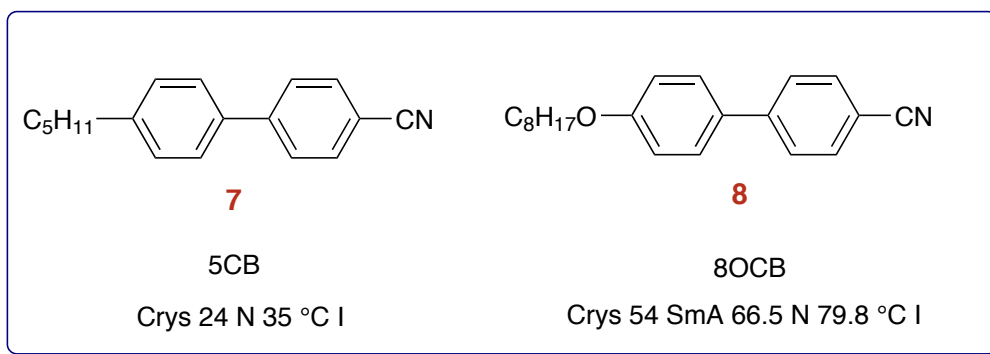


Figure 21. Liquid crystal hosts 5CB and 8OCB with their transition temperatures.

Gray et al in Hull University developed achiral host material for ferroelectric display system based on the discoveries made from the nematic materials. They developed low viscosity and wide temperature range SmC phases without any linking group in between the core rings. The key advance was the development of the terphenyl core unit with one or more lateral fluoro substituents to modify the central core unit. The introducing of fluorine in the central core normally reduces the melting point along with the suppression of unwanted ordered smectic phases such as SmB. A carbon fluorine bond generates a large dipole moment in the molecule and make them tilt in the SmC phase. Monofluoroterphenyls for instance 9 in Figure 23, have a high smectic tendency. More ordered tilted SmC

phase will result in the compound **9** in Figure 23 because of the polarity of the lateral fluoro substituent and the ether oxygen in the terminal chain.^{41,42, 43}

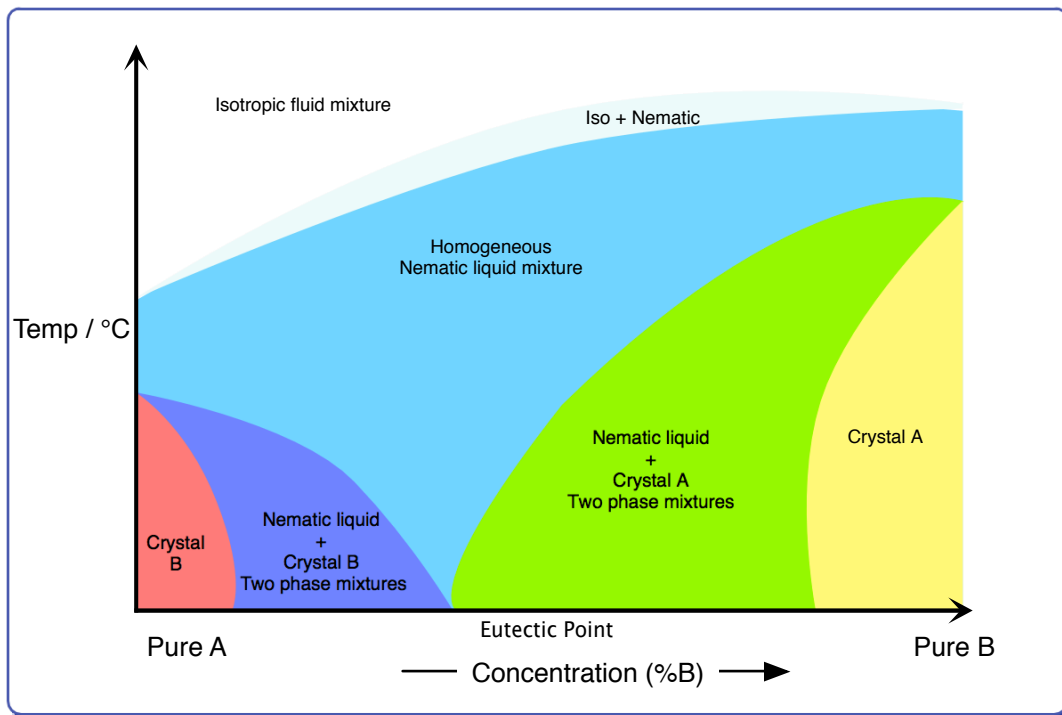


Figure 22. Phase diagram similar to that for the binary mixture of 5BC and 8OCB.^{41,42}

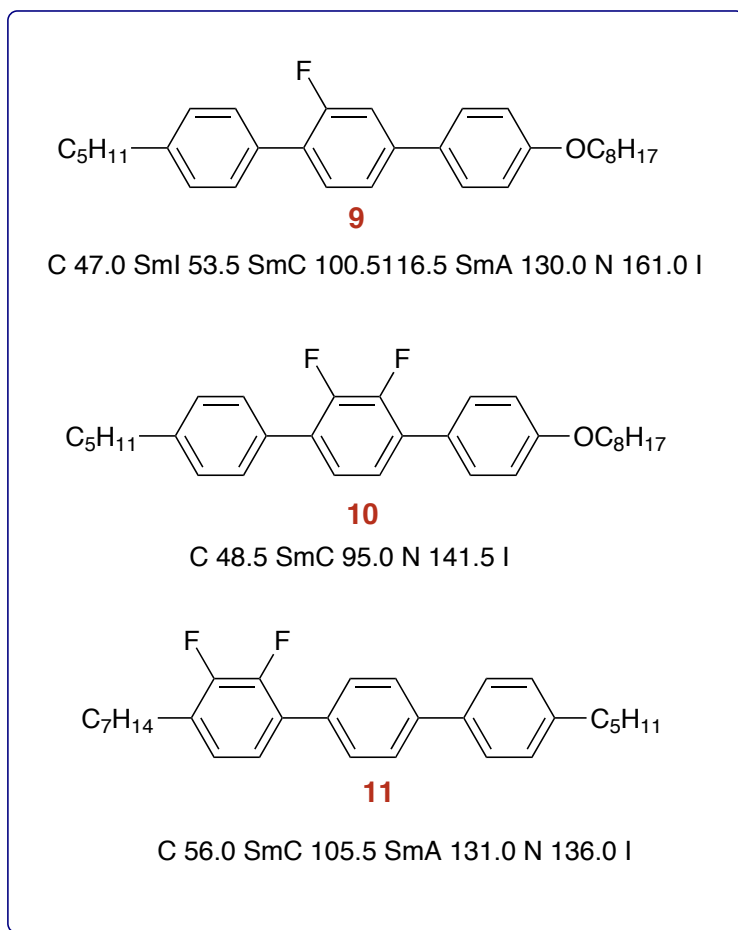


Figure 23. Achiral fluorinated terphenyl host compounds.

Figure 23 *O*-fluoro-substituted terphenyls. *Ortho* monofluoroterphenyls **9** and difluoroterphenyls **10** Figure 23 outstanding ferroelectric host materials. Preferably both the fluoro substituents are placed on one side of the molecule to enhance the net dipole moment of the molecule as they reinforce with other. Consequently the difluoroterphenyl materials have a high negative dielectric anisotropy and moderately high SmC phase stability.

The 2,3- or 2',3'-difluoroterphenyls (Figure 23) are no broader than the monofluoro substituted terphenyls and hence the dielectric anisotropy increases without drastic changes in melting point and viscosity. A most important advantage of the *ortho*-difluoroterphenyls is that a relatively high SmC phase stability can be generated from dialkyl substituents. This avoids the use of terminal alkoxy chains which increases viscosity relative to similar alkyl chain lengths.

The location of ortho and difluoro substituent on the terphenyl core unit will effect mesomorph in conjunction with melting and clearing points. The 'middle ring' 2',3' difluoroterphenyls - **10** (Figure 23) have a lower melting point and lower Sm-C mesophase stability with a better nematic tendency than the 'end' or 'outer' ring 2,3-difluoroterphenyls (*e.g.* The SmC phase is enhanced when the two fluoro substituent are on an outer ring and gives the lateral dipole near one end of the molecule. Both substitution positions, in conjunction with a reasonably long terminal chain, show a SmC phase. The compounds exhibit high negative dielectric anisotropies and high clearing points and the phase sequence of N \rightarrow SmA \rightarrow SmC on cooling. The central terphenyl core unit provides anisotropy required to give mesomorphic behaviour. The terminal chains will help to trim down the melting point so that a mesophases can be observed. The flexible parts of the calamitic liquid crystal are alkyl or alkoxy chains which also affect the transition temperatures with mesophase morphology. Kelly has studied the effect of the position of a double bond along a chain and Goulding and co-workers have studied the effect of an oxygen atom at different positions along a chain. Coates studied the effect of a methyl branching at various positions along the chain and showed that if the branching point is closer to the core unit the mesophase stability will disappear more strictly. The melting points of the materials are also much reduced. When the branching point moves further away from the core, its influence on the mesophase stability is less, but the melting points are still reduced.^{41,44-48}

1.4.3 Liquid Crystal Chiral Dopants

The properties of a chiral nematic LC phase are result of its helical ordering. In the case of doped liquid crystals, the helical order is caused by the interaction of a chiral dopant with an achiral nematic host, which can be expressed in the dopants helical twisting power. Doped liquid crystal research has divided into two major fields. The first focuses on the development of shape persistent dopants, mainly aiming at reaching high helical twisting powers and investigation of the interactions between chiral dopants and LC host molecules. In the second field the focus lies on the switchable dopants, which can change shape in reaction to an external stimulus, usually light or heat. In this area the focus lies more on future application, for instance in liquid crystal displays.^{49–54}

The chiral dopant mainly accounts for less than 10% of the total ferroelectric mixture, but it is a most essential component. Though the chiral dopant need not be mesogenic in order to be useful in imparting ferroelectric properties to the smectic C host mixture, it should have a mesogenic-like structure, rather similar to that of the host materials in order to help maintain the properties of the host mixture. Care should be taken when considering the structural nature of the chiral dopant to ensure it does not depress the SmC phase stability of the host mixture. More attention should be given to the other important features of the dopant like high spontaneous polarisation (P_S), tilt angle (θ), good solubility and long chiral nematic pitch length (P).

The common chiral dopants used in ferroelectric mixtures have a polar group at the chiral centre (*e.g.*, Cl, F, or CN) which provides the required high P_S . Figure 24 illustrates the chemical structure of two chiral dopants. The cyanohydrin ester, compound **12**, has a polar cyano substituent at the chiral centre. The large dipole associated with the cyano unit ensures the generation of high P_S magnitude. However, compound **13** is non-mesogenic; it has a mesogenic-like architecture and accordingly, should be useful as a chiral dopant for ferroelectric mixtures.

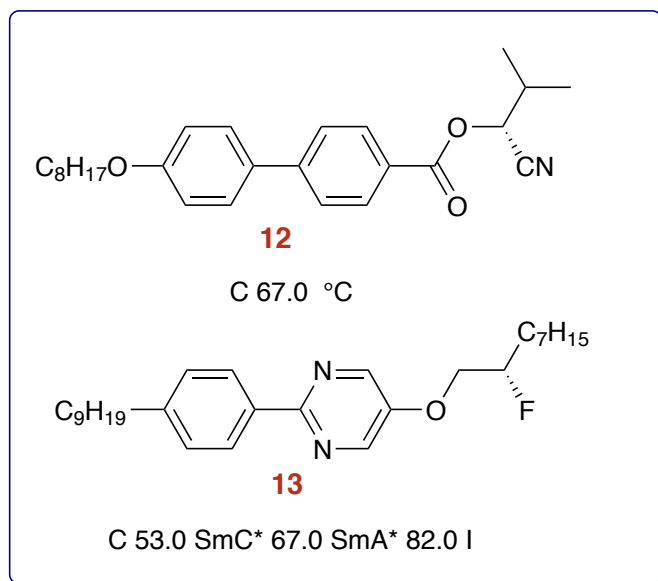


Figure 24. The structure of chiral dopants.

The use of a fluorine at the chiral centre offers many advantages while designing chiral dopant materials. Its small size and high electronegativity ensure the generation of high P_S values without enhancing viscosity or adversely affecting solubility. In addition, the small size of the fluoro substituent upholds, or even enhances, the SmC phase stability of the original host mixture. This is particularly important for ferroelectric host mixtures based on phenylpyrimidines which have particularly low SmC phase stabilities.^{22,43 55 38}

A common use of chiral dopants in liquid crystal phases formed by rod-like (calamitic) molecules is the induction of chiral bulk properties such as the helical pitch of the N* phase or the spontaneous polarisation of a SmC* phase. Molecular design of cholesteric dopants is usually aimed at inducing high chirality evidenced by a tight helical pitch and this usually makes these dopants unsuitable for FLC applications, since a long pitch is essential for a stable bookshelf alignment.

Dopants with axial chiral such as from biaryl cores as shown in Figure 25 suggest that a core with helical topography is more effective at chirality transfer in the N* phase than a core in which the two aromatic rings are nearly orthogonal, which is consistent with previous observations made by Gottarelli and others.^{56 57 58}

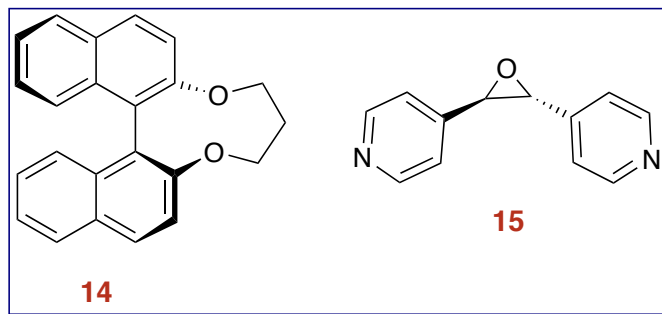
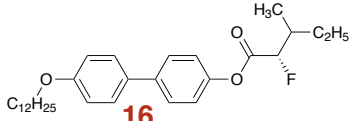
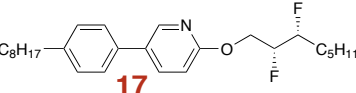
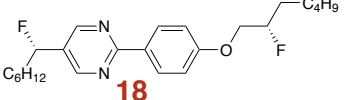
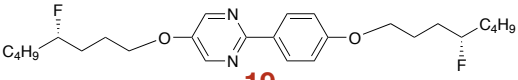
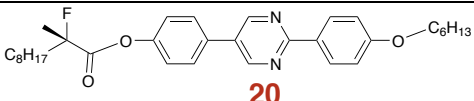
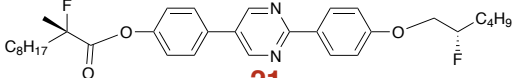


Figure 25. A typical examples of axial chiral dopants.⁵⁶

In the molecular design of dopants for FLC applications, chemical stability, a large dipole at the chiral centre and a minimum of disruption to liquid crystalline ordering by bulky branching groups led to the investigation of fluoro-substituents at the chiral centre. Some examples are tabulated with P_s and transition temperature in Table 1. In general, fluoro-substituents at a chiral centre are more complex to synthesise as there is not a source of such fluorinated units available from nature's chiral pool. Advanced asymmetric synthesis is required although this an area where improvement in methodology is rapid. It turns out that a fluoro-substituent does not necessarily confer a high P_s , unless of course lot of dopant is used in the mixture. The table gives extrapolated values for 100% ee but, in some cases it was not possible to obtain the original sources and so the method of obtaining the P_s values is uncertain, not sure about CF_3 , but I do not think that is so high either unless used in high percentages.

Table 1. The examples of dopants with transition temperatures and P_s^{59-63}

Dopant	P_s /nC cm^{-2}	Transition temperature / °C
 16	200	Cr 71 C* 81 A 93 I
 17	400	Not found in lit
 18	335	Cr 73 S 76 C* 79 A 86 I
 19	310	Not found in lit
 20	450	Cr 81 S 112 C* 144 I
 21	602	Cr 102 S 122 C* 128 I

A number of FLC chiral dopant were synthesised and characterised by different research groups which are mainly developed from trifluorinated, dihydrofurones and tetrahydrofurans. Optically active trifluoromethylated materials with a tetrahydrofuran tail unit proved to be better chiral dopants for preparing FLC compositions.⁶⁴

The amplification of molecular chirality by liquid crystalline systems is widely applied in investigations towards enantioselective solvent – solute interactions, chiral supramolecular assemblies, smart materials, and the development of liquid crystal displays.^{65 66} . Some of the chiral dopants will help to increase the helical twisting power in the smectic C* mixture.^{67 68 69}

1.4.4 Amplification of Chirality in Liquid Crystals

Chiral nematic liquid crystals possess a supramolecular chiral unit. In general these materials exhibit very high optical rotation and circular dichroism properties. The chiroptical properties are magnified in the mixture compared to those of individual dopants. The best example is menthol, which has a 30,000 times larger specific molar optical rotation ($[\phi]$) in liquid crystal host MBBA **22** ($[\phi]_{578} \sim 2,400,000^\circ$) than in methanol ($[\phi]_D = 78^\circ$). These chiral liquid crystal molecules show huge chiral properties that can be used as a measure of their chiral environment and also as a measure of the chirality of the dopant.^{70 71–73}

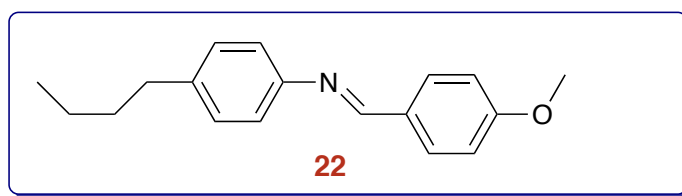


Figure 26. The structure of MBBA

In the designing of chiral molecule the introduction of fluorine at the chiral centre can enhance the desired chiral properties. The small size and high electro negativity ensure the generation of high P_s values without increasing viscosity or adversely affecting solubility. Also, the small size of the fluoro substituent will support or even increases the SmC phase stability of the original host mixture. This is particularly important for ferroelectric host mixtures based on phenylpyrimidines which have particularly low SmC phase stabilities.^{22,43}

Molecules containing bulky cyano group at the chiral centre confer a large energy difference between most possible time-averaged conformations of the chiral centre and results in high P_s value, even though low transition temperature are noticed. This is may be due to the steric effect of the cyano chiral unit near to the central core unit leading to low transition temperatures for the pure chiral compounds as in the example in Figure 27.^{74,75}

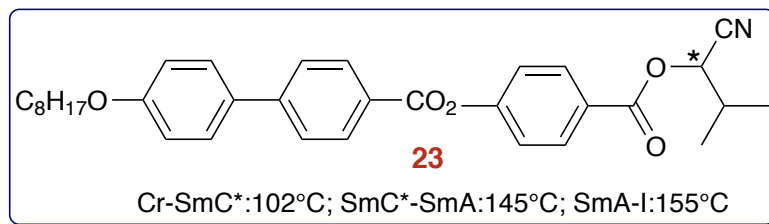


Figure 27. The structure where cyano group close to the molecular core⁷⁴

1.5 Fluorinated Liquid Crystals

Introduction of fluorine in designing the FLC molecule is a vital approach, as it influences the mesomorphic behaviour and also considerable effect on the physical and electro-optical properties. Molecules with a liquid crystalline mesophase have a degree of intermolecular association between that of a three dimensional crystal and an isotropic liquid. To alter these intermolecular organisations, a perturbing substituent or group can be introduced in the molecular structure which modify the separation of the molecules and adjust the strength of the intermolecular force.^{22,76–80}

The fluorine atom is frequently used in the design of liquid crystal molecules to obtain a lot of exciting effects such as a stronger dipole moment, lower viscosity and a higher chemical stability. The introduction of a fluorine atom normally leads to a noticeable variation of properties and also imparts advantageous properties due to its small size (1.47 Å) comparable to the size of hydrogen (1.20 Å). A fluorine atom is a suitable hydrogen mimic due to its insignificant steric impact and the ability to impart substantial electronic and polarity influences.⁷⁶

1.5.1 Effect of the Location of Fluoro Substituents

Maintenance of thermotropic liquid crystalline phase, in most cases, requires a balance of attractive molecular forces along the length of a rod or the surface of a disk versus the disorder of fluidity which is aided by flexible units at the periphery Figure 28. The substitution of hydrogen for fluorine, particularly on the rigid core, has proved one of the most successful ways of reducing melting points, and achieving the desired dielectric properties for display applications. These beneficial properties have been reached with the bonus that the compounds are very stable and can be synthesised in high purity and with very low ionic contamination.^{43,79–81}

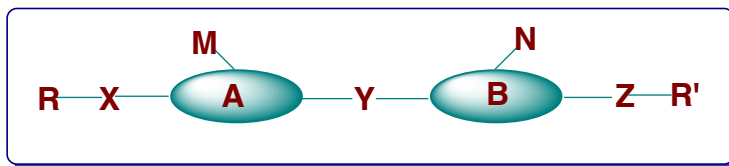


Figure 28. A typical structural template for a calamitic liquid crystal.

1.5.2 Fluoro Substitution at a Lateral Position

The attributes of fluorine that have made it so successful in liquid crystal science and applications is firstly due its small size (1.47 Å) when compared to hydrogen (1.20 Å). This means that packing in the nematic or smectic phase is not as efficient when one or two fluorine atoms replace hydrogens on an aromatic rigid core, but although clearing points are reduced markedly, so are melting points. It has the additional advantage of suppressing ordered smectic phases when ferroelectric materials are the target. Figure 29 shows how introduction of fluorine into the molecule has results in the reduction melting point and clearing point of the hydrocarbon to give practically useful materials. It also exhibits the large change in phase type caused by moving the position of the fluorine, *e.g* the middle ring difluoro example is a nematogen but when the fluorines are moved to the end ring, the smectic phase is supported, as well as a broad temperature range SmC phase.^{82–84}

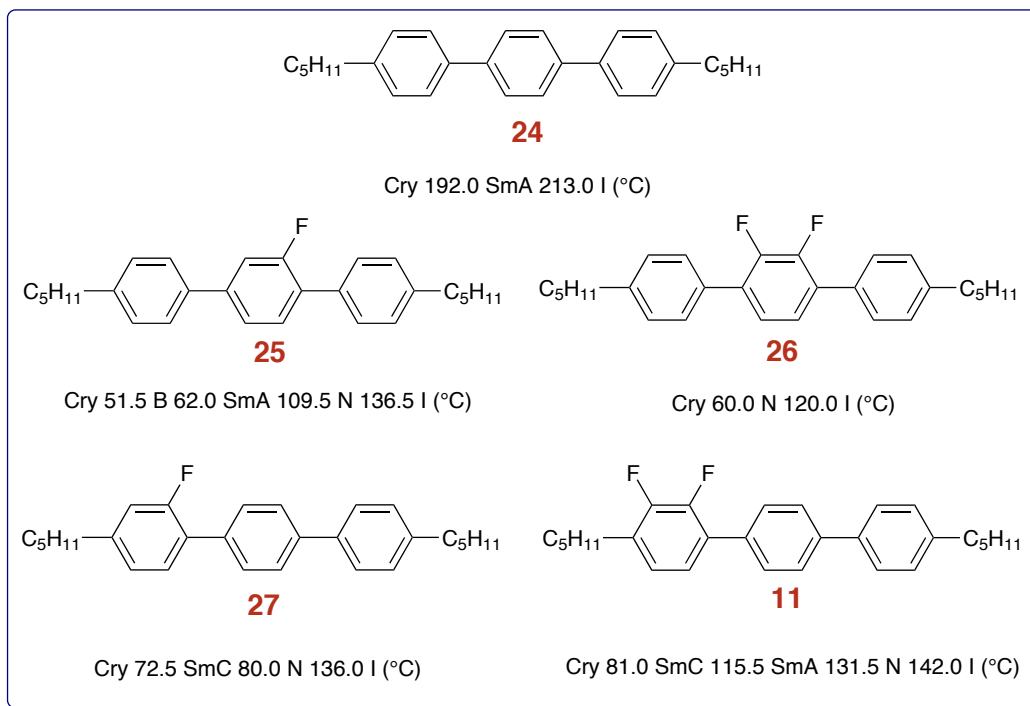


Figure 29. Effect of transition temperatures on fluoro substitution.⁴³

A second advantageous property of fluorine is that it has the highest electronegativity in the periodic table. All display and photonic applications of liquid crystal require an anisotropic distribution of dipoles in the molecules giving rise to negative or positive dielectric anisotropy. This is what allows liquid crystals to be manipulated by an electric field and thus change the optical properties within the pixel of a display or photonic device. Attachment laterally gives a negative ΔE which is used in VAN, IPS and FLC devices whereas terminally attached fluoro-substituent give positive ΔE materials and are used in conventional TN displays.

Finally the carbon-fluorine bond is very strong $441.3 \text{ KJ mol}^{-1}$ versus $413.7 \text{ KJ mol}^{-1}$ for a carbon hydrogen bond. Fluorine is also a very weak ligand and so it will not bind to metal ions, which could enable current flow in a display cause degradation of performance. The net result is the large area, long life TVs that can be seen in many households and are a great testimony to the years of research in academic and industrial laboratories.^{43,85}

2 Research Aim

2.1 Current FLC Mixtures

As shown in the previous section, the small size, low polarisability, mono-atomic nature, high electronegativity and strength of the C-F bond has been essential in enabling stable liquid crystals to be prepared with the desired electro-optic and viscoelastic properties required for display applications. Compounds very similar to compounds in Figure 41 are found in today's large TVs and in smaller LCDs and thus, a multi billion pound industry relies on the benefits of fluorinated liquid crystals. The nematic phase is exploited in most displays, but as already demonstrated, minor variations in the location of the fluoro-substituents can yield materials with wide SmC phase temperature profiles. In general, increasing the length of the terminal chains can also be employed to increase smectic vs nematic phase stability. It has already been discussed that an FLC mixture is best formulated from an achiral host mixture and a chiral dopant. A low viscosity mixture was developed during the collaboration between The Defence Evaluation Research Agency (DERA), now QinetiQ and the liquid crystal research group at Hull University. It consists of dialkyldifluoroterphenyls, with fifty percent of the mixture made of a middle ring difluorinated-material and the other half from two end-ring substituted compounds. The resultant mixture has a low melting point, wide SmC phase temperature range and an I - N - SmA - SmC phase sequence that provides good alignment. It is very stable, has low viscosity and the tilt angle is high enough to give good optical contrast⁸⁶⁻⁸⁸.

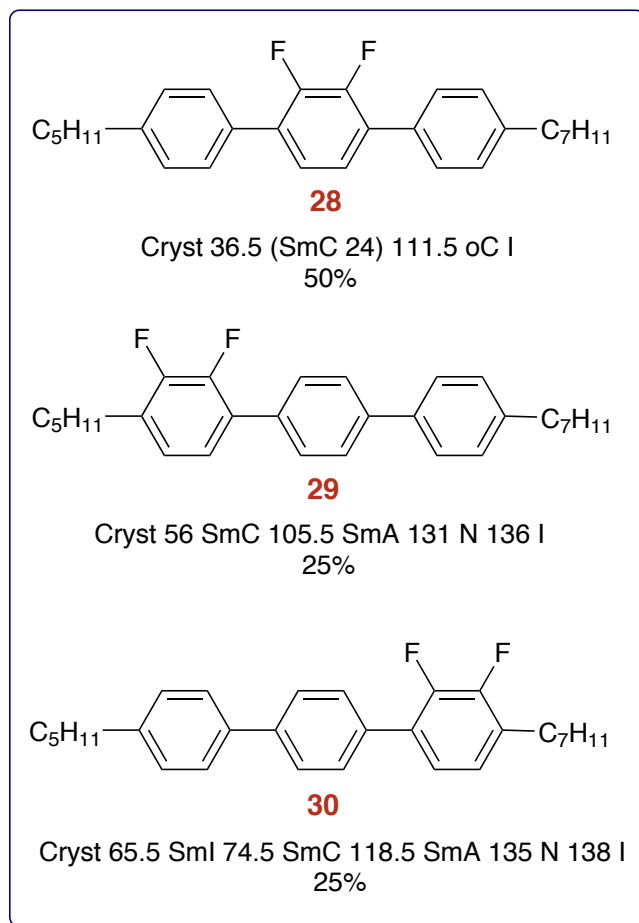


Figure 30. The structures and transition temperature of host mixture KCHM211.

It is interesting to note that 50% of the mixture only as a SmC phase up to 25 °C and is essentially a nematogen but the transition temperature of the final mixture which we will refer to as KCHM211 has a much higher SmC – SmA phase transition.

KCHM211 Cryst ~ 11 SmC 87.2 SmA 99.5 N 122.5 °C I

KCHM211 + BE8OF2N (7 % w/w) **31** (Figure 31) SmC* 67.2 SmA* 97.7 N* 117 °C I

The FLC mixture KCHM211 used throughout my work has suitable properties :

- Very stable
- Tilt angle 20 °

- I N SmA SmC phase sequence aids better alignment
- Similar compounds used in VAN displays

Mixing the three components has led to a reduced m.p, although not really low enough for a commercial device, however the mixture can be held below this temperature for long periods without crystallising. The chiral dopant BE8OF2N **31** (Figure 31) selected by DERA as part of the FLC research programme with Hull University was originally synthesised by Merck. A 7 % w/w mixture with KCHM211 produces a mixture with a P_S of 16 nC cm⁻² and a pitch length of 14 μ m at the N* - SmA* phase transition and provided good alignment. The transition temperatures shows that the most dramatic effect is the reduction of the SmC* – SmA* phase transition by 20 °C. The SmA* – N* transition is barely altered and the clearing temperature is reduced by nearly 9.0 °C; however the latter is beneficial since it reduces the temperature at which electro-optics cells need to be filled.

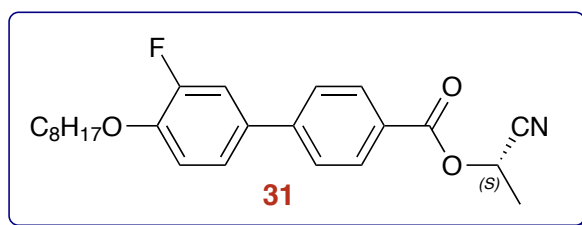


Figure 31. The structure of BE8OF2N.

The main drawback of this dopant is the instability of the ester group. The electron withdrawing nature of the nitrile makes the ester more sensitive to hydrolytic cleavage; this is borne out by the fact that containing compounds are rarely found in modern LC mixtures. There has been one previous report in 1989 of a cyanohydrin ether as the chiral portion of a ferroelectric liquid crystal **32** (Figure 32). The paper described the syntheses following the well known asymmetric synthesis method developed by Evans. One example was prepared with sufficient purity for liquid crystal evaluation, R1 = n-decyl, R2 = n-pentyl and only a melting point was reported. The paper mentioned that publication of liquid crystal properties would follow but none have appeared.

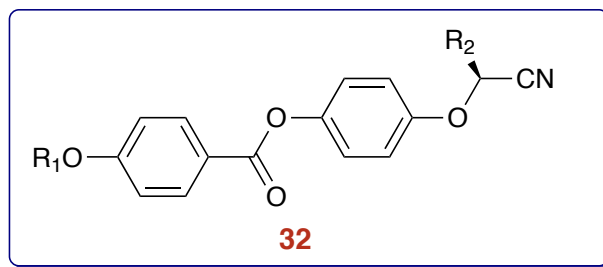


Figure 32. The general structure of cyanohydrin ether linked FLC.

The motive for this project is to prepare dopants that maintain the moderate P_S and long pitch when added to mixtures related to KCHM211, but with increased chemical and photochemical stability. This is part of a larger goal of formulating a commercially viable FLC mixture based on the fluorinated terphenyl materials.

2.2 Project Outline

Due mainly to the probable instability of BE8OF2N **31**, a new non-mesogenic dopant **36** and **35**, shown in Figure 34 was selected. Esters are more unstable than ethers; from this basis the ester group is replaced with an ether group at the chiral centre of the BE8OF2N which may give more stability to the compound. The aim was to maintain a moderate P_S and a long pitch length and this required confirmation. The replacement of an ether group by an ester was achieved using the key intermediates (*R*) and (*S*)-1-amino-1-oxopropan-2-yl 4-methylbenzenesulfonate **33** and **34** as shown in Figure 33 which were synthesised from the cheap commercially available (*R*)- and (*S*)-lactamide which also has a built in unit of chiral centre shown in Scheme 1 and Scheme 6.

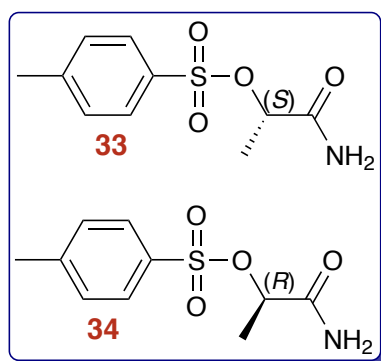


Figure 33. (*R*) and (*S*)-1-amino-1-oxopropan-2-yl 4-methylbenzenesulfonate

Both enantiomers were synthesised to confirm any racemisation that may occur during the synthesis. The intermediate compounds **33** and **34** were selected as they include an amide which can readily be converted to the nitrile group. The tosylate is a good leaving group for S_N2 reactions, gives crystalline derivatives and therefore is convenient to purify and can increase enantiomeric purity from recrystallisation.

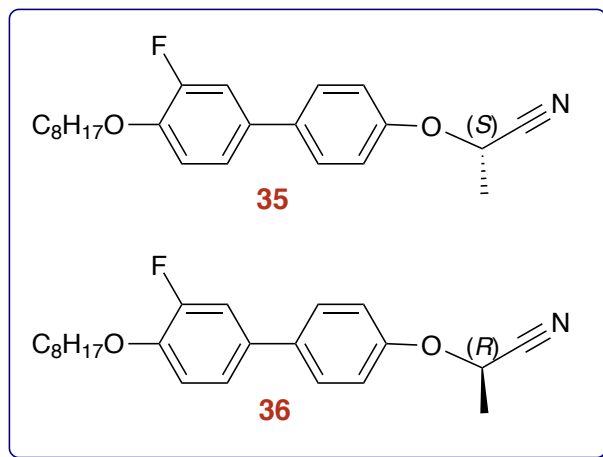


Figure 34. The targeted non-mesogenic liquid crystal dopant

The synthetic route of the *S* and *R* chiral unit **33** and **34** and the target **35** and **36** are shown in Scheme 1 and Scheme 6. Scheme 7 is not that efficient in terms of yield but to avoid any racemisation the chiral unit was attached at the last step and this took precedence over the chemical yield.

The study of mesogenic dopants led to the interest in the design of more liquid crystalline dopants. The targeted dopants are mesogenic alkyl difluoro terphenyls with ortho-difluoro substituents in one of the rings of a terphenyl. The structures mimic quite closely those used in the achiral host mixture KCHM211 and should maintain higher liquid crystal phase temperatures. The general format of the targeted compound is shown in the Figure 80. The targeted compounds **67**, **77** and **87** were synthesised using similar methods as used for **35**. The related Schemes are shown below with some of the intermediate compound schemes.⁸⁹

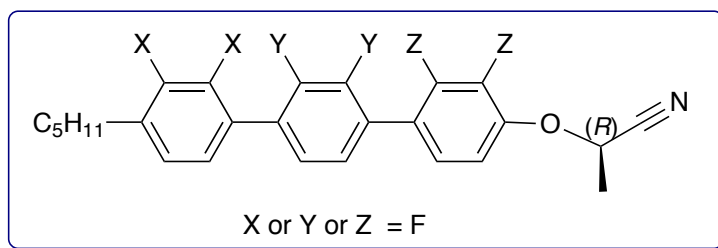
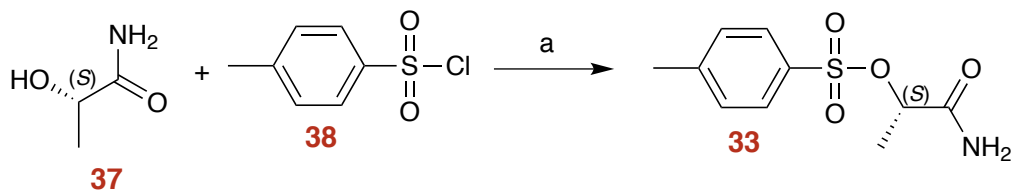


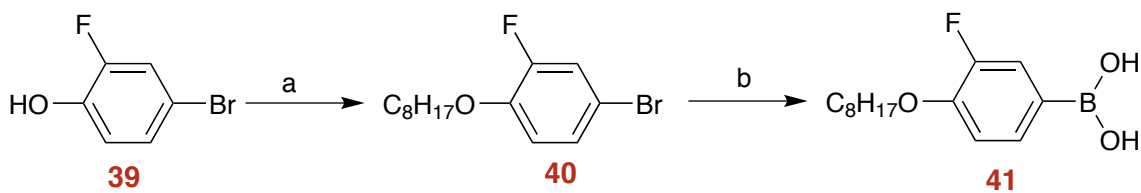
Figure 35. Mimic of targeted mesogenic liquid crystal dopants.

2.3 Schemes and Mechanisms



a: DCM, Diisopropylethylamine, DMAP, 0 °C

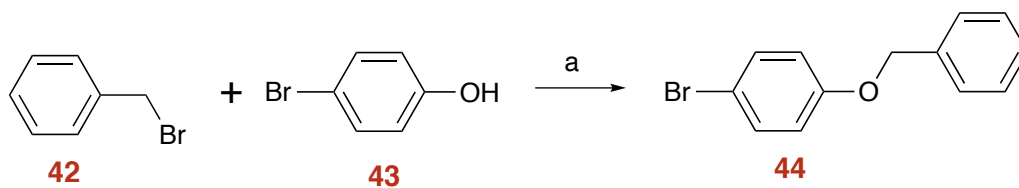
Scheme 1. Synthesis of (S)-lactamide tosylate, **33**



a: 1-Bromooctane, K_2CO_3 and butanone

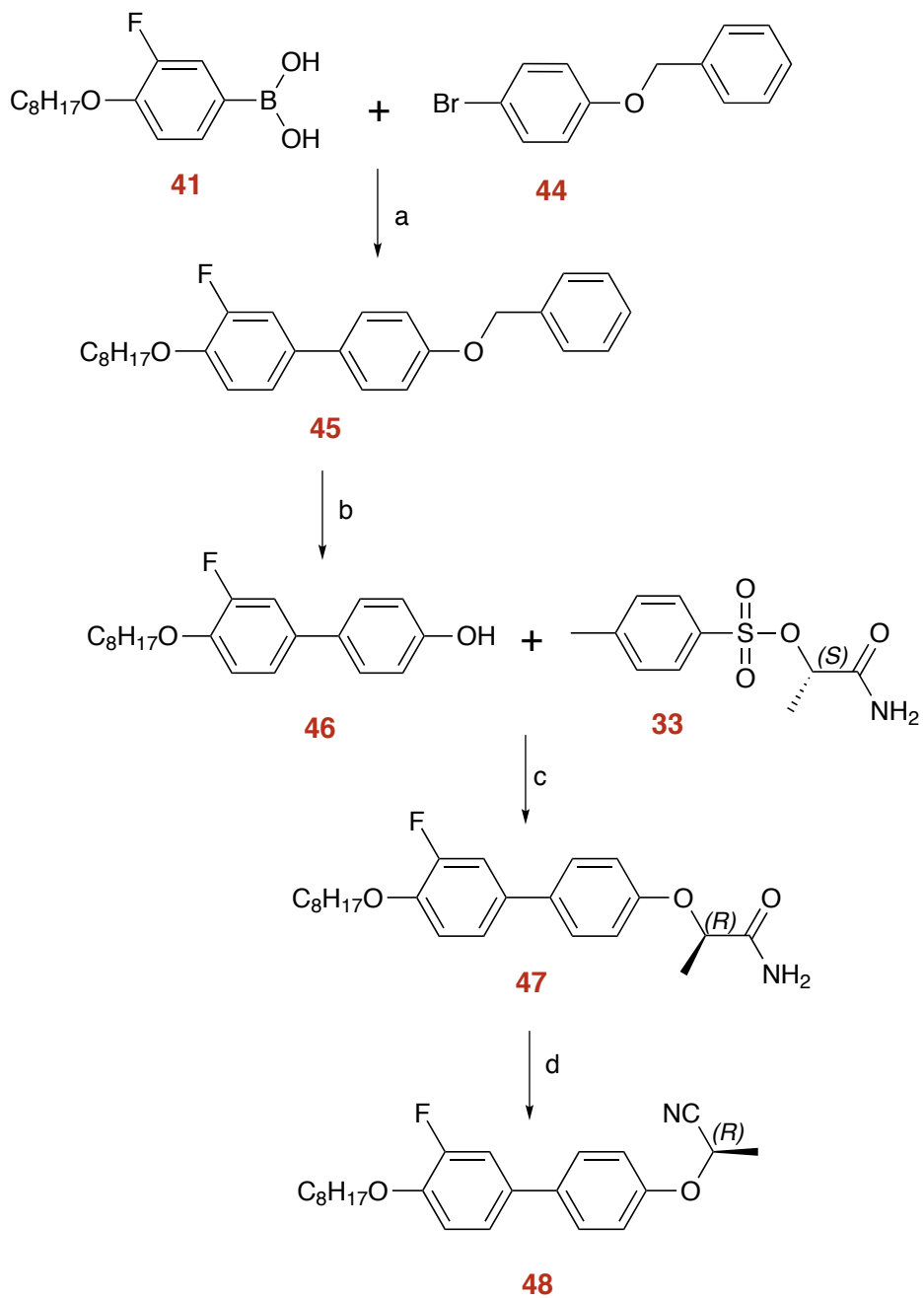
b: (i) n-BuLi (ii) THF, -78 °C (iii) $B(OMe)_3$ (iv) 10% HCl

Scheme 2. Synthesis of boronic acid **41**



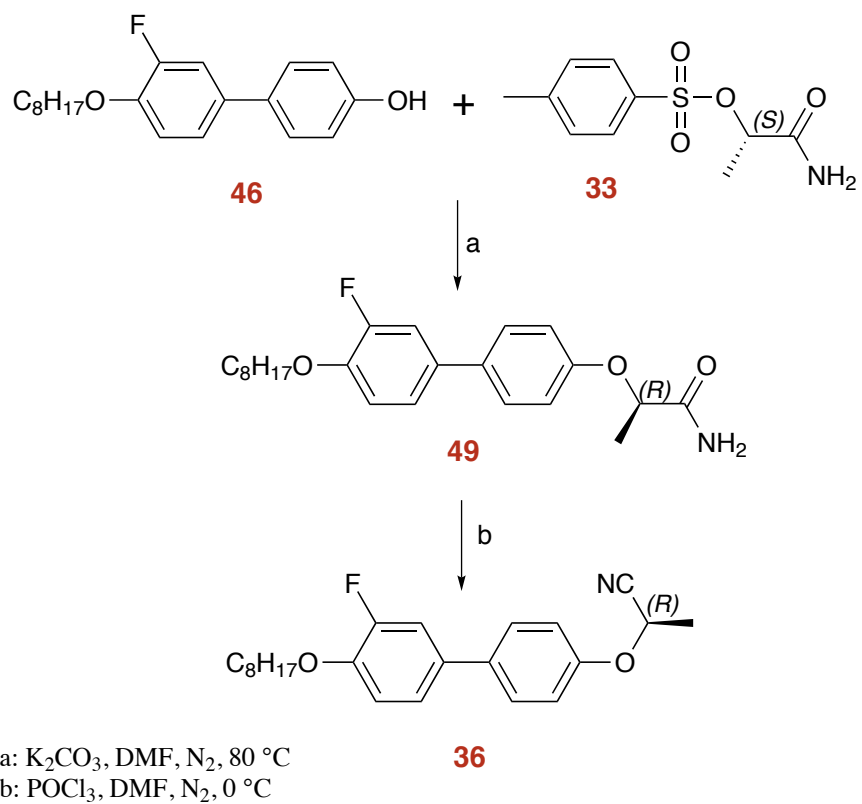
a) Butanone, K_2CO_3 , 80 °C

Scheme 3. Synthesis of 1-(benzyloxy)-4-bromobenzene **44**

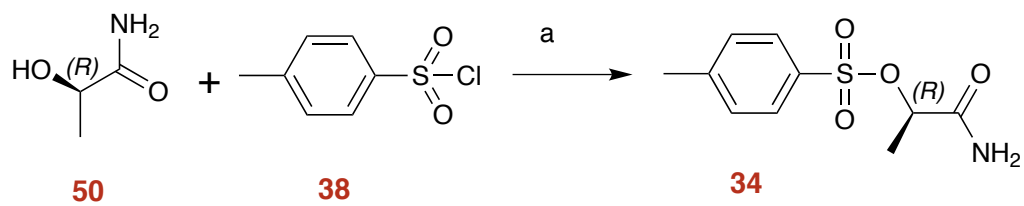


a: H₂O, DME, Na₂CO₃, Pd(PPh₃)₄
 b: H₂, Pd/C
 c: K₂CO₃, DMF, KI, N₂, 80 °C
 d: POCl₃, DMF, N₂, 0 °C

Scheme 4. Synthesis of (*R*)-2-((3'-fluoro-4'-(octyloxy)-[1,1'-biphenyl]-4-yl)oxy)propane-nitrile **48**

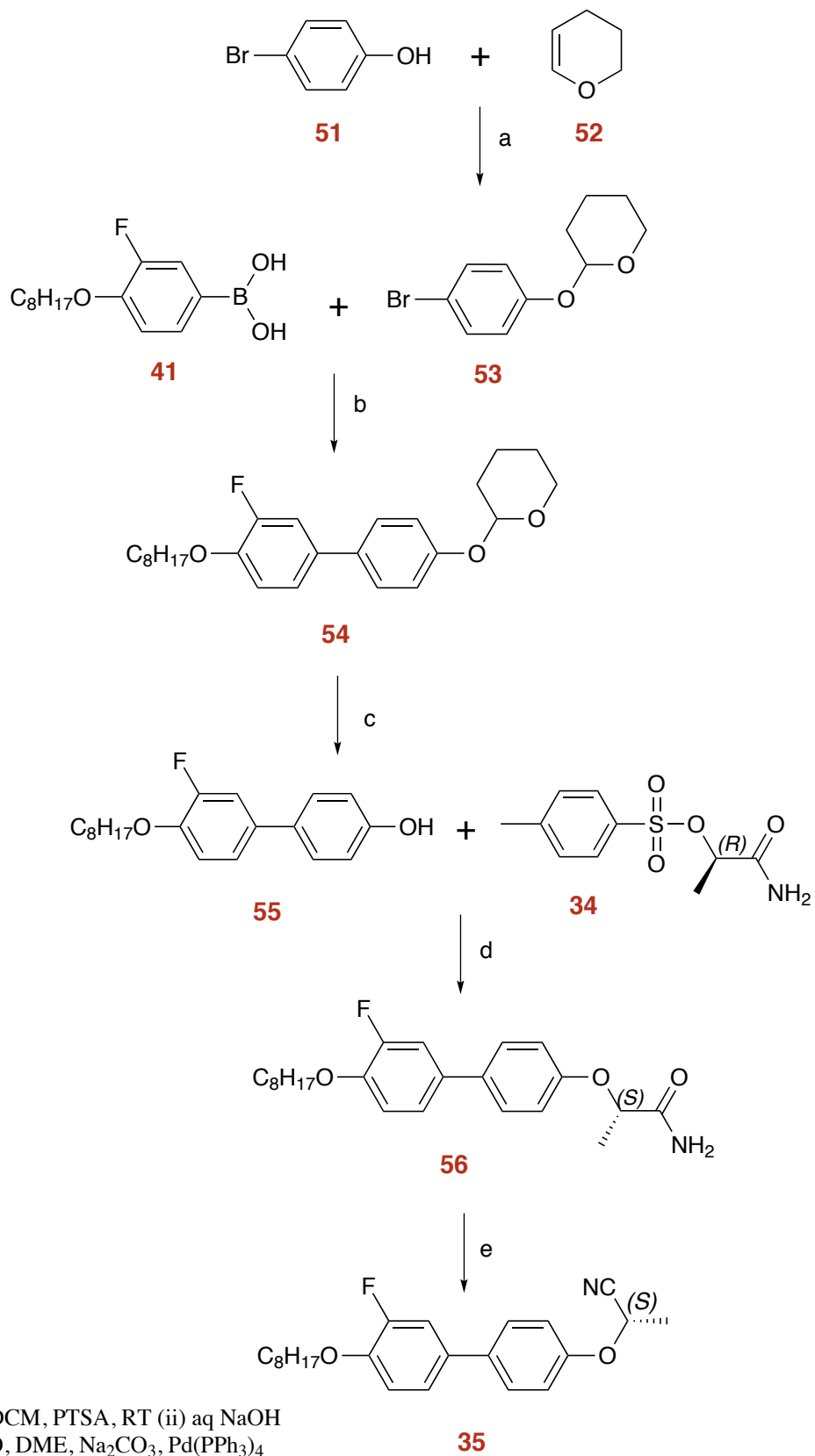


Scheme 5. Synthesis of (*R*)-2-((3'-fluoro-4'-(octyloxy)-[1,1'-biphenyl]-4-yl)oxy)-propanenitrile **36** without KI

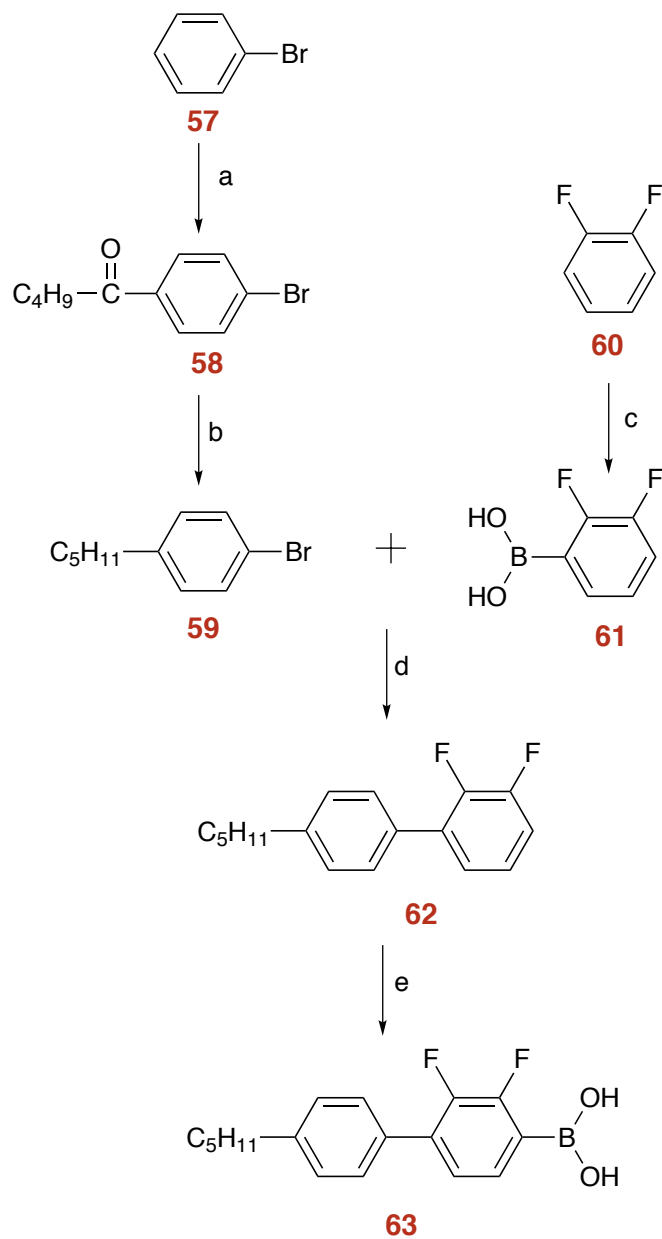


a: DCM, Diisopropylethylamine, DMAP, $0\text{ }^\circ\text{C}$

Scheme 6. Synthesis of (*R*)-lactamide tosylate, **34**

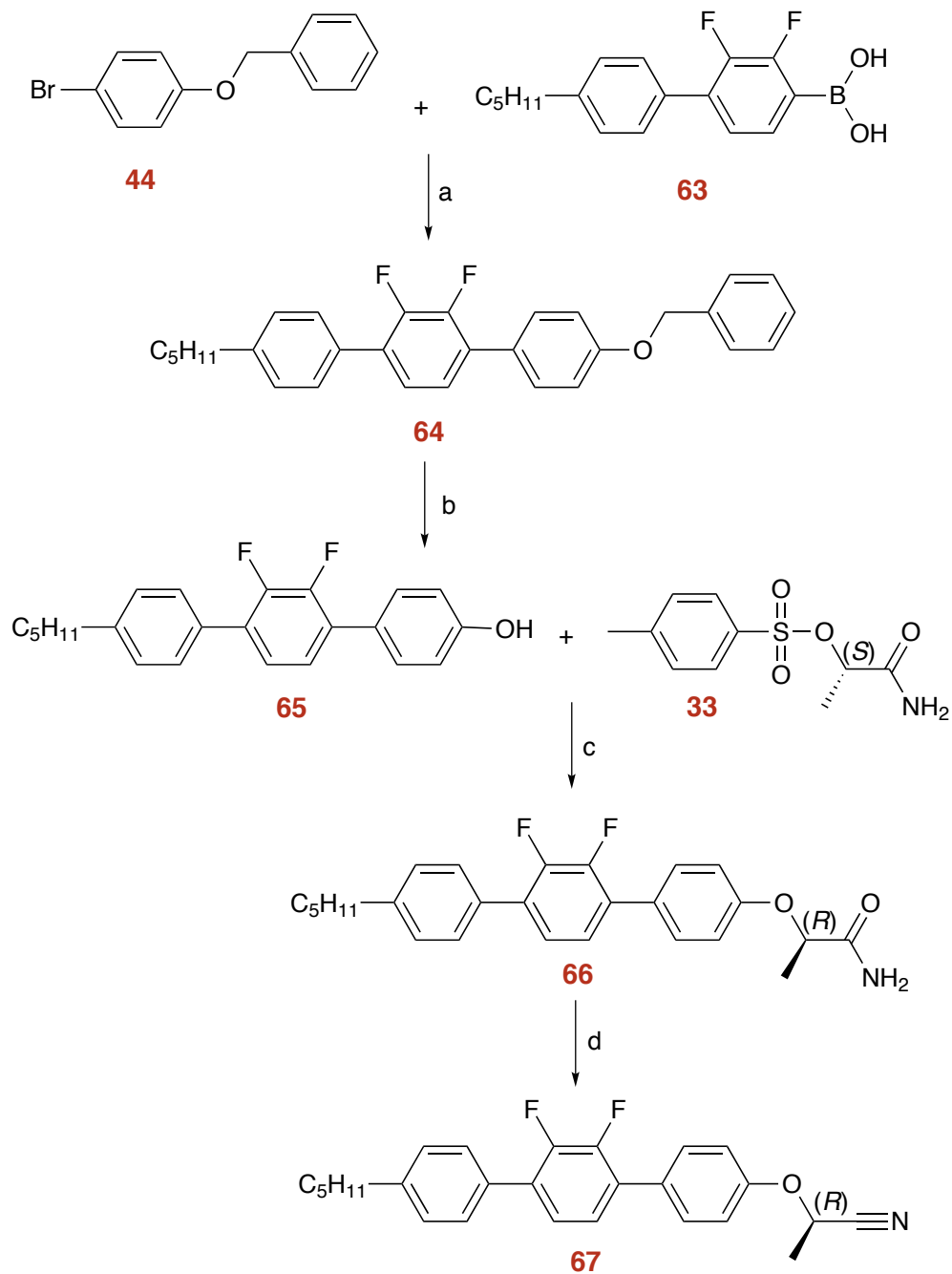


Scheme 7. Synthesis of (S)-2-((3'-fluoro-4'-(octyloxy)-[1,1'-biphenyl]-4-yl)oxy)-propane-nitrile **35**



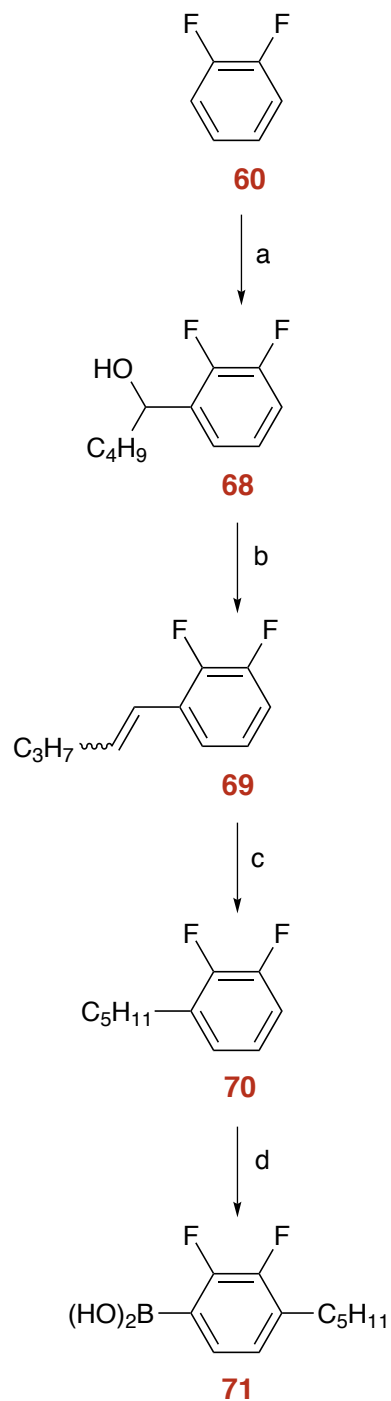
- a: (i) Valeryl chloride, AlCl_3 in DCM (ii) 36% HCl
 b: (i) $\text{NH}_2\text{NH}_2 \cdot \text{H}_2\text{O}$, DEG (ii) KOH (iii) 36% HCl
 c: (i) $n\text{-BuLi}$ (ii) THF, -78°C (iii) $\text{B}(\text{OMe})_3$ (iv) 10% HCl
 d: H_2O , DME, Na_2CO_3 , $\text{Pd}(\text{PPh}_3)_4$
 e: (i) $n\text{-BuLi}$ (ii) THF, -78°C (iii) $\text{B}(\text{OMe})_3$ (iv) 10% HCl

Scheme 8. Synthesis of (2,3-difluoro-4'-pentyl-[1,1'-biphenyl]-4-yl)boronic acid **63**



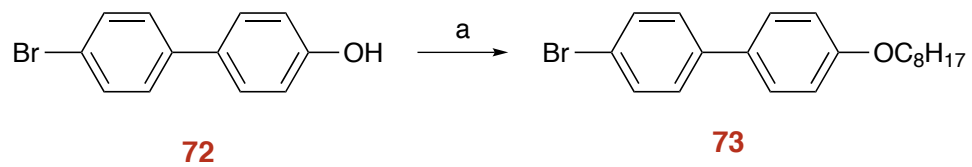
a: H₂O, DME, Na₂CO₃, Pd(PPh₃)₄
 b: DCM, BBr₃, 0 °C
 c: POCl₃, DMF, 80 °C
 d: POCl₃, DMF, 0 °C to RT

Scheme 9. Synthesis of (*R*)-2-((2',3'-difluoro-4''-pentyl-[1,1':4',1''-terphenyl]-4-yl)oxy)propanenitrile **67**



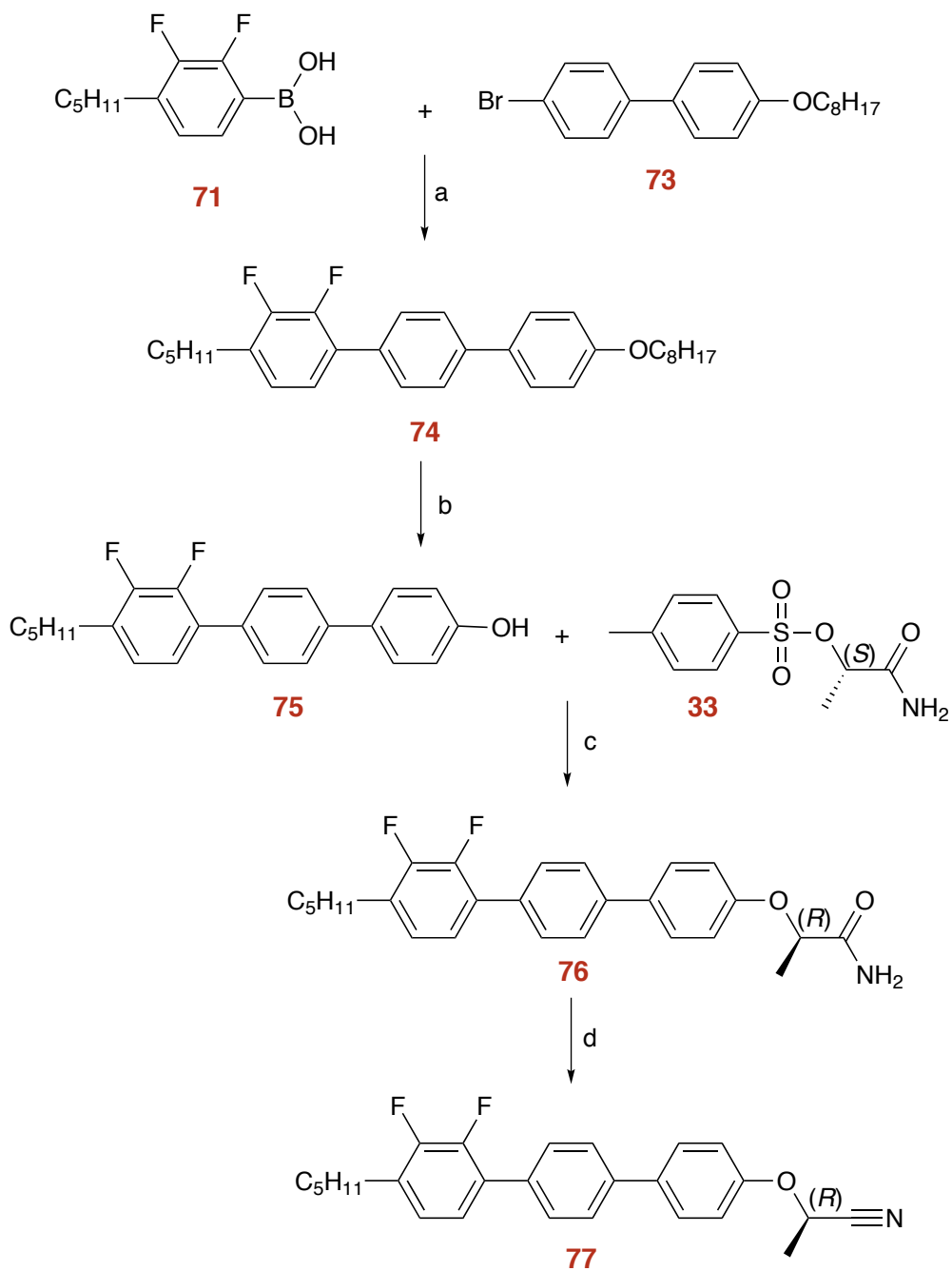
a: (i) *n*-BuLi, THF; (ii) C₄H₉CHO, THF; (iii) NH₄Cl (aq).
 b: *Para*-toluenesulfonic acid (PTSA), toluene.
 c: H₂, 10% Pd/C, toluene.
 d: (i) *n*-BuLi, THF; (ii) B(OMe)₃, THF; (iii) 10% HCl.

Scheme 10. Synthesis of (2,3-difluoro-4-pentylphenyl)boronic acid **71**



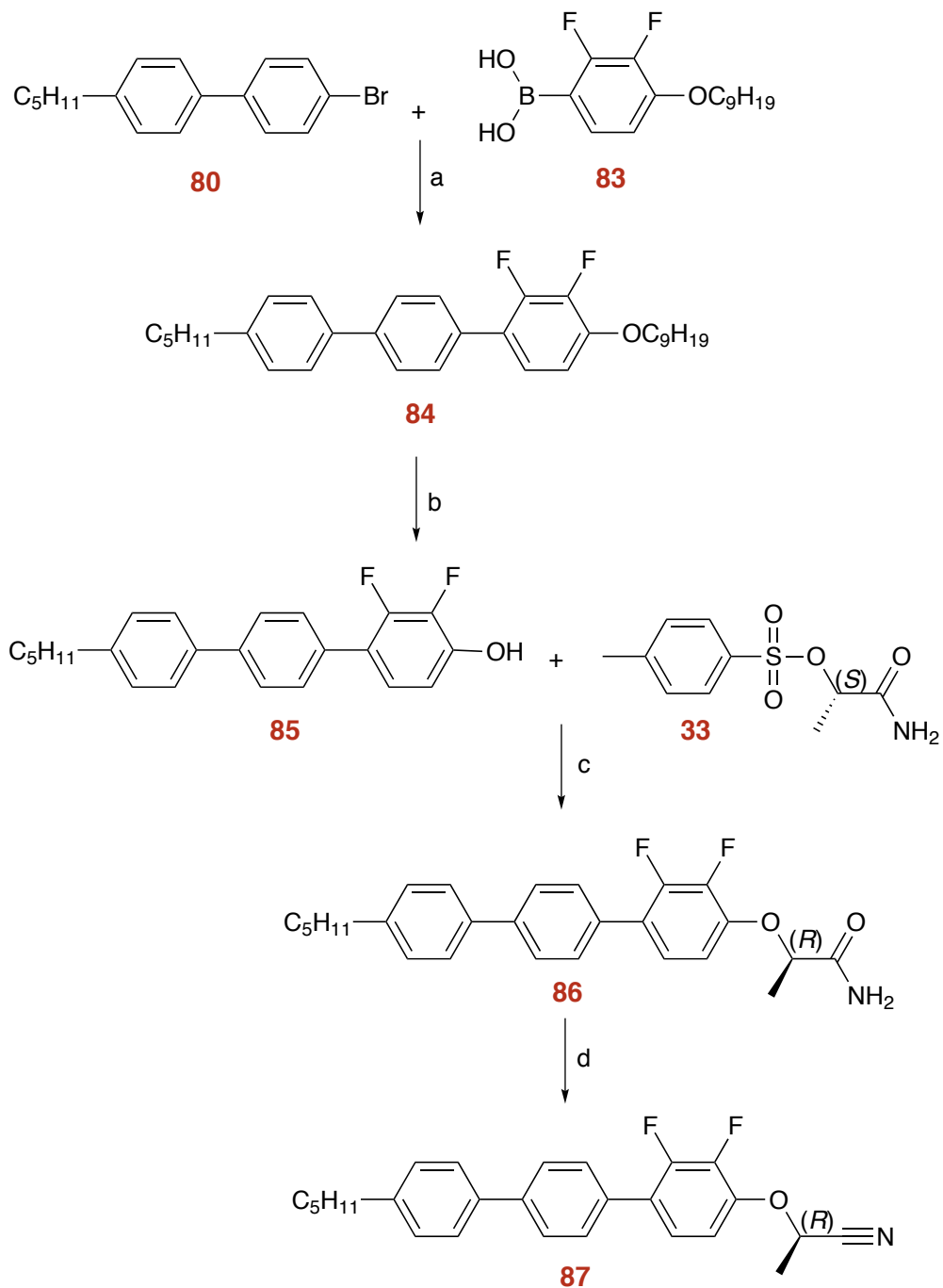
a: Bromooctane, butanone and K₂CO₃

Scheme 11. Synthesis of 4-bromo-4'-(octyloxy)-1,1'-biphenyl **73**



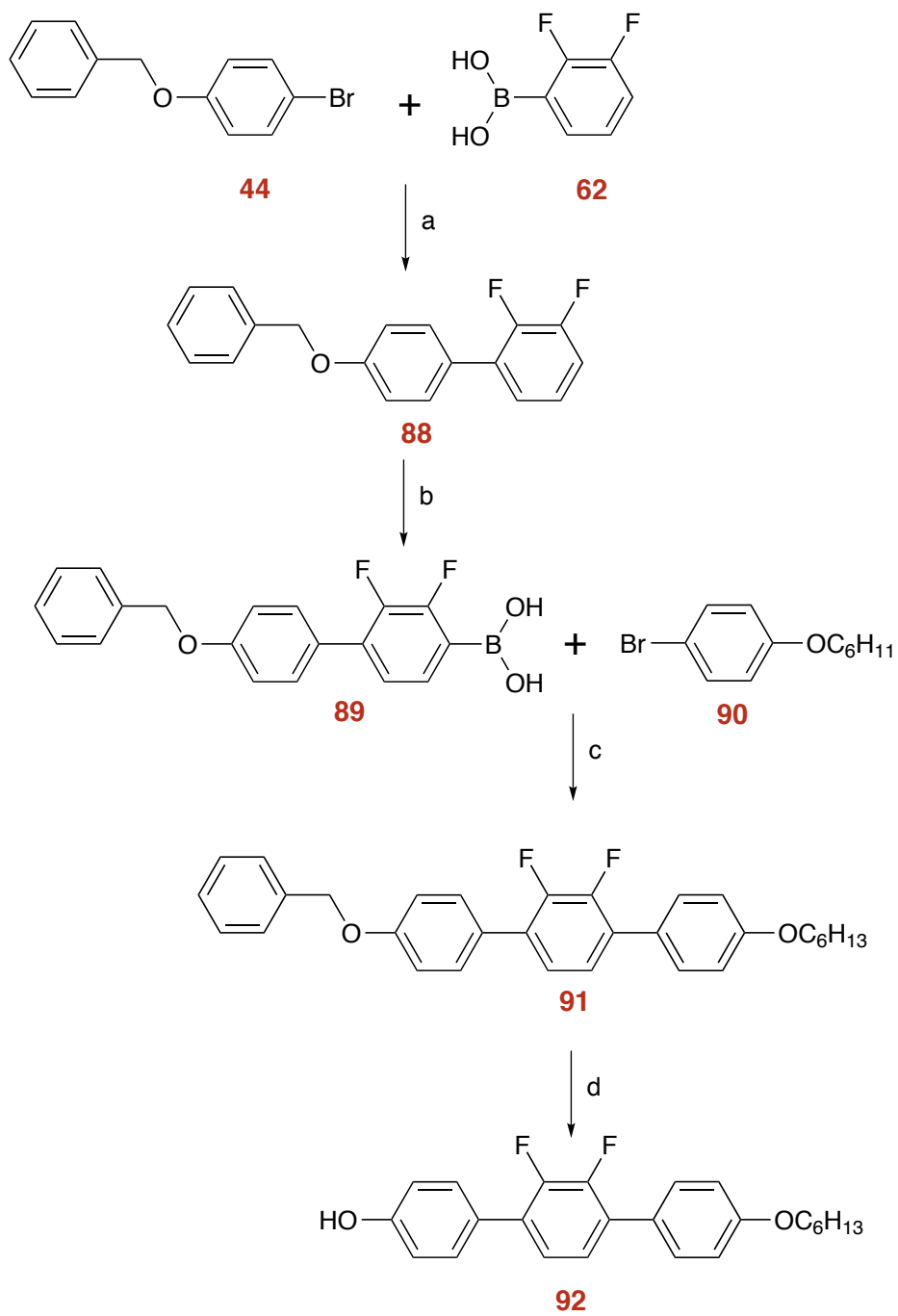
a: H_2O , DME, Na_2CO_3 , $\text{Pd}(\text{PPh}_3)_4$
 b: DCM, Br_2 , $0\text{ }^\circ\text{C}$
 c: POCl_3 , DMF, $80\text{ }^\circ\text{C}$
 d: POCl_3 , DMF, $0\text{ }^\circ\text{C}$ to RT

Scheme 12. Synthesis of (*R*)-2-((2',3'-difluoro-4'-pentyl-[1,1':4',1''-terphenyl]-4-yl)oxy)propanenitrile **77**



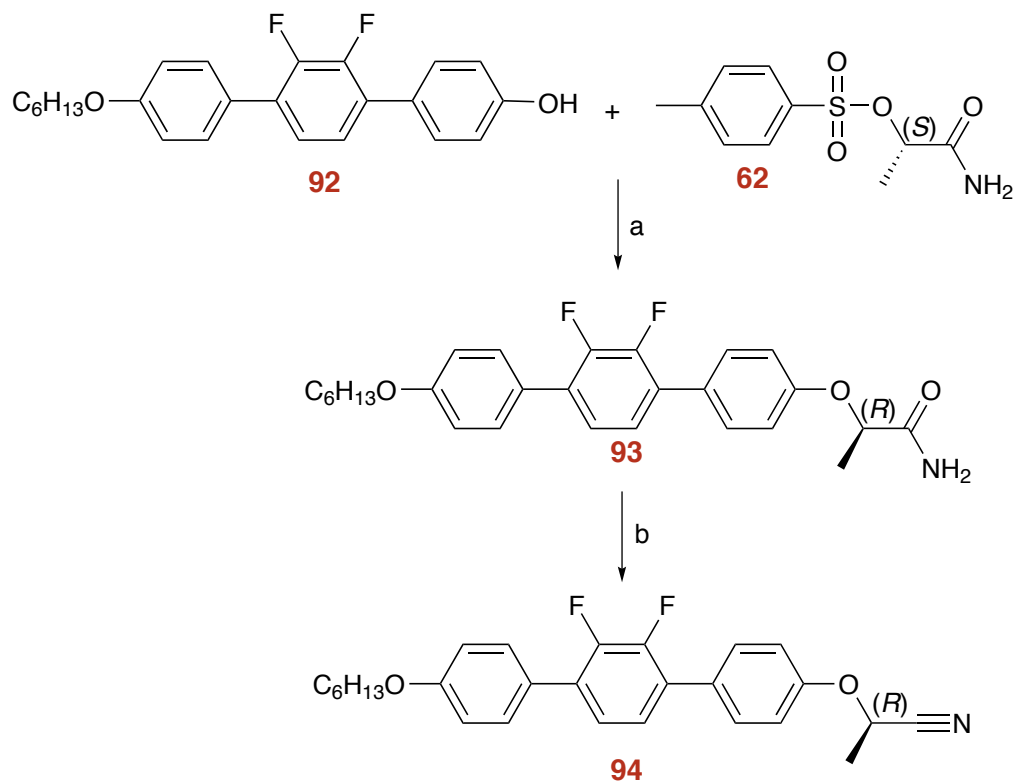
a: H₂O, DME, Na₂CO₃, Pd(PPh₃)₄
 b: DCM, BBr₃, 0 °C
 c: POCl₃, DMF, 80 °C
 d: POCl₃, DMF, 0 °C to RT

Scheme 15. Synthesis of (R)-2-((2,3-difluoro-4''-pentyl-[1,1':4',1''-terphenyl]-4-yl)oxy)propanenitrile **87**

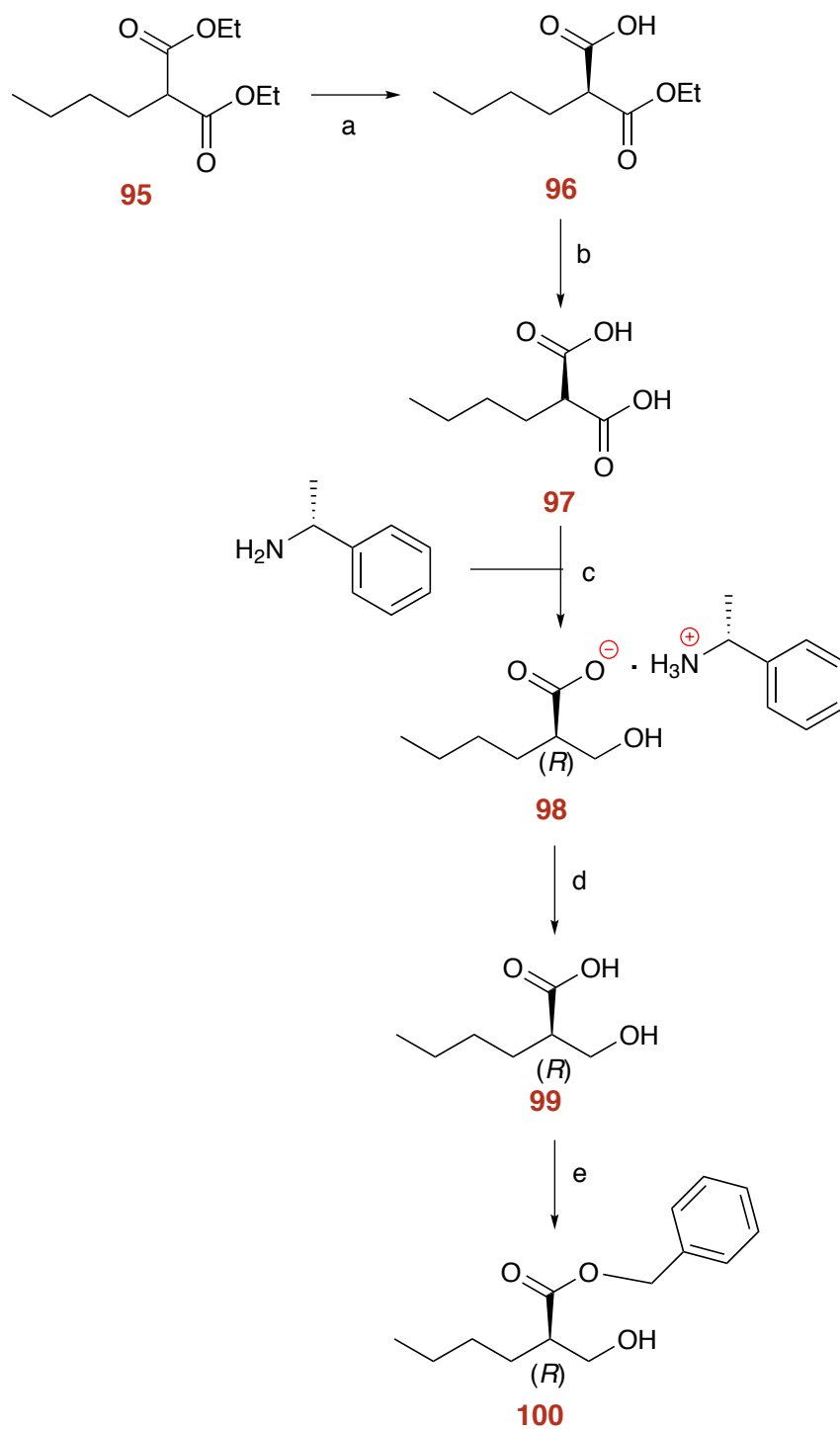


a: H₂O, DME, Na₂CO₃, Pd(PPh₃)₄
 b: (i) *n*-BULi, THF, -78 °C; (ii) B(OMe)₃, THF; (iii) 10% HCl
 c: H₂O, DME, Na₂CO₃, Pd(PPh₃)₄.
 d: H₂, Pd/C

Scheme 16. Synthesis of 2',3'-difluoro-4''-(hexyloxy)-[1,1':4',1''-terphenyl]-4-ol **92**

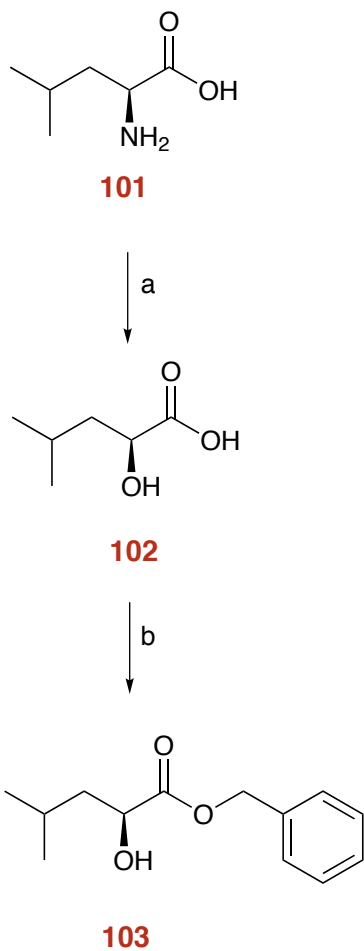


Scheme 17. Synthesis of (*R*)-2-((2',3'-difluoro-4''-(hexyloxy)-[1,1':4',1''-terphenyl]-4-yl)-oxy)propanenitrile **94**



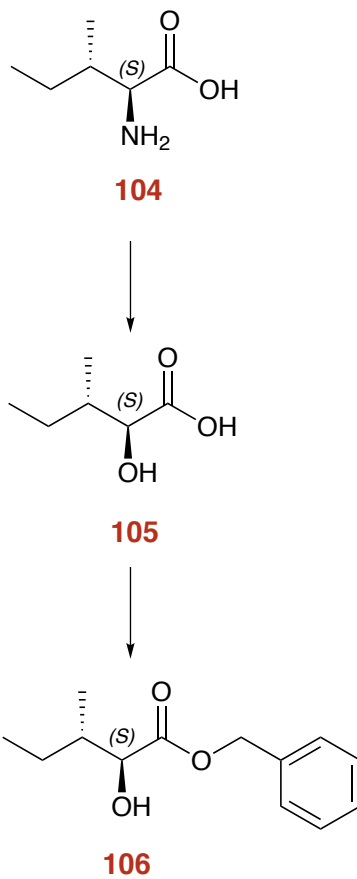
- a. KOH, water, EtOH
 b. (i) 2-propanol (ii) LiBH₄ in THF (iii) 2N HCl
 c. 2-propanol and EtOAc
 d. 2N HCl and EtOAc
 e. (i) MeOH and H₂O (ii) Cs₂CO₃ in H₂O (iii) DMF (iv) Benzyl bromide (v) brine

Scheme 18. Synthesis of (*R*)-benzyl 2-(hydroxymethyl)hexanoate **100**⁹⁰



a: (i) 2.5 N H₂SO₄, (ii) NaNO₂ in H₂O
b: (i) 20% CsCO₃, (ii) BnBr, DMF

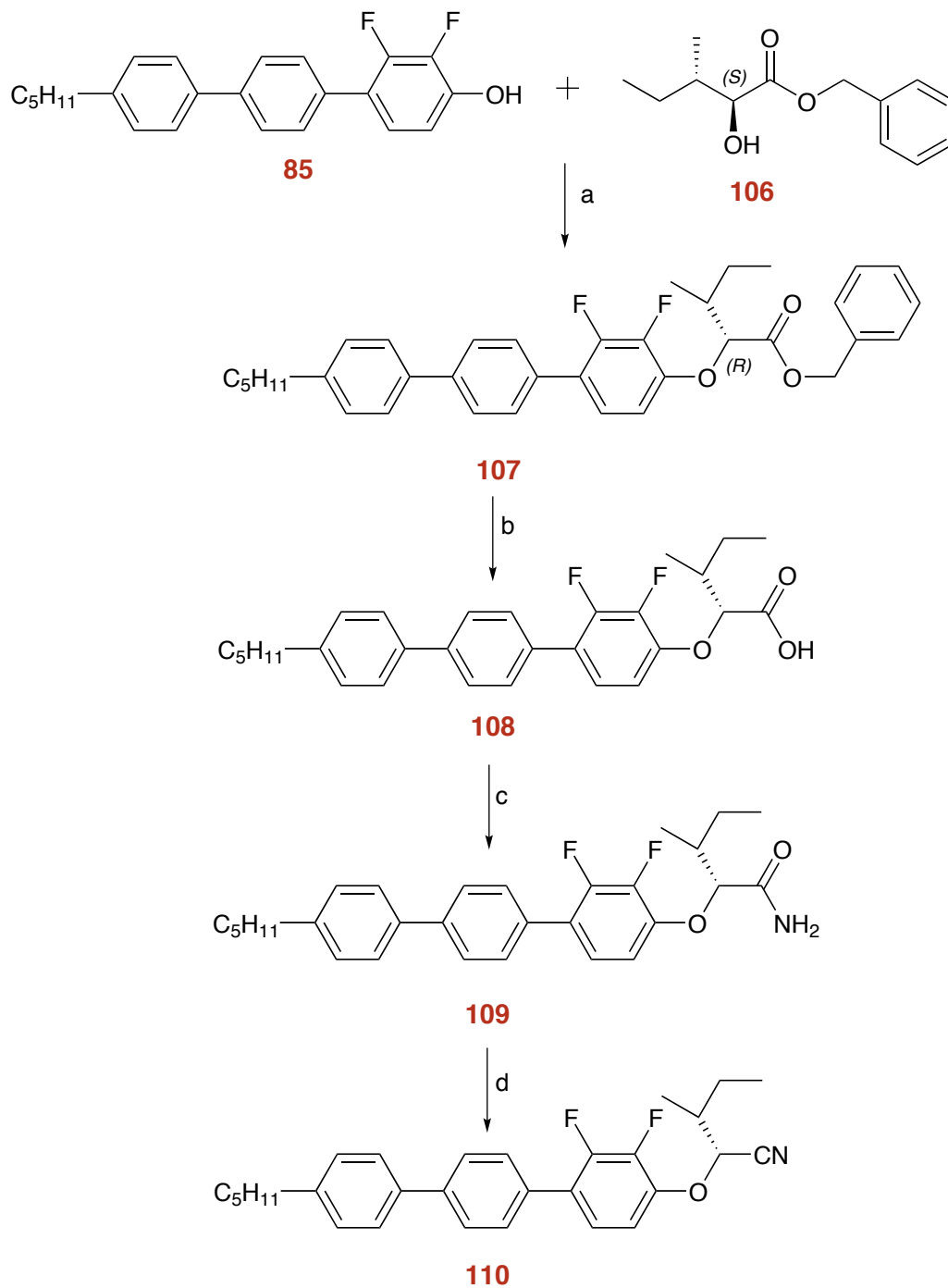
Scheme 19. Synthesis of (S)-benzyl 2-hydroxy-4-methylpentanoate **103**



a: (i) 2.5 N H₂SO₄, (ii) NaNO₂ in H₂O
b: (i) 20% CsCO₃, (ii) BnBr, DMF

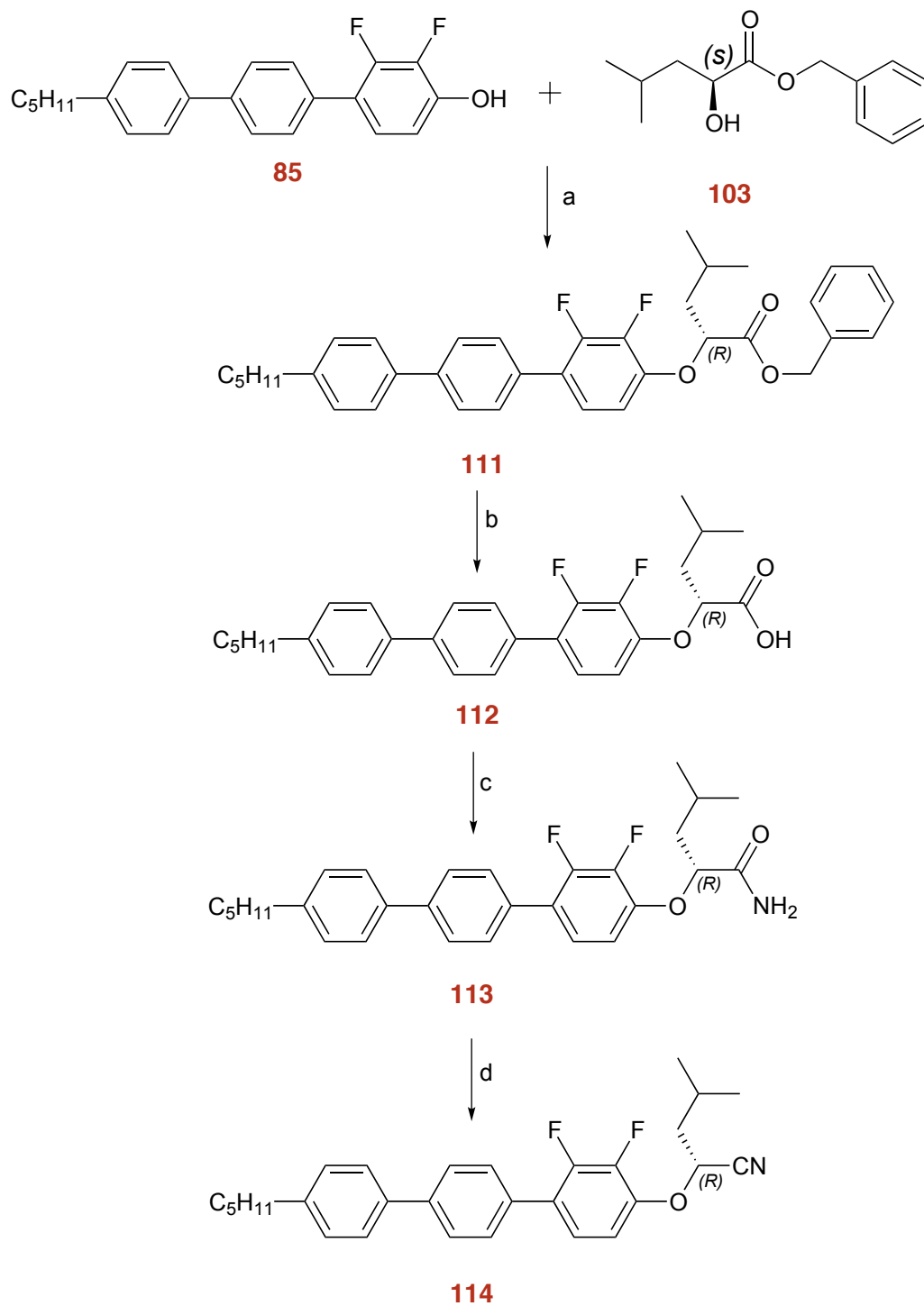
Scheme 20. Synthesis of (2S,3S)-benzyl 2-hydroxy-3-methylpentanoate **106**

10



a: (i) PPh_3 , THF (ii) DEAD
 b: H_2 , Pd/C, Ethyl acetate
 c: (i) Oxalyl chloride, DCM (ii) Aq NH_3
 d: POCl_3 , DMF, 0°C to RT

Scheme 21. Synthesis of (2*R*,3*S*)-2-((2,3-difluoro-4'-pentyl-[1,1':4',1''-terphenyl]-4-yl)-oxy)-3-methylpentanenitrile **110**



a: (i) PPh₃, THF (ii) DEAD
 b: H₂, Pd/C
 c: (i) Oxalyl chloride, DCM (ii) Aq NH₃
 d: POCl₃, DMF, 0 °C to RT

Scheme 22. Synthesis of (*R*)-2-((2,3-difluoro-4''-pentyl-[1,1':4',1''-terphenyl]-4-yl)-oxy)4-methylpentanenitrile **114**

2.4 Mechanistic Discussion of the Synthetic Routes

The target compound **48** was synthesised following the route in Scheme 4 and showed an optical rotation of -0.2° which is much lower than expected. In addition when it was formulated as a 7 % w/w mixture with KCHM211, it was not possible to measure the tilt angle due to poor alignment and this suggested that there was little chirality *i.e.* a degree of racemisation had occurred. This was traced to the addition of KI, which racemised the compound; the mechanism is discussed as shown in Figure 36

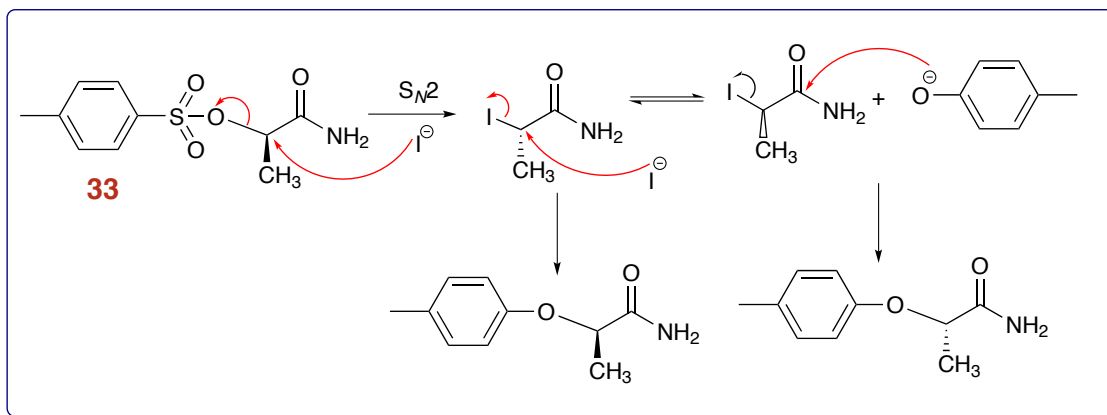


Figure 36. Proposed mechanism for the racemisation.

By carrying out Scheme 4 without addition of KI during the tosylation step; the target compound shows reasonably high optical rotation *i.e.* $+32.04^\circ$ for (*R*)-2-((3'-fluoro-4'-(octyloxy)-[1,1'-biphenyl]-4-yl)oxy)propanenitrile **36** and -41.1° for (*S*)-2-((3'-fluoro-4'-(octyloxy)-[1,1'-biphenyl]-4-yl)oxy) **35** propanenitrile and also shows moderate tilt angles of the SmC* phase when doped in KCHM211.

The original approach of Scheme 3 was devised around the tetrahydropyran (THP) acetal protecting group and necessitated the synthesis of the THP protected 4-bromophenol **44**. The THP is easy and cheap to attach, is stable to strong base such as *n*-BuLi but can easily be cleaved under mild acidic conditions. The proposed mechanism for the transformation of 4-bromophenol to the tetrahydropyranyl intermediate **44** is illustrated in Figure 37. The THP group proved too easy to cleave and made the work up problematic. The first solution

to this problem was to replace THP with benzyl as the protecting group and this will be discussed later.

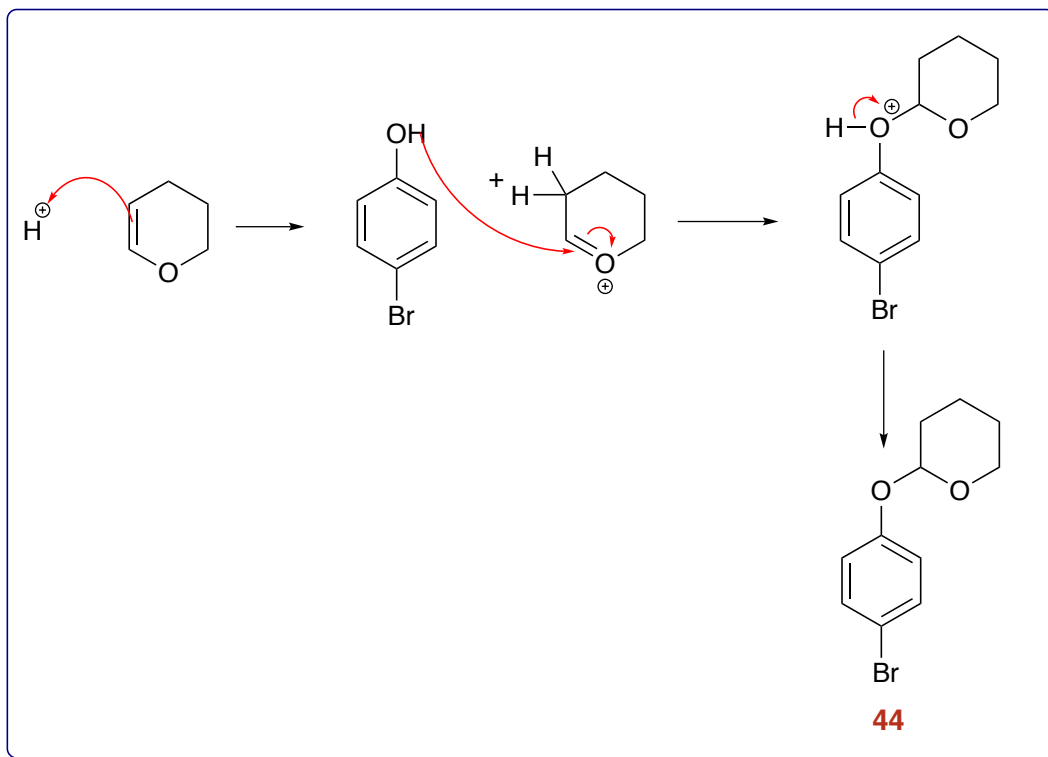


Figure 37. Proposed mechanism for the transformation of a 4-bromophenol to 2-(4-bromophenoxy)tetrahydro-2H-pyran.

The intermediate compound **45** is synthesised by Suzuki coupling of the THP protected phenol **44** and the difluorophenylboronic acid **41**. This reaction has been key to the synthesis of all the fluorinated terphenyls developed over many years and is used by industry. The general Suzuki coupling reaction mechanism illustrated in Figure 38.

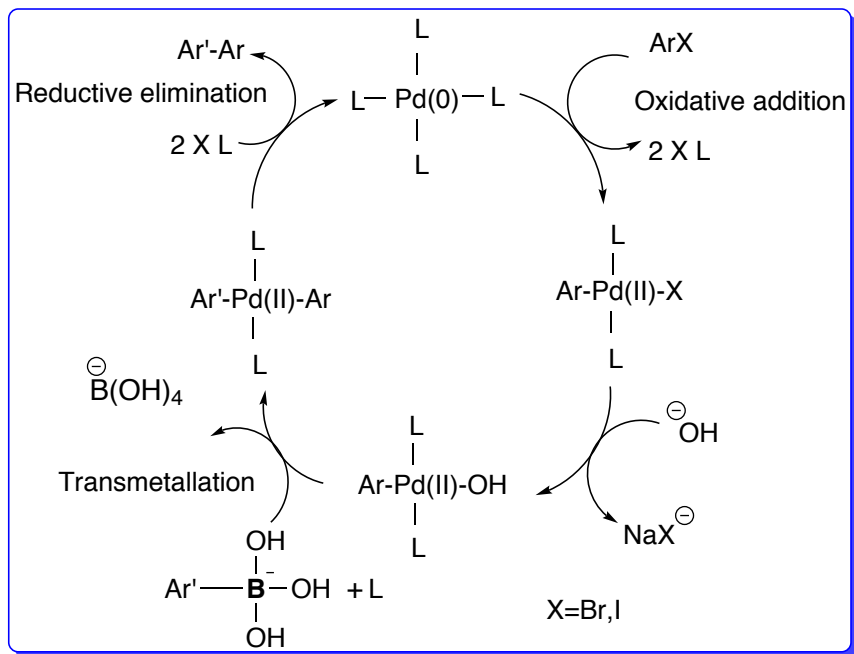


Figure 38. Catalytic cycle for Suzuki coupling reaction.

The intermediate step in the synthesis of compound **45** is a Suzuki coupling reaction. Palladium-catalysed coupling between an aryl bromide and an aryl boronic acid formed a C-C bond and generated the desired biphenyl structure of **45**. A catalytic cycle of this Suzuki coupling reaction is drawn in Figure 38. The cycle was initiated by the oxidative addition of the aryl bromide to the stabilized Pd (0) species. A base RO^- was introduced in the coordination sphere of Pd. The transmutation step transferred the Ar' group from the metal boron to the metal palladium to generate an intermediate containing Ar , Ar' , $B(OH)_2$, and RO in the coordination sphere of palladium. Two reductive eliminations from this intermediate produced the coupling $Ar-Ar'$ product.**45**.^{91,92}

The compound **49** is synthesised by tosylation of **46** with **33**. The proposed mechanism for the transformation of **46** to **49** is shown in Figure 39

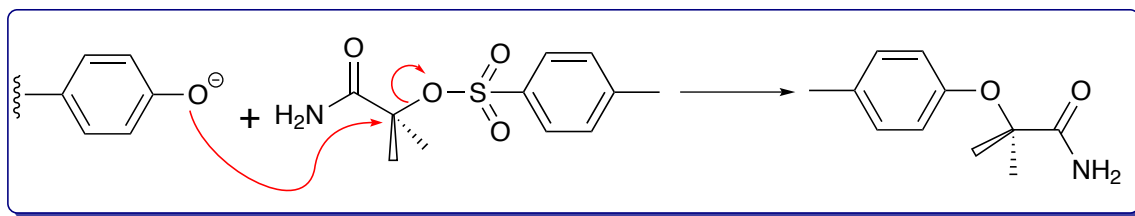


Figure 39. The S_N2 mechanism for tosylation of phenol to form lactamide ethers.

The intermediate compound **33** was synthesised from lactamide and 4-methylbenzene-1-sulfonyl chloride. The proposed mechanism for the transformation of lactamide to the (*S*)-1-amino-1-oxopropan-2-yl 4-methylbenzenesulfonate **33** is illustrated in Figure 39 and is presumed to proceed extitvia an S_N2 mechanism. The targeted cyanoether **36** was synthesised using a Vilsmeier reagent generated from DMF and $POCl_3$. The proposed mechanism is shown in the Figure 40.

2.5 Second Generation Dopants

The synthesis of second generation liquid crystal dopants **110** and **114**, and the intermediate compounds **107** and **111** are synthesised using the Mitsunobu reaction.⁹³ The mechanism is shown in the Figure 42. The chiral units compounds **103** (Scheme 19) and **106** (Scheme 20) were prepared by MSc student Anthony Umendiego following conventional diasotization and benzylation of amino acid starting materials. The diazotisation step, it should be noted involves a double inversion of configuration *i.e* retention of configuration. Attaching the chiral unit to the phenolic mesogens was carried out as part of this project and that part will be discussed here.

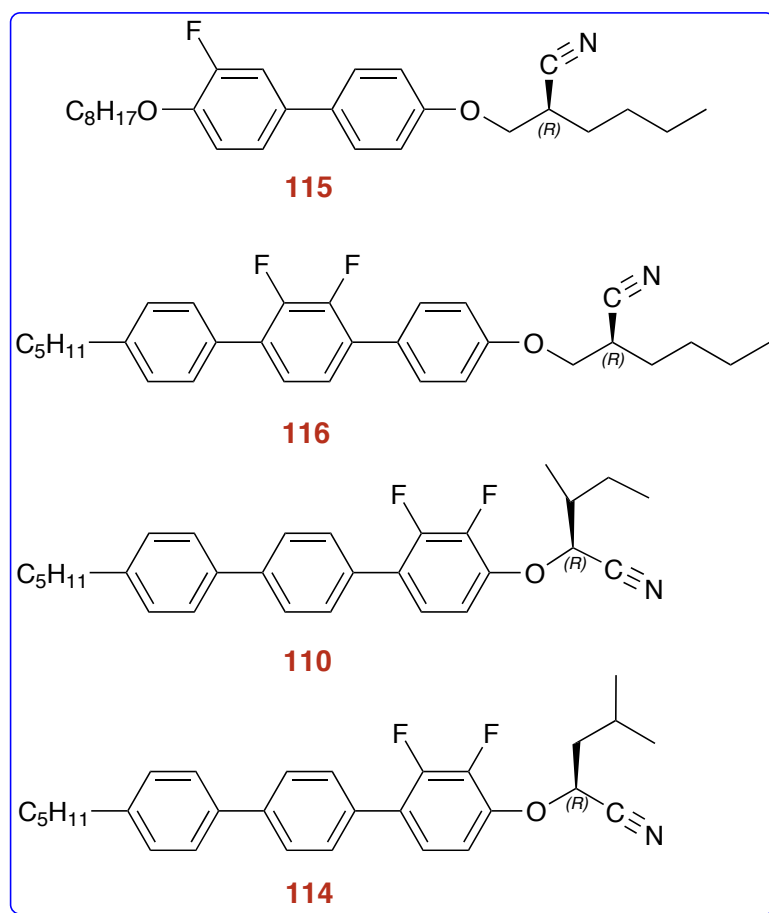


Figure 41. The structures of second generation dopants.

Mitsunobu reaction is used to convert a primary or secondary alcohol into a variety of compounds using triphenylphosphine and diethoxycarbonyldiazene

solution (DEAD). The final product depends on the acidic reagent *i.e* the conjugate acid of the nucleophile. The mechanism initiates with attack of triphenylphosphine on DEAD and forms a zwitterionic intermediate. The intermediate formed deprotonates the acidic compound to reveal the anionic nucleophile. The starting material alcohol binds to the phosphonium ion and the nucleophile performs a S_N2 attack to yield the final substitution product with inversion of stereochemistry. The formation of a strong P=O bond in the by-product drives this reaction forward.^{94,95}

The final synthetic targets were based on dopants in which the chiral cyano ether is one methylene group carb further away from the aromatic core. It appeared at the time, that the low P_s observed in several compounds may have been due to the C-O dipole in the ether link opposing the dipole of the nitrile. This in turn producing a very low net transverse dipole and ultimately a low P_s . Moving the nitrile one bond farther away may negate this factor and should lead to a longer N^* pitch. It might also provide a means of employing the pitch compensation approach for obtain long pitch FLC materials as pitch direction usually alternates for the same configuration as the chiral centre down the terminal chain from the core.

There seemed to be several good reason to target chiral unit **100** (Scheme 18). This particular example was chosen as the synthesis was published⁹⁰ and was described in details and the process was presumably reliable. Scheme 18 begins with hydrolysis of a malonate ester with 1 equivalent of KOH to produce a half ester **96**. This enabled a selective reduction to be carried out on the more reactive ethyl ester using LiBH₄ to give a hydroxy acid. The racemic hydroxyl acid was resolved by crystallisation of the diastereomeric salt using (*R*) - benzylethylamine. Once the chiral acid was freed from its salt, it was converted to the benzyl ester using benzyl bromide and caesium carbonate in water. All these steps worked well just as described in the literature. The final step was to link this unit to the phenol extitvia the hydroxy moiety and this did not seem to be a major hurdle. Many attempts were made to link this to either the middle ring difluoro terphenyl **65** or the biphenyl **55**. Many variations of the Mitsunobu to synthesis the targeted dopants **115** and **116** respectively reaction were tried but none produced any of the desired ether. One explanation for the failures of these reactions is that the benzyl ester insufficiently labile and reacts with the hydroxy unit and removing it from the desired reaction. A second explanation- s is that although the benzyl ester is one carbon further away for the hydroxy which was successfully employed extitvia the amino acid based dopants in Mitsunobu chemistry, adopts a conformation that produces high steric hindrance. Unfortunately, lack of time and shortage of material meant that we could not continue solving this synthetic bottleneck and this step awaits another researcher to solve.

3 Evaluation of Liquid Crystals

The properties of liquid crystal materials are analysed mainly by using polarised optical microscopy (POM), differential scanning calorimetry (DSC) and X-ray scattering. POM is used to study the transition temperatures and phase identification from texture analysis. Phase identification is best made while cooling from isotropic phase to crystallisation phase, but heating values should also be obtained as these are thermodynamic values. The ferroelectric liquid crystal mixtures are prepared by combining dopants with host materials and heating it to the isotropic liquid; by repeated heating and cooling, combined with mixing, one can get a homogeneous mixture. The homogeneity of the mixture can be verified by using POM. Subtle phase changes which lead to small changes in enthalpies in the liquid crystal materials can be studied by DSC to confirm the transitions from POM and to provide enthalpy data. More detailed phase analysis is available by using small angle X-ray scattering (SAXD)

3.1 Polarized Optical Microscopy

POM is used to study the liquid crystal phase transitions and optical textures for different mesophases. The operational principle of POM is the magnified view of a thin layer of a mesogenic compound sandwiched with glass slide and a glass cover slip. The microscopic slide of compound is usually placed on a hot stage, which is connected with temperature controller and two polarisers that are crossed at 90°. Mesophase identification is possible because anisotropy leads to birefringence and thus, light is not extinguished. This gives information about the arrangement of the molecules within the particular phase.

In an isotropic phase the polarised light will propagate through the material with the same velocity irrespective of the direction. The liquid crystal materials are anisotropic in nature in turn they exhibit birefringence property. When the material has biaxial phases they have different indices of refraction. Uniaxial liquid crystal materials exhibit birefringence property where Δn .

$$\Delta n = n_e - n_o$$

Where n_e extraordinary index and n_o ordinary index.

3.2 Differential Scanning Calorimetry

The application of DSC is to study the characterisation of liquid crystal mesophase transitions. Most materials only show a transitions from solid to isotropic state, but anisotropic liquid crystals may show several additional smaller changes in enthalpy during transition changes and this can be measured by DSC.

The principle of DSC is, when a material experience physical change like phase transition, which needs more or less heat to flow through the sample. The flow of heat is maintained equally for both a sample and a reference pan. The difference in heat which passes through the sample depends whether the process is exothermic or endothermic. The sample temperature is increased linearly with time. The reference material should have defined heat capacity over the temperature range. The heat flow in the material is a function of temperature and time. The whole process is carried out in the controlled atmosphere.

The experiment will give qualitative and quantitative information on the physical changes of the material during exothermic or endothermic process. The change in enthalpy gives a typical curve of the heat flow as a function of temperature over time. Depending on the method used, the DSC gives a positive or negative peak. Based on a DSC curve, the transition enthalpies can be calculated by integrating the desired peak. DSC cannot be used to identify what phase we are in, so it must be used in conjunction with POM and X-ray scattering data to put together an accurate phase diagram.

3.3 Electro-Optical Studies

The electro optical properties of single liquid crystal compounds and mixtures are studied by placing the sample in between two indium tin oxide coated glass plate (cell) using hot stage. Cells can be commercially purchased from companies such as Instec and several others. The alignment of the material in a cell is very important to measure the electro optical properties even in actual display

applications. Polyimide alignment layers or nylon on top of a conducting layer in the cell help to align the molecules, especially rod like liquid crystals. The alignment direction is managed by creating grooves by rubbing in anti-parallel or parallel direction when studying ferroelectric liquid crystals. The cell gap is normally in the range of $2\ \mu\text{m}$ to $20\ \mu\text{m}$. After filling with the liquid crystal material the both sides of the cell must be connected to a function generator to supply various types of waveforms. Connection can be made directly to contacts in special cell holders or soldered with wires. The function generator is linked to an amplifier which enables applied voltages of up to 100 V to be obtained.

The tilt angle of ferroelectric liquid crystal materials is measured by using applied electric field in SmC^* phase. When an electric field is applied to the tilted molecules (a) molecules will rotate to one side of the cone; by switching the direction of the field the molecule rotate to the other side of the cone (b) as shown in the Figure 43. There will be minimum light transmission when the long axis of the molecules is parallel to one of the polarisers and this can be done by manipulating a rotating stage. Changing the direction of the field in this arrangement gives maximum light transmission because of the change of tilt. By rotating the stage to bring it to minimum transmission and noting down the angle of rotation. The difference between these two angles is twice the optical tilt angle 2θ .

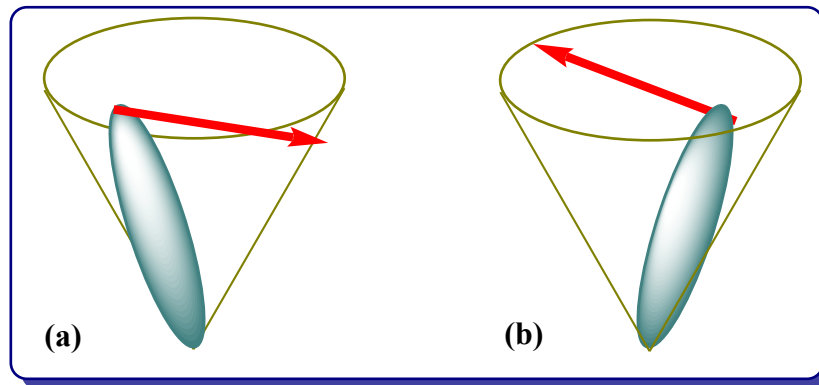


Figure 43. The molecular tilt by applying applied field in SmC^* phase.

The spontaneous polarisation is another important property of FLC materials which can be measured by electro optical experiments. In the determination of P_s an oscilloscope is used to read the current output from the cell versus time. The input blue signal and response of FLC (red signals) are measured using

Instec automatic liquid crystal testing (ALCT) system and WinLC software. The red output wave arises because reversing the polarity of the field liquid crystal molecules will rotate and results in brief flow of current which results in a single peak Figure 44. Integration of the area under this current peak gives the quantity of charge, which can then be used to obtain the spontaneous polarisation. Initially, all other sources of capacitance in the circuit are identified, such as from the wires and empty cell so that only the capacitance from the ferroelectric material is calculated.

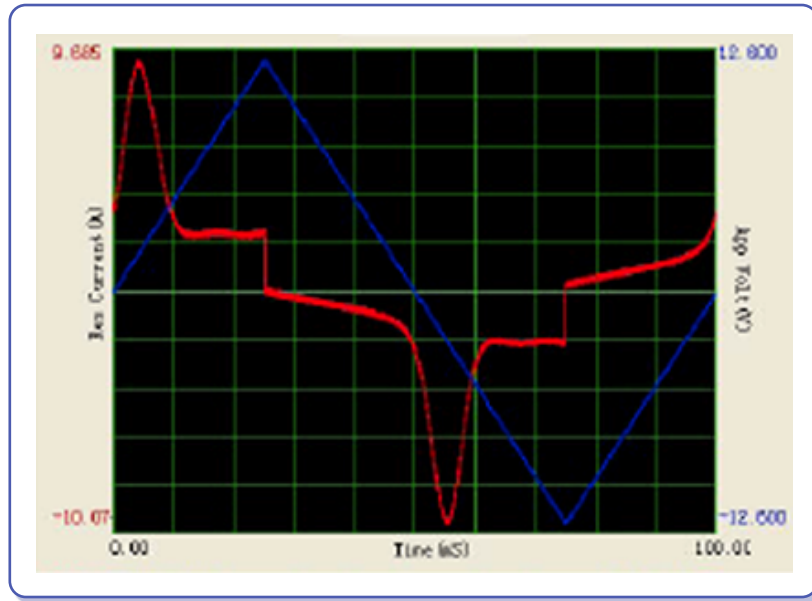


Figure 44. Current versus time for a ferroelectric liquid crystal, using the ALCT system and software.⁹⁶

The change in spontaneous polarisation requires a charge $2P$, where P is the spontaneous polarisation of the molecules per area of the device. So with the area of the electrodes given by a , the total charge $Q = 2Pa$. The total charge is also equal to the integral of the current over time, which is the area we see under the peak. The area under the peak equal to A can be calculated using the following equation.⁹⁶

$$P = A/2a$$

4 Results and Discussion

4.1 Characterisation Of Ferroelectric Liquid Crystal Dopants

4.1.1 NMR Shift Experiment

Knowledge of the optical purity of the chiral materials is essential in the measurement of electro-optical analysis. In virtue of this the optical purity of the targeted compound **36** was investigated by synthesising both *R* and *S* enantiomers and conducting a chiral NMR shift experiment using europium tris (3-heptafluoropropyl hydroxymethylene) - (+) -camphorate. This chiral shift reagent and ligand produces a rapid equilibrium of different diastereomeric complexes in which the europium coordinates to donor sites on the substrate. The process is fast on the NMR time scale and results in a shift to higher ppm. Since the two enantiomers produce diastereomeric complexes, different changes in chemical shift may be observed and integration of the separate signals can quantify the relative amounts of each isomer. The NMR shift reagent experiment showed no separation of the signals from the two enantiomers, so it was not possible to determine optical purity quantitatively (Figure 45).

R and *S* chiral dopants were synthesised using *R* and *S* chiral units as shown on the Scheme 1, Scheme 6. However, optical rotations for the (*R*)-isomer was -41.1° and for the (*S*)-isomer was $+39.04^\circ$; the fact that the magnitude is quite large and are nearly equal and opposite, is not proof but supports the conclusion that almost no loss of optical purity occurred.

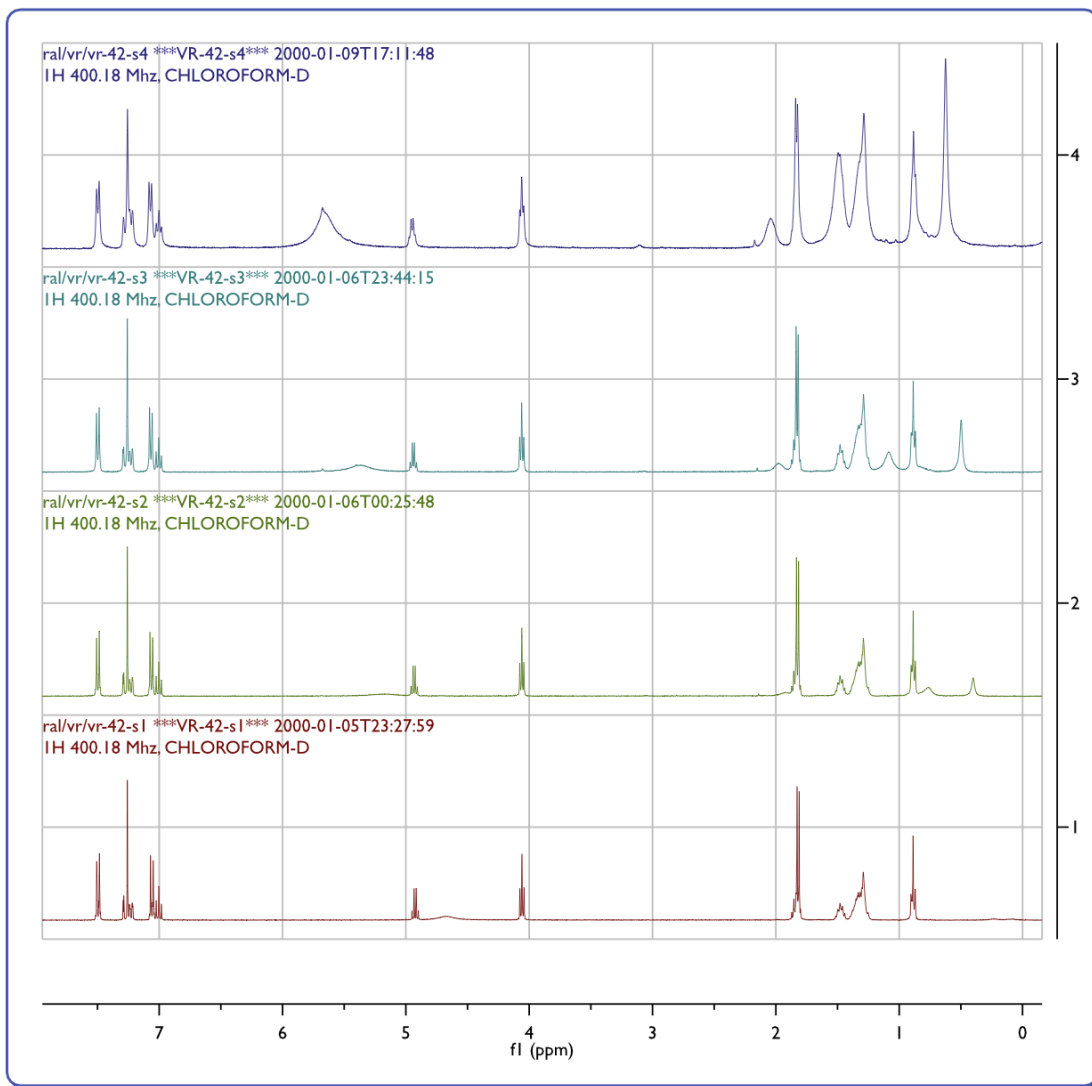


Figure 45. The NMR shift reagent experimental signals of compound **36**.

4.1.2 Optical Rotation

The optical rotation of the non-mesogenic dopants **36** and **35** prepared from (*S*)- and (*R*)-lactamide was found by measuring the angle of rotation in DCM solvent by using an automatic digital polarimeter. The optical rotation was calculated using the following equation.

$$[\alpha] = a/c.l$$

$[\alpha]$ = specific rotation;

a = Measured rotation;

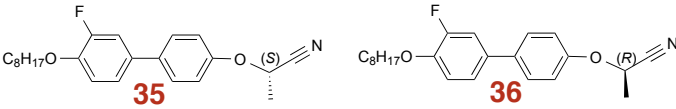
c = concentration (g/ml);

l = length of the cell (dm).

The (*R*) and (*S*) stereo centres dopants dextrorotatory (clockwise) and levorotatory (counter clockwise) behaviour can be observed. The specific rotation of both enantiomers are almost equal and opposite, as shown in Table 2. This shows the compound is optically pure or little racemisation occurred.

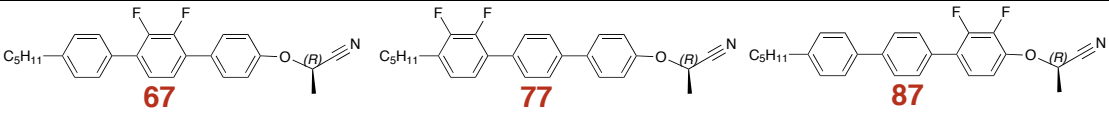
Table 2. The optical rotation of non-mesogenic dopants

Dopant	Weight / g	Solvent (D-CM) / ml	Cell Length /dm	Measured Rotation / °	Optical Rotation / °
35	0.017	2.0	0.417	- 0.15	- 41.1
36	0.016	2.0	0.417	+ 0.13	+ 39.04



The optical rotation of mesogenic dopants **67**, **77** and **87** were determined as shown in Table 3. The optical rotation of dopant **67** is higher than the other two dopants **67** and **77**, this is may be due to the presence fluorines on the core unit are near to the chiral unit. However, the optical rotations of the terphenyl mesogenic dopants are higher than those of biphenylnon-mesogenic dopants.

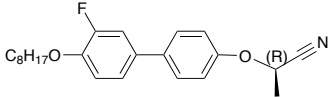
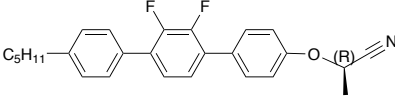
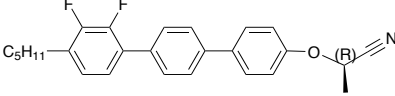
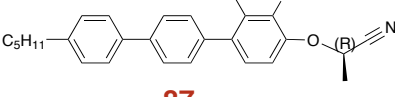
Table 3. The optical rotation of mesogenic dopants

					
Dopant	Weight / mg	Solvent (D-CM) / ml	Cell Length / dm	Measured Rotation / °	Optical Rotation / °
67	23.5	2.0	0.417	+ 0.53	+ 71.4
77	21.3	2.0	0.417	+ 0.3	+ 75.5
87	23.0	2.0	0.417	+ 0.49	+ 102.1

4.1.3 The Phase Transition Temperatures

The phase transition temperatures of the targeted ferroelectric liquid crystal dopants **35**, **67**, **77** and **87** determined by using polarising optical microscopy (POM) are summarised in Table 4

Table 4. The phase transition temperatures of targeted chiral dopants

Dopant	The phase transition temperatures / °C
 <p style="text-align: center;">35</p>	cooling: I 72.3 N* 69.8 Crys
 <p style="text-align: center;">67</p>	cooling: I 99.5 BP 96.1BP (mosaic) 94.8 N* 83.5 Crys
 <p style="text-align: center;">77</p>	Cooling: I 119.0 BP (Fog Phase) 118.7 Blue Green Phase 118.0 BP (Mosaic Phase) 115.5 Crys
 <p style="text-align: center;">87</p>	Cooling: I 131.1 N* 99.1 Crys

The dopant **35** did not show any phase behaviour as it is a non-mesogenic compound. The mesogenic dopants **67**, **77** and **87** shown liquid crystal phase behaviour dependent on the position of the fluorines on the core unit as well as distance from the chiral centre. The transition temperature of dopant **67** where fluorines are located on the central unit are less than that of dopant **77** and **87** where fluorines are at the end ring. The dopants **67** and **77** shown an interesting blue phase where dopant **87** where fluorines are located near to the chiral centre do not show any blue phases. The textures of compound dopant **77** are as shown in Figure 46 taken from camera fitted POM. The dopant **77** shows (1) BP I at 115.6 °C, (2) BP II (mosaic) at 117.9 °C, (3) BP II (mosaic) at 118.2 °C and (4) BP III (fog phase) 118.9 °C Figure 46. Blue phase stabilised overed aide temperature range have recently been shown to be useful in fast switching displays as explained in the blue phase section. However, no further developments

have been published in this field following the initial publicity.

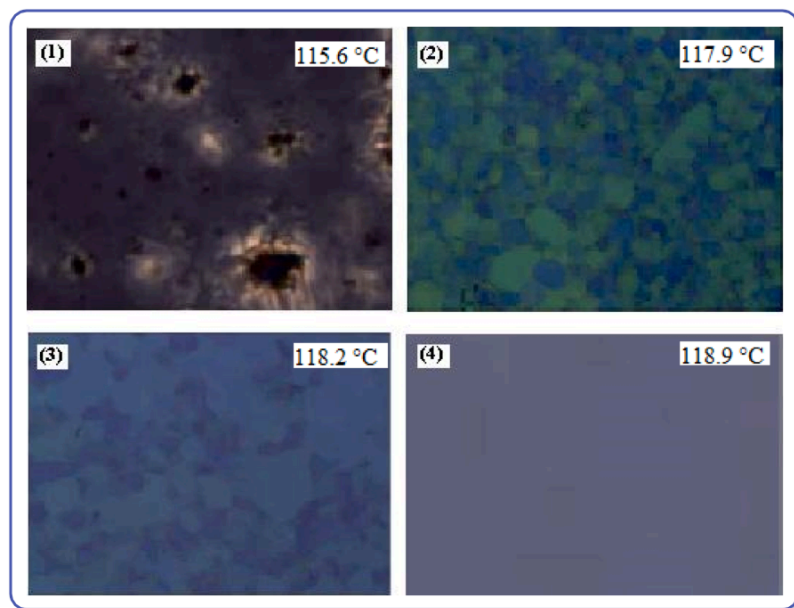


Figure 46. The blue phases of the compound **77** are shown in the following pictures taken from camera fitted POM; (1) BP I, (2) BP II, (3) BP II (mosaic) and (4) BP III (fog phase)

4.1.4 Phase Characterisation of Host Mixture KCHM211 Doped with Compounds **35**, **67**, **77** and **87**

The phase characterisations of the targeted compounds were carried out by mixing with the achiral host material KCHM211 (7 % w/w) supplied by the Kingston chemicals using POM in conjunction with DSC. The host mixture KCHM211 shown in Figure 41 was discussed in section current FLC mixtures. The dopant and host was mixed (7 % w/w), the mixture was heated to the isotropic and cooled to room temperature in ultrasonic bath, homogeneous mixing can be achieved by repeating the procedure several times.

The ITO coated homogeneous cells having an area of $5\text{ mm} \times 5\text{ mm}$ with $5\text{ }\mu\text{m}$ spacing (tolerance is $\pm 0.2\text{ }\mu\text{m}$) are obtained from Instec Inc., USA. Homogeneous alignments are obtained in the sandwich cell with surfaces, which were treated with an anti parallel rubbing method. The chiral ether linked dopants with host mixture KCHM211 (7 % w/w) mesogens were introduced into liquid-crystal cells through capillary action on heating the sample to the isotropic state on a hot bench (System Kofler). Phase transitions can be observed in POM at the time of heating and cooling the cell. Good alignment can be achieved by cooling down the cell very slowly particularly at the N^* to SmA^* transition and sometimes with the aid of an applied field (square wave). The flowing direction of the FLC mixture during the cell filling is found to influence the molecular alignment in the resultant liquid crystal layer. Obviously the appearance will be strictly controlled by the nature of the alignment surface in the cells that are used. An Olympus polarizing optical microscope is used to record the respective transformation phases of FLC mixture textures, as a function of temperature with its auxiliary attachments like hot stage.

The transition temperatures of the targeted novel FLC mesophases dopants while cooling **35**, **67**, **77**, **87** and BE80F2N with KCHM211 (7 % w/w) and on its own are tabulated in Table 5 and graphically represented in Figure 47.

Table 5. Phase transitions (°C) from POM of FLC chiral dopants with KCHM211 mixture (7% w/w)

Mesophases	KCHM211	Host + BE8OF2N	Host+35	Host+67	Host+77	Host+87
SmC - SmA	87.2	67.2	77.6	83.2	83.2	82.78
SmA - N	99.5	97.7	89.6	95.6	99.8	99.98
N - I	122.5	113.5	114.5	121	124.4	121.49

The SmC* - SmA* transitions of the targeted ether linked compounds are almost similar to that of KCHM211 mixtures. The SmA* phase temperature was larger for BE8OF2N than all targeted dopants. Interestingly the SmA* phase temperature range of non-mesogenic dopant **35** and mesogenic dopant **67** where fluorines on the middle ring have similar LC phase temperature range and other two mesogens where fluorines on the end ring have a similar LC transition temperature range.

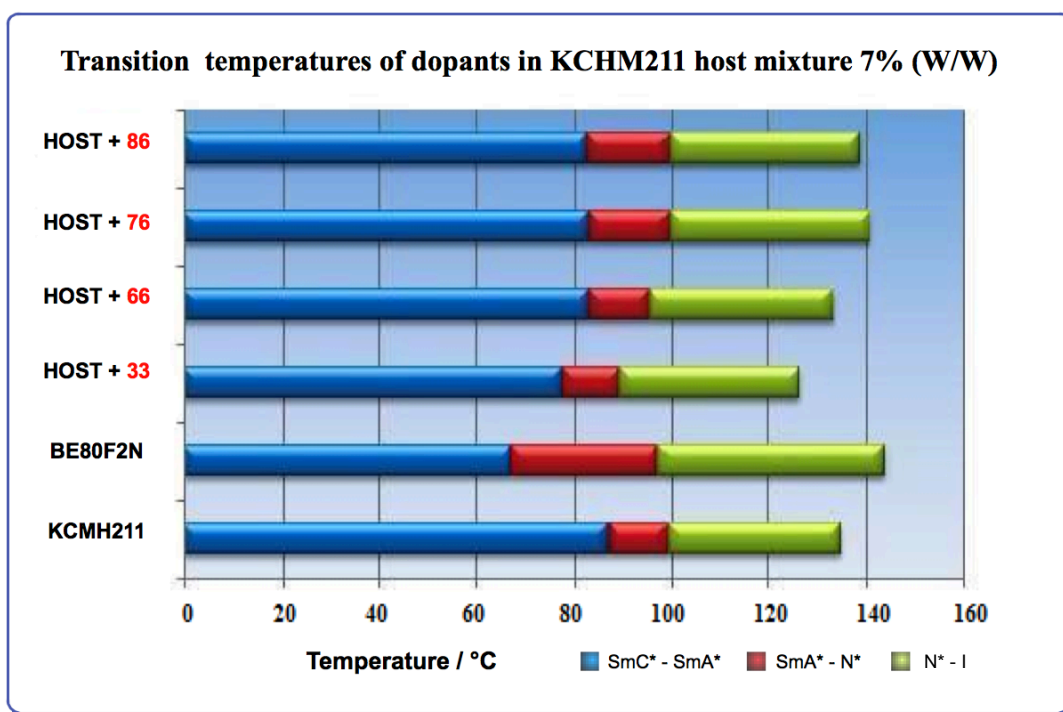


Figure 47. The comparison of phase transitions of FLC chiral dopants with KCHM211 mixture (7% w/w).

The reduction in the SmA* phase temperature range is probably advantageous

for providing a higher tilt angle. The clearing point was drastically reduced in dopant **35**. The clearing points of end fluorinated rings dopants **77** and **87** are higher than that of middle ring dopant **67**. Reduction of clearing point will reduce the temperature required for cell filling which is important when considering a manufacturing process.

Some of the interesting textures of the targeted dopants with mixture KCHM211 were recorded. Optical textures were recorded using POM as a function of temperature. The textures of the samples were recorded at a heating / cooling rate of 0.2 °C per minute from the solid phase of the sample to isotropic phase (I) on heating and reverse on the cooling from isotropic phase to solid phase. The non-mesogenic ether linked chiral dopant **35** shows the SmA* phase in KCHM211 at 88.9 °C (1) and by increasing the temperature further to at 116.4 °C shows the fingerprint texture of the cholesteric (N*) phase (2) as shown in the Figure 48

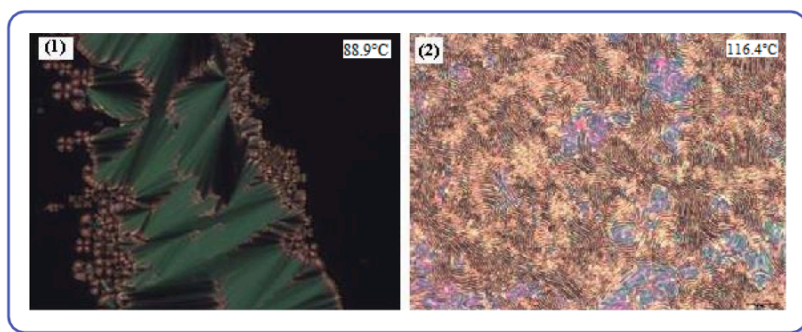


Figure 48. Photograph of dopant **35** with KCHM211 (7 % w/w) shows (1) focal conic and homeotropic texture of SmA* and (2) finger print textures of the N* phase

Micrographs taken from thermal POM measurements of the mesogenic ether linked chiral dopant dopant **77** recorded at (1) SmA* at 96.3 °C and rest of them shows cholesteric phases. (2) 111.9 °C (3) 120.2 °C (4) 122.6 °C shown in Figure 49

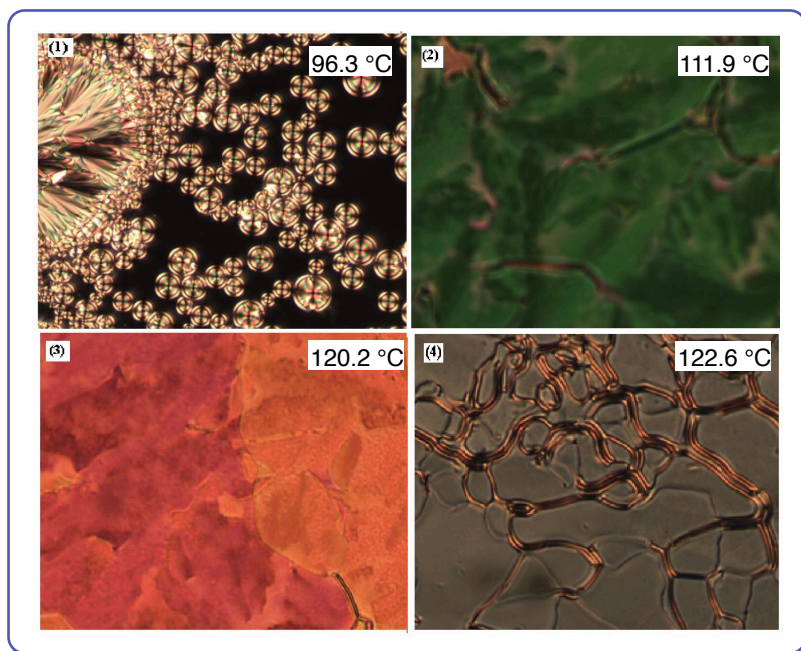


Figure 49. Photograph of dopant **77** with KCHM211 (7 % w/w)

The ether linked chiral dopant **67** shows finger print textures (1) 93.8 °C (2) 116.5 °C shown in Figure 50. At 93.8 °C the fingerprint texture was clear but as the temperature increases to 116.5 °C, the pitch length decreases until it is hard to recognise the pitch by eye.

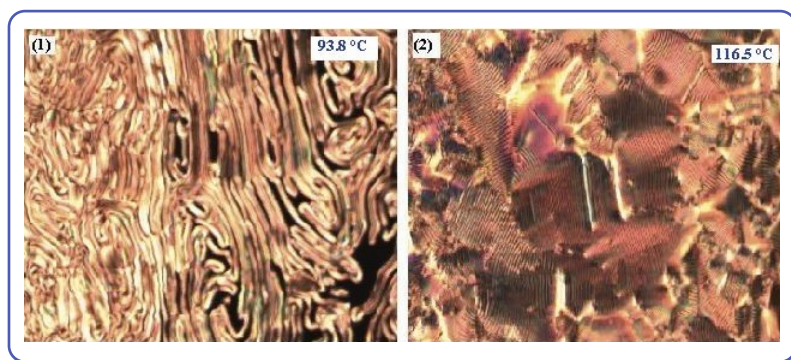


Figure 50. Photograph of dopant **67** with KCHM211 (7 % w/w)

The ether linked chiral dopant **87** shows (1) 99.1 °C (2) 129 °C shown in Figure 51. At 99.1 °C there was a pretansitional behaviour before forming the N* phase and the psuedo focal conic N* texture was observed at 99 °C. Often this

spontaneously changes to the Grandjean texture, but in these examples shearing was usually required to produce the planar aligned texture.

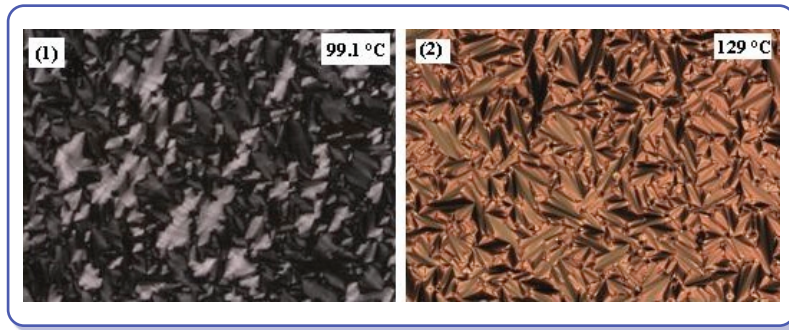


Figure 51. Photograph of dopant **87** with KCHM211 (7 % w/w)

4.1.5 Pitch Length and Helical Twisting Power

In cholesteric or chiral nematic liquid crystals the director \mathbf{n} (the local average direction of the molecular long axes) makes a helix perpendicular to \mathbf{n} . The distance corresponding to a full rotation of the director is called the pitch, \mathbf{P} . The pitch length value can be determined by different methods, some of which are relatively simple but lacking in accuracy.

Initially pitch length of the dopants mixtures of the cholesteric phase were determined with using POM and measuring the separation of dark lines in the fingerprint texture Figure 48 (2). The distance between two dark lines is equal to half the pitch length. The accuracy of the results was not satisfactory, so pitch length were determined using Cano wedge method for determination of \mathbf{P}^{97} , which were supplied by EHC, a Japanese company. A diagram of a Cano wedge is shown in Figure 52, the slides are coated to produce homogeneous alignment. The angle between two sides θ is shown with the help of double headed arrow mark. The pitch length was calculated using the following mathematical expression.

$$P = d * 2 * \tan\theta$$

Where θ is the angle between two sides, where $\tan\theta = 0.0083$ and d is the distance between two lines at different temperatures. The dotted lines shown in Figure 52, when viewed from above, separate areas where there is a jump in the number of half turns of the helix.

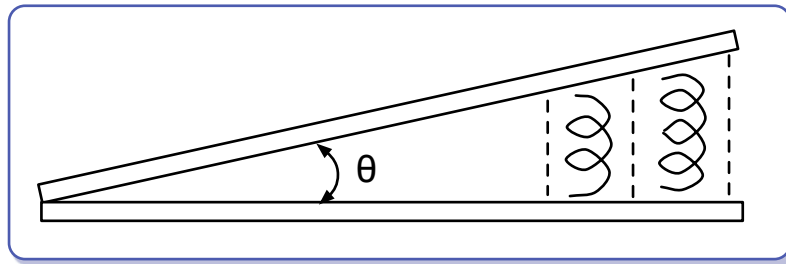


Figure 52. The schematic diagram of Cano wedge

Microphotograph of a stripe–wedge Grandjean–Cano cell filled with dopant **35**

with KCHM211. The wedge thickness increases from left to right. The disclinations (vertical) are perpendicular to the cell thickness gradient and at the stripe edge the disclinations shift the distance d as shown in Figure 53.

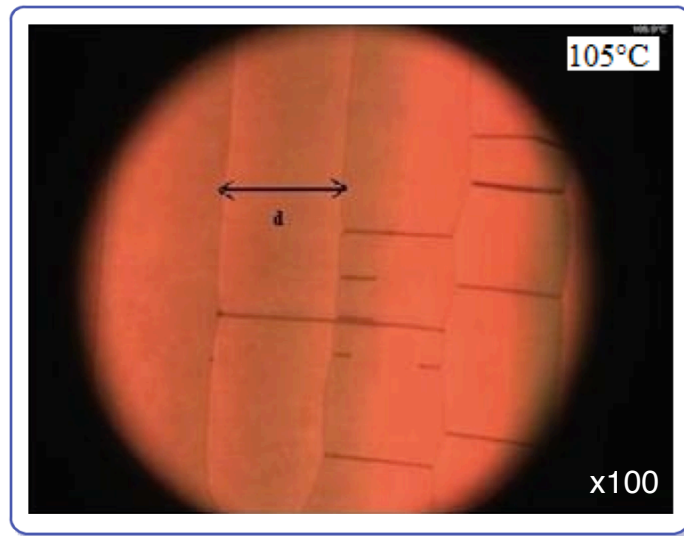


Figure 53. Microphotograph of a stripe – wedge Grandjean – Cano cell filled with dopant **35** with KCHM211 (7 % w/w)

The pitch length of dopants **35** and **67** and KCHM211 were determined and tabulated in Table 6. The pitch length at the N* - SmA* is $12.8 \mu\text{m}$ and $11.2 \mu\text{m}$. Publications and patents from Displaytech quote > 8 times the cell gap as a target for avoiding alignment problems caused by twisted states. That would give a target pitch length of $40 \mu\text{m}$ and this material falls well short of that value. However, most current microdisplay devices have a cell gap of less than $1 \mu\text{m}$ so the pitch should be quite acceptable and testing of similar mixtures by a company (Forth Dimension Displays, Dalgety Bay, Scotland) supports this. The SmC* pitch length data could not be measured directly from POM studies although this value is also important in the likelihood of obtaining good alignment. However, by altering the percentage of the dopant in host mixture will alter the pitch length P , which was proved by the data obtained by measuring 5 % , 7 % and 10 % of dopant (w/w) in KCHM211 host mixture Table 6.

Table 6. Pitch length of dopant **35** with 5,7 and 10% mixture of KCHM211.(w/w)

Temp / $^{\circ}\text{C}$	5%		7%		10%	
	Average $d / \mu\text{m}$	$P / \mu\text{m}$	Average $d / \mu\text{m}$	$P / \mu\text{m}$	Average $d / \mu\text{m}$	$P / \mu\text{m}$
109	1520.34	25.24	-	-	-	-
108	1535.34	25.48	717.34	11.91	-	-
107	1567.00	26.01	707.64	11.75	-	-
106	1598.67	26.54	718.00	11.92	-	-
105	1621.67	26.92	733.67	12.18	-	-
104	1674.67	27.80	737.33	12.24	-	-
103	1725.67	28.65	752.67	12.50	-	-
102	1768.67	29.36	759.67	12.61	459.34	7.62
101	1818.00	30.18	769.00	12.76	481.67	7.99
100	1854.67	30.79	769.00	12.76	491.00	8.15
99	1911.34	31.73	772.34	12.82	491.67	8.16
98	1989.34	33.03	-	-	508.34	8.44
97	2041.67	33.89	-	-	527.00	8.74
96	-	-	-	-	534.00	8.86
95	-	-	-	-	541.34	8.98
94	-	-	-	-	543.34	9.02
93	-	-	-	-	560.00	9.30
92	-	-	-	-	580.00	9.63
91	-	-	-	-	594.00	9.86
90	-	-	-	-	616.00	10.22
89	-	-	-	-	617.67	10.25

The various composition of pitch length shown in Figure 54 explains that, increasing in the in the percentage of the dopant tightens the helical pitch. The Figure 54 shows a linear relationship between percentage of the dopant in host and pitch length P or helical twisting power βm .

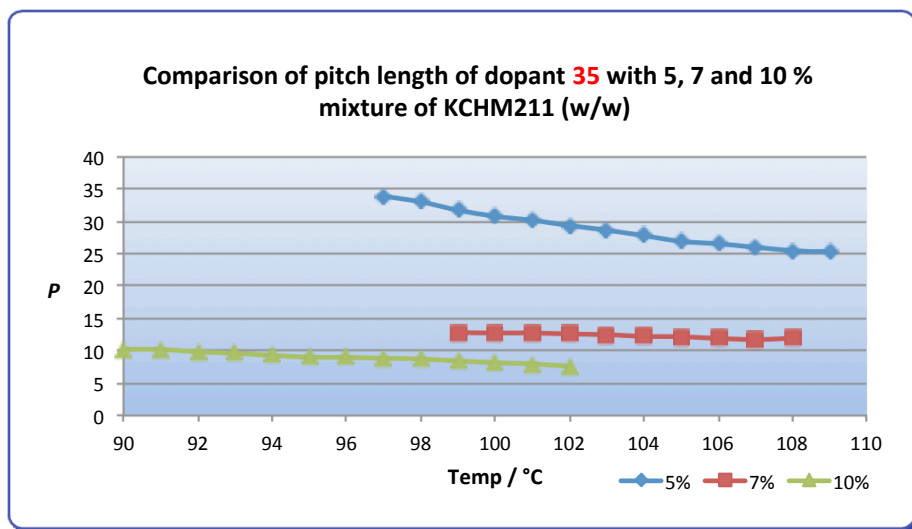


Figure 54. Comparison of pitch length of dopant **35** with 5, 7 and 10% mixture of KCH-M211 (w/w)

Chiral materials are widely used in liquid crystal display devices to supply a twisting power. In the construction of twisted nematic liquid crystal displays, the achiral host materials are mixed with small amount of chiral dopants to ensure only one direction of twist. The understanding of helical twisting power (HTP) is vital for the construction of liquid crystal displays. In general HTP are measured indirectly. First the pitch lengths of the material is measured as shown in pitch length measurement section. This method is more accurate than measuring from fingerprint textures. In this method the shift of the disclination line formed in a Cano Wedge following overnight annealing in a chiral nematic phase and is easy to measure from a calibrated POM. HTP is measured from the following equation.

$$\beta_m = 1/(P * C * ee)$$

β_m =helical twisting power;

P=pitch length;

C=concentration;

ee=enantiomeric excess;

In this case the enantiomeric excess is 100% because the amount of host and dopant (w/w) is 100%.

Table 7. The helical twisting power **35** with 5,7 and 10% mixture of KCHM211.(w/w)

Temp / °C	5%		7%		10%	
	$P \mu\text{m}$	βm	$P \mu\text{m}$	βm	$P \mu\text{m}$	βm
102	29.36	0.0068	12.61	0.0113	7.62	0.0131
101	30.18	0.0066	12.76	0.0112	7.99	0.0125
100	30.79	0.0065	12.76	0.0112	8.15	0.0123
99	31.73	0.0063	12.82	0.0111	8.16	0.0123

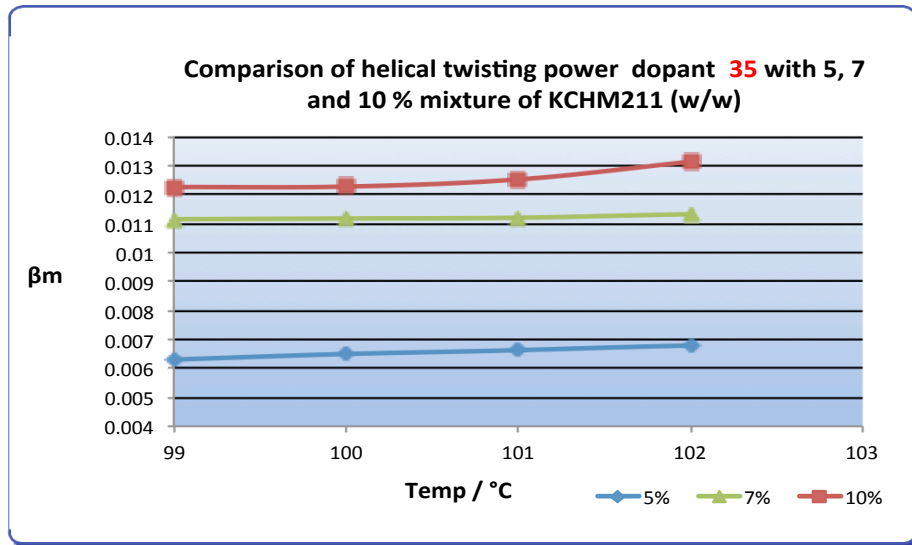


Figure 55. Comparison of helical twisting power **35** with 5, 7 and 10 % mixture of KCHM211 (w/w)

4.1.6 Pitch Length and Helical Twisting Power of Dopant 67

Table 8. Determination of pitch length and helical twisting power of dopant **67** with KCHM211 mixture (7% w/w).

Temp / °C	Pitch length / μm	βm
100	9.7	0.0147
98	11.2	0.0128
96	12.4	0.0115
94	15.8	0.0090
92	18.45	0.0077

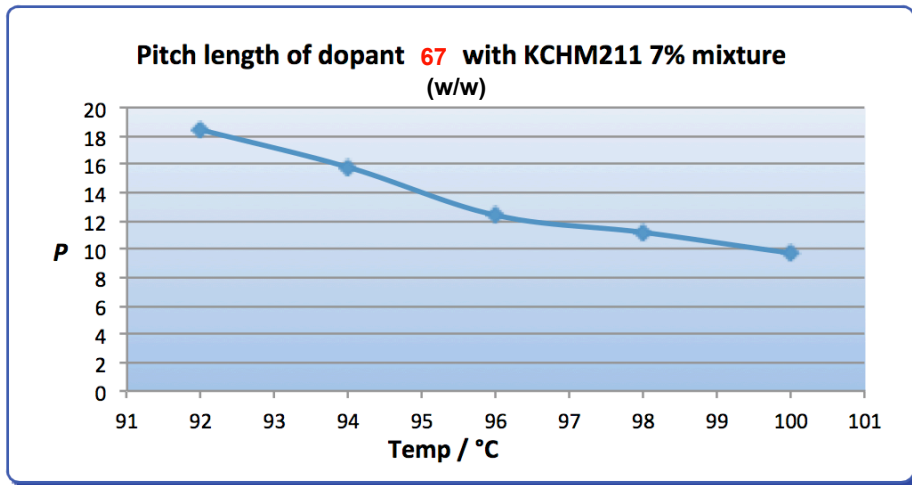


Figure 56. Pitch length of dopant 67 with KCHM211 mixture (7% w/w).

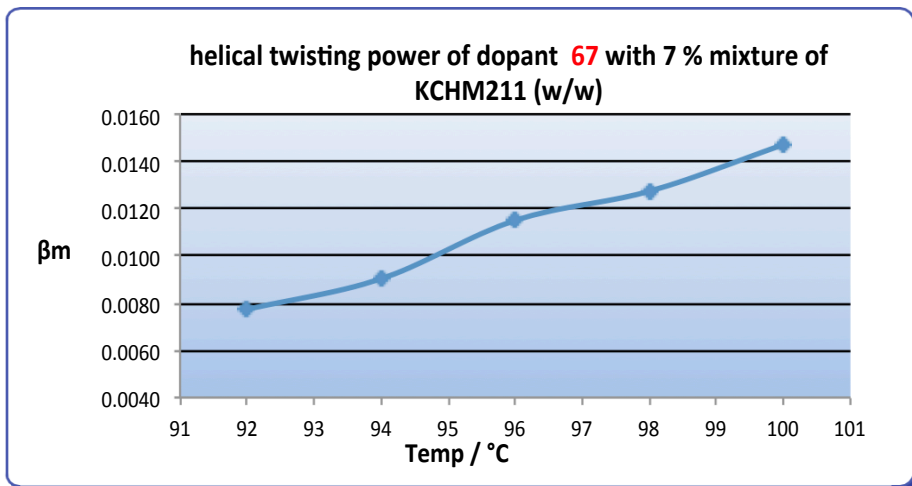


Figure 57. Helical twisting power of dopant 67 with KCHM211 mixture (7% w/w).

4.1.7 Tilt Angle

A tilt angle of 22.5 ° will give the maximum contrast ration for the SSFLC device so it is an important parameter to measure. The tilt angles were obtained from ferroelectric switching of the new dopants as 7 % w/w mixtures with KCHM211 by applying a low frequency DC voltage to an electro optic cell viewed under crossed polarisers. The microscope's rotating stage was turned to find the angle of maximum extinction which is equal to the twice the tilt angle. A voltage of 40 V amplitude was employed to ensure complete switching.

The accurate measurements of electro optical properties of the compounds were determined in anti-parallel rubbed planar aligned 5 μm cells supplied by Instec. Tilt angle, P_s data and phase transitions were obtained using Instec Automatic Liquid Crystal Tester (ALCT), in conjunction with Instec temperature controller and hot-stage and a polarising microscope. Data was captured on a PC and processed using Instec software. The triangular wave method was used to determine P_s .⁹⁸

The cell gap plays important role in electro optical measurements which was determined by using a UV spectrometer and measuring the wavelength of interference fringes using the following formula.

$$d = \frac{n \times lw \times hw}{2(hw - lw)} \mu m$$

Where, n-no of fringes; lw-low wavelength; hw-high wavelength.

$$d = \frac{14 \times 372 \times 780}{2(780 - 372)} \mu m$$

$$d = 4.978 \mu m$$

The 5 μm cell gap quoted by Instec was shown to be quite accurate. The tilt angle data of dopants **35** and **67** with KCHM211 mixture (7% w/w) were tabulated in Table 9 and Table 10 respectively and a comparison graph was drawn of tilt angles versus temperature shown in Figure 58.

Table 9. Tilt angles of dopant **35** with KCHM211 mixture (7% w/w).

Temp / °C	Tilt angle / θ	Temp / °C	Tilt angle / θ
78	2.85	66	5.50
77	3.10	64	5.75
76	3.20	62	6.50
75	3.50	60	6.75
74	3.75	55	7.50
73	4.00	50	8.00
72	4.10	45	9.50
71	4.25	40	11.00
70	4.75	35	12.50
68	5.00	30	15.00

Table 10. Tilt angles of dopant **67** with KCHM211 mixture (7% w/w).

Temp / °C	Tilt angle / θ	Temp / °C	Tilt angle / θ
85	5.15	70	16.85
84	8.5	65	17.00
83	8.35	60	17.30
82	10.3	55	17.75
81	10.8	50	18.35
80	11.7	45	19.10
78	11.9	40	19.20
76	12.25	35	19.35
74	14.00	30	19.10
72	15.35		

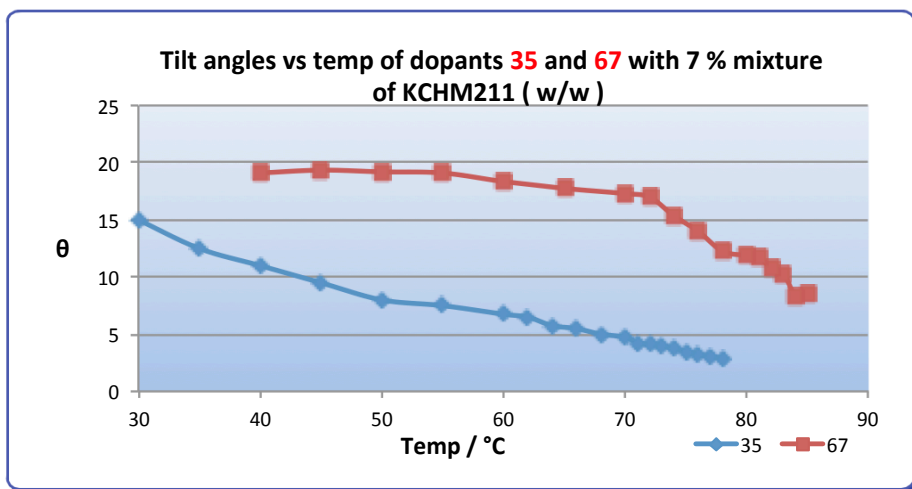


Figure 58. Tilt angles *vs* temperatures of dopants **35** and **67** with KCHM211 mixture (7% w/w).

The tilt angle data shows that the terphenyl generally has a higher tilt than the biphenyl. The earlier transition temperature results did not show that the biphenyl was a SmA* promoter so unlike BE8OF2N, that property cannot be used to rationalize the results. However, the dialkoxyterphenyl dopant would be expected to have SmC properties and since the molecules will match the size of the host mixture compounds and support the layer structure, perhaps it is not surprising that the tilt is larger. These results should be confirmed by X-ray diffraction studies.

4.1.8 Spontaneous Polarisation (P_s)

The spontaneous polarisation P_s is one of the most important characteristic properties of ferroelectric liquid crystals. The P_s of most FLC materials are indirectly proportional to the temperature at SmC* phase as P_s approaches zero with increase in temperature approaching the Curie point. As a result the SmC* to SmA* phase transition of FLCs has been considered as a typical second-order transition. The P_s considered as independent of experimental conditions, but earlier research shows that P_s depend on the thickness of the cell measured frequency.^{99 100 101 102 102}

Methods of spontaneous polarisation enhancement.

In FLC material the P_s exists orthogonal to the layer normal; as a result the intensity of P_s depends on the presence of lateral molecular dipole moments. P_s can be increased by a number of ways, increasing the number and type of aromatic rings. P_s is reduced from what would be a very high value arising if all the dipoles simply added, by rotation of the molecules along the long axis and intramolecular rotations; so by hindering these rotations, P_s increases drastically. These approaches focussed on the chiral unit attached to the central core unit, such as the number asymmetric centres and the way it connected to the core. The dipole moment of the central core unit rotates with chiral unit as a whole around the long axis, but this rotation is normally hindered by the nature of the central core unit as well as the chiral unit. This leads to an overall preferred orientation in space on average. The length of the alkyl or alkoxy chain plays a considerable role in the P_s values. P_s with increases with longer the chain lengths, but there is an optimum length, after which P_s starts decreasing. The nature of the chain, whether branched or not and the nature of linking atoms also alters the thermal stability of the mesophase. In general, P_s show higher value when the molecule possesses a stronger dipole moment at the chiral centre and closer to the central core unit, but these may reduce the SmC* and N* pitch length. Commonly used groups such as carbonyl C=O, halogens (F, Cl, Br), nitrile C≡N or methyl groups CH₃ attached to an oxygen have been commonly employed near or at the chiral centre. Chiral molecules with P_s values up to 300 nC cm⁻² have been found for individual compounds.¹⁰³

The choice of molecular design for the dopants for this thesis was based on accepted principles and previous experience within the Dr R. Lewis research group. However, the values of P_s have been unpredictable, the octyloxyfluorobiphenyl ether compound **35** gives a useful moderate value of 19 nC cm^{-2} at room temperature when doped (7 % w/w) in KCHM211 but similar dopants which have an alkyldifluoroterphenyl core gave low or very low values of P_s . Optical purity is not quantified but the consistent $[\alpha]_D$ values indicate that optical purity is fairly high. Dilution of the chirality due to the increase molecular mass does not account for the size of the reduction in P_s either and we are left with considering changes in conformation of the chiral centre and its orientation relative to other strongly dipolar parts of the dopant *e.g.* fluoro substituents, the ether link and the aromatic rings. Detailed molecular modelling and single crystal structure of compound were employed to investigate these.

Table 11. Spontaneous polarisation of dopant **35** with KCHM211 mixture (7% w/w).

Temp / °C	P_s / nCcm^{-1}
30	19.90
35	17.50
40	13.56
45	12.09
50	9.90
55	7.76
60	5.40
65	4.70
70	3.83
72	3.46

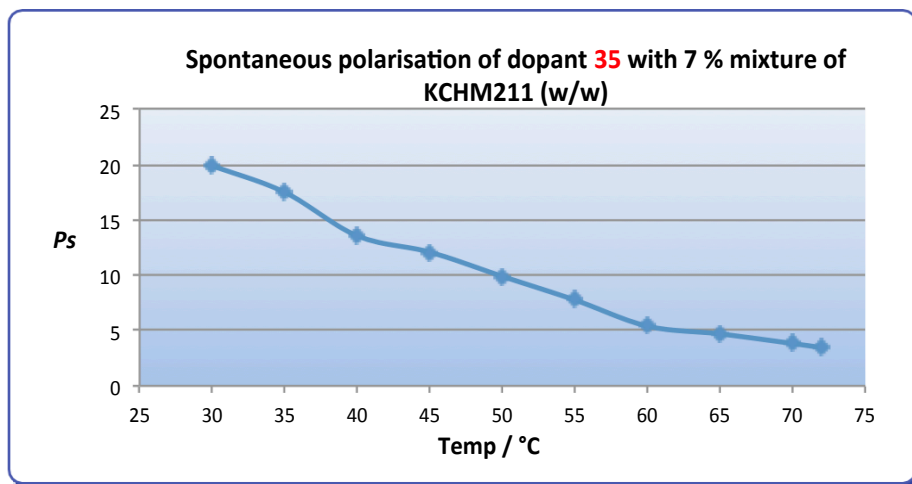


Figure 59. Spontaneous polarisation of dopant **35** with KCHM211 mixture (7% w/w).

The P_s for this biphenyl ether dopant **35** follows typical trend of increase with decreasing temperature. The relationship between P_s and temperature is almost linear and mirrors the increase in tilt angle with decreasing temperature Table 9. There is even a similar dip that occurs, although it is not certain whether this significant or a chance similarity. The maximum P_s at 7 % w/w in host mixture KCHM211 at 30 °C is 19.9 nC cm^{-2} is much higher than the maximum for BE8OF2N, which is 18 nC cm^{-2} at the same concentration. This is an important result in that it confirms that a less labile ether group can replace the ester in BE8OF2N and provide similar electro-optic switching behaviour. The N^* pitch length for the ether dopant **35** in the same mixture is 12.8 micron at the N^* - SmA^* transition and this compares to 12 microns for BE8OF2N under the same conditions.

This could provide a mechanism for producing high P_s FLC mixtures without increasing P_s to the point where it causes alignment to break down. Mixing of BE8OF2N and compound **35**, if the pitch directions are of opposite handedness may result in a high P_s dopant with very long pitch.

Table 12. Spontaneous polarisation of dopant **67** with KCHM211 mixture (7% w/w).

Temp / °C	$P_s / nCcm^{-1}$	Temp / °C	$P_s / nCcm^{-1}$
25	5.73	63	2.85
30	5.51	65	2.69
35	5.13	67	2.45
40	4.70	69	2.37
45	4.32	71	2.20
47	4.13	73	2.02
49	3.98	75	1.78
51	3.77	77	1.65
53	3.53	79	1.37
55	3.47	81	1.13
57	3.32	83	0.93
59	3.06	85	0.56
61	2.97		

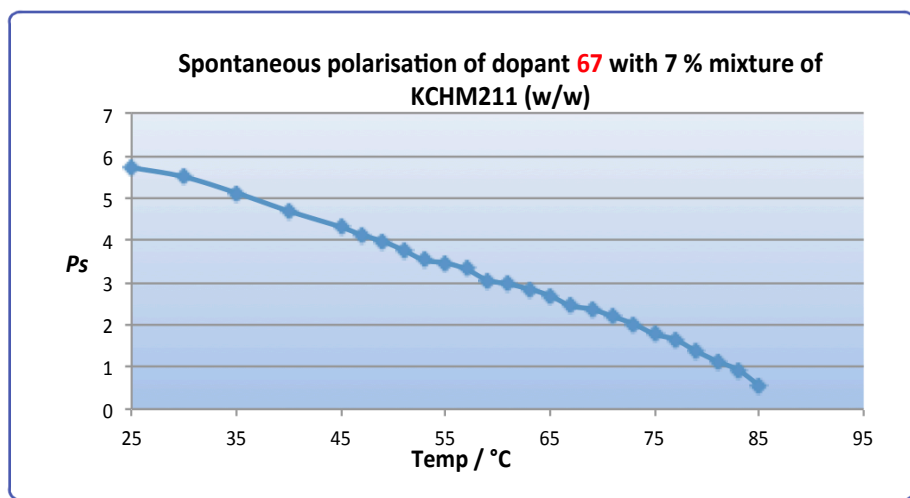


Figure 60. Spontaneous polarisation of dopant **67** with KCHM211 mixture (7% w/w)

The P_s data from biphenyl **35**, was very promising but a biphenyl would always reduce the SmC* phase temperature of the FLC mixture, especially if high concentrations are required. It seemed that improved phase behaviour could be achieved by attaching the same chiral group to a mesogenic terphenyl. To that end, terphenyls **67**, **77** and **87** were prepared and discussed previously, there

is no evidence to suggest that the optical purity was not high. However, compounds **77** and **87** that have the difluoro-units in the end rings, either adjacent or remote from the chiral centre. However, the *Ps* for these two analogues was very small and therefore the data was considered too unreliable for reproduction in this thesis.

The *Ps* for the middle ring analogue was much lower than expected for the middle ring difluorterphenyl since the optical purity was judged to be quite high but there is no data available for other cyanohydrins ethers to make a comparison. The other two terphenyl dopants were studied to help confirm this *Ps* data and molecular modeling was also carried out. Calculated dipole moments from the most stable conformation of the chiral centre can shed some light on the magnitude of *Ps*, at least qualitatively.

Molecular modelling was performed on the dopant using Gaussian 09W *via* Gaussview, but a collaboration with Dr David Benoit in our department enabled more rigorous study to be carried out. The results from this work is discussed in section molecular modelling.

4.2 The Study of Alkoxyterphenyl Mesogenic Dopant 94

The alkoxyterphenyl mesogenic dopant **94** as shown in Figure 61 was designed and synthesised to be structurally similar to the alkyl terphenyl dopant **67**. The idea was to test whether replacement of an alkyl chain by an alkoxy chain would increase P_s when the dopant was mixed with KCHM211 (7% w/w). This was based on the observations that the biphenyl dopant **35** has an octyloxy chain and a moderately high P_s but all the terphenyl analogues that exhibited a low P_s possessed pentyl chains; surprisingly there is no much change in the P_s values (P_s 7.2 nC cm⁻²) in comparison to the pentyl analogue **67**.

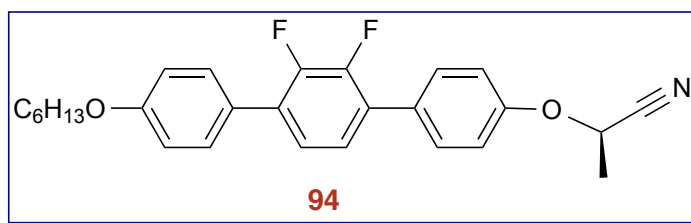


Figure 61. The alkoxyterphenyl mesogenic dopant **94**.

The transition temperatures of dopant **94** are:

Heating: Cryst 106.4 SmC* 109.8 SmA* 115.4 N* 139.1 I

Cooling: I 138.8 N* 115.1 SmC* 108.3 SmA* 92.0 Cryst

The transition temperatures shows interesting finger print textures as shown in Figure 62 and Figure 63. There is a general increase in transition temperatures when compared to **67**; this is quite an expected trend due to the occurrence of the alkoxy chain. The optical rotation is + 27 which is lower than **67** (+ 71.4).

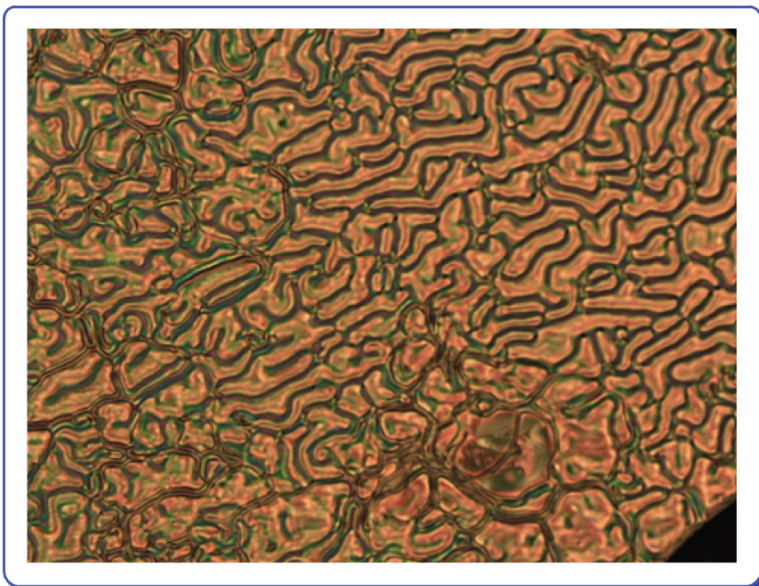


Figure 62. The N* pitch unwinding at transition to SmA* phase for compound **94** at 115.4 °C.

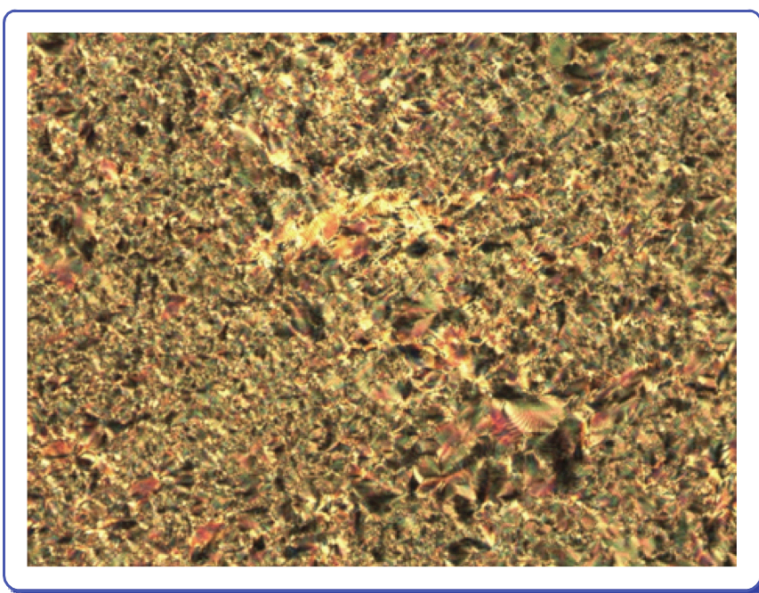


Figure 63. The fingerprint texture of N* phase for compound **94** at 138.3 °C.

4.3 Characterisation of Second Generation FLC Dopants

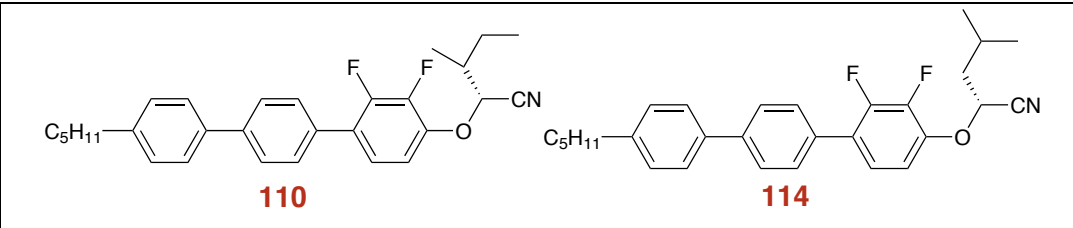
It is known that a longer chain attached to the chiral centre reduces rotational freedom and this leads to higher P_s but this is counteracted by a tighter N^* pitch length in the resulting FLC mixture. A longer terminal chain would also provide a more mesogenic unit, perhaps with lower melting points. The amino acid based synthesis was described in this section. The synthetic targets were chosen before the electrooptic measurements were carried out and the available material was used to prepare terphenyl derivatives (dopants **110** and **114**). With hindsight the two analogues should also have been prepared, since the terphenyl yielded vanishingly small values of P_s . The optical activity of compounds did not hint that racemisation had occurred so it must be concluded that it is a quirk of the molecular structure and conformation. The details of the characterisation of these dopants is presented here.

4.3.1 Optical Rotation

The optical rotation of second generation FLC dopants **110** and **114** were determined as shown in Table 13. The optical rotation of these compounds are surprisingly less than that of non-mesogenic first generation dopant **35**, though they are mesogenic compounds. This is may be due to branched chain near the chiral unit. However, the optical rotations of first generation FLC dopants are higher than those of second generation FLC dopants.

Table 13. The optical rotation of second generation FLC dopants

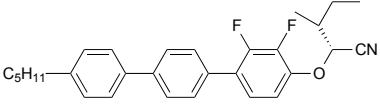
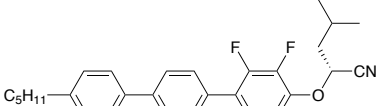
Dopant	Weight / mg	Solvent (D-CM) / ml	Cell Length /dm	Measured Rotation / °	Optical Rotation / °
110	25.0	1.0	0.417	+ 0.72	+ 69.2
114	25.0	1.0	0.417	+ 0.503	+ 48.36



4.3.2 The Phase Transition Temperatures

The phase transition temperatures of the targeted ferroelectric liquid crystal dopants dopants **110** and **114** were determined by polarising optical microscopy (POM) and are summarised in Table 14

Table 14. The phase transition temperatures of second generation FLC dopants

Dopant	The phase transition temperatures / °C
 110	Heating: Cr 33.6(DSC) (SmC* 34.5) SmA* 90.9 I Cooling: I 90.9 SmA* 33.6 SmC*
 114	Heating: Cr 33.1 SmA* 95.4 I Cooling: I 94.5 SmA* 31.7 Cr

The dopants **110** and **114** are structurally similar to dopant **87** where fluorines are nearer to the chiral centre. The transition temperatures are much lower than that of lactamide dopant **87** this is may be because of extended branched alkyl chain in the chiral centre and in conjunction with the straightforward synthesis led us to believe that these may be good candidates as FLC chiral dopants.

4.3.3 Characterisation of compound **110** doped with host mixture KCHM211

The phase characterisations of the targeted compound was carried out by mixing with the achiral host material KCHM211 (7% w/w) using POM in conjunction with DSC. The dopant and host was mixed (w/w), the mixture was heated to the isotropic and cooled to a room temperature in ultrasonic mixture, homogeneous mixture can be achieved by several repeating the procedure.

The transition temperatures of the targeted novel FLC mesophases dopant **110** with KCHM211 (7% w/w) is tabulated in Table 15.

Table 15. Phase transitions of dopant **110** with KCHM211 mixture (7% w/w)

Mixture	SmC* - SmA*	SmA* - N*	N* - I
110 + KCHM211	82.4 °C	96.8 °C	119.5 °C

Although the phase transition temperatures of the FLC mixture was promising, P_s was very low and was considered too unreliable to report. The reason for the low P_s is presumably related to the same observation that occurred for the similar lactamide dopant.

4.4 X-Ray Analysis

X-ray diffraction is vital in the determination of crystalline structures. This technique is also widely used to understand the structure and conformation in single liquid crystals in addition to phase composition in detail. In my work, X-ray diffraction was used to investigate the detailed molecular structure of some materials and phase behaviour. The fundamental principle of X-ray diffraction and Bragg's law are explained in order to understand the single crystal diffraction and small angle X-ray scattering (SAXS).

A focused X-ray beam interacts with crystal atoms and are scattered by the surrounding electrons. The scattering process of X-rays is the emission of coherent secondary waves from the electrons of the atoms when they are excited and resonate with the frequency of periodically changing electric field of X-rays. The outgoing waves will superimpose and the result of interference depends on amplitude, wavelength and relative phase of the waves. We can measure the distances between the planes of the atoms that constitute the sample by using Bragg's Law.¹⁰⁴

4.4.1 Bragg's Law

Crystalline solids consist of regular arrays of atoms, ion, or molecules with inter atomic spacing on the order of 100 pm or 1 Å

The Bragg's law, expressed as follows:

$$n\lambda = 2d \sin \theta$$

λ - Wavelength of incident X-ray beam;

d - Distance between diffracting atomic planes;

θ - Angle of diffraction;

n - An integer.

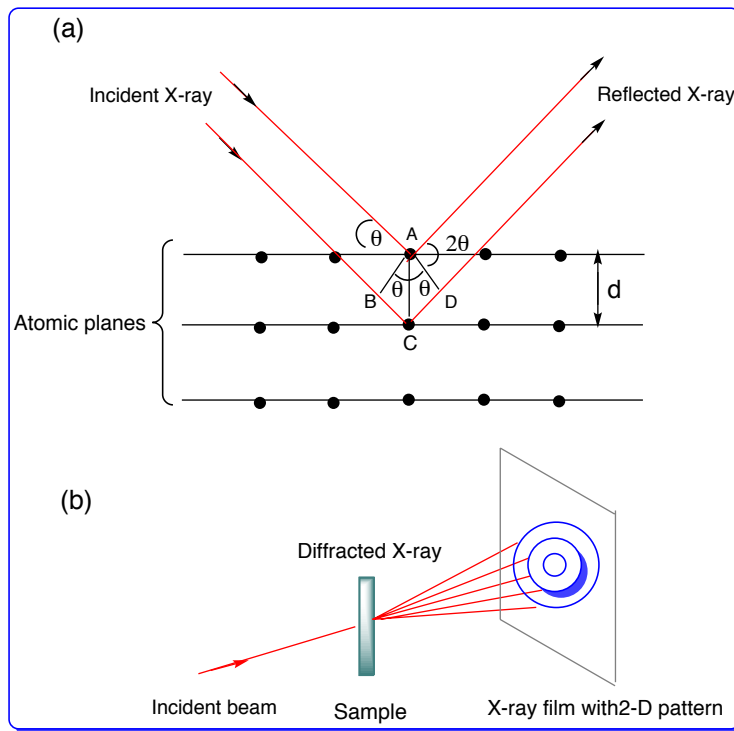


Figure 64. description of a) Bragg's Diffraction Law b) 2-D X-ray diffraction pattern.^{105,106}

The Bragg's law explains the relationship between the wavelength of an incident X-ray beam, the distance between diffracting atomic planes (or d-spacing) and the angle of diffraction as shown in Figure 64 (a) and the composed diffraction data confer information about the structure of the materials shown in Figure 64 (b).^{105,106}

The mesophase pattern in liquid crystal materials can be analysed by 2-D X-ray diffraction pattern of oriented samples as shown in Figure 65. Due to the short range of positional order, the isotropic phase shows diffused rings. The appearance of a nematic phase can be confirmed by diffuse arcs along the meridian at small angles in unaligned samples whereas in aligned samples sharp arcs are produced. The diffuse arc at the bigger radius characterises the distance between molecules along their widths. Smectic phases are distinguished by sharp Bragg spots resulting from the repeating layer. In the SmA phases, the director is normal to the smectic layer, resulting in the Bragg reflections being placed along the meridian. In the case of SmC phases several possible patterns can be noticed, the angle between the smectic layers normal and the director θ is no longer collinear. This tilt can straightforwardly be observed in the diffraction

pattern as the diffuse peaks at smaller and larger angles are no longer orthogonal to each other. Diffraction arcs along the equator revealed at the wide angle region are related to the intermolecular packing distance.^{107 108 109 110}

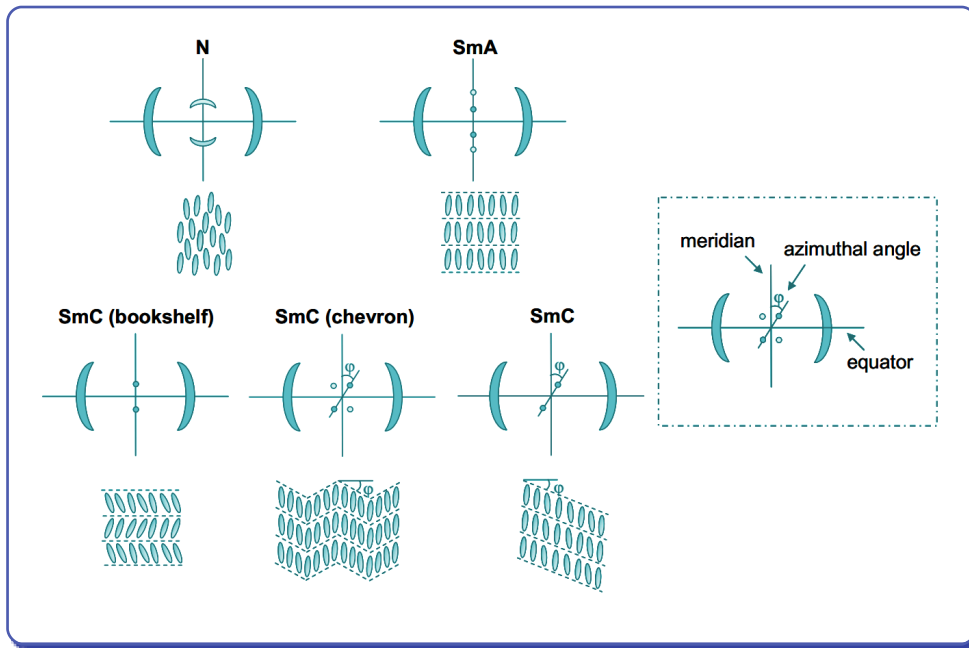


Figure 65. 2-D X-ray diffraction pattern of oriented samples.^{105,106}

4.4.2 Single Crystal X-Ray Diffraction

The aim of this study was to examine whether the conformation obtained from molecular modelling matched the structure obtained experimentally by diffraction. It is not possible to assume that the structure in a liquid crystal phase would be the same as in a crystal as intermolecular interactions may cause a change in conformation to achieve the lowest energy packing in the crystal. However it is one of the experimental techniques that give this level of structural detail. The structure of one of the dopant **35** crystalline structure was determined by single-crystal X-ray diffraction. Detail of the machine created with CONVERT.DLL (www.crystalimpact.com). The unit cell is triclinic and contains three crystallographically independent molecules with similar overall conformations.

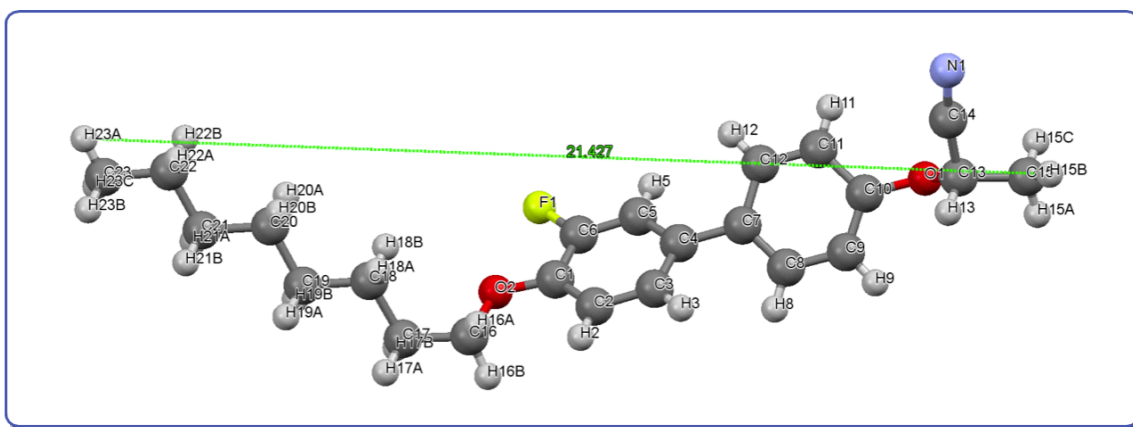


Figure 66. ORTEP diagram of (*S*)-2-((3'-fluoro-4'-(octyloxy)-[1,1'-biphenyl]-4-yl)oxy)propanenitrile **35** with atom numbering.

The molecular geometry is surprisingly nonlinear Figure 66, having an overall I bend shaped structure rather than the more extended type of conformation found in the crystal structure of many mesogenic materials.¹¹¹

In view of the high spontaneous polarisation observed parallel to the (presumed) molecular layers of the SmC* phase, it is of particular interest in the crystal of the cyano- groups (whose alignment undoubtedly contributes very significantly to the spontaneous polarisation of the mesophase) are also arranged so as to produce a macroscopic dipole with a substantial component parallel to the layer

direction and normal to the planes of 'red', 'blue' and 'green' molecules which constitute the layers.¹¹²

In general, it is difficult to grow superior quality crystals of mesogenic compounds carrying flexible alkyl and alkoxy chains. In spite of this, we managed to obtain colourless crystals of the dopant **35** by slow evaporation of a solution (benzene and methanol in a 1 : 2 ratio). This was achieved using a wide neck sample tube and making a small hole in the plastic stopper to enable evaporation. The crystal structure was determined by SCXRD and the procured crystal data are presented in Table 16.

The compound crystallizes in the triclinic centrosymmetric space group $\overline{P1}$ and its cell parameters are

$$a=44.75(1) , b = 4.7146(6) , c = 9.9643(19) , \beta = 95.826(17)^\circ$$

$$a/b = 9.4918 \quad b/c = 0.4731 \quad c/a = 0.2227$$

$$\text{Cell volume } 2091.39(70)^3$$

Interestingly, the structure was found to be non-planar as evidenced by the observed large torsion angles of $175.055(614)^\circ$ (C17–C16–O2–C1) created by the fluorinated ring with the alkoxy chain and $-81.6(9)^\circ$ (C10–O1–C13–C14) created by the chiral unit attached ring and chiral centre. The octyloxy chain is completely staggered. The nitrile is on the same side of the ring as the fluorine although they are certainly not coplanar. The ether bonds linked to the chiral centre are almost orthogonal to the nitrile which means that the C–O dipole does not oppose the that of the nitrile. Both observations, at least, fit with having a substantial transverse dipole moment that will contribute to the *Ps*. Unfortunately there is no comparable data for the low *Ps* terphenyl dopants that might have shown dipoles opposing one another.^{113–115}

The powder pattern of the dopant **35** is also shown in Figure 67

Table 16. Crystal data and structure refinement for compounds **35**.

General								
Code	VR55							
Bibliographic data								
Creation method	Created with CONVERT.DLL (www.crystalimpact.com)							
Phase data								
Formula sum	C92 H128 F4 O8 N4 B16							
Formula weight	1667.02 g/mol							
Crystal system	monoclinic							
Space-group	P 1 21/c 1 (14)							
Cell parameters	a=44.75(1) Å b=4.7146(6) Å c=9.9643(19) Å β=95.826(17)°							
Cell ratio	a/b=9.4918 b/c=0.4731 c/a=0.2227							
Cell volume	2091.39(70) Å ³							
Calc. density	1.32351 g/cm ³							
Pearson code	mP252							
Formula type	NOP2Q23R32...							
Wyckoff sequence	e63							
Atomic parameters								
Atom	Ox.	Wyck.	Site	S.O.F.	x/a	y/b	z/c	U [Å ²]
C1		4e		1	0.2393(2)	0.4414(14)	0.5191(6)	
C2		4e		1	0.2631(2)	0.3027(15)	0.4701(6)	
H2		4e		1	0.2595	0.1677	0.3995	
C3		4e		1	0.2923(2)	0.3598(13)	0.5235(6)	
H3		4e		1	0.3083	0.2612	0.4878	
C4		4e		1	0.2995(2)	0.5575(11)	0.6284(5)	
C5		4e		1	0.2747(2)	0.7009(14)	0.6761(6)	
H5		4e		1	0.278	0.8396	0.7452	
C6		4e		1	0.2461(2)	0.6385(14)	0.6220(6)	
F1		4e		1	0.2224(1)	0.7732(9)	0.6713(4)	
C7		4e		1	0.3306(1)	0.6123(12)	0.6830(6)	
C10		4e		1	0.3899(1)	0.7363(10)	0.7821(5)	
O1		4e		1	0.4191(1)	0.8011(9)	0.8296(4)	
C8		4e		1	0.3527(2)	0.627(3)	0.5999(11)	
H8		4e		1	0.3479	0.5964	0.5059	
C9		4e		1	0.3819(2)	0.683(3)	0.6484(10)	
H9		4e		1	0.3969	0.6861	0.5875	
C11		4e		1	0.3663(2)	0.730(3)	0.8695(10)	
H11		4e		1	0.3712	0.7618	0.9634	
C12		4e		1	0.3378(2)	0.681(3)	0.8224(10)	
H12		4e		1	0.3224	0.6914	0.8811	
C13		4e		1	0.4417(3)	0.5931(17)	0.8426(8)	
H13		4e		1	0.4398	0.4615	0.7635	
C14		4e		1	0.4402(3)	0.436(2)	0.9694(11)	
N1		4e		1	0.4438(3)	0.271(3)	1.0788(10)	
C15		4e		1	0.4728(3)	0.735(2)	0.8587(12)	
H15A		4e		1	0.4756	0.8449	0.7774	
H15B		4e		1	0.4884	0.5889	0.8718	
H15C		4e		1	0.4742	0.8614	0.9371	
O2		4e		1	0.2097(1)	0.4047(10)	0.4768(5)	
C16		4e		1	0.2019(2)	0.1947(17)	0.3746(7)	
H16A		4e		1	0.2106	0.009	0.4037	
H16B		4e		1	0.21	0.2499	0.2896	
C17		4e		1	0.1684(2)	0.173(2)	0.3528(7)	
H17A		4e		1	0.1628	0.0475	0.2745	
H17B		4e		1	0.16	0.3634	0.3301	
C18		4e		1	0.1540(2)	0.059(2)	0.4738(7)	
H18A		4e		1	0.1628	-0.1292	0.4986	
H18B		4e		1	0.1589	0.1877	0.5515	
C19		4e		1	0.1206(2)	0.031(3)	0.4472(8)	
H19A		4e		1	0.1158	-0.1118	0.3752	
H19B		4e		1	0.1121	0.2145	0.4142	
C20		4e		1	0.1060(2)	-0.057(3)	0.5715(9)	
H20A		4e		1	0.1104	0.0874	0.6426	
H20B		4e		1	0.115	-0.2387	0.6056	
C21		4e		1	0.0719(2)	-0.095(4)	0.5462(10)	
H21A		4e		1	0.0627	0.0896	0.5175	
H21B		4e		1	0.0673	-0.231	0.4714	
C22		4e		1	0.0577(3)	-0.200(4)	0.6697(11)	
H22A		4e		1	0.0665	-0.3858	0.6981	
H22B		4e		1	0.0622	-0.0648	0.745	
C23		4e		1	0.0251(3)	-0.230(5)	0.6414(16)	
H23A		4e		1	0.0167	-0.3035	0.7216	
H23B		4e		1	0.0205	-0.3623	0.5662	
H23C		4e		1	0.0162	-0.0448	0.6174	
C8B		4e		1	0.3522(2)	0.393(2)	0.7005(13)	
H8B		4e		1	0.3463	0.203	0.6794	
C9B		4e		1	0.3818(2)	0.450(2)	0.7480(13)	
H9B		4e		1	0.3963	0.303	0.7577	
C11B		4e		1	0.3698(2)	0.945(2)	0.7577(13)	
H11B		4e		1	0.3759	1.1363	0.7722	
C12B		4e		1	0.3404(2)	0.885(2)	0.7117(13)	
H12B		4e		1	0.3264	1.0364	0.6994	

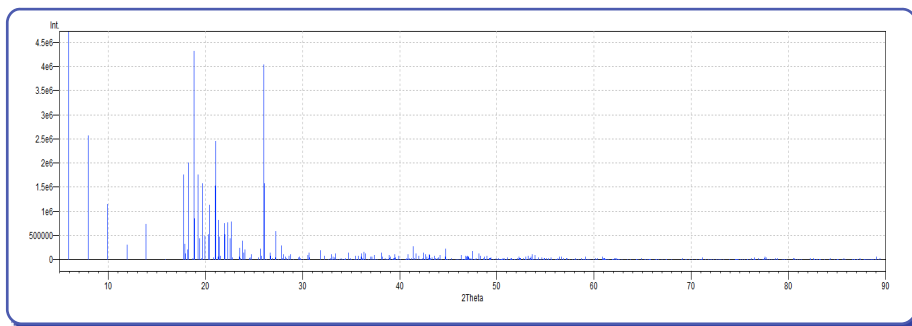


Figure 67. The powder pattern of the dopant **35**.

The conformation of the individual molecule was obtained by selecting one molecule from the packed structure. The diagram above shows how four molecules pack to yield two pairs of orthogonal nitrile dipoles that oppose each other. Similarly the fluorines are arranged to almost oppose each other.

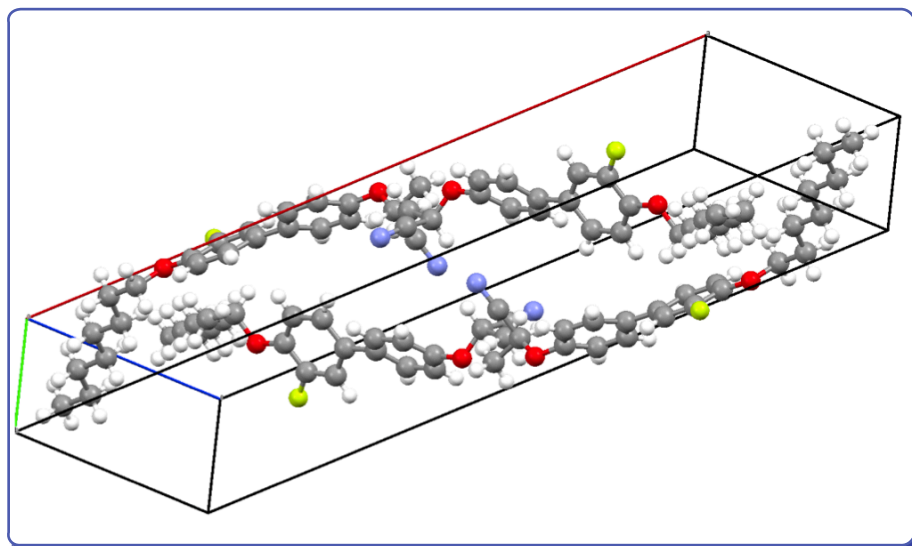


Figure 68. Molecular packing of dopant **35** in the crystal

The extended sheet shows the alkyl chains appearing above and below the planes of the aromatic core as shown in Figure 69. Looks like the C-F dipoles should cancel each other out. Note the space group is again centrosymmetric suggesting an equal number of left and right handed molecules. This does not agree with the equal opposite optical rotations observed when starting with the either enantiomer of lactamide. Perhaps crystallisation selected a racemic crystal or the long period in solution during crystallisation led to racemisation. It was

an unexpected result and requires reinvestigation of the materials by alternative methods. The enormous number of molecules in the asym unit must be a result of many subtle differences in alkyl chain and aromatic ring orientations. It is amazing that these are ordered in this way. Molecules are arranged in layers but the orientation is important: head groups are adjacent to head groups and alkyl chains are adjacent to alkyl chains.

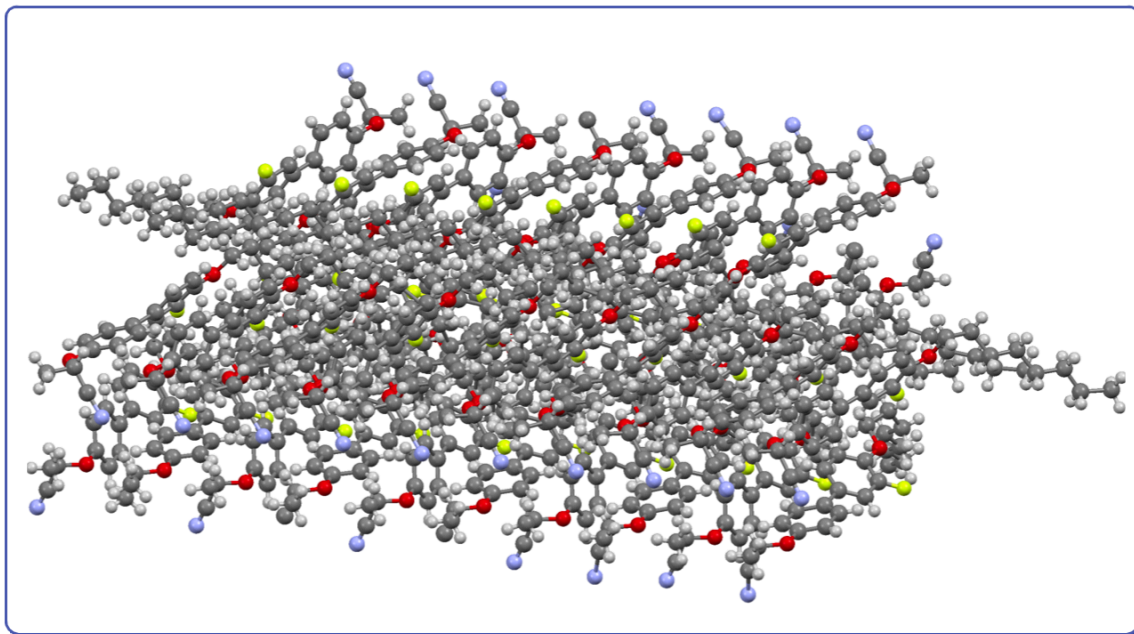


Figure 69. Molecular packing of dopant **35** in the crystal, projected along the crystallographic direction.

4.5 X-Ray Diffraction Experiments (XRD)

Small angle X-ray diffraction scattering (SAXS) is one of the most important methods for the identification of type of phases and molecular arrangements in liquid crystal phases. Limited information can be gleaned about the nematic phases from the SAXS patterns. There are only two diffuse scatterings, one at small angles related to the average longitudinal distance between the molecules and one at medium or wide angles related to the mean lateral distance between the molecules. The diffuse pattern can be analysed to obtain a value of the order parameter S , but this was not carried in our case.^{116 117}

The mesophase behaviour of compound **35** with KCHM211 host (7% w/w) has been confirmed by XRD. In the nematic phase at 110 °C two reflections are seen Figure 70. In the small angle, the reflection at 3.54 ° corresponds to a distance of 24.92 Å. In the wide angle, the diffuse reflection at 18.41 °, corresponds to a distance of 4.81 Å; this is due to the disordered nature of nematics.

Table 17. SAXS data of dopant **35** with 5,7 and 10% mixture of KCHM211.(w/w)

		Small angle		Wide angle	
Phase	Temp / °C	$2\theta / ^\circ$	D / Å	$2\theta / ^\circ$	D / Å
SmC*	23	3.6	24.5	19.4	4.6
SmA*	85	3.4	26.2	18.9	4.7
N*	110	3.5	24.9	18.4	4.8

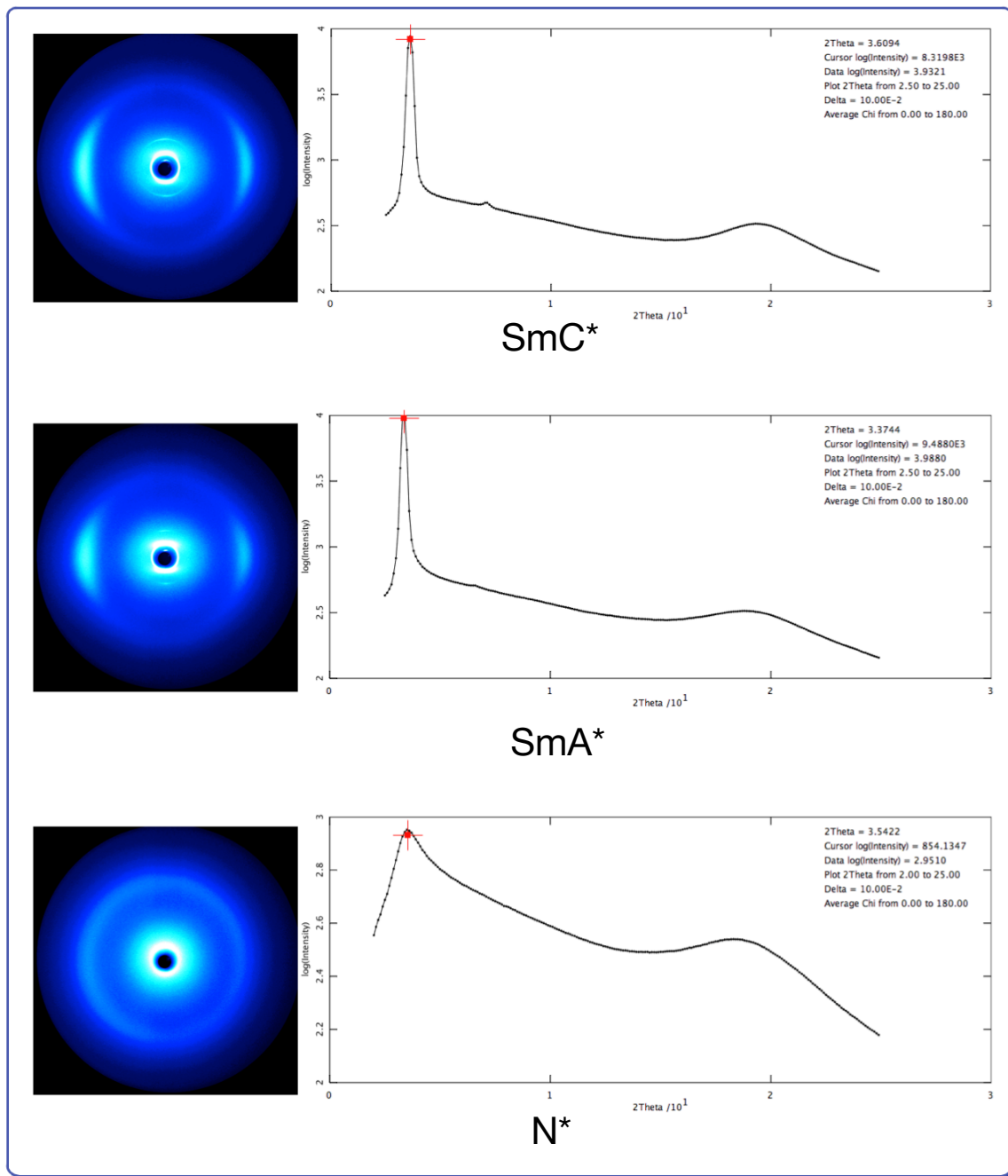


Figure 70. XRD of dopant **35** with KCHM211 (7% w/w) N* at 114.5 °C.

The XRD patterns of the SmA* and SmC* phases appear similar. The tilt of the SmC* is not seen on XRD. This could be due to the helical nature of the chiral material causing the tilt to average to zero. Thus a tilt angle was not calculated from the XRD data. However, the presence of the SmC* phase is supported by the shrinkage of the layer spacing. The maximum tilt (15 °) obtained by POM

and switching between the two ferroelectric states occurs at 30 °, although not large, it was clearly switching between two tilted states. The X-ray derived layer spacing for the SmA* phase is 26.16 Å and in the SmC* phase, it is only slightly smaller at 24.46 Å, as shown in Table 17. The phase transition of the dopant **35** with KCHM211 from SmA* to SmC* is confirmed by the observation of broken fan textures and a simultaneous change from homeotropic to Schlieren textures in POM studies and from the DSC which shows a weak reversible second order transition as shown in Figure 71.

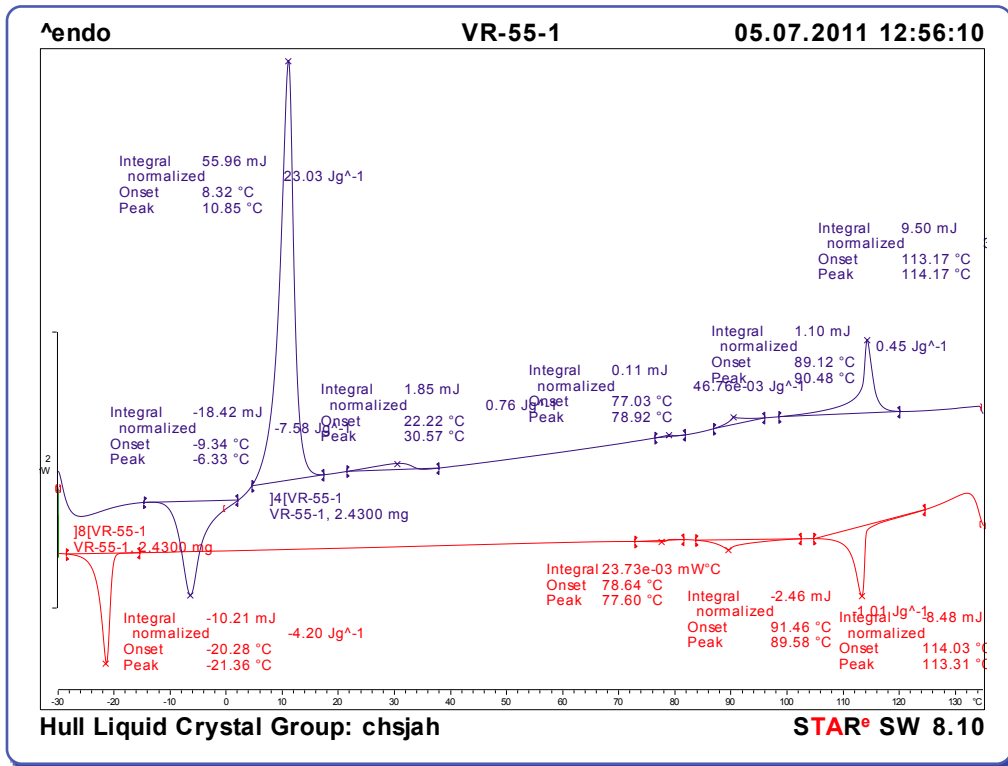


Figure 71. DSC thermograph of dopant **35** with KCHM211 (7% w/w).

5 Molecular Modeling

Computation was aimed at rationalising the unexpectedly low P_s measured for most of the chiral dopants by calculating dipole moments, as these are available from most quantum mechanical computational methods. Ultimately the aim was to measure the dipole moment of the dopant dissolved in either a non-polar solvent or a suitable nematic liquid crystal. If the experimental dipole moments were in agreement with theoretical values, it follows that the conformations were probably close to the real geometry and the values could be used to rationalise the experimental P_s data and in the future, may be used as a predictive tool. Due to time constraints, the experimental dipole moments were not measured and will have to wait until a later date. Modelling studies began with in our own laboratory, but it became apparent that collaborating with a specialist computational chemist (Dr David Benoit) would give a more rigorous investigation. The investigations are described below.

Initial dipole moment calculations used the Gaussian 09W programme and Gauss view as the graphical interface. The structures were first minimised using the MM2123 force field followed by zero point calculation on these conformers using density function theory (DFT) and Hartree Fock (HF) methods. It was decided that these conformations based on the default MM2 minimisation process carried out in the gas phase at 0K could not be assumed, with any confidence, to be global minima. Advanced calculations were then started in collaboration with Dr David Benoit in our department. The next section describes are own modelling study.

The discussion on the reasons for ferroelectricity in the SmC* phase show that dipole components along the director *ie* the principle molecular axis do not contribute to the P_s in the SmC* phase.

The following Initial method was performed:

1. Minimise the energy of the molecule by molecular mechanics
2. Refine optimum geometry using *ab initio* methods and obtain the electronic distribution
3. Calculate Dipole moment and obtain x, y and z components

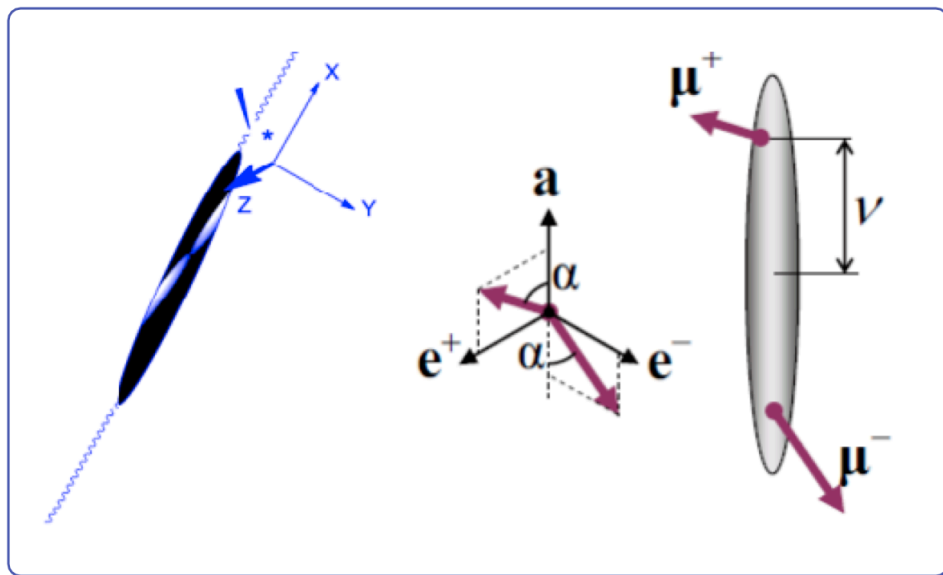
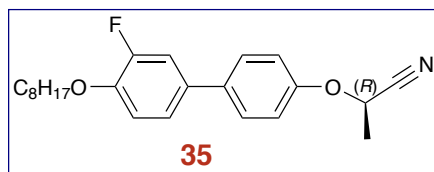


Figure 72. Schematic of a molecule with a pair of off-centre dipoles μ^\pm , which lie in orthogonal planes and determine molecular chirality, polarity and biaxiality. The orientation of the molecular hard core is defined by the unit vector \mathbf{a} . The unit vectors e^\pm denote the short dipole-related molecular axes parallel to the μ^\pm , a planes.

Initially dopant **35** was examined using molecular modeling.



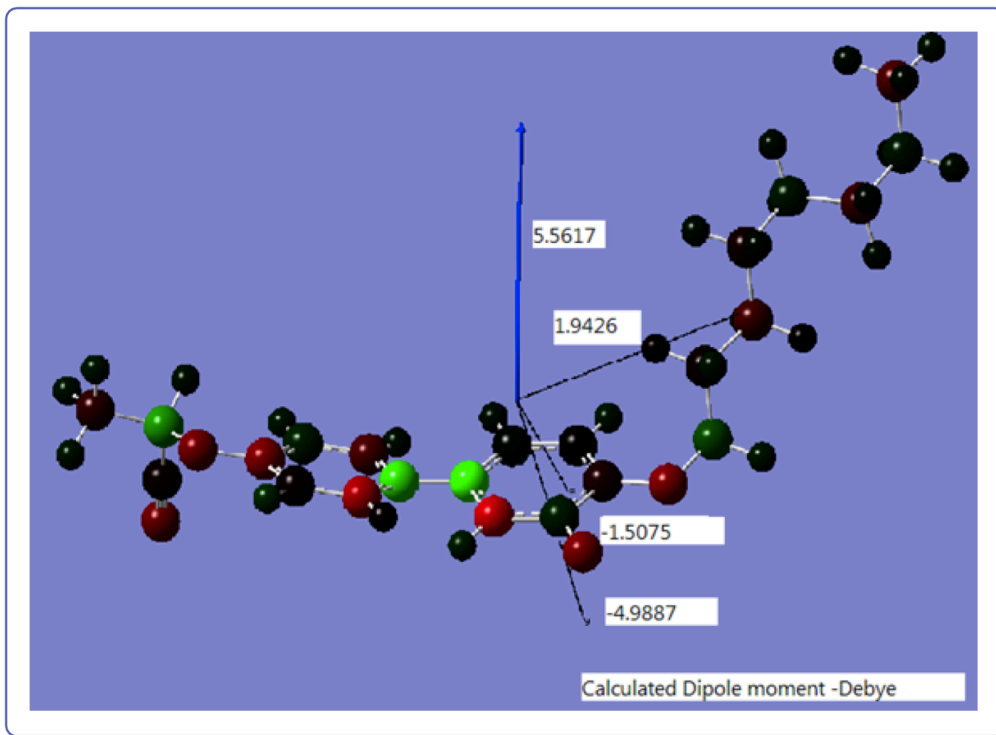


Figure 73. The colour-coded Mulliken Charge distribution of dopant **35**.

The minimum energy conformation was obtained using Gaussian 09W for dopant **35**, the ether analogue of BE8OF2N using HF method and 6-31++G (d, 2p) dataset. Figure 73 shows the calculated colour-coded Mulliken Charge distribution, the overall dipole moment and the x, y and z contributions. There is a substantial component orthogonal to the long axis of the molecule which is the main contributor to the P_s . This agrees with the moderate P_s observed for the biphenyl ether. The calculation was carried out at 0 K in the gas phase, and a more in depth investigation of conformations populations at the temperatures employed in experimental measurements was required.

5.1 Advanced Molecular Modeling

This section describes these more advanced calculations by in collaboration with Dr David Benoit. In order to determine the dipole interactions, the Open–Babel¹¹⁸ program was used and a UFF force field to generate 5000 random conformations. The initial structure was input from Chemdraw and using Lasso, a free structure selection tool into Open Babel. Each of the 5000 conformers was optimised by DFT calculations (2000 iterative steps per conformer) to produce its ideal geometry and set of coordinates. One explanation for the low *Ps* was that the ether oxygen bond dipole opposed that of the nitrile and partially cancelled out the effect of the polar group. To this end thioether analogues were also investigated. Ether groups based on oxygen are small, rigid and strongly electron withdrawing and sulphur is larger, more flexible and weakly electron withdrawing. This difference should show whether the ether oxygen played a major role in determining overall dipole moment and ultimately, the *Ps*.

Accurate determination of electronic properties required an advanced DFT method. The molecular orbitals were calculated using a series of different basis of sets of atomic orbitals and hybrid functional values, and the dipole values of the structure were determined from the resulting electron distribution.

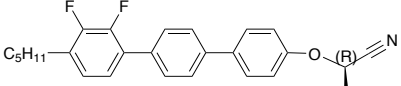
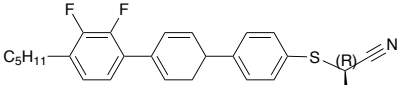
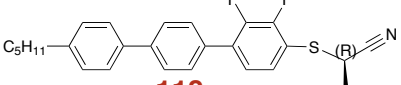
5.1.1 Calculating Dipole Moments

Using the Open–Babel program, the six different dopants structures were created in their most stable optimised energy conformations. Orca¹¹⁹ is a free general purpose quantum chemistry tool. From this and using molecular data their vector co-ordinates and dipole moment results were calculated. The XYZ co-ordinates of all atoms were viewed in Text Wrangler, a free text editor for the Mackintosh computer, in order to show the basic results.

In order to eliminate a possibility or error in the minimisation method, the following molecules **77**, **118** and **117** were re optimised to see if the results were consistent. To do this the optimised structures were used as the basis data for generating a further 5000 conformers and 2000 iterations steps to recheck the data. These results for **77**, **118** and **117** are shown in Table 18. The dopants **77**

and **117** results had similar energies to those obtained in the first optimisation so, the initial results and coordinates were used for the rest of the calculation. The two energy values were quite consistent except for compound **87** which was reduced by 5% and so this second set of results was used.

Table 18. Repeat conformational search and energy minimisation to show reproducibility.

Dopant Conformation	Lowest Energy value (I) / kJ mol^{-1}	Lowest Energy value (II) / kJ mol^{-1}	Percentage difference %
 <p style="text-align: center;">77</p>	313.142	315.804	0.850
 <p style="text-align: center;">117</p>	360.524	363.639	0.864
 <p style="text-align: center;">118</p>	362.627	346.913	4.529

Two ‘flavours’ of DFT theory were used to calculate the hybrid molecular orbitals required, namely PBE¹²⁰ and B3LYP_G.¹²¹ The latter method involves the usage of hybrid functions for more realistic orbitals. For complex structures, that possess a large variety of atoms, hybrid functions enable more realistic molecular orbitals to be created and it should follow that a more accurate electronic distribution should be obtained.

The dipole moment data for the two methods are shown in Table 19 and the graphical representation is shown in Figure 74. The trends and absolute values are consistent with the exception of the thioterphenyl analogue **77**.

Table 19. Total dipole difference between results of the two methods

Dopant	Calculation Method PBE RT Magnitude (Debye)	Calculation methods B3LYP_G Magnitude (Debyes)	Difference between results of the two methods
35	2.08	2.15	0.07 (3.37%)
77	3.13	3.38	0.25 (7.40%)
117	5.46	4.43	1.03 (18.87%)
67	4.32	4.61	0.29 (6.29%)
87	3.52	3.62	0.10 (2.84%)
118	2.42	2.44	0.02 (0.82%)

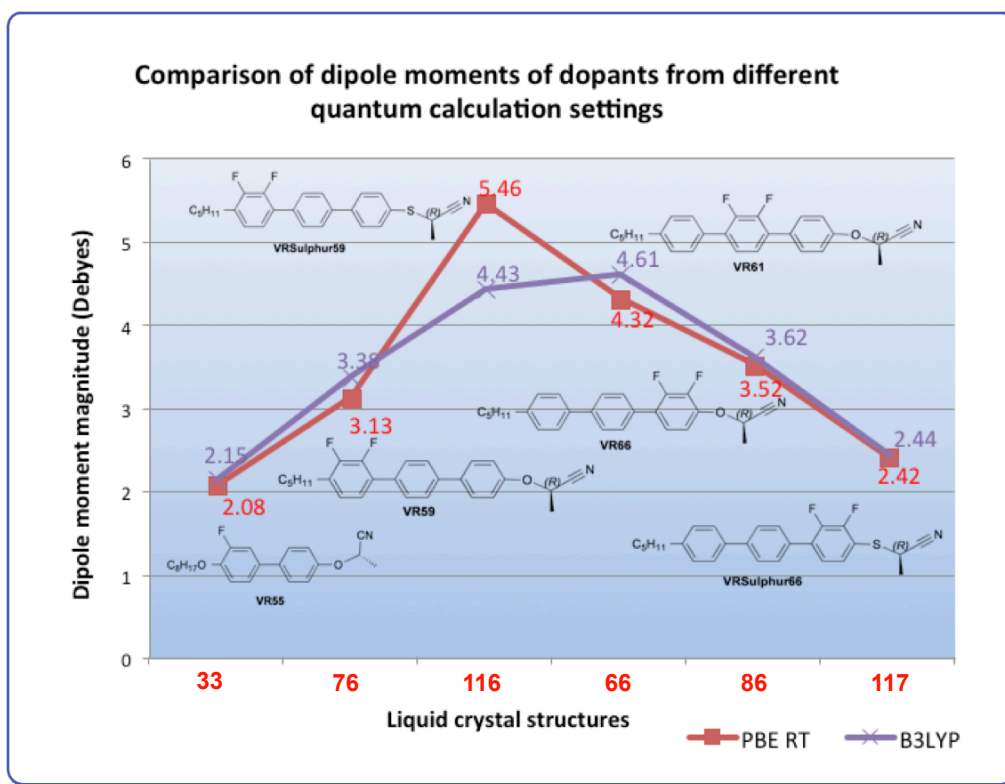


Figure 74. The total dipole moment from the two methods.

The main observation was that the trend in total dipole moment was not that of the *Ps* measurements i.e. the higher *Ps* compound **35** gave the lowest dipole moment. Sulphur atoms gave a substantially higher value over oxygen in one

case (**77**, **117**) and a substantially lower value (**87**, **118**). Thus it is difficult to make definitive conclusions, except to say that the preferred conformations in each case made a substantial difference to the dipole moment as well as the atoms in the structure.

Table 20. The lowest conformation energy values

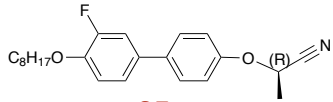
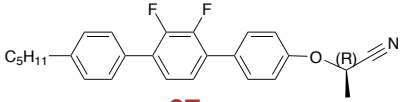
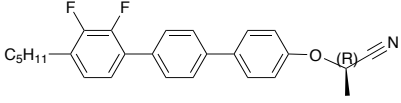
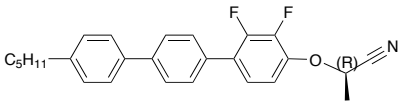
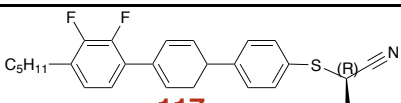
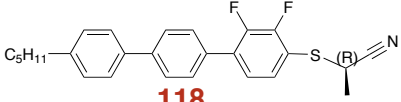
Dopant Conformation	Lowest Energy value / kJ mol^{-1}
 <p style="text-align: center;">35</p>	210.521
 <p style="text-align: center;">67</p>	333.769
 <p style="text-align: center;">77</p>	313.142
 <p style="text-align: center;">87</p>	314.895
 <p style="text-align: center;">117</p>	360.524
 <p style="text-align: center;">118</p>	362.627

Table 21 and Table 22 show the total dipole moments and the x,y and z vectors from the two DFT calculation methods. These data are used to exclude the z component and obtain the final orthogonal component of the dipole which is presented in Figure 77

Table 21. Total dipole coordinates from optimisation in XYZ vectors using PBE RT Magnitude

Dopant	Calculation Method <i>RT</i> Magnitude (Debye)	Total dipole coordinates from optimisation in XYZ vectors		
		X	Y	Z
35	2.08	-0.01672	0.59245	-0.56167
77	3.13	0.17251	-0.92187	-0.79888
117	5.46	-2.12415	-0.20773	0.22579
67	4.32	-0.08318	1.49363	0.80962
87	3.52	-1.10865	-0.77125	-0.309
118	2.42	0.08527	-0.93159	-0.17701

5.1.2 B3LYP_G Method

Table 22. Total dipole co-ordinates from optimisation in XYZ vectors using B3LYP_G Magnitude

Dopant	Calculation Method B3LYP_G Magnitude (Debye)	Total dipole coordinates from optimisation in XYZ vectors		
		X	Y	Z
35	2.15	-0.05402	0.55191	-0.63602
77	3.38	0.26842	-1.05256	-0.76432
117	4.43	-1.68328	0.16432	-0.42491
67	4.61	0.01886	1.56869	0.91009
87	3.62	-1.06648	-0.93143	-0.13382
118	2.44	0.10083	-0.95454	0.04273

5.1.3 Temperature Calculations

All the optimisations and dipole moments were carried at 0K have been determined using the two different DFT functional methods of B3LYP_G and PBE. The next step was to use this data and method at the operating temperature (300 K), when the molecules may well occupy a number of conformations.

The temperature study involved use of the program CP2K an open source molecular dynamics package. The DFT approach uses a mixed Gaussian and plane waves approach. The wave-function is described using a combination of Gaussian type orbitals, but the density is calculated on a grid. The program allows all data on the atoms of a molecule to be placed within a force field and experience change with temperature. This is an easy approach to input data and is capable of producing a wide range of results with temperature control. Once the CP2K

system was in place the structure was left to run on a 10,000 step cycle at 300K. This provides a wide range of geometries to use their coordinates to calculate the dipole moment.

Here the force field was created that allowed all the data from the molecular orbital's to be included and to go through the DFT calculations. The PM3 method acts to use Gaussian repulsion functions for the structure. This system was ideal for these liquid crystal structures. The molecules are at a temperature of 300K and are preformed at a series of step to acquire data on the molecular orbitals. Each frame was a femtosecond.

5.1.4 Molecular Dynamics Results

A realistic temperature study would be to sample a selection of the molecular dynamics conformations, and either average the dipole moments or optimise these geometries prior to averaging the dipole moments. The dipole moments from this preliminary study is given in Table 23. The main message is that the flexibility of these systems can give large changes in electron distribution. This is confirmed by viewing the structures below Figure 75, Figure 76 and Figure 78 which shows very different conformations between the molecular dynamics and the O K minimised geometries.

Table 23. Total dipole difference between results of CP2K and B3LYP_G methods

Dopant	Calculation methods- CP2K program 4000 (Debyes)	Calculation methods B3LYP_G Magnitude (Debyes)	Difference between results of the two methods
77	4.41	3.38	1.03 (23.4%)
117	3.72	4.43	0.71 (16.0%)
67	6.08	4.61	1.47 (24.2%)
87	3.73	3.62	0.11 (2.95%)
118	2.23	2.44	0.21 (8.61%)

5.1.5 Visual Comparison of Conformations from 0 K and 300 K Random Snapshots

The liquid crystals dopants **67** and **118** different conformations with different methods are shown in Figure 75 and Figure 76 respectively. The left hand picture is a snapshot taken from a molecular dynamics simulation at 300K and the right hand picture is of an optimised OK minimisation.

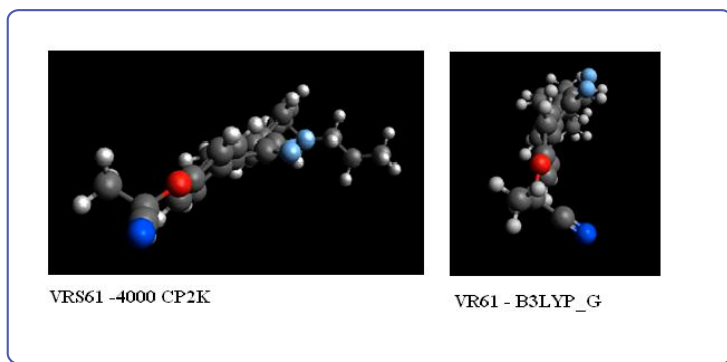


Figure 75. The dopant **67** showing different conformations obtained from minimisation and dynamics simulations at 300 K

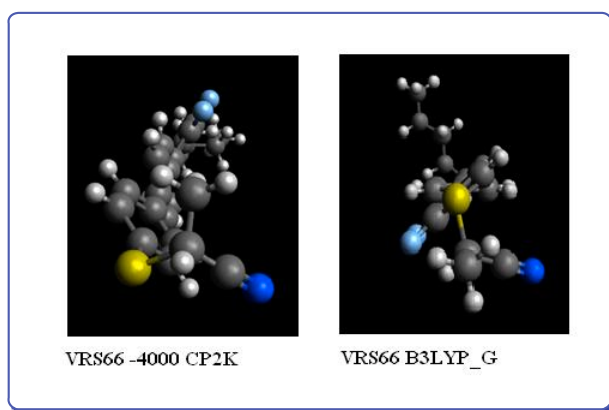


Figure 76. The dopant **87** showing different conformations obtained minimisation and dynamics simulations at 300 K

The data for the overall dipole moment gave a minimum value for the higher P_s biphenyl dopant **35**, but the component along the director, which is the molecular axis does not contribute to the P_s . The components orthogonal to the long molecular axis are key to the magnitude of P_s . Assuming that there is no preferred spatial arrangement around the C_2 axis in the SmC* phase, the components along x and y could be considered to be degenerate around the C_2 axis, as if the axes formed a disk. Thus the square roots of the sum of the squares of the x and y components should provide values that describe this disk. Figure 77 shows these results which are a very similar curve to that obtained from the total dipole moment. Figure 78 shows the axes mapped onto the molecular structures. The two dipoles orthogonal to the long axes are used to obtain the result in Figure 77

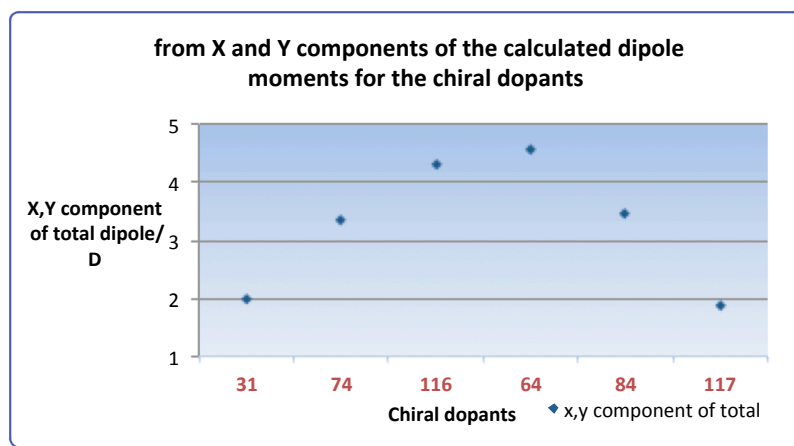


Figure 77. The dipole moment using x,y components.

There are a few explanations of this data; one is that there is no link between P_s and the transverse dipole moments but these seems unlikely. A second explanation is that at room temperature, the conformational flexibility of the dopant means that using a minimum energy conformation, no matter how carefully obtained, to calculate dipole is unrealistic. Future modelling studies could sample many conformations from a molecular mechanism simulation at a particular temperature and average the dipole moments of each conformation. That should provide a more realistic value and it would also be useful to measure dipole moments experimentally to check whether the trends followed those of modelling data.

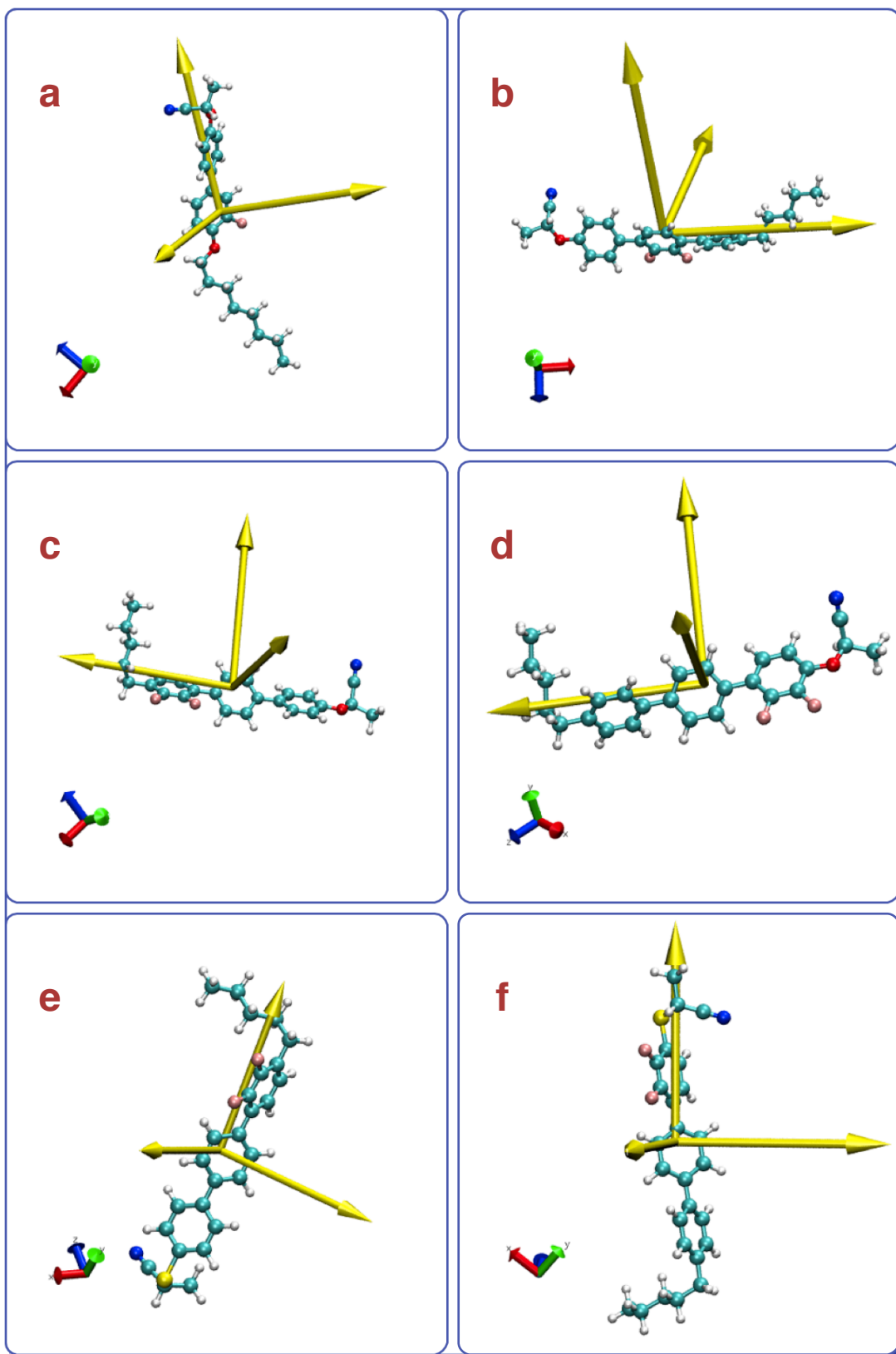


Figure 78. The dipole projection in chiral dopants a. **35**, b. **67**, c. **77**, d. **87**, e. **117** and f. **118**.

6 Conclusion

The initial aim was to synthesise a more stable chiral dopant than the ester BE8OF2N but maintain the beneficial properties, long N^* pitch and the moderately high P_s of the difluoroterphenyl based FLC mixture and if possible enhance them. The chosen targets contained an ether link to the chiral nitrile as opposed to an ester. Synthetic routes to these chiral dopants were developed and the synthetic approach required few steps, relatively low cost starting materials and was suitable for scale-up. Racemisation of the final product was considered to be of little threat and was reduced further by always attaching the chiral group in the final steps. The evidence that compound **35** Figure 79 was prepared in high ee was indirect but reasonably compelling.

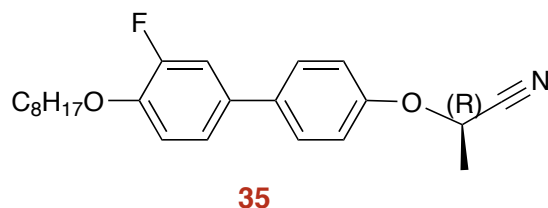


Figure 79. The biphenyl dopant **35**.

This material was doped as a 5, 7 and 10 % w/w mixture in the stable, low viscosity FLC host KCHM211. In comparison with the standard achiral host mixture, although there was still a marked reduction in transition temperatures, the reduction in the SmC^* to SmA^* transition was much lower relative to that of BE8OF2N and this result indicated that the biphenyl ester acts as a SmA^* promoter. The N^* pitch length of the 7 % mixture was 18.7° at the N^* - SmA^* transition, the maximum SmC^* tilt angle was 15° , and the P_s at $30^\circ C$ of 19.9 nC cm^{-2} were suitable for practical applications and an improvement on BE8OF2N. No stability assessment was carried out but one can assume that the ether would be an improvement over the ester.

This successful first step led us to employ the same synthetic route to prepare terphenyl dopants of the general structure which matched that of the host materials, with the aim of enhancing the upper temperature limit of the SmC^* phase. This would allow a higher percentage of dopant to be used, if necessary.

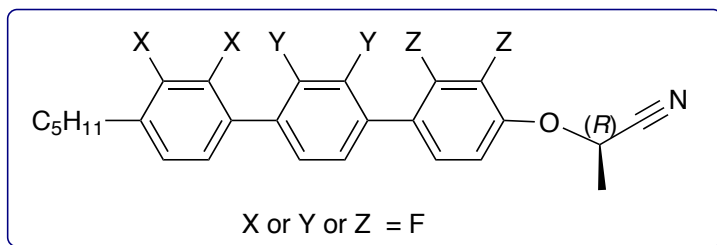


Figure 80. Difluoroterphenyl mesogenic liquid crystal dopants where X=F=**77**, Y=F=**67** and Z=F=**87**.

The individual compounds **77**, **67**, (X or Y = F) Figure 80 showed the fascinating blue phase which also indicated a high degree of chirality and therefore was further evidence that racemisation was not an issue. The example **87** (Z = F) Figure 80 with fluoro-substituents next to the chiral centre only possessed an N* phase. The phase behaviour was very promising with only a reduction of 3 °C in the SmC* - SmA* transition which confirms that a larger percentage of this dopant could be employed. The tilt angle (19.6 ° at 30 °C) and N* pitch length (18.5 ° at the N* - SmA* transition) were both suitable for FLC devices, but the maximum P_s value of compound **87** was only 5.7 nC cm⁻² at 25 °C and the values obtained from the other two examples were equally low. This was a considerable reduction in P_s from that of the biphenyl. A moderate reduction might be expected due to the increased molecular weight of the dopant and the same w/w percentage employed, however this drop was much more than predicted. It may be a true consequence of the change in molecular structure, or perhaps poor alignment, but is unlikely to be due to racemisation as the P_s values are low, but consistent. Racemisation would be expected to give almost zero P_s or would vary much more from sample to sample. A low P_s is not crucial to produce a functioning FLC material; as long as the material switches and with a high tilt angle and has the required birefringence, the material may be useful. Low viscosity and a combination of the various electric and optic properties may give acceptable FLCD performance, but switching speed will generally be lower than for high P_s materials. In addition switching may only be partial and bistability will be limited. The higher P_s biphenyl dopant **35** possessed an octyloxy chain so alkoxy version of the middle ring terphenyl dopant was prepared. In the event this material also gave a low P_s in the standard mixture (7 % w/w). SAXS was used to analyse the phase structure in more detail. The N* and SmA* diffraction-

s patterns were as expected but the SmC* phase did not show the typical tilt in the wide angle peaks, but did show a modest layer shrinkage. Helical averaging to cancel out the tilt direction may account for the SmC* phase appearing as a SmA* phase. More advanced diffraction studies are needed to confirm this hypothesis.

The unexpectedly low P_s led to an attempt to rationalise the results using molecular modelling and X-ray diffraction analysis. Advanced molecular modelling methods were used to identify the minimum energy conformation and dipole moments were calculated at room temperature using two DFT methods. Both methods gave similar results and the same trends. The non-mesogenic, higher P_s fluorobiphenyl chiral dopant **35** gave a low dipole moment (2.8 Debyes) whereas the mesogenic difluoroterphenyl chiral dopants gave higher values. Surprisingly the low dipole moment biphenyl dopant showed a higher P_s , which was the opposite of what was expected. The overall dipole moment is not directly proportional to P_s as only the component parallel to the long axis would contribute to the P_s . The dipole moments of the dopants were determined as single molecules in the gas phase whereas the P_s was measured at 7 % mixture by w/w in KCHM211. Advanced molecular modelling of the real mixtures would be one approach and it would be obtain experimental dipole moments in order to support (or not) the trends in the calculated values.

The second method employed to rationalise the P_s data was to examine the molecular geometry by single crystal X-ray diffraction. Crystal growth of these dopants was difficult, but after considerable effort, the biphenyl dopant **35** produced a crystal sufficiently good to generate a structure from which some conclusions can be drawn. Terphenyl dopants did not yield suitable crystals and so a full comparison was not possible. It turned out that the biphenyl crystal was not completely uniform, but was made of many fragments. However, a sufficiently well resolved structure was produced by Dr Prior. Careful examination of the conformation of **35** showed that the nitrile dipole was roughly orthogonal to the aromatic fluorine bond and did not oppose the ether bond. That qualitative assessment agrees with the experimentally observed moderate value of P_s .

The aim was to support the modelling results with experimental dipole moment data but time constraints made that impossible but it would be desirable to com-

plete these measurements, either in our laboratory or from collaborating with colleagues from other institutions.

A second generation of dopants were designed and synthesised. The new chiral units **100**, **103** and **106** Figure 81 had a longer branched alkyl group than the simple methyl group at the chiral centre of the first generation. This made use of amino-acids as the starting material. The chiral unit **100** where the chiral centre is one methylene farther away from the core was also selected as a potentially advantageous target, which may provide the opposite pitch length to the other dopants and therefore could be used as in a pitch compensated mixture of dopants. The chiral unit was prepared but we were unable to join it to bi- or ter - phenol cores after testing several methods including variants of the Mitsunobu reaction. This final step needs further study as the synthesis does not appear to have major drawbacks on paper.

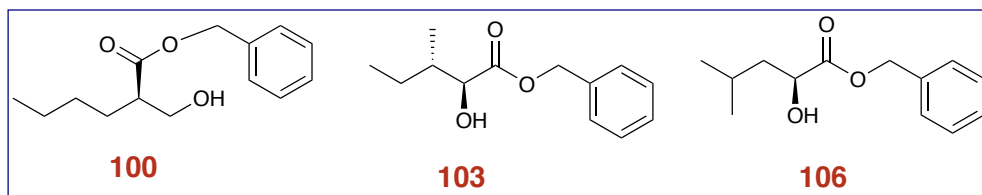


Figure 81. The new chiral units **100**, **103** and **106**.

The chiral units **103** and **106** were successfully attached to the alkyl difluoroterphenyls using the Mitsunobu reaction. The transition temperatures and phase characterisation in KCHM211 (7 % w/w) were determined by POM and DSC. The electrooptics results were similar to those of first generation difluoroterphenyls.

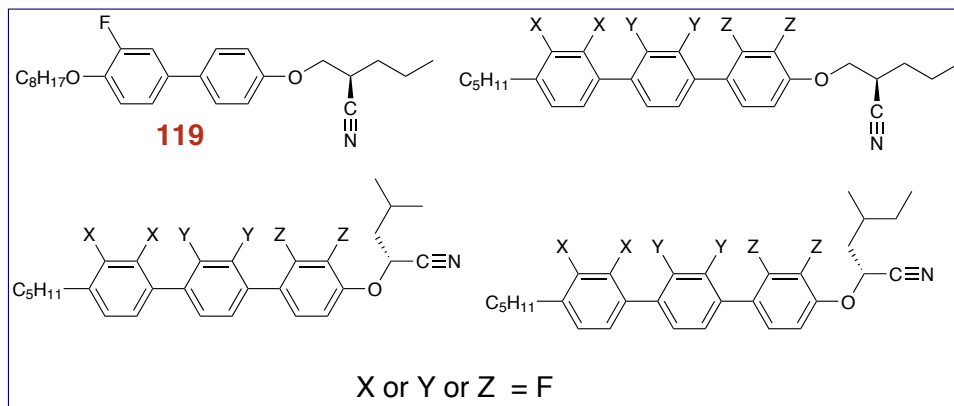


Figure 82. The targeted new chiral dopants.

In conclusion, this new family of dopants Figure 82 with a chiral cyano group linked *via* an ether has been synthesized for use in FLC mixtures and electro optic studies carried out. The phase behaviour and electro optic properties of the biphenyl analogue and the one terphenyl example so far studied show promise, but there is a question mark over the low P_s value of the terphenyls.

7 Experimental

7.1 General Instrumentation and Techniques

7.1.1 ^1H , ^{13}C and ^{19}F Nuclear Magnetic Resonance(NMR)

NMR were recorded on a Jeol JNM ECP400 or a Jeol JNM LA-400 spectrometer, with TMS $\delta_H = 0$ as the internal standard or residual protic solvent [CDCl_3 , $\delta_H = 7.26$; $(\text{CD}_3)_2\text{SO}$, $\delta_H = 2.50$]. Chemical shifts are given in ppm (δ) and coupling constants J are given in Hertz (Hz). Peak types in the spectra are denoted by the following notations: singlet (s), doublet (d), triplet (t), quartet (quin) and multiplet (m). ^1H -NMR were recorded at 400 MHz; ^{13}C -NMR recorded at 100.5 MHz with the central peak of CDCl_3 ($\delta_C = 77.0$ ppm) as the internal reference; ^{19}F were recorded at 376 MHz, reference CFCl_3 $\delta_F = 0$ ppm.

7.1.2 Infrared Spectrometry

Infrared spectroscopy was useful for the confirmation of certain groups. The analysis was carried-out using a Nicolet 380 FT-IR spectrometer with Smart Orbit, Diamond ATR. Analyses were carried out using EZ OMNIC software. Some samples required preparation in KBr discs.

7.1.3 Mass Spectrometry

The mass spectrometer used for analysis was a Shimadzu GCMS-QP5050A gas chromatography mass spectrometer with Electron Impact (EI) at a source temperature of 200 °C. Results are quoted where M^+ represents the molecular ion of the material.

7.1.4 Chromatography

The progress of reactions was frequently monitored by thin layer chromatography (TLC) and capillary gas chromatography (GC). Aluminium backed TLC

plates coated with silica gel (60 F₂₅₄ Merck) were utilised. GC was carried out using a Varian CP3800 gas chromatograph equipped with a 10 m CP-SIL 5CB column. Purification of intermediates and final products was mainly accomplished by column chromatography, using silica gel 60 (230 - 400 mesh). The purity of the final products was normally confirmed by elemental analysis using a Fisons EA 1108 CHN.

7.1.5 Purity of Intermediates and Final Compounds

The purity of the majority of the reaction intermediates was checked by gas chromatography using a chromopack CP3800 capillary gas chromatograph fitted with a CP-SIL 5CB capillary column. The purity of the intermediates was found to be >95%.

7.1.6 Melting Points and Transition Temperatures

The melting point and other transition temperatures for each compound were measured using a Mettler DSC822e with STARe software calibrated with indium (156.6 °C 28.45 J/g) and zinc (419.47 °C), checked daily with indium \pm 0.3 °C. The reference, an empty aluminium pan was used to calculate the enthalpies of transition for materials exhibiting liquid crystalline phases and to confirm the melting points and transition temperatures of all final products. Thermal polarising microscopy to identify liquid crystal phase was carried out using an Olympus BH2 polarising microscope, Mettler FP52 and FP82 heating stage and controller and Photos- Nikon INFINITY little, Olympus U-PMT VC, JVC TK-C1481 colour video cameras using Mettler Studio Capture software. Samples were prepared as thin films between a glass slide and a glass cover slip.

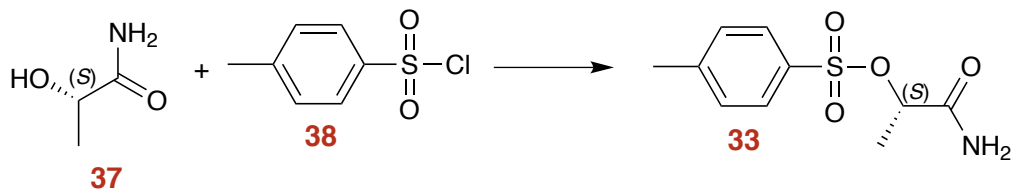
7.2 Reagents and Reaction Solvents

Some intermediates were supplied from Kingston chemicals and others were purchased from Acros Organics, Avocado, Aldrich and Fisher and were used

without further purification. Anhydrous solvents such as THF, ether and DMF were purchased from Aldrich.

7.3 Experimental Procedures

7.3.1 (S)-1-Amino-1-oxopropan-2-yl 4-methylbenzenesulfonate — 33

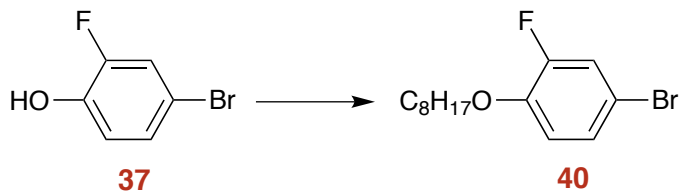


4-Methylbenzene-1-sulfonyl chloride, **37** (64.24 g, 0.34 mol), N,N - diisopropylethylamine, **38** (43.54 g, 0.33 mol) and dimethylaminopyridine (3.43 g, 0.03 mol) were added sequentially to a stirred mixture of (S)-lactamide (25.0 g, 0.28 mol) in dry DMF (300 ml) at 0 °C. The stirred mixture was allowed to warm to room temperature overnight and the solvent was removed and the product was partitioned between ethyl acetate and 2M sodium carbonate (2 x 50 ml). The ethyl acetate extract was washed with water (2 x 100 ml), dil HCl (2 x 100 ml) and brine (2 x 100 ml) solution and dried over magnesium sulphate. The solvent was removed and the crude product was purified by column chromatography (silica gel; hexane-ethyl acetate: 3:1) and recrystallised from cyclohexane, ethyl acetate (8:2) to yield colourless crystals of the tosylate, **33**.¹²²

Yield: 25 g, 38 %

δ^H : 1.44 (3H, d, J 7.0, CH_3CH), 2.47 (3H, s, ArMe), 4.85 (1H, q, J 7.0, $CHCH_3$), 5.76 (1H, b s, NH), 6.32 (1H, b s, NH), 7.38 (2H, d, J 8.1, ArH) and 7.81 (2H, d, J 8.1, ArH)

7.3.2 4-Bromo-2-fluoro-1-(octyloxy)benzene — 40



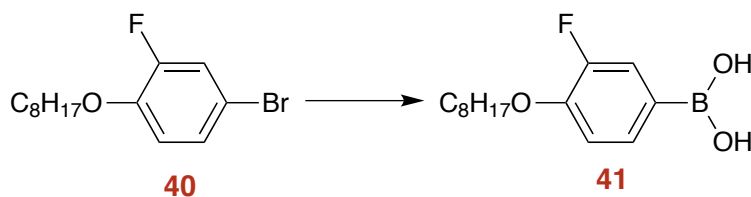
4-Bromo-2-fluorophenol, **121** (30.00 g, 0.16 mol), bromobutane (30.33 g, 0.16 mol) and K_2CO_3 (64.99 g, 0.47 mol) in butanone (250 ml) were heated under reflux for 24 h. The K_2CO_3 was removed by filtration and the solvent removed under vacuum. The crude product was purified by column chromatography (silica gel, 5:1 hexane/ DCM). The solvent was removed to yield a white solid, **122**.¹²³

Yield: 55.89 g, 92 %.

Boiling point = 130.0 °C (bp 140-142 °C *Lit*)¹²³

δ^H : 0.87 (3H, t, *J*, 6.6, CH_3), 1.29 (8H, m, 4 X CH_2), 1.44 (2H, quin, *J* 8.1, CH_2), 1.79 (2H, t, *J* 6.9, CH_2), 3.95 (2H,t, *J* 6.5, CH_2), 6.79 (1H, t, *J* 8.8, 6-*H*), 7.13 (1H, ddd, *J* 8.8, 2.2, 1.5, *ArH*) and 7.19 (1H, dd, *J* 10.3, 2.2, 3-*H*)

7.3.3 3-Fluoro-4-((octyloxy)phenyl)boronic acid – **41**



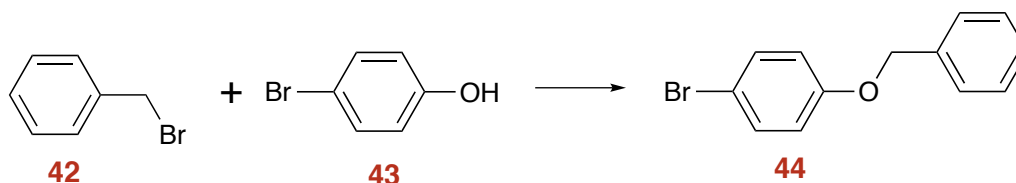
4-Bromo-2-fluoro-1-(octyloxy)benzene **40** (30.00 g, 0.1 mol) in THF (350 mL) and under nitrogen was cooled to -78 °C. 2.5 M *n*-BuLi (44.00 mL, 0.11 mol) was added dropwise ensuring that the temperature was below -60 °C. After complete addition of 2.5 M *n*-BuLi the reaction was stirred for 1 h at -78 °C. Trimethylborate (60.65 g, 0.20 mol) was added dropwise while ensuring that the temperature was below -60 °C. The reaction was stirred for 1 h at -78 °C before being allowed to warm to room temperature overnight. 10 % HCL was added and the solution stirred for 1 h. Product was extracted into ether and washed with water and brine. The organic extract was dried over $MgSO_4$, filtered and the solvent removed under reduced pressure. The crude product was stirred in hexane (water added to remove anhydride) for 1 h. Solid white powder filtered off yielding boronic acid, **41**.¹²⁴

Yield: 27 g, 70 %

Melting point = 158.9 °C (bp 132 – 135 °C *Lit*)¹²⁴

δ^H : 0.86 (3H, t, J 6.6, CH_3), 1.3 (8H, m, 4 X CH_2), 1.44 (2H, quin, J 8.2, CH_2), 1.79 (2H, t, J 6.9, CH_2), 3.95 (2H, t, J 6.5, CH_2), 6.76 (1H, t, J 8.8, ArH), 7.15 (1H, ddd, J 8.8, 2.2, 1.56, ArH), 7.22 (1H, dd, J 10.3, 2.2, ArH) and 8.05 (2H, b s)

7.3.4 1-(Benzyloxy)-4-bromobenzene — 44



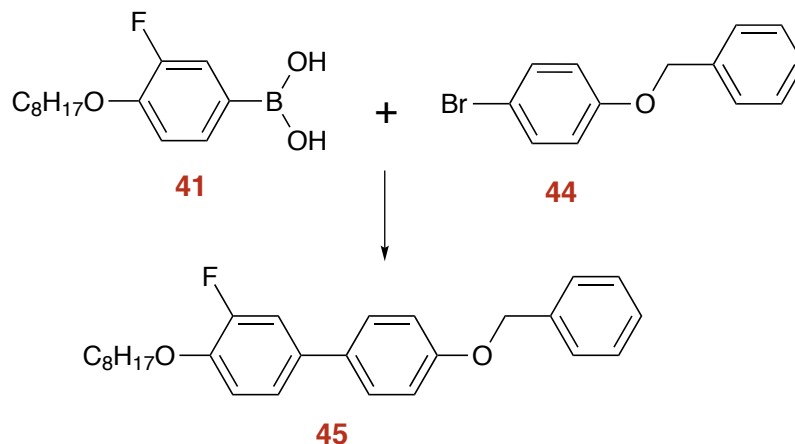
Bromomethyl benzene **42** (25.0 g, 0.15 mol), 4-bromophenol **43** (25.28 g, 0.15 mol) and potassium carbonate (60.48 g, 0.45 mol) was stirred in butanone (300 ml) at 80 °C under dry nitrogen. The reaction mixture was heated under reflux overnight. After confirming the completion of reaction by GLC and filtering off the potassium carbonate using a sintered glass crucible; the reaction mixture was washed with 10% NaOH a (100ml x 2) and the product was extracted into ether (x2). The combined ethereal extracts were washed with brine (100ml x 2), dried over magnesium sulphate and the solvent was removed. The compound was recrystallised from methanol.¹²⁵

Yield: 34.30 g, 85 %

Melting point : 60-63 °C (mp 61-63 °C *Lit*)

δ^H : 5.04 (2H, s, CH_2), 6.86 (2H, m, ArH) and 7.38 (7H, m, ArH)

7.3.5 4'-(Benzyloxy)-3-fluoro-4-(octyloxy)-1,1'-biphenyl — 45



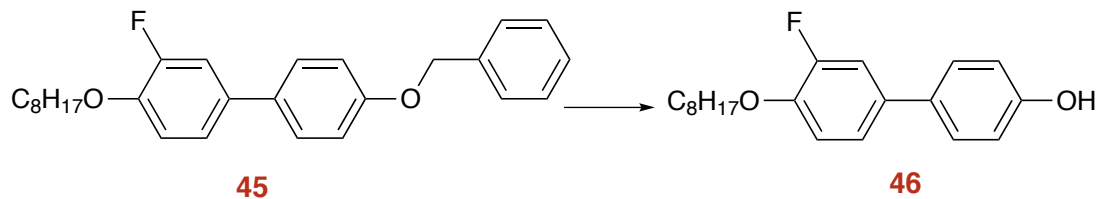
1-(Benzyloxy)-4-bromobenzene **44** (0.8 g, 0.003 mol), DME (20 ml) and sodium carbonate (20 ml, 2M) aqueous solution was stirred under dry nitrogen, evacuated and flush through with nitrogen. Tetrakis (triphenylphosphine) palladium (0.035g 0.00003 mol) was added, the reaction mixture was evacuated and filled with nitrogen. (3-Fluoro-4-(octyloxy) phenyl) boronic acid (1.16 g, 0.0043 mol) was added, and the reaction mixture was heated under reflux for overnight. After confirming the completion of reaction by GC, and allowing to cool copious and water, and the product was extracted into ether (x2). The combined organic extracts were washed with brine (20 ml x 2), dried over magnesium sulphate and the solvent was removed. The obtained white solid compound 4'-(benzyloxy)-3-fluoro-4-(octyloxy)- 1,1'-biphenyl **45** was recrystallised from ethanol and toluene.

Yield: 1.2 g, 95 %

Melting point : 60-63 °C

δ^H : 0.87 (3H, t, J 6.9, CH_3), 1.3 (8H, m, 4 X CH_2), 1.48 (2H, quin, J 7.2, CH_2), 1.82 (2H, quin, J 7.3, CH_2), 4.05 (2H, t, J 6.6, CH_2), 5.1 (2H, s, CH_2), 6.98 (1H, d, J 7.0, ArH), 7.03 (1H, d, J 8.8, ArH), 7.22 (1H, ddd, J 8.5, 2.1, 1.0, ArH), 7.3 (1H, m, ArH), 6.98 (1H, d, J 7.0, ArH), 7.35 (1H, d, J 7.1, ArH), 7.39 (1H, d, J 5.9, ArH), 7.41 (1H, d, J 7.0, ArH) and 7.45 (4H, m, ArH)

7.3.6 3'-Fluoro-4'-(octyloxy)-[1,1'-biphenyl]-4-ol — 46

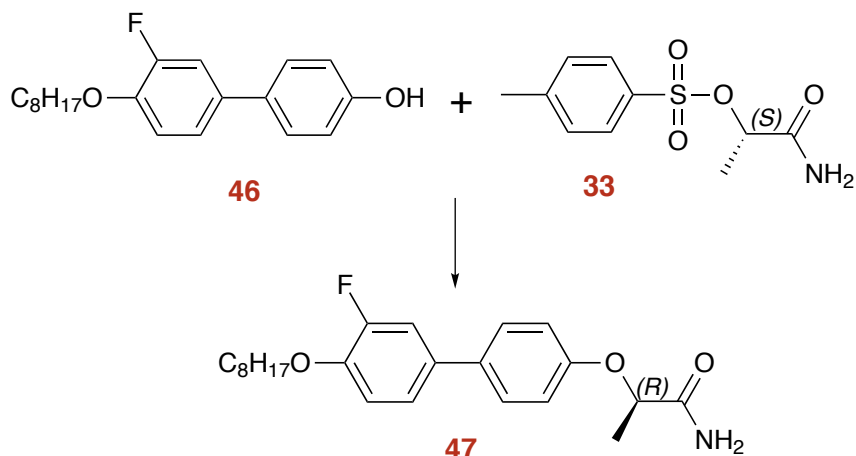


A suspension of Pd/C in a solution of **45** (1.94 g, 0.0048 mol) in ethyl acetate (100 ml) in a Parr hydrogenator was evacuated using a vacuum pump and flushed with hydrogen gas repeated the process for three times, the reaction was maintained in an atmosphere of hydrogen overnight with constant mixing unit. TLC was used to check for the completion of the reaction. The mixture was then filtered through high flow and solvent removed under reduced pressure to afford a white solid powder. The product was re-crystallised with methanol to afford white crystals as product. **46**.

Yield: 1.31 g, 87 %

δ^H : 0.89 (3H, t, J 7.00, CH_3CH_2), 1.31 (8H, m, 4 X CH_2CH_3), 1.15 (2H, quin, J 7.7, CH_2CH_2), 1.82 (2H, quin, J 6.9, CH_2CH_2), 4.05 (2H, t, J 6.6, CH_2O), 4.94 (1H, b s, HO), 6.88 (1H, d, J 8.7, ArH), 6.99 (2H, t, J 8.6, ArH), 7.21 (1H, ddd, J 8.4, 2.1, 1.3, ArH), 7.25 (1H, dd, J 12.6, 2.0, ArH) and 7.4 (2H, d, J 8.7, ArH)

7.3.7 (*R*)-2-((3'-Fluoro-4'-(octyloxy)-[1,1'-biphenyl]-4-yl)oxy)propanamide —
47



3'-Fluoro-4'-(octyloxy)-[1,1'-biphenyl]-4-ol **46** (1.2 g, 0.0079 mol) was added to a solution of potassium carbonate (3.89 g, 0.028 mol), potassium iodide (0.1 g) in DMF (50 ml) under dry nitrogen. This mixture was stirred for 15 min at 80 °C and (*S*)-1-amino-1-oxopropan-2-yl 4-methylbenzenesulfonate **33** (1.02 g, 0.0042 mol) was added and stirring was continued overnight. After confirming the completion of reaction by GLC, the cooled reaction mixture was poured into ice cooled water. The precipitate was filtered using sintered glass crucible, and dried in a desiccator using a vacuum pump. The crude compound was recrystallised from methanol and purified by column chromatography (silica gel; hexane-ethyl acetate, 8:2) to give a colourless solid of the (*R*)-2-((3'-fluoro-4'-(octyloxy)-[1,1'-biphenyl]-4-yl)oxy)propanamide **47**.

Yield: 0.74 g, 50 %.

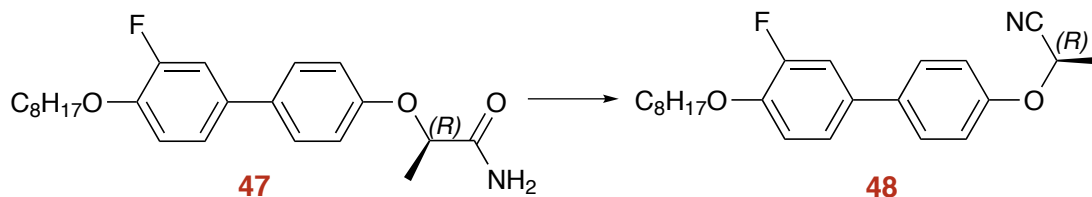
Melting point: 195.0 °C

Optical Rotation $[\alpha]_D^{21} = -0.12.75$ (c 0.008 in DCM)

δ^H : 0.89 (3H, t, *J* 6.8, CH₃CH₂), 1.31 (8H, m, 4 X CH₂CH₃), 1.48 (2H, quin, *J* 7.5, CH₂CH₂), 1.62 (3H, d, *J* 6.8, CH₂CH), 1.82 (2H, quin, *J* 7.8, CH₂CH₂), 4.05 (2H, t, *J* 6.6, CH₂O), 4.70 (1H, q, *J* 6.8, HCH₃), 5.6 (1H, b s, HN), 6.41 (1H, b s, HN), 6.96 (2H, d, *J* 8.7, ArH), 6.99 (1H, t, *J* 8.6, ArH), 7.21 (1H, ddd, *J* 8.5, 2.2, 0.9, ArH), 7.26 (1H, dd, *J* 12.5, 2.2, ArH) and 7.46 (2H, d, *J* 8.8, ArH)

δ^C : 14.1, 18.7, 22.7, 26.0, 29.3, 29.4, 31.9, 69.7, 75.0, 114.4, 114.6, 115.2, 115.8, 122.2, 128.1, 133.6 (1C, d, J 6.45), 146.4 (1C, d, J 10.9), 151.7, 154.1, 156.4 and 174.9 δ^F : -134.13 (dd, J 11.8, 9.1)

7.3.8 (*R*)-2-((3'-Fluoro-4'-(octyloxy)-[1,1'-biphenyl]-4-yl)oxy)propanenitrile — 48



POCl_3 (2.36 g, 0.015 mol) was added to dry DMF (25 ml) at 0°C , with stirring the mixture under dry nitrogen and allowed to attain 0°C (the colour of the solution became orange), and add (*S*)-2-((3'-fluoro-4'-(octyloxy)-[1,1'-biphenyl]-4-yl) oxy)propanamide (0.6 g, 0.0015 mol) was added. The reaction mixture temperature was maintained from 0°C for 10 min, and then allowed to attain the room temperature. The cooled reaction mixture was poured into ice cooled water. The precipitate was filtered using a sintered glass crucible, dried and in a desiccator using vacuum pump. The compound was micro-filtered with ethyl acetate and recrystallised from ethyl acetate.

Melting point: 85.5°C

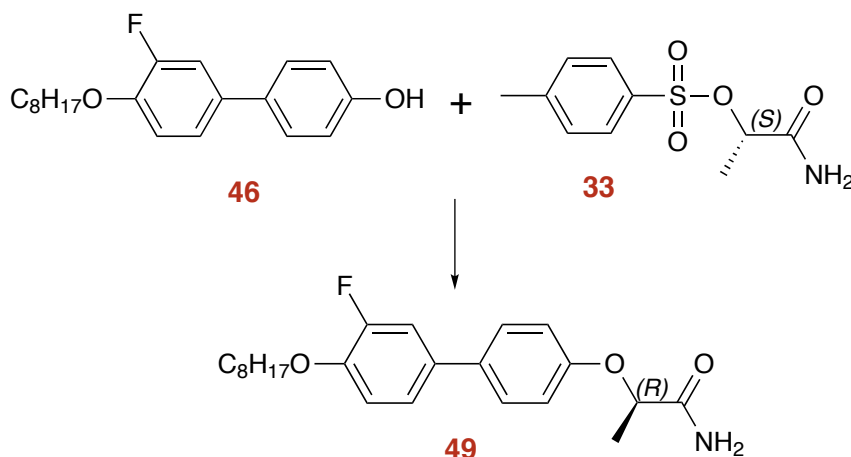
Optical Rotation $[\alpha]_D^{20} = -4.76$ (c 0.015 in DCM)

δ^H : 0.88 (3H, t, J 6.8, CH_3CH_2), 1.32 (8H, m, 4 X CH_2CH_3), 1.48 (2H, quin, J 7.00, CH_2CH_2), 1.82 (3H, d, J 6.8, CH_2CH), 1.83 (2H, quin, J 6.8, CH_2CH_2), 4.06 (2H, t, J 6.6, CH_2O), 4.90 (1H, q, J 6.8, HCH_3), 7.00 (1H, t, J 8.60, ArH), 7.06 (2H, d, J 8.8, ArH), 7.23 (1H, ddd, J 8.4, 2.1, 1.0, ArH), 7.28 (1H, dd, J 12.5, 2.2, ArH), and 7.50 (2H, d, J 8.8, ArH)

δ^C : 14.2, 20.0, 22.7, 26.0, 29.3, 29.4, 39.9, 62.6, 69.6, 114.5, 114.7, 115.1, 116.2, 118.2, 122.4, 128.1, 135.5 (1C, d, J 6.8), 135.0, 146.5 (1C, d J 10.8) 152.9 (1C, d, J 245.4, CF) and 155.7

δ^F : -134.11 (dd, J 12.0, 9.3)

7.3.9 (*R*)-2-((3'-Fluoro-4'-(octyloxy)-[1,1'-biphenyl]-4-yl)oxy)propanamide —
49



Quantities:

3'-Fluoro-4'-(octyloxy)-[1,1'-biphenyl]-4-ol **46**, (0.5 g, 0.0016 mol)

Potassium carbonate, (0.47 g, 0.017 mol)

DMF, (10 ml)

(S)-1-Amino-1-oxopropan-2-yl 4-methylbenzenesulfonate **123**, (1.02 g, 0.0042 mol)

The experimental procedure was as described for the preparation of compound **47** without potassium iodide to give a white solid of (*R*)-1-amino-1-oxopropan-2-yl 4-methylbenzenesulfonate **49**.

Yield: 0.60 g, 98 %.

Melting point: 159.0 °C

Optical Rotation $[\alpha]_D^{19} = -12.75$ (c 0.021 in DCM)

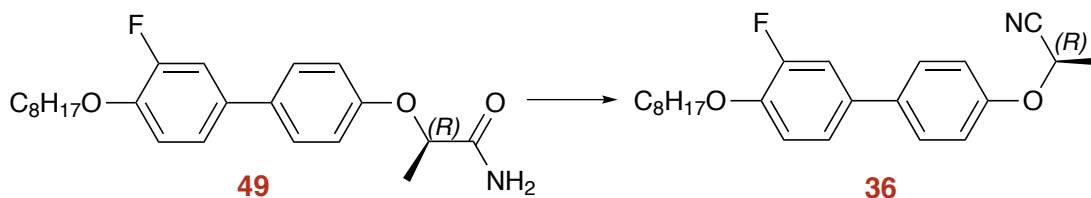
δ^H : 0.89 (3H, t, J 6.8, CH_3CH_2), 1.31 (8H, m, 4 X CH_2CH_3), 1.48 (2H, quin, J 7.5, CH_2CH_2), 1.62 (3H, d, J 6.8, CH_3CH), 1.82 (2H, quin, J 7.8, CH_2CH_2), 4.05 (2H, t, J 6.6, CH_2O), 4.70 (1H, q, J 6.8, HCH_3), 5.6 (1H, b s, HN), 6.41 (1H, b s, HN), 6.96 (2H, d, J 8.7, ArH), 6.99 (1H, t, J 8.6, ArH), 7.21 (1H, ddd, J 8.5, 2.2, 0.9, ArH), 7.26 (1H, dd, J 12.5, 2.2, ArH) and 7.46 (2H, d, J 8.8, ArH)

δ^C : 14.1, 18.7, 22.7, 26.0, 29.3, 29.4, 31.9, 69.7, 75.0, 114.4, 114.6, 115.2, 115.8, 122.2, 128.1, 133.6 (1C, d, J 6.45), 146.4 (1C, d, J 10.9), 151.7, 154.1, 156.3

and 174.9

δ^F : -134.13 (dd, J 11.8, 9.1)

7.3.10 (R)-2-((3'-Fluoro-4'-(octyloxy)-[1,1'-biphenyl]-4-yl)oxy)propanenitrile
— **36**



Quantities:

POCl_3 , (0.55 g, 0.036 mol)

DMF, (15 ml)

(R)-2-((3'-Fluoro-4'-(octyloxy)-[1,1'-biphenyl]-4-yl)oxy)propanamide, (0.14 g, 0.0036 mol)

The experimental procedure was as described for the preparation of compound **48** to give a white solid of (R)-1-amino-1-oxopropan-2-yl 4-methylbenzenesulfonate **36**.

Yield: 60.00 mg, 46 %

Melting point: 85.5 °C

Optical Rotation $[\alpha]_D^{21} = + 39.04$ (c 0.008 in DCM)

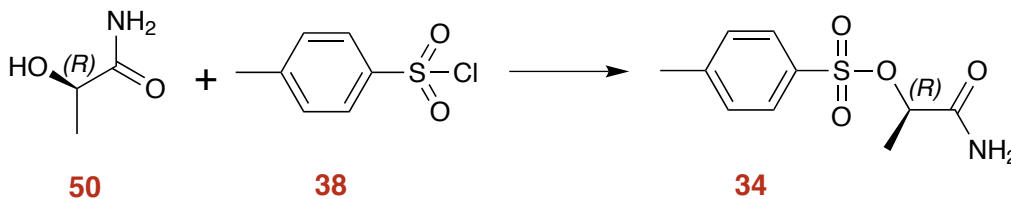
δ^H : 0.88 (3H, t, J 6.8, CH_3CH_2), 1.32 (8H, m, 4 X CH_2CH_3), 1.48 (2H, quin, J 7.00, CH_2CH_2), 1.82 (3H, d, J 6.8, CH_3CH), 1.83 (2H, quin, J 6.8, CH_2CH_2), 4.06 (2H, t, J 6.6, CH_2O), 4.9 (1H, q, J 6.8, HCH_3), 7.00 (1H, t, J 8.6, ArN), 7.06 (2H, d, J 8.8, ArH), 7.23 (1H, ddd, J 8.4, 2.1, 1.0, ArH), 7.28 (1H, dd, J 12.5, 2.2, ArH) and 7.50 (2H, d, J 8.8, ArH)

δ^C : 14.2, 20.0, 22.7, 26.0, 29.3, 29.4, 31.9, 62.6, 69.9, 114.5, 114.7, 115.1, 116.2, 118.2, 122.4, 128.1, 133.5 (1C,d, J 6.8), 135.0, 146.5 (1C, d, J 10.8), 152.9 (1C, d, J 245.4, CF), 155.7

δ^F : -134.11 (dd, J 12.0, 9.3)

CHN elemental analysis: (Found: C, 74.58; H, 7.75; N, 3.95. C₂₃H₂₈FNO₂ requires C, 74.77; H, 7.64; N, 3.79%)

7.3.11 (*R*)-1-Amino-1-oxopropan-2-yl 4-methylbenzenesulfonate — 34



Quantities:

4-Methylbenzene-1-sulfonyl chloride **37**, (25.70 g, 0.13 mol)

N,N-diisopropylethylamine **38**, (17.42 g, 0.13 mol)

Dimethylaminopyridine, (1.37 g, 0.01 mol)

Dichloromethene, 100 ml

The experimental procedure was as described for the preparation of compound **33** to give a white solid of (*R*)-1-amino-1-oxopropan-2-yl 4-methylbenzenesulfonate **34**.

Yield: 24.27g, 88 %

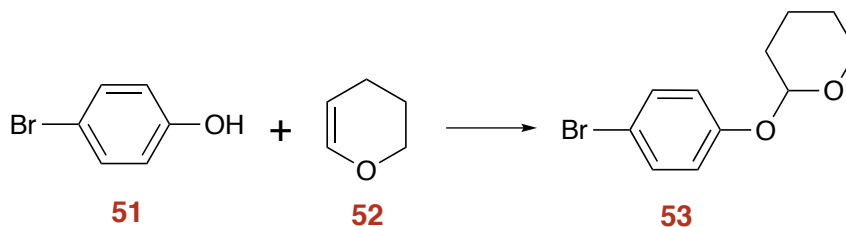
Optical Rotation $[\alpha]_D^{19} = + 47.5$ (c 0.0192 in DCM)

δ^H : 1.44 (3H, d, *J* 6.9, CH₃CH), 2.46 (3H, s, ArMe), 4.85 (1H, q, *J* 6.9, CHCH₃), 5.72 (1H, b s, NH), 6.31 (1H, b s, NH), 7.37 (2H, d, *J* 8.6, ArH) and 7.81 (2H, d, *J* 8.4, ArH)

δ^C : 18.5, 21.1, 127.9, 130.2, 132.9, 145.7, 171.4

V_{max}/cm^{-1} : 3416 (N-H), 3175, 3175, 1632, 1449, 1337, 1177, 924, 813.

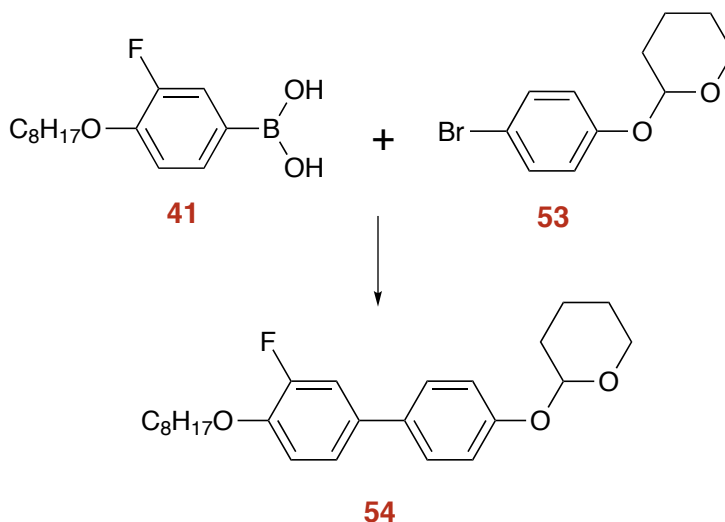
7.3.12 2-(4-Bromophenoxy)tetrahydro-2H-pyran — 53



4-Bromophenol (10.0 g, 0.0304 mol) and 2-3 small crystals of PTSA were added to excess of 3,4 dihydro-2H-pyran (50 ml) at room temperature, stirring under dry nitrogen for 2 h. The reaction was quenched by the addition of 5% NaOH aqueous solution and stirring was continued for another 30 min. After confirming the completion of reaction by GLC, the mixture was extracted into ether (x2). The combined ethereal extracts were washed with water, dried over (Na_2SO_4) and the solvent was removed. The compound was purified by column chromatography (hexane; ether 95:5) to give a white solid of the THP protected phenol 2-(4-bromophenoxy)tetrahydro-2H-pyran **53**.¹²⁶

Yield: 12.68 g, 85 %. (*Lit* 100%)

7.3.13 2-((3'-Fluoro-4'-(octyloxy)-[1,1'-biphenyl]-4-yl)oxy)tetrahydro-2H-pyran — 54



Quantities:

2-(4-Bromophenoxy)tetrahydro-2H-pyran, (15.6g 0.085 mol)

n-Butyllithium, (2.5 M in hexane , 34 ml, 0.085 mol)

Trimethyl borate, (13.3 g, 0.13 mol)

HCl (10 %), (100 ml)

THF, (200 ml)

The experimental procedure was as described for the preparation of compound **41** to give a white solid.¹²⁷

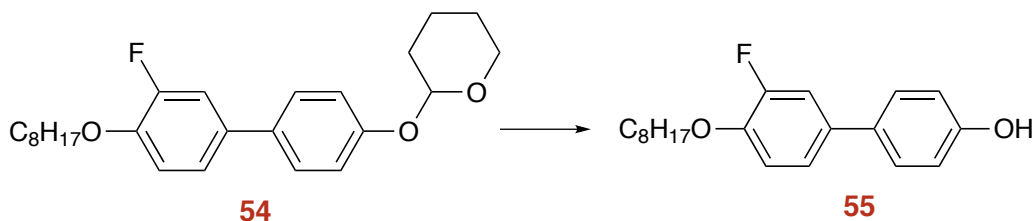
Yield: 14.2 g, 62 %

δ^H : 0.88 (3H, t, *J* 8.0, CH_3CH), 1.33 (9H, m, CH_2CH_3), 1.47 (2H, quin, *J* 7.1, CH_2CH_2), 1.66 (2H, m, CH_2CH_2), 1.85 (2H, quin, *J* 7.9, CH_2CH_2), 1.88 (2H, m, CH_2CH_2), 2.02 (1H, m, PyH), 3.62 (1H, m, PyH), 3.93 (1H, m, PyH), 4.02 (2H, t, *J* 6.6, CH_2O), 5.46 (1H, t, *J* 3.0 PyH), 6.99 (1H, t, *J* 8.6 ArH), 7.10 (2H, d, *J* 8.7 ArH), 7.23(1H, d m, *J* 7.9 ArH) , 7.28 (1H, m, ArH) and 7.44 (2H, d, *J* 8.8 ArH)

M/Z 316 (M^+)

V_{max}/cm^{-1} : 2929, 2853, 1502, 1477, 1276, 1104, 1039, 965

7.3.14 3'-Fluoro-4'-(octyloxy)-[1,1'-biphenyl]-4-ol — **55**



Dissolve the 2-((3'-fluoro-4'-(octyloxy)-[1,1'-biphenyl]-4-yl)oxy)tetrahydro-2H-pyran **54** (1.50 g, 0.0037 mol) in MeOH (20 ml) and DCM (10 ml) then PTSA (0.5 g) was added to the solution, the solution was stirred for 30 min. The completion of the reaction was checked by using TLC. Solvent was removed by using vacuo. The compound was dissolved in ether (100 ml) then washed with sodium

bicarbonate (X3). The solvent was removed in vacuo. The pure compound was collected after column chromatography (Hexane and DCM, 1:2)

Yield: 1.33 mg, 90 %

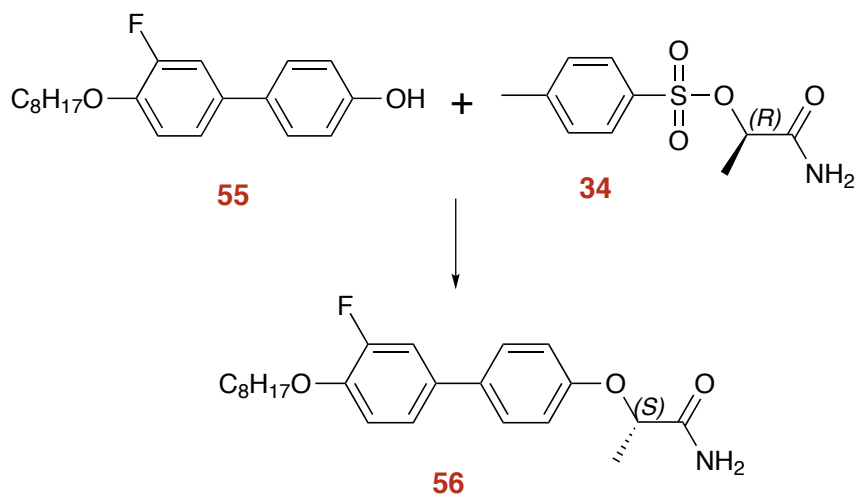
δ^H : 0.88 (3H, t, J 7.00, CH_3CH_2), 1.32 (8H, m, 4 X CH_2CH_3), 1.47 (2H, quin, J 7.0, CH_2CH_2), 1.82 (2H, quin, J 6.1, CH_2CH_2), 4.05 (2H, t, J 6.7, CH_2O), 4.8 (1H, bs, HO), 6.98 (1H, d, J 8.6, ArH), 7.20 (2H, d, J 8.1, ArH), 7.26 (1H, dd, J 12.6, 2.0, ArH) and 7.40 (2H, d, J 8.6, ArH)

δ^C : 14.2, 22.7, 26.0, 29.3, 29.3, 29.4, 31.9, 69.7, 114.4, 114.6, 115.2, 115.7, 122.1, 128.0, 132.7, 134.1, 146.1, 146.2, 151.7, 154.1, 155.0.

M/Z 316 (M^+)

V_{max}/cm^{-1} : 3400 (O-H), 2917, 2850, 1596, 1505, 1469, 1238, 1135, 803

7.3.15 (S)-2-((3'-Fluoro-4'-(octyloxy)-[1,1'-biphenyl]-4-yl)oxy)propanamide — 56



Quantities:

3'-Fluoro-4'-(octyloxy)-[1,1'-biphenyl]-4-ol **55**, (0.5 g, 0.0015 mol)

(S)-1-Amino-1-oxopropan-2-yl 4-methylbenzenesulfonate **34**, (1.02 g, 0.0017 mol)

Potassium carbonate, (3.89 g, 0.0316 mol)

DMF, (10 ml)

The experimental procedure was as described for the preparation of compound **47** to give a white solid of compound **56**.

Yield: 0.5 g, 80 %

Melting point: 192.0 °C

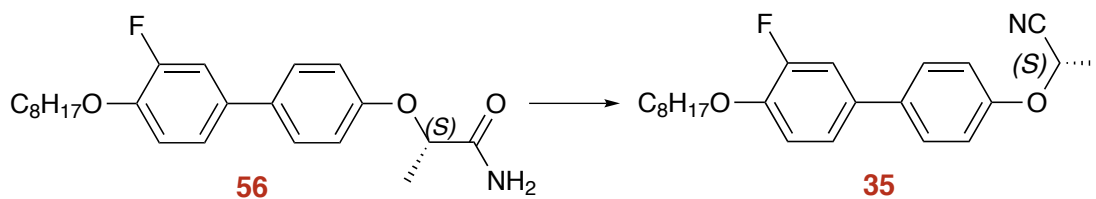
Optical Rotation $[\alpha]_D^{20} = -38.7$ (c 0.009 in DCM)

δ^H : 0.89 (3H, t, J 6.5, CH_3CH_2), 1.31 (8H, m, 4 X CH_2CH_3), 1.47 (2H, quin, J 7.4, CH_2CH_2), 1.62 (3H, d, J 6.8, CH_2CH), 1.83 (2H, quin, J 6.3, CH_2CH_2), 4.05 (2H, t, J 6.6, CH_2O), 4.70 (1H, q, J 6.8, HCH_3), 5.59 (H, b s, NN), 6.4 (H, b s, NN), 6.96 (2H, d, J 8.7, ArH), 7.00 (1H, d, J 8.6, ArH), 7.22 (1H, d m, J 8.3, ArH), 7.26 (1H, dd, J 12.5, 2.0, ArH) and 7.46 (2H, d, J 8.8, ArH)

δ^C : 14.1, 18.7, 22.7, 26.0, 29.3, 29.4, 31.9, 69.7, 75.0, 114.4, 114.6, 115.2, 115.8, 122.2, 128.1, 133.6 (1C, d, J 6.3), 133.9, 146.4 (1C, d, J 10.8), 152.9 (1CF, d, J 245.7), 156.3, and 174.9

δ^F : -134.13 (dd, J 10.6, 8.0)

7.3.16 (S)-2-((3'-Fluoro-4'-(octyloxy)-[1,1'-biphenyl]-4-yl)oxy)propanenitrile — **35**



Quantities:

POCl₃, (2.36 g, 0.015 mol)

DMF, (25 ml)

(S)-2-((3'-Fluoro-4'-(octyloxy)-[1,1'-biphenyl]-4-yl) oxy)propanamide, (0.60 g, 0.0016 mol)

The experimental procedure was as described for the preparation of compound **36** to give a white solid of (S)-1-amino- 1-oxopropan-2-yl 4-methylbenzenesulfonate **35**.

Yield: 0.42 mg, 75 %

Melting point: 74.8 °C

Optical Rotation $[\alpha]_D^{19} = -41.10$ (c 0.008 in DCM)

Transition / °C 69.8 N* 72.3 I

δ^H : 0.88 (3H, t, J 7.1, CH_3CH_2), 1.30 (8H, m, 4 X CH_2CH_3), 1.48 (2H, quin, J 7.00, CH_2CH_2), 1.82 (3H, d, J 6.7, CH_2CH), 1.83 (2H, m, CH_2CH_2), 4.06 (2H, t, J 6.5, CH_2O), 4.92 (1H, q, J 6.8, HCH_3), 7.00 (1H, t, J 8.60, ArH), 7.06 (2H, d, J 8.8, ArH), 7.23 (1H, ddd, J 8.5, 2.2, 1.1, ArH), 7.27 (1H, dd, J 11.0, 2.2, ArH), and 7.50 (2H, d, J 8.9, ArH)

δ^C : 14.2, 21.0, 22.7, 26.0, 29.3, 29.4, 31.9, 62.6, 69.7, 144.8, 114.7, 115.1, 116.3, 118.2, 122.4, 128.5, 133.5 (1C, d J 6.5) 135.0, 146.5 (1C, d, J 10.9), 152.9 (1C, d, J 245.5 CF) and 155.7

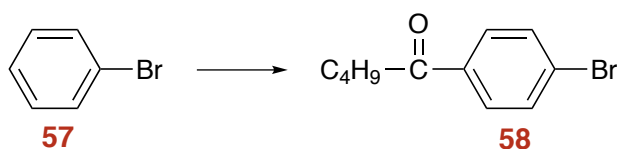
δ^F : -134.11 (dd, J 12.0, 9.3)

CHN elemental analysis: (Found: C, 75.01; H, 7.88; N, 3.50. $C_{23}H_{28}FNO_2$ requires C, 74.77; H, 7.64; N, 3.79%)

M/Z 369 (M^+)

V_{max}/cm^{-1} : 2953, 2930, 2871, 2173 ($C\equiv N$), 1639, 1463, 1235, 1235, 806

7.3.17 1-(4-Bromophenyl)pentan-1-one — 58



Bromobenzene, **57** (105.98 g, 0.675 mol) was added to a cooled ($\sim 5^\circ\text{C}$) mixture of aluminium chloride (66.00 g, 0.495 mol) in DCM (200 ml). Valeryl chloride (54.26 g, 0.45 mol) was added dropwise. The mixture was allowed to warm to room temperature overnight. The mixture was poured slowly into an excess mixture of ice and 36% HCL. The product was extracted into DCM before being washed with water. The organic extracts were dried over $MgSO_4$, filtered and

the solvent removed under vacuum. The product was distilled and collected at 140-150 °C to yielding a orange/yellow solid, **58**¹²⁷

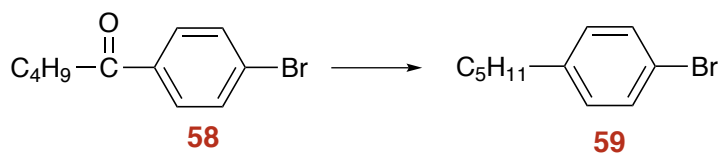
Yield: 60.02 g, 55 %

Boiling Point: 187 °C (*Lit* b.p. 180 - 184 °C)

δ^H : 0.94 (3H, t, *J* 7.3, CH_3CH_2), 1.39 (2H, sext, *J* 7.4, CH_2CH_2), 1.70 (2H, quin, *J* 7.5, CH_2CH_2), 2.92 (2H, t, *J* 7.3, $CH_2C=O$), 7.58 (2H, d, *J* 8.4, *Ph*) and 7.81 (2H, d, *J* 8.5, *Ph*).

δ^C : 14.02, 22.53, 26.44, 38.38, 128.08, 129.69, 131.94, 135.86, 199.57.

7.3.18 1-Bromo-4-pentylbenzene — **59**



The same procedure was carried out as for compound **80** using the following quantities: compound **58** (55.46 g, 0.23 mol), hydrazine monohydrate (31.45 g, 0.69 mol), potassium hydroxide (38.71 g, 0.69 mol). The crude product was distilled and collected at 120-130 °C. Yielding an colourless oil, **59**¹²⁷

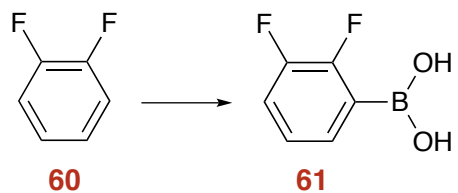
Yield: 36 g, 69 % . 145-148 °C

Boiling Point: 146.5 °C (*Lit* b.p. 145 - 148 °C)

δ^H : 0.94 (3H, t, *J* 6.9, CH_3CH_2), 1.33 (4H, m, CH_2CH_2), 1.63 (2H, quin, *J* 7.5, CH_2CH_2), 2.59 (2H, t, *J* 7.7, CH_2CH_2), 7.08 (2H, d, *J* 8.2, *Ph*) and 7.43 (2H, d, *J* 8.3, *Ph*).

δ^C : 14.1, 22.6, 31.1, 31.5, 35.4, 119.4, 130.3, 131.3, 141.9.

7.3.19 (2,3-Difluorophenyl)boronic acid — 61



Quantities:

Difluorobenzene, **60**, (289.00 g, 2.53 mol)

2.5 M *n*-BuLi (840.00 mL, 2.75 mol)

Trimethylborate (526.24 g, 5.06 mol)

THF, 2.5 L

HCl (10 %) 1.0 L

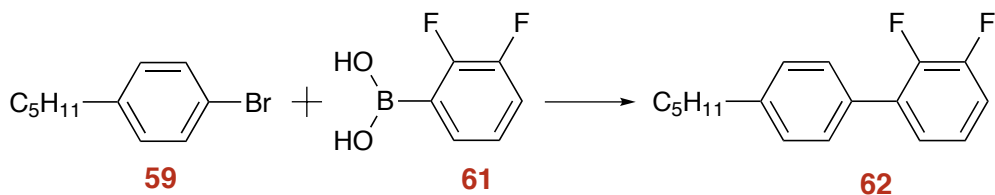
The experimental procedure was as described for the preparation of compound **41** to give a white solid (2,3-difluorophenyl)boronic acid **61**.¹²⁷

Yield: 240.60 g, 72 %

Boiling Point: 136 °C (*Lit* b.p. 234 - 237 °C)

δ^H : 7.16(1H, m, ArH), 7.33 (1H, m, ArH), 7.40 (1H, m, ArH), 8.49 (2H, b s, B(OH)₂)

7.3.20 2,3-Difluoro-4'-pentyl-1,1'-biphenyl — 62



Quantities:

1-Bromo-4-pentylbenzene, (10.00 g, 0.04 mol)

DME, (25 ml)

Sodium carbonate, (25 ml, 2M)

Tetrakis(triphenylphosphine)palladium (0.035g 0.000022 mol)

(2,3-Difluorophenyl)boronic acid (8.50 g, 0.045 mol)

The experimental procedure was as described for the preparation of compound **45** to give a white solid 2,3-difluoro-4'-pentyl-1,1'-biphenyl **62**.¹²⁷

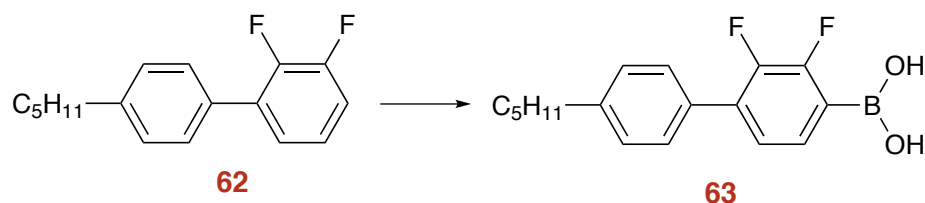
Yield: 10.00 g, 96 %

δ^H : 0.97 (3H, t, J 7.4, CH_3CH_2), 1.41 (4H, m, 4 x CH_2CH_3), 1.71 (2H, quin, J 7.4, CH_2CH_2), 2.70 (2H, t, J 7.5, CH_2CH_2), 7.15 (2H, m, ArH), 7.23 (1H, m, ArH), 7.32 (2H, d, J 8.3, ArH) and 7.51 (2H, dd, J 8.2, 1.7, ArH)

δ^C : 14.1, 22.7, 31.2, 31.71, 35.8, 115.8 (1C, d, J 17.15), 124.0 (1C, dd, J 7.2, 4.9), 125.3 (1C, m), 128.7, 128.9, 131.4 (1C, d, J 10.1), 132.1 (1C, d, J 2.7), 143.2, 148.1 (1CF, dd, J 249.1, 13.1) and 151.2 (1CF, dd, J 247.5, 13.8)

δ^F : -143.68 (d, J 20.3) and -137.95 (dt, J 20.6, 6.7)

7.3.21 (2,3-Difluoro-4'-pentyl-[1,1'-biphenyl]-4-yl)boronic acid — **63**



Quantities:

2,3-Difluoro-4'-pentyl-1,1'-biphenyl, **62**, (10.00 g, 0.038 mol)

2.5 M *n*-BuLi (16.00 mL, 0.041 mol)

Trimethylborate (8.00 g, 0.076 mol)

THF, 100 mL

HCl (10 %) 100 mL

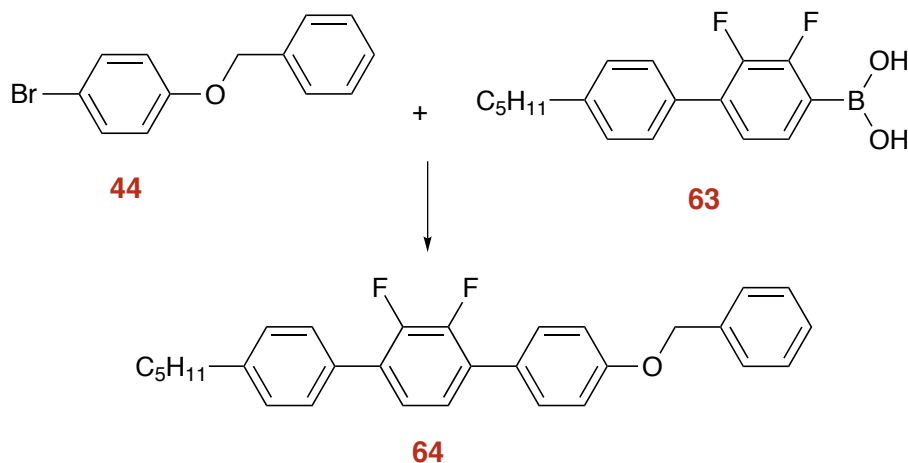
The experimental procedure was as described for the preparation of compound **41** to give a white solid 2,3-difluoro-4'-pentyl-[1,1'-biphenyl]-4-yl)boronic acid **63**.¹²⁷

Yield: 9.89 g, 86 %

δ^H : 0.87 (3H, t, J 6.8, CH_3CH_2), 1.31 (4H, m, 4 X CH_2CH_3), 1.61 (2H, quin, J 7.4, CH_2CH_2), 2.62 (2H, t, J 7.6, CH_2CH_2), 7.28 (1H, d, J 7.6, ArH), 7.32 (2H, d, J 8.3, ArH), 7.32 (2H, d, J 8.3, ArH), 7.41 (1H, m, ArH) and 7.49 (2H, d, J 7.5, ArH)

δ^F : -146.12 (dd, J 22.4, 4.8) and -130.72 (dd, J 22.5, 4.3)

7.3.22 4-(Benzyloxy)-2',3'-difluoro-4''-pentyl-1,1':4',1''-terphenyl — 64



Quantities:

1-Bromo-4-pentylbenzene, (8.00 g, 0.03 mol)

DME, (200 ml)

Sodium carbonate, (100 ml, 2M)

Tetrakis(triphenylphosphine)palladium (0.035g 0.0003 mol)

(2,3-Difluorophenyl)boronic acid (11.09 g, 0.036 mol)

The experimental procedure was as described for the preparation of compound 45 to give a white solid 4-(benzyloxy)-2',3'-difluoro-4''-pentyl-1,1':4',1''-terphenyl 64.

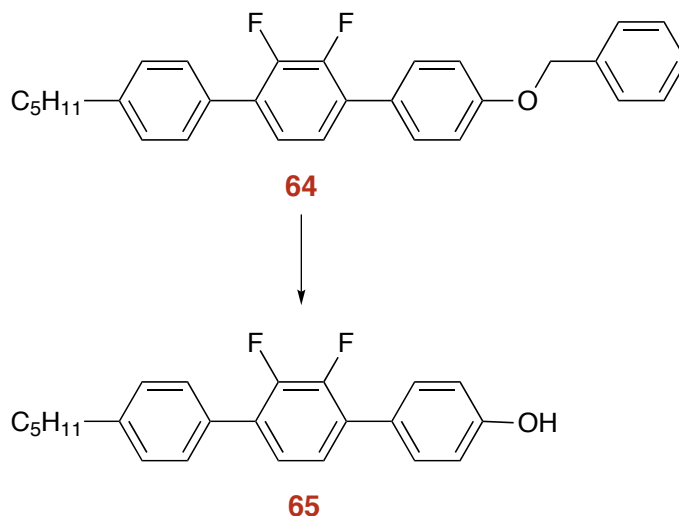
Yield: 11.80 g, 87 %

δ^H : 0.93 (3H, t, J 7.4, CH_3CH_2), 1.36 (4H, m, 4 X CH_2CH_3), 1.67 (2H, quin, J 7.4, CH_2CH_2), 2.67 (2H, t, J 7.4, CH_2CH_2), 5.13 (2H, s, CH_2Bn), 7.09 (2H, d, J 8.8, ArH), 7.32 (2H,md, ArH), 7.29 (2H, d, J 8.1, ArH), 7.37 (1H, m, ArH), 7.41

(1H, d, *J* 5.9, *ArH*), 7.43 (1H, d, *J* 7.1 *ArH*), 7.47 (2H, d, *J* 7.2, *ArH*), 7.51 (2H, m, *ArH*) and 7.49 (2H, m, *ArH*)

M/Z 442.0 (*M*⁺)

7.3.23 2',3'-Difluoro-4''-pentyl-[1,1':4',1''-terphenyl]-4-ol — 65



Quantities:

4-(Benzyloxy)-2',3'-difluoro-4''-pentyl-1,1':4',1''-terphenyl **64**, (3.00 g, 0.0067 mol)
Pd/C, (1.00 g)

EtOAc, (100 ml)

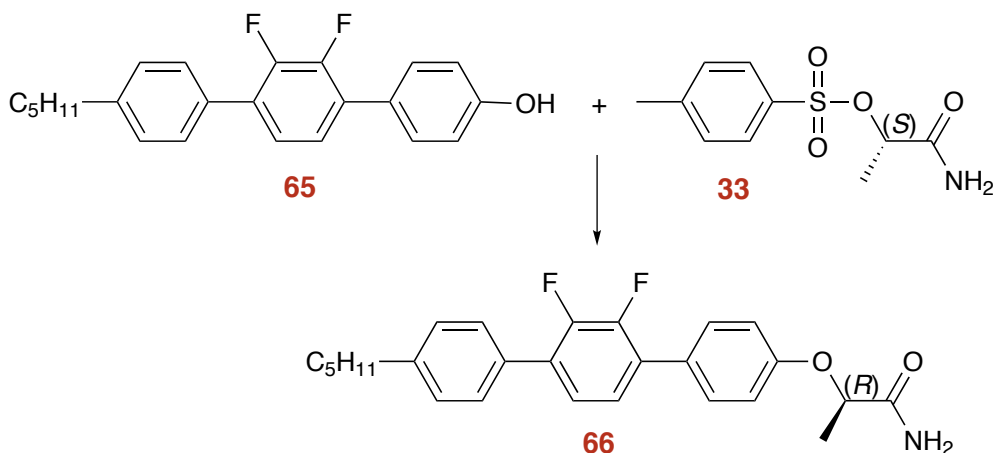
The experimental procedure was as described for the preparation of compound **46** to give a white solid 2',3'-difluoro-4''-pentyl-[1,1':4',1''-terphenyl]-4-ol **65**.¹²⁸

Yield: 2.00 g, 87 %

Boiling Point: 187 °C (*Lit* b.p. 185 - 186 °C)

δ^H : 0.92 (3H, t, *J* 7.00, CH_3CH_2), 1.37 (4H, m, 4 X CH_2CH_3), 1.66 (2H, m, CH_2CH_2), 2.66 (2H, t, *J* 7.5, CH_2CH_2), 4.92 (1H, b s, OH), 6.94 (2H, d, *J* 8.8, *ArH*), 7.22 (2H, m, *ArH*), 7.29 (H, d, *J* 8.3, *ArH*), and 7.49 (4H, m, *ArH*)

7.3.24 (*R*)-2-((2',3'-Difluoro-4''-pentyl-[1,1':4',1''-terphenyl]-4-yl)oxy)propanamide — **66**



Quantities:

2',3'-Difluoro-4''-pentyl-[1,1':4',1''-terphenyl]-4-ol **65**, (1.50 g, 0.0043 mol)

(*S*)-1-Amino-1-oxopropan-2-yl 4-methylbenzenesulfonate **123**, (1.20 g, 0.0051 mol)

Potassium carbonate, (1.70 g, 0.0085 mol)

DMF, (50 ml)

The experimental procedure was as described for the preparation of compound **49** to give a white solid (*R*)-2-((2',3'-difluoro-4''-pentyl-[1,1':4',1''-terphenyl]-4-yl)-oxy)propanamide **66**.

Yield: 0.84 g, 47 %

Melting point: 197.4 °C

Optical Rotation $[\alpha]_D^{21} = -16.3$ (c 0.0117 in DCM)

δ^H : 0.91 (3H, t, *J* 7.2, CH_3CH_2), 1.36 (4H, m, 4 X CH_2CH_3), 1.65 (3H, d, *J* 6.8, CH_3CH), 2.67 (2H, m, CH_2CH_2), 2.86 (2H, t, *J* 7.8, CH_2CH_2), 4.74 (1H, quin, *J* 6.8, *H*), 5.58 (1H, b s, *NH*), 6.41 (1H, b s, *NH*), 7.02 (2H, d, *J* 8.9, *ArH*), 7.22 (2H, m, *H*), 7.29 (2H, d, *J* 8.2, *ArH*), 7.50 (2H, m, *ArH*) and 7.55 (2H, m, *ArH*)

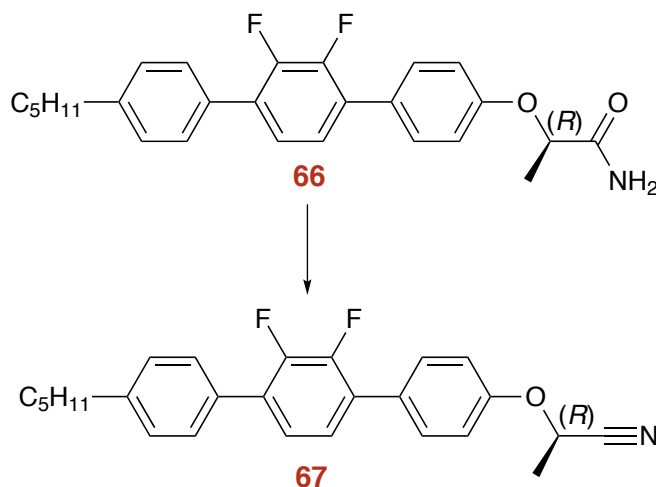
δ^C : 14.1, 18.7, 22.6, 31.1, 31.6, 35.7, 74.9, 115.5, 124.4, 124.7, 128.7, 128.8, 130.4, 131.9, 143.2, 156.8, 174.6.

δ^F : -143.38 (dd, J 19.8, 5.4) and -143.00 (dd, J 19.8, 5.4)

M/Z 423 (M^+)

V_{max}/cm^{-1} : 3387, 3186, 2926, 1738 (C=O), 1637 (N-H), 1458, 1234, 798

7.3.25 (*R*)-2-((2',3'-Difluoro-4''-pentyl-[1,1':4',1''-terphenyl]-4-yl)oxy)propanenitrile – 67



Quantities:

$POCl_3$, (1.81 g, 0.012 mol)

DMF, (50 ml)

(*R*)-2-((2',3'-Difluoro-4''-pentyl-[1,1':4',1''-terphenyl]-4-yl)oxy)propanamide **66**, (0.50 g, 0.0048 mol)

The experimental procedure was as described for the preparation of compound **36** to give a white solid of (*R*)-2-((2',3'-difluoro-4''-pentyl-[1,1':4',1''-terphenyl]-4-yl)oxy)propanenitrile **67**.

Yield: 0.29 g, 60 %

Melting point: 102.8 °C

Optical Rotation $[\alpha]_D^{20} = + 71.4$ (c 0.011 in DCM)

Transition / °C 83.5 N* 94.8 BP (mosaic) 96.1 BP 99.5 I

δ^H : 0.91 (3H, t, J 6.8, CH_3CH_2), 1.36 (4H, m, 4 X CH_2CH_3), 1.67 (2H, d, J 7.4, CH_3CH), 1.84 (3H, d, J 6.8, CH_2CH_2), 2.66 (2H, t, J 7.2 CH_2CH_2), 4.96 (1H, quin, J 6.8 H), 7.11 (2H, d, J 8.7, ArH), 7.29 (2H, d, J 8.1 ArH), 7.50 (2H, d, J 6.8, ArH) and 7.58 (2H, d, J 7.4, ArH)

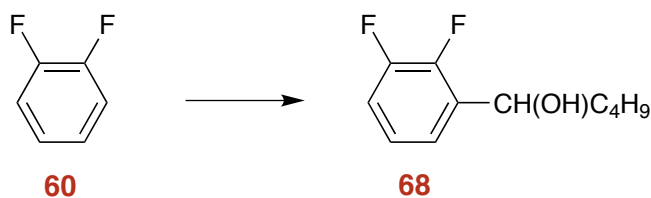
δ^C : 14.1, 20.0, 20.0, 31.1, 31.6, 35.7, 62.4, 115.9, 118.2, 124.4, 124.7, 128.6, 128.8, 130.4, 130.4, 143.2, 156.2.

δ^F : -143.27 (dd, J 19.6, 5.3) and -142.96 (dd, J 20.1, 5.0)

M/Z 405 (M^+)

V_{max}/cm^{-1} : 2972, 2657($C\equiv N$), 2163, 1605, 1482, 1458, 1237, 1097, 799

7.3.26 1-(2,3-Difluorophenyl)pentan-1-ol — 68



n-Butyllithium in hexane (82 ml, 2.5 M in hexane, 0.22 mol) was added dropwise to a stirred, cooled ($-78\text{ }^\circ\text{C}$) solution of compound 1,2-difluorobenzene **60** (25 g, 0.22 mol) in dry THF (200 cm^3). The mixture was maintained under these conditions for 1 h and a solution of pentanal (20.1 g, 0.24 mol) in dry THF (100 ml) was added drop wise at $-78\text{ }^\circ\text{C}$. The mixture was allowed to warm to room temperature overnight and then ammonium chloride (aq) (55 ml, 11.2 g, 0.22 mol) solution was added. The product was extracted into ether ($2 \times 100\text{ cm}^3$), washed with water ($2 \times 100\text{ cm}^3$), dried over magnesium sulphate, and the solvent removed under reduced pressure to get colourless oil 1-(2,3-difluorophenyl)pentan-1-ol **68**.¹²⁷

Boiling Point = $182\text{-}184\text{ }^\circ\text{C}$

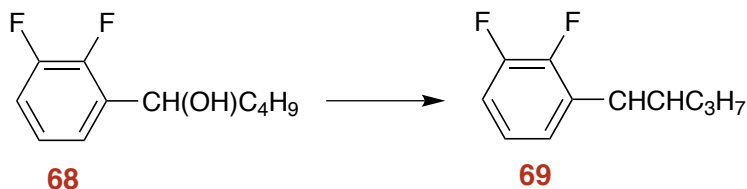
Yield: 32 g, 72 %

Boiling Point: $180\text{-}184\text{ }^\circ\text{C}$ (*Lit* BP $182\text{-}184\text{ }^\circ\text{C}$)

m/z 200 (M^+), 149, 143, 127, and 115.

δ^H : 0.92 (3H, t, CH_3CH_2), 1.28 (4H, m, CH_2CH_3), 1.56 (2H, quin, CH_2CH_2), 3.56 (1H, s, HO), 4.47 (1H, t, $CHCH_2$) and 7.91 (3H, m, ArH)

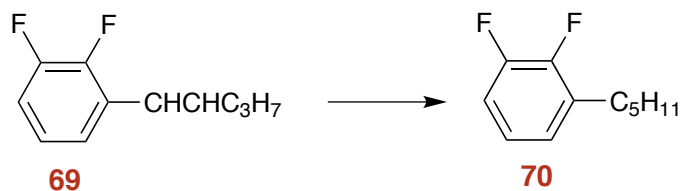
7.3.27 *E*-1,2-Difluoro-3-(pent-1-en-1-yl)benzene — 69



A stirred solution of crude compound 1-(2,3-difluorophenyl)pentan-1-ol **68** (20 g, 0.08 mol) and para-toluene sulfonic acid (PTSA) (3.25 g) in toluene (200 ml) was heated under reflux in a Dean and Stark apparatus overnight, completion of the reaction was monitored using GC analysis. The cooled mixture was poured into a saturated solution of sodium hydrogen carbonate, stirred for 1 h, and the product extracted into ether (2 x 50 cm³). The ethereal extracts were washed with water (2 x 100 cm³), dried over magnesium carbonate and the solvent removed under reduced pressure to get 1,2-Difluoro-3-(pent-1-enyl)benzene **69**.

Yield: 12 g, 82 %

7.3.28 1,2-Difluoro-3-pentylbenzene — 70



Compound 1,2-Difluoro-3-(pent-1-enyl)benzene **69** (39.3 g, 0.216 mol) was dissolved in toluene (500 ml) and hydrogenated overnight in a Parr apparatus at room temperature and pressure using 10 % palladium on-carbon (5 g), check the completion of the reaction using GC analysis. The palladium catalyst was filtered off, the solvent was removed and the product distilled to give a colourless oil.¹²⁷

Yield: 15.6 g, 63 %

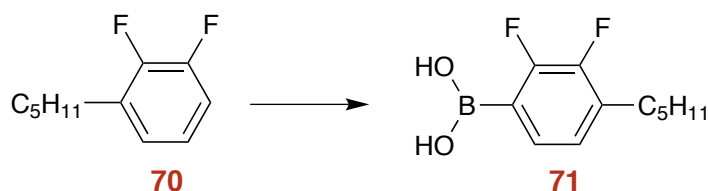
Boiling Point: 206-208 °C (*Lit* BP 206-208 °C)

δ^H : 0.90 (3 H, t), 1.35 (4H, m), 1.60 (2 H, quintet), 2.65 (2 H, t), and 6.90-7.00 (3 H, m)

m/z 184 (M^+), 143, 127, 115, and 101.

7.3.29 (2,3-Difluoro-4-pentylphenyl)boronic acid — 71

129



Quantities: Compound **70** (15.6g 0.085 mol) *n*-Butyllithium (2.5 M in hexane , 34 ml, 0.085 mol) Trimethyl borate (13.3 g, 0.13 mol) HCl (10 %) (100 ml) THF (200 ml)

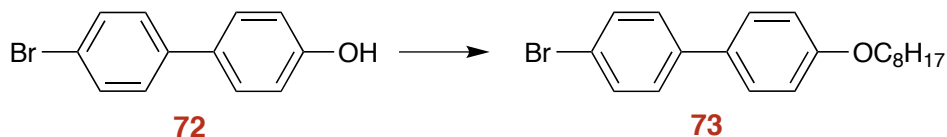
The experimental procedure was as described for the preparation of compound **41** to give a white solid.¹²⁷

Yield: 14.2 g, 62 %

δ^H : 0.90 (3 H, t), 1.30 (4 H, m), 1.60 (2 H, quin), 2.65 (2 H, t), 6.95 (1 H, m), and 7.45 (1 H, m); no obvious OH absorption

m/z 228 (M^+), 211, 205, 197, 193, 184, 171, 153, 149, and 143.

7.3.30 (4-Bromo-4'-(octyloxy)-1,1'-biphenyl — 71



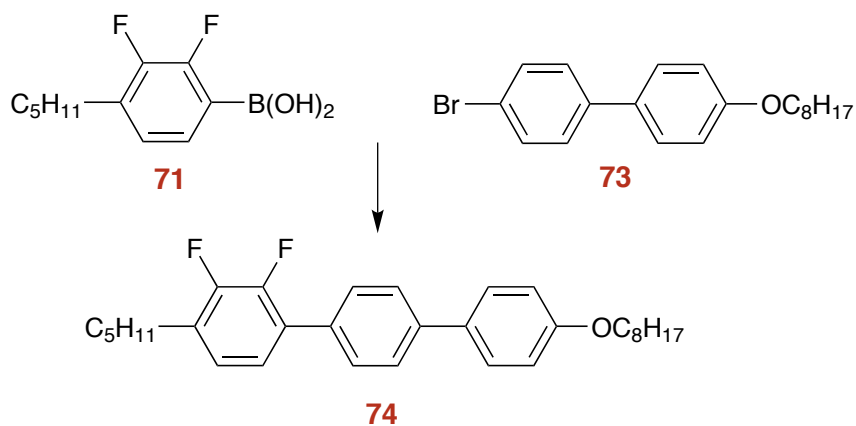
A stirred mixture of 4'-bromo-[1,1'-biphenyl]-4-ol (5.0 g, 0.020 mol), 1-bromooctane (4.25 g, 0.022 mol), and potassium carbonate (8.28 g, 0.060 mol) in butanone (150 ml) was heated under reflux for 24 h. The mixture was cooled, the potassium carbonate was filtered off, and the butanone was removed. The residue was distilled to yield a colourless oil 4-bromo-4'-(octyloxy)-1,1'-biphenyl **71**.¹³⁰

Yield: 6.8 g, 94 %

Melting point : 128.3 °C (*Lit* mp 121-122 °C)¹³⁰

δ^H : 0.90 (3H, t, *J* 6.9, CH_3CH_2), 1.33 (6H, m, CH_2CH_3), 1.48 (2H, m, CH_3CH), 1.80 (2H, m, CH_3CH), 3.99 (2H, t, *j* 6.5, CH_3O), 6.95 (2H, d, *J* 8.7, *ArH*), 7.40 (2H, d, *J* 8.5, *ArH*), 7.46 (2H, d, *J* 8.7, *ArH*) and 7.52 (2H, d, *J* 8.5, *ArH*)

7.3.31 2,3-Difluoro-4''-(octyloxy)-4-pentyl-1,1':4',1''-terphenyl — **74**



Quantities:

(4-Bromo-4'-(octyloxy)-1,1'-biphenyl **71**, (6.00 g, 0.016 mol)

DME, (100 ml)

Sodium carbonate, (100 ml, 2M)

Tetrakis(triphenylphosphine)palladium (0.035g 0.00066 mol)

(2,3-Difluoro-4-pentylphenyl)boronic acid, **71** (4.92 g, 0.022 mol)

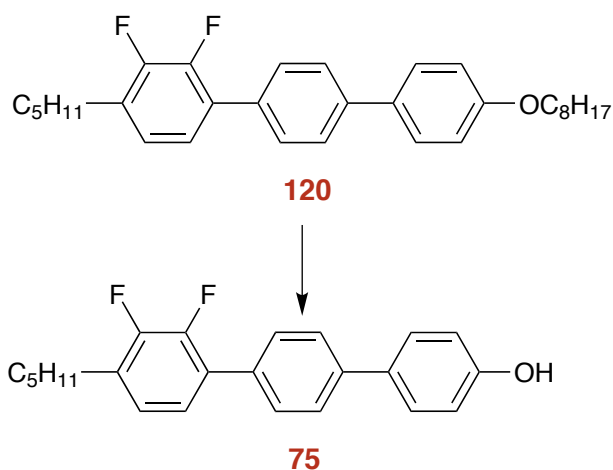
The experimental procedure was as described for the preparation of compound **45** to give a white solid 2,3-difluoro-4''-(octyloxy)-4-pentyl-1,1':4',1''-terphenyl **74**.¹²⁷

Yield: 6.00 g, 69 %

Transitions / °C 89.0 SmC, 155.5 SmA, 165.0 N 166.0 I¹²⁷

δ^H : 0.89 (3H, t, *J* 6.9, CH_3CH_2), 0.91 (3H, t, *J* 7.0, CH_3CH_2), 1.33 (12H, m, CH_2CH_3), 1.48 (2H, quin, *J* 7.6, CH_3CH), 6.8 (CH_2CH_2), 2.69 (2H, t, *J* 7.7, CH_2CH_2), 4.0 (2H, t, *J* 6.6, OCH_2), 6.90 (2H, d, *J* 8.8, ArH), 7.00 (1H, m, ArH), 7.14 (1H, td, *J* 7.3, 7.3, 1.7, ArH), 7.57 (4H, m ArH) and 7.63 (2H, d, *J* 8.5, ArH)

7.3.32 2'',3''-Difluoro-4''-pentyl-[1,1':4',1''-terphenyl]-4-ol — 75



2,3-Difluoro-4''-(octyloxy)-4-pentyl-1,1':4',1''-terphenyl **74** (3.50 g, 0.075 mol) was stirred in DCM (80 ml) at 0 °C under dry nitrogen. Boron tribromide (26.50 g, 0.027 mol) was added drop wise with rapid stirring. Continued the stirring overnight. After confirming the completion of reaction by GLC, add the reaction mixture to cold water with stirring and product was extracted into EtOAc (100x2). The combined ethereal extracts were washed with water (100ml x 2), dried over magnesium sulphate and the solvent was removed. Purified by column chromatography (silica gel; DCM, 8:2) to give a colourless solid **75**.¹²⁸

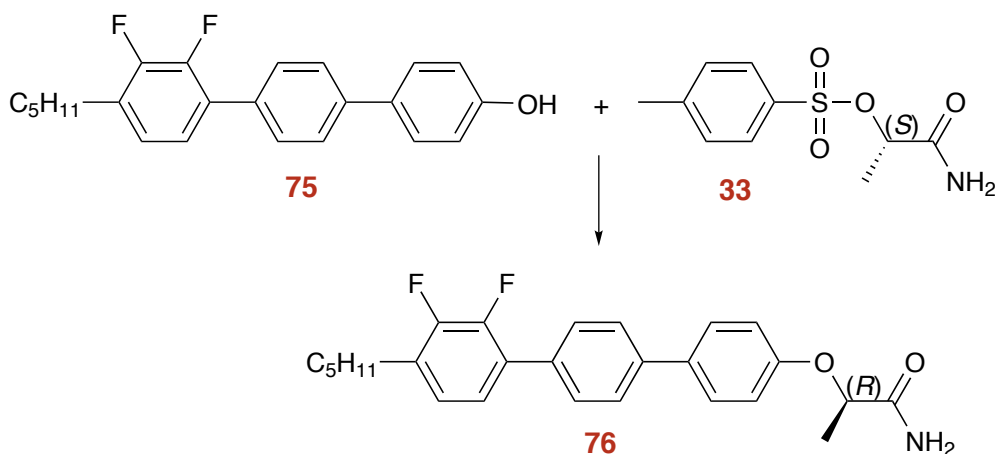
Yield: 2.60 g, 98 %

Transitions / °C 168 N 176,5 I¹²⁸

δ^H : 0.92 (3H, t, *J* 7.0, CH_3CH_2), 1.37 (4H, m, CH_2CH_3), 1.66 (2H, quin, *J* 7.6, CH_3CH), 2.69 (2H, t, *J* 7.5, CH_2CH_2), 6.90 (2H, d, *J* 6.0, ArH), 7.00 (1H, td, *J*

7.8, 7.5, 1.5, ArH), 7.14 (1H, td, *J* 7.7, 7.0, 1.7 ArH), 7.53 (2H, d, *J* 8.6 ArH), 7.59 (2H, d, *J* 8.9, ArH) and 7.62 (2H, d, *J* 8.4, ArH)

7.3.33 (R)-2-((2'',3''-Difluoro-4''-pentyl-[1,1':4',1''-terphenyl]-4-yl)oxy)propanamide — 76



Quantities:

2'',3''-Difluoro-4''-pentyl-[1,1':4',1''-terphenyl]-4-ol, **75**, (1.50 g, 0.0043 mol)

(S)-1-Amino-1-oxopropan-2-yl 4-methylbenzenesulfonate **123**, (1.20 g, 0.0051 mol)

Potassium carbonate, (1.170 g, 0.0085 mol)

DMF, (50 ml)

The experimental procedure was as described for the preparation of compound **49** to give a white solid **76**.

Yield: 0.53 g, 30 %

Melting point: 208.6 °C

Optical Rotation $[\alpha]_D^{20} = -15.9$ (c 0.01 in DCM)

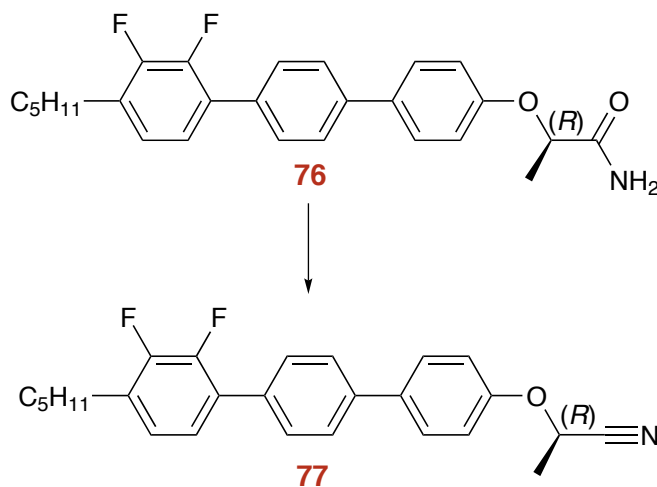
δ^H : 0.93 (3H, t, *J* 7.0, CH₃CH₂), 1.37 (4H, m, CH₂CH₃), 1.64 (3H, d, *J* 6.7, CCH₃), 1.68 (2H, m, CH₃CH), 2.69 (2H, t, *J* 7.6, CH₂CH₂), 4.73, (1H, quin, *J* 6.8, CH), 5.61 (1H, b s, NH), 6.43 (1H, b s, NH), 6.99 (2H, m, ArH), 7.01 (2H, d, *J* 8.9, ArH), 7.14 (1H, td, *J* 7.6, 7.0, 1.8, ArH) and 7.60 (6H, m, ArH)

δ^F : -144.04 (dd, J 20.0, 6.2) and -143.50 (dd, J 20.3, 5.9)

M/Z 423 (M^+)

V_{max}/cm^{-1} : 3183, 2954, 2869, 1640 (N-H), 1497, 1462, 1235, 1087, 805

7.3.34 (*R*)-2-((2'',3''-Difluoro-4''-pentyl-[1,1':4',1''-terphenyl]-4-yl)oxy)propanenitrile— 77



Quantities:

$POCl_3$, (1.81 g, 0.012 mol)

DMF, (50 ml)

(*R*)-2-((2'',3''-Difluoro-4''-pentyl-[1,1':4',1''-terphenyl]-4-yl)oxy)propanamide, **76**, (0.50 g, 0.0048 mol)

The experimental procedure was as described for the preparation of compound **36** to give a white solid of **77**.

Yield: 0.20 g, 50 %

Melting point: 115.5 °C

Optical Rotation $[\alpha]_D^{21} = + 72.72$ (c 0.0033 in DCM)

Transition / °C 115.5 BP (Mosaic Phase) 118.0 Blue Green Phase 118.7 BP (Fog Phase) 119.0 I

δ^H : 0.93 (3H, t, J 6.9, CH_3CH_2), 1.37 (4H, m, CH_2CH_3), 1.66 (2H, quin, J 7.6, CH_2CH_2), 1.83 (3H, d, J 6.8, CCH_3), 2.70 (2H, t, J 7.8, CH_2CH_2), 4.95, (1H, quin, J 6.7, CH), 7.01 (1H, ddd, J 7.8, 7.5, 1.4, ArH), 7.10 (2H, d, J 8.8 ArH), 7.14 (1H, td, J 7.8, 7.1, 1.7 ArH) and 7.62 (6H, m, ArH)

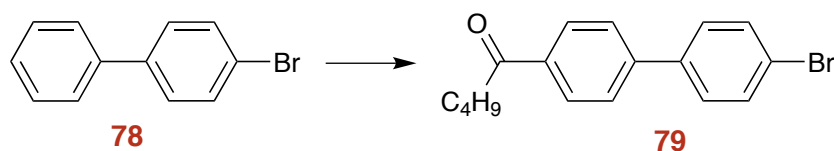
δ^F : -144.01 (dd, J 20.2, 6.4) and -143.50 (dd, J 20.1, 5.8)

δ^C : 14.1, 20.0, 22.5, 28.8, 29.8, 31.5, 62.6, 116.2, 118.3, 124.2, 124.8, 127.0, 127.9 (1CF, d, J 10.4), 128.5, 129.3, 131.1 (1CF, d, J 13.3), 133.9, 135.7, 139.8, 156.0.

M/Z 405 (M^+)

V_{max}/cm^{-1} : 2954, 2870, 2360 ($C\equiv N$), 2031, 1605, 1486, 1457, 1240, 807

7.3.35 1-(4'-Bromo-[1,1'-biphenyl]-4-yl)pentan-1-one— 79



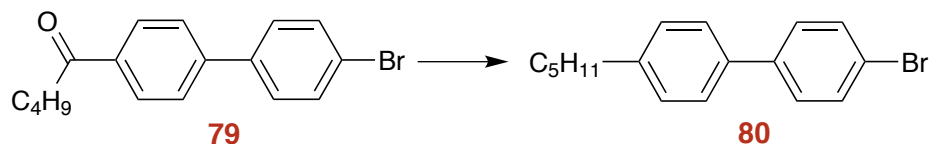
Aluminium chloride (51.34 g, 0.385 mol) in DCM (200 mL) was cooled below 5 °C. Valeryl chloride (42.2 g, 0.35 mol) was added quickly and the solution cooled to 0 °C. Solid 4-bromobiphenyl, **78** (122.4 g, 0.525 mol) was added slowly. The reaction mixture was allowed to warm to room temperature overnight. The mixture was poured slowly into an excess mixture of ice and 36% HCl acid. The product was extracted into DCM before being washed with water, 8% potassium hydroxide and a second water wash. The organic extracts were dried over magnesium sulphate, filtered and the solvent removed under reduced pressure. The crude product was recrystallised from ethanol (~100 mL) to yield an orange/yellow solid, **79**.

Yield: 111.00 g, 100 %

δ^H : 0.96 (3H, t, J 7.4, CH_3CH_2), 1.43 (2H, m, CH_2CH_3), 1.74 (2H, quin, J 7.4, CH_2CH_2), 7.48 (2H, d, J 8.3, ArH), 7.59 (2H, d, J 8.2, ArH), 7.63 (2H, d, J 8.2, ArH) and 8.03 (2H, d, J 8.2, ArH)

δ^C : 14.0, 22.6, 26.6, 38.5, 122.6, 127.1, 128.8, 128.9, 132.1, 136.1, 138.9, 144.3 and 200.1.

7.3.36 4-Bromo-4'-pentyl-1,1'-biphenyl— 80



Compound **79** (95.17 g, 0.30 mol) in DEG (300 ml) was heated to form a solution. Hydrazine monohydrate (45.00 g, 0.90 mol) was added all at once. The mixture was heated to 130 °C and stirred for 3 h. The temperature was raised to 180 °C and the excess hydrazine monohydrate was distilled out. The solution was allowed to cool to room temperature overnight. The mixture was again heated to form a solution before adding potassium hydroxide (50.49 g, 0.90 mol) all at once. The mixture was heated to 180 °C for 3 h. After cooling slightly the solution was poured into an excess mixture of ice and 36% HCL. The product was extracted into DCM and washed with lots of water and brine. The organic extracts were dried over magnesium sulphate, filtered and the solvent removed under vacuum. The crude product was recrystallised from ethanol to yield an orange solid, **80**.¹²⁸

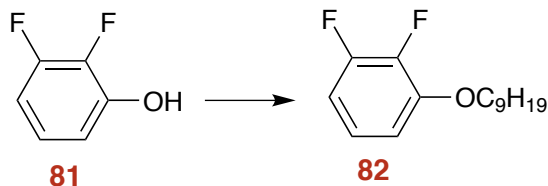
Yield: 90.97 g, 94 %

Boiling Point: 195-198 °C (*Lit* BP 195-197 °C)

δ^H : 0.99 (3H, t, J 7.4, CH_3CH_2), 1.53 (2H, m, CH_2CH_3), 1.79 (2H, quin, J 7.3, CH_2CH_2), 4.01 (2H, t, J 6.5, CH_2O), 6.98 (2H, d, J 8.8, ArH), 7.42 (2H, d, J 8.5, ArH), 7.48 (2H, d, J 8.8, ArH) and 7.53 (2H, d, J 8.5, ArH)

^{13}C -NMR: 14.1, 22.6, 31.2, 3.6, 35.6, 121.2, 126.8, 128.6, 129.0, 131.8, 140.1 and 142.7.

7.3.37 1,2-Difluoro-3-(nonyloxy)benzene — 82



Quantities:

2,3-Difluorophenol, (25.0 g, 0.19 mol)

1-Bromononane, (47.65 g, 0.23 mol)

Potassium carbonate, (8.28 g, 0.060 mol)

Butanone, (200 ml)

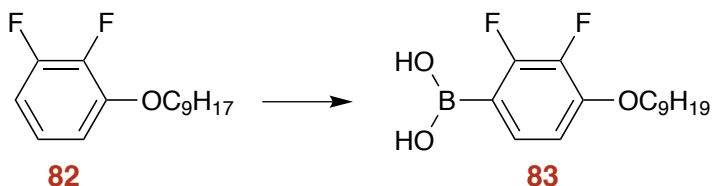
The experimental procedure was as described for the preparation of compound **71** to give a white solid of **82**.¹³¹

Yield: 41.00 g, 88 %

Boiling Point: 94-99 °C at 0.2 mmHg

δ^H : 0.89 (3H, t, J 7.0, CH_3CH_2), 1.33 (10H, m, CH_2CH_3), 1.43 (2H, quin, J 7.9, CH_3CH), 1.72 (2H, quin, J 7.9, CH_3CH), 4.02 (2H, t, J 6.6, OCH_2), 6.8 (1H, dd, J 7.2, 6.8, ArH) and 6.95 (1H, m, ArH)

7.3.38 (2,3-Difluoro-4-(nonyloxy)phenyl)boronic acid — 83



Quantities:

Difluorobenzene, **60**, (40.69 g, 0.16 mol)

2.5 M *n*-BuLi (64.5 ml, 0.16 mol)

Trimethylborate (33.49 g, 0.32 mol)

THF, 300 ml

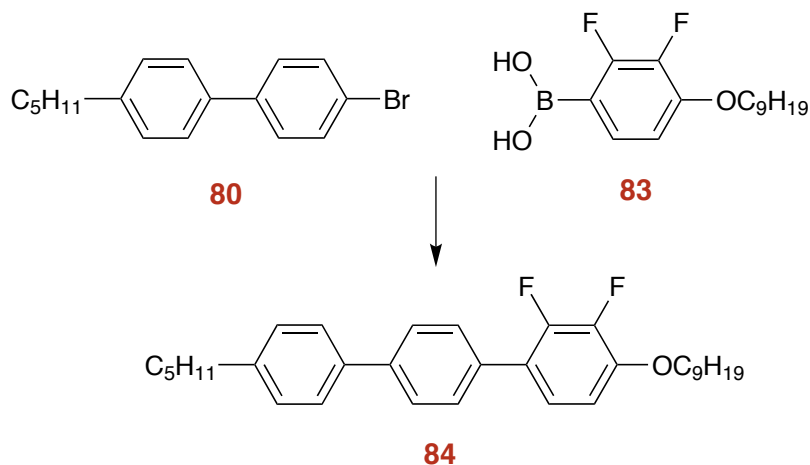
HCl (10 %) 200 ml

The experimental procedure was as described for the preparation of compound **41** to give a white solid **83**.

Yield: 30.00 g, 64 %

δ^H : 0.86 (3H, t, J 7.1, CH_3CH_2), 1.30 (10H, m, CH_2CH_3), 1.43 (2H, quin, J 7.9, CH_3CH), 1.72 (2H, quin, J 7.9, CH_3CH), 4.06 (2H, t, J 6.8, OCH_2), 6.90 (1H, ddd, J 7.2, 6.8, 1.2 ArH), 7.30 (1H, m, ArH) and 8.16 (2H, s, $B(OH)_2$)

7.3.39 2,3-Difluoro-4-(nonyloxy)-4''-pentyl-1,1':4',1''-terphenyl — **84**



Quantities:

4-bromo-4'-pentyl-1,1'-biphenyl **80**, (5.00 g, 0.016 mol)

DME, (100 ml)

Sodium carbonate, (100 ml, 2M)

Tetrakis(triphenylphosphine)palladium, (0.035g 0.00016 mol)

2,3-Difluoro-4-(nonyloxy)phenylboronic acid, **83** (6.50 g, 0.021 mol)

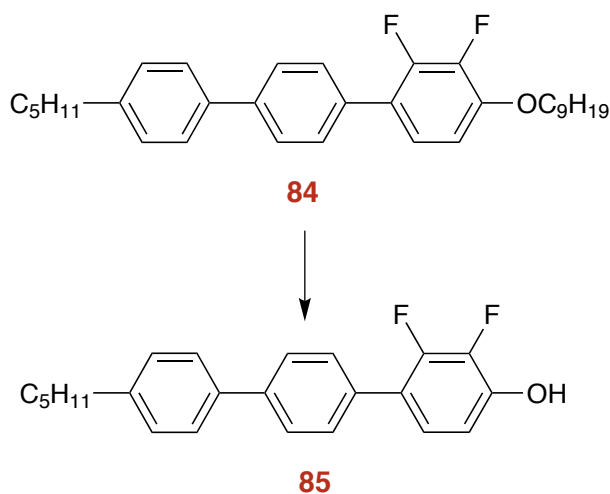
The experimental procedure was as described for the preparation of compound **45** to give a white solid 4-(benzyloxy)-2',3'-difluoro-4''-pentyl-1,1':4',1''-terphenyl **64**.¹²⁷

Yield: 5.40 g, 79 %

Transitions / °C 91.5 S, 142.0 S, 146.0 N 150.0 I

δ^H : 0.89 (3H, t, J 7.0, CH_3CH_2), 0.91 (3H, t, J 7.0, CH_3CH_2), 1.34 (14H, m, CH_2CH_3), 1.49 (2H, quin, J 7.6, CH_2CH_2), 1.66 (2H, quin, J 7.4, CH_2CH_2), 1.85 (2H, quin, J 7.5, CH_2CH_2), 2.65 (2H, t, J 7.7, CH_2CH_2), 4.08 (2H, t, J 6.6, OCH_2), 6.81 (1H, ddd, J 9.1, 7.6, 1.9, ArH), 7.14 (1H, td, J 8.5, 8.3, 2.4, ArH), 7.27 (2H, d, J 8.3, ArH), 7.55 (2H, d, J 8.1, ArH) 7.57 (2H, d, J 7.6, ArH) and 7.66 (2H, d, J 8.5, ArH)

7.3.40 2,3-Difluoro-4''-pentyl-[1,1':4',1''-terphenyl]-4-ol — 85



2,3-Difluoro-4-(nonyloxy)-4''-pentyl-1,1':4',1''-terphenyl (5.0 g, 0.01 mol) is stirred in DCM (100 ml) at 0 °C under dry nitrogen. Borontribromide (41.8 ml, 0.042 mol) was added drop wise with rapid stirring. The stirring continued overnight. After confirming the completion of reaction by GLC, the reaction mixture was added to cold water with stirring and the product was extracted into ethyl acetate (x2). The combined ethereal extracts were washed with water (100 ml x 2), dried magnesium sulphate and the solvent was removed, Purified by column chromatography (silica gel; DCM), and recrystallisation using isopropyl alcohol with de colourising charcoal gave the pure phenol.¹²⁸

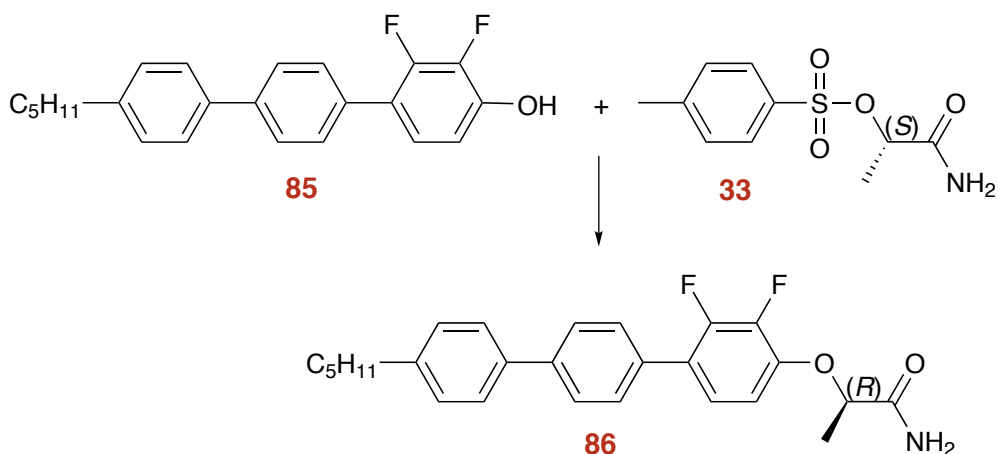
Yield: 2.5 g, 69 %.

Melting point : 164 °C (*Lit* mp 162-163 °C)

δ^H : 0.91 (3H, t, J 7.0, CH_3CH_2), 1.36 (4H, m, CH_2CH_3), 1.67 (2H, quin, J 7.4, CH_2CH_2), 2.66 (2H, t, J 7.8, CH_2CH_2), 5.32 (1H, b s, OH), 6.87 (1H, td, J 8.9, 8.7, 1.8, ArH), 7.14 (1H, ddd, J 8.4, 8.3, 2.2, ArH), 7.28 (2H, d, J 8.1, ArH), 7.56 (4H, m, ArH) and 7.66 (2H, d, J 8.3, ArH)

δ^F : -163.31 (dd, J 20.6, 7.2) and -141.54 (dd, J 20.7, 7.1)

7.3.41 (R)-2-((2,3-Difluoro-4''-pentyl-[1,1':4',1''-terphenyl]-4-yl)oxy)propanamide — 86



Quantities:

2,3-Difluoro-4''-pentyl-[1,1':4',1''-terphenyl]-4-ol **85**, (2.20 g, 0.0063 mol)

(S)-1-Amino-1-oxopropan-2-yl 4-methylbenzenesulfonate **123**, (1.82 g, 0.0075 mol)

Potassium carbonate, (1.72 g, 0.0125 mol)

DMF, (50 ml)

The experimental procedure was as described for the preparation of compound **49** to give a white solid **86**.

Yield: 2.00 g, 74 %

Melting point: 115 °C

Optical Rotation $[\alpha]_D^{19} = + 21.10$ (c 0.009 in DCM)

Transition / °C cry 115.5 BP (mosaic Phase) 118.0 Blue Green Phase 118.7 BP (Fog Phase) 119.0 I

δ^H : 0.92 (3H, t, J 7.2, CH_3CH_2), 1.36 (4H, m, 4 X CH_2CH_3), 1.66 (2H, m, CH_3CH), 1.68 (3H, d, J 6.8, CCH_3), 2.66 (2H, t, J 7.6, CH_2CH_2), 4.76 (1H, quin, J 6.8 H), 5.67 (1H, b s, NH), 6.58 (1H, b s, NH), 6.85 (1H, ddd, J 9.0, 7.6, 1.8, ArH), 7.18 (1H, td, J 8.7, 8.6, 2.3 ArH), 7.28 (2H, d, J 8.2 ArH), 7.56 (4H, m, ArH) and 7.68 (2H, d, J 8.4 ArH)

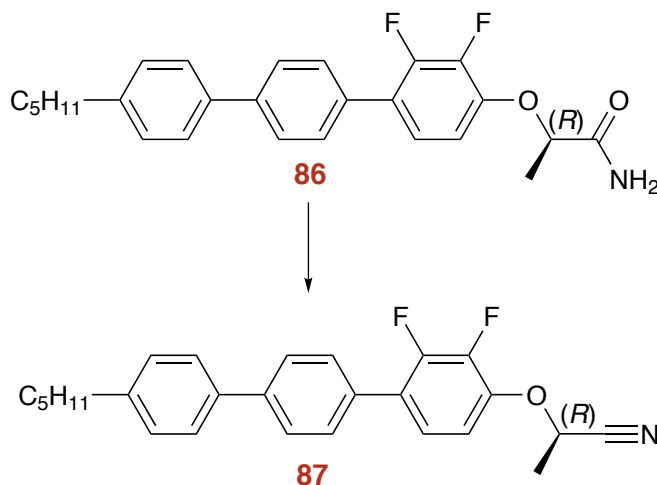
δ^C : 14.1, 18.5, 22.6, 31.2, 31.6, 35.7, 111.5, 124.0 (1C, m), 124.79 (1C, m), 127.0, 127.2, 129.0, 129.1 (1C, d, J 2.9), 133.0, 137.8, 140.9, 142.6 and 173.8

δ^F : -156.00 (dd, J 19.8, 6.6) and -140.11 (dd, J 19.8, 7.5)

M/Z 423 (M^+)

V_{max}/cm^{-1} : 3376 (N-H), 3191, 2925, 2362, 1639, 1493, 1288, 1088, 797

7.3.42 (*R*)-2-((2,3-Difluoro-4''-pentyl-[1,1':4',1''-terphenyl]-4-yl)oxy)propane-nitrile — 87



Quantities:

$POCl_3$, (1.30 g, 0.003 mol)

DMF, (50 ml)

(*R*)-2-((2,3-Difluoro-4''-pentyl-[1,1':4',1''-terphenyl]-4-yl)oxy)propanamide 86, (1.30 g, 0.003 mol)

The experimental procedure was as described for the preparation of compound **36** to give a white solid of **87**.

Yield: 0.45 g, 31 %

Melting point: 111.28 °C

Optical Rotation $[\alpha]_D^{19} = + 102.1$ (c 0.0115 in DCM)

Transition / °C 99.1 N* 131.1 l

δ^H : 0.92 (3H, t, J 6.7, CH_3CH_2), 0.87 (3H, t, J 7.6, CH_2CH_3), 0.98 (3H, d, J 6.7, CH_3CH), 1.29 (5H, m, CH_2CH_2), 1.29 (5H, m, CH_2CH_2), 1.55 (3H, t, J 7.9 CH_2CH_2), 1.99 (1H, m, CH_2CH_2), 2.56 (2H, t, J 7.5, CH_2 Ar), 4.58 (1H, d, J 4.1 H), 5.10 (1H, d, J 12, $ArOCH$), 5.16 (1H, d, J 1, CH_2Ar), 6.94 (1H, dt, J 8.4, 2.0), 7.23 (7H, m, ArH) and 7.51 (2H, d, J 8.2, ArH)

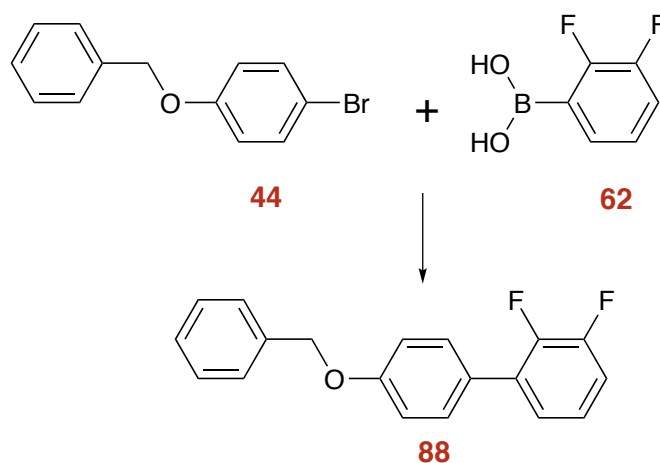
δ^C : 14.1, 20.0, 22.7, 31.3, 31.7, 35.7, 63.1, 113.5 (2C, d, J 3.7), 117.7, 124.2 (1C, m), 126.5 (1C, d, J 10.9), 127.0, 127.3, 129.0, 129.2, 132.9, 137.8, 141.1, 142.63, 143.5 (1C, d, J 147.5) and 149.0 (1C, d, J 251.0)

δ^F : -154.98 (dd, J 20.0; 6.8) , -139.59 (dd, J 19.9; 7.4).

M/Z : 405 (M^+)

V_{max}/cm^{-1} : 2922, 2852, 2167 ($C\equiv N$), 1974, 1492, 1467, 1286, 1099, 1061, 799

7.3.43 4'-(Benzyloxy)-2,3-difluoro-1,1'-biphenyl — **88**



Quantities:

1-(Benzyloxy)-4-bromobenzene, (18.00 g, 0.069 mol)

DME, (250 ml)

Sodium carbonate, (250 ml, 2M)

Tetrakis(triphenylphosphine)palladium (0.08g 0.000069 mol)

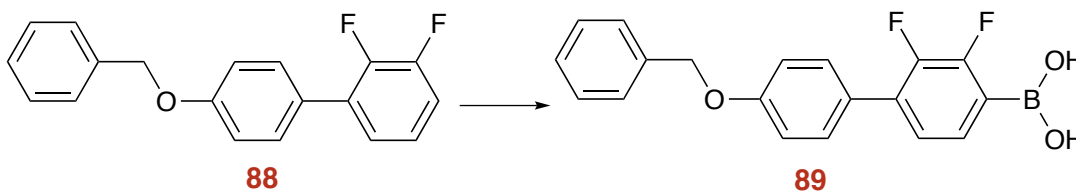
(2,3-Difluorophenyl)boronic acid (15.20 g, 0.096 mol)

The experimental procedure was as described for the preparation of compound **45** to give a white solid 4'-(benzyloxy)-2,3-difluoro-1,1'-biphenyl **88**.

Yield: 16.80 mg, 28 %

δ^H : 5.12 (2H, s, CH_2O), 7.07 (2H, d, J 8.9), 7.10 (1H, t, J 9.2), 7.11-7.51 (5H, m), 7.32-7.37 (1H, m), 7.38-7.44 (2H, d, J 8.6) and 7.45-7.51 (4H, m)

7.3.44 (4'-(Benzyloxy)-2,3-difluoro-[1,1'-biphenyl]-4-yl)boronic acid— **89**



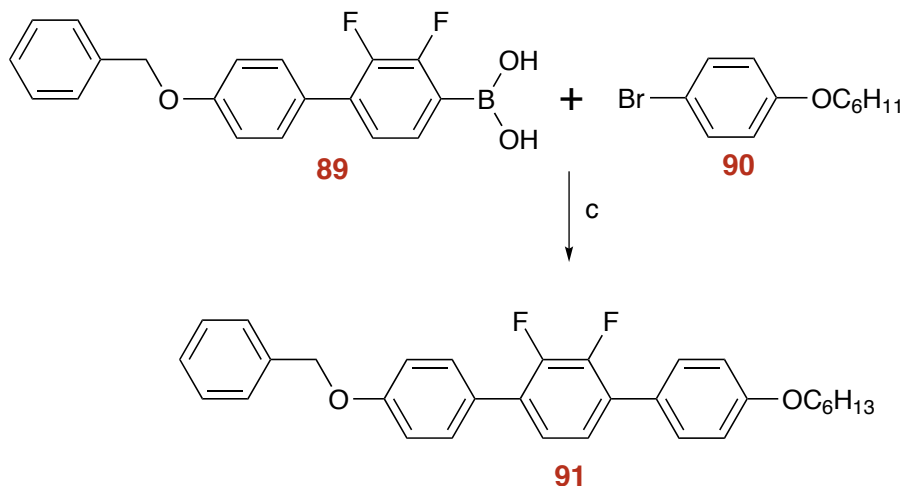
Quantities: Compound **88** (15.0 g 0.51 mol) *n*-Butyllithium (2.5 M in hexane , 22.4 ml, 0.056 mol) Trimethyl borate (10.53 g, 0.101 mol) HCl (10 %) (300 ml) THF (300 ml)

The experimental procedure was as described for the preparation of compound **41** to give a white solid **89**.¹²⁷

Yield: 11.2 g, 66 %

δ^H : 5.18 (2H, s, CH_2O), 7.14 (2H, d, J 8.4), 7.28 (1H, m), 7.31-7.45 (5H, m), 7.48 (2H, d, J 6.9), 7.53 (2H, d, J 8.6) and 8.42 (2H, bs, BOH_2)

7.3.45 (4-(Benzyloxy)-2',3'-difluoro-4''-(hexyloxy)-1,1':4',1''-terphenyl— **91**



Quantities:

4'-(Benzyloxy)-2,3-difluoro-[1,1'-biphenyl]-4-yl)boronic acid **89**, (7.0 g, 0.027 mol)

DME, (200 ml)

Sodium carbonate, (200 ml, 2M)

Tetrakis(triphenylphosphine)palladium (0.02g 0.000027 mol)

(2,3-Difluorophenyl)boronic acid (12.00 g, 0.027 mol)

The experimental procedure was as described for the preparation of compound **45** to give a white solid 4-(benzyloxy)-2',3'-difluoro-4''-(hexyloxy)-1,1':4',1''-terphenyl **91**.

Yield: 8.0 g, 63 %

Melting point: XXX °C

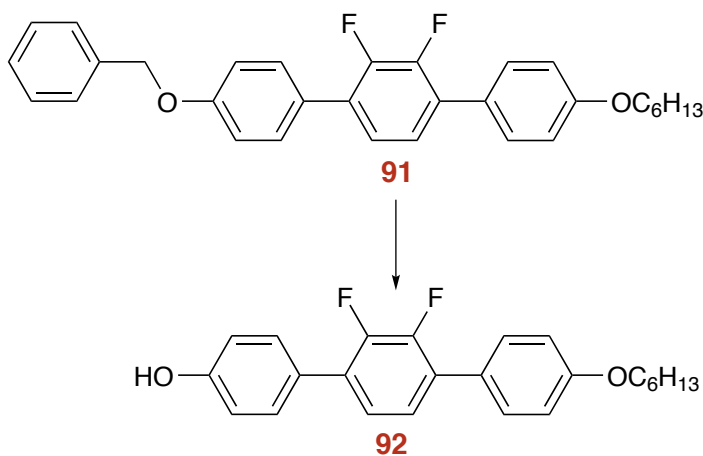
δ^H : 0.92 (3H, t, J 7.1, CH_3CH_2), 1.36 (4H, h, J 3.7, CH_2CH_3), 1.49 (2H, m, CH_2CH_2), 1.82 (2H, dt, J 14.5, 6.6, CH_2CH_2), 4.01 (2H, t, J 6.6, CH_2-O). 5.13 (2H, s, OH), 6.99 (2H, d, J 8.7, Ar H), 7.08 (2H, d, J 8.6, Ar H), 7.21 (2H, d, J 4.1, ArH), 7.32-7.38 (1H, m, ArH), 7.41 (2H, t, J 7.3, ArH), 7.47 (2H, d, J 7.0, ArH) and 7.52 (4H, m, ArH)

δ^C : 14.1, 22.7, 25.8, 29.3, 31.7, 68.1, 70.1, 114.7, 115.0, 124.4, 126.9, 127.4, 127.6, 128.1, 128.7, 136.9, 148.5 (dd, J 250.8, 15.0), 158.8 and 159.2

δ^F : -143.49 (m)

M/Z 472 (M^+)

7.3.46 (2',3'-Difluoro-4''-(hexyloxy)-[1,1':4',1''-terphenyl]-4-ol – 92



Quantities:

4-(Benzyloxy)-2',3'-difluoro-4''-(hexyloxy)-1,1':4',1''-terphenyl **91**, (7.00 g, 0.015 mol)

Pd/C, (2.00 g)

EtOAc, (200 ml)

The experimental procedure was as described for the preparation of compound **46** to give a white solid 2',3'-difluoro-4''-(hexyloxy)-[1,1':4',1''-terphenyl]-4-ol **92**.

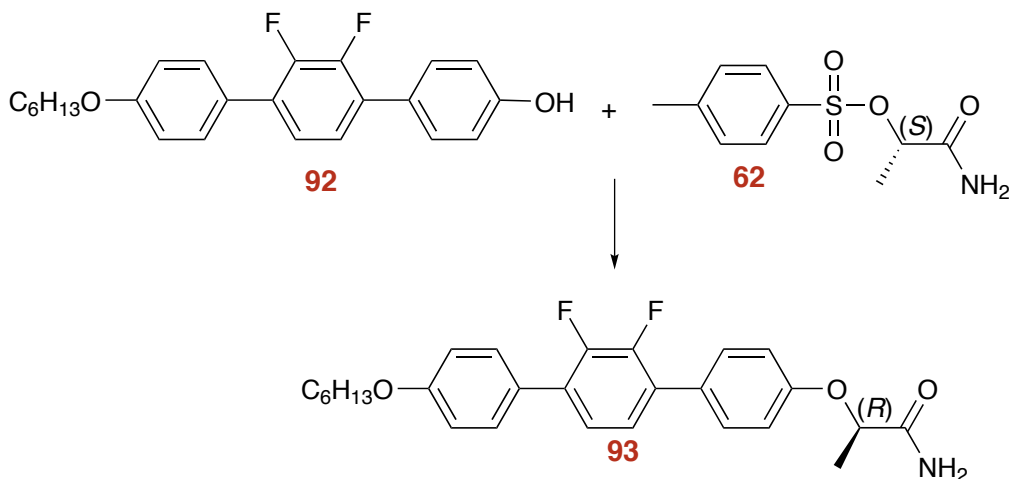
Yield: 4.5 g, 80 %

δ^H : 0.92 (3H, t, J 7.00, CH_3CH_2), 1.37 (4H, m, 4 X CH_2CH_3), 1.66 (2H, m, CH_2CH_2), 2.66 (2H, t, J 7.5, CH_2CH_2), 4.92 (1H, b s, OH), 6.94 (2H, d, J 8.8, ArH), 7.22 (2H, m, ArH), 7.29 (H, d, J 8.3, ArH), and 7.49 (4H, m, ArH)

δ^C : 14.1, 22.7, 25.8, 29.3, 30.4, 31.6, 68.2, 114.7, 115.6, 124.4, 126.9, 127.4, 128.9 (1CF, dd, J 33.6, 9.8), 130.0 (1CF, d, J 2.5), 130.3 (1CF, d, J 2.4), 148.5 (1CF, dd, J 250.5, 15.5), 155.6, 159.2.

M/Z 298 (M^+)

7.3.47 (R)-2-((2',3'-Difluoro-4''-(hexyloxy)-[1,1':4',1''-terphenyl]4-yl)oxy)propanamide –93



Quantities:

2',3'-Difluoro-4''-(hexyloxy)-[1,1':4',1''-terphenyl]-4-ol **92**, (2.0 g, 0.00523 mol)

(S)-1-Amino-1-oxopropan-2-yl 4-methylbenzenesulfonate **123**, (1.4 g, 0.00573 mol)

Potassium carbonate, (1.44 g, 0.011 mol)

DMF, (200 ml)

The experimental procedure was as described for the preparation of compound **49** to give a white solid (R)-2-((2',3'-difluoro-4''-(hexyloxy)-[1,1':4',1''-terphenyl]-4-yl)oxy)propanamide **93**.

Yield: 0.6 g, 26 %

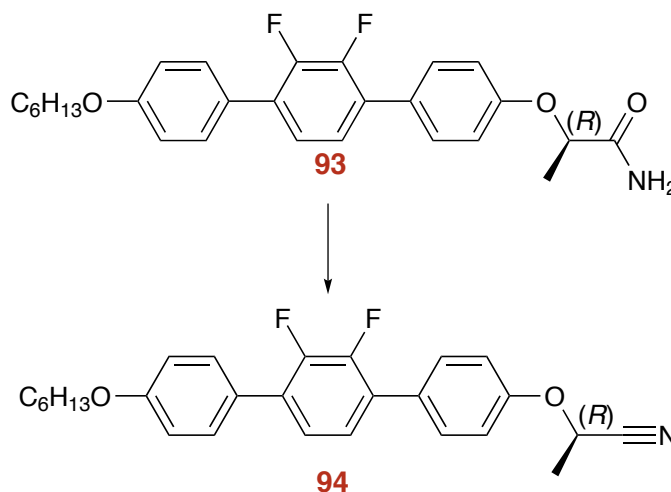
δ^H : 0.86-0.96 (3H, m, CH_3CH_2), 1.35 (4H, m, CH_2CH_3), 1.48 (2H, quin, J 7.2, CH_2CH_2), 1.64 (3H, d, J 6.7, CH_2CH_2), 1.81 (2H, dt, J 14.5, 6.7 CH_2CH_2), 4.01 (2H, t, J 6.5, CH_2-O), 4.74 (H, quin, J 6.7 H), 5.54 (1H, b s, NH), 6.41 (1H, b s, NH), 6.99 (2H, d, J 8.9, CH_2 Ar), 7.02 (2H, d, J 9.5 CH_2 Ar), 7.20 (2H, t, J 5.7, CH_2 Ar), 7.51 (2H, d, J 8.5, CH_2 Ar), 7.54 (2H, d, J 9.3, CH_2 Ar)

δ^C : 14.1, 18.7, 22.7, 25.8, 29.3, 31.6, 68.2, 74.9, 114.7, 115.2, 124.4 (1C, d, J

13.2), 126.8, 128.4 (1C, d, J 10.4), 128.7, 129.4 (1C, d, J 10.1), 130.0 (1C, d, J 3), 130.4 (1C, d, J 3.0), 158.0 (1C, d, J 247.5), and 174.7

δ^F : -143.44 (dd, J 20.1, 4.0) and -143.27 (dd, J 19.6, 4.2)

7.3.48 (*R*)-2-((2',3'-Difluoro-4''-(hexyloxy)-[1,1':4',1''-terphenyl]-4-yl)oxy)propanenitrile **94**



Quantities:

POCl_3 , (0.9 g, 0.0011 mol)

DMF, (25 ml)

(*R*)-2-((2',3'-Difluoro-4''-(hexyloxy)-[1,1':4',1''-terphenyl]-4-yl)oxy)propanamide **93**, (0.5 g, 0.001 mol)

The experimental procedure was as described for the preparation of compound **36** to give a white solid of (*R*)-2-((2',3'-difluoro-4''-(hexyloxy)-[1,1':4',1''-terphenyl]-4-yl)oxy)propanenitrile **94**.

Yield: 350.00 mg, 73 %

Melting point: 111.28 °C

Optical Rotation $[\alpha]_D^{22} = +27$ (c 0.005 in DCM)

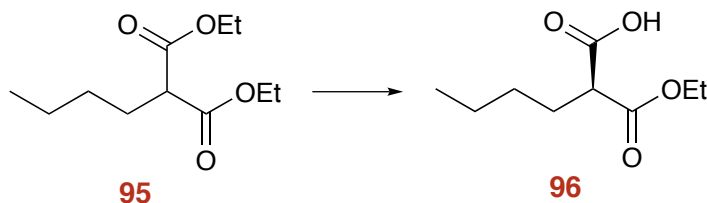
δ^H : 0.92 (3H, t, J 7.0, CH_3CH_2), 1.36 (2H, sext, J 6.9, CH_2CH_3), 1.48 (2H, quin, J 7.1, CH_3CH_2), 1.84 (3H, d, J 6.7, CH_2CH_2), 4.01 (2H, t, J 6.6, $\text{CH}_2\text{-O}$), 4.96

(H, quin, J 6.7 Hz), 7.00 (2H, d, J 8.6, CH_2 Ar), 7.11 (2H, d, J 8.7 CH_2 Ar), 7.22 (2H, d, J 5.2, CH_2 Ar), 7.52 (2H, d, J 7.5, CH_2 Ar), 7.58 (2H, d, J 7.7, CH_2 Ar)

δ^{C} : 11.6, 14, 22.5, 31.1, 35.5, 38.2, 62, 68, 7 (2C, t, J 4.19), 114.6, 115.8, 130 and 131.0

δ^{F} : -140.9, -156.8 (dd, J 20.8; 6.9).

7.3.49 (S)-2-(Ethoxycarbonyl)hexanoic acid⁹⁰ – 96

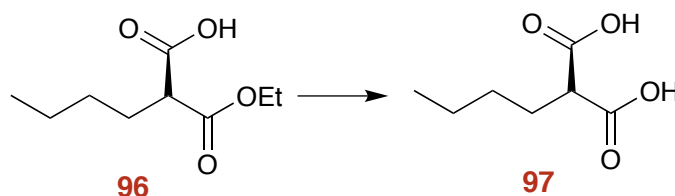


A 1-L 3-necked flask was charged with diethyl butylmalonate (98.2 g, 0.454 mol) and ethanol (300 ml). The solution was cooled to an internal temperature of 15-18 °C (keep water bath underneath the flask) over a period of 30 min, and a solution of potassium hydroxide (25.47 g, 0.454 mol 90 % purity) in ethanol (300 ml) was added over a period of 40 min while maintaining an internal temperature of 15-25 °C. The lines were rinsed with ethanol (50 ml), and the rinse was added to the reaction mixture. The hazy solution was stirred for 8 h. The reaction mixture was concentrated under a vacuum (20 mbar; jacket temperature 35-40 °C) to collect solvent and to obtain a cloudy viscous suspension. This suspension was diluted with water (500.0 ml) and diethyl ether (25 ml), and the biphasic mixture was stirred for 15 min. The organic layer was separated, and the aqueous layer was extracted with diethyl ether (25 ml). The aqueous layer was cooled to 15-18 °C (internal temperature) and acidified with concentrated sulphuric acid (15 ml) to pH 1-2 (addition time of sulphuric acid was 30 min while maintaining the internal temperature at < 25 °C). Hexane (50 ml) was added, and the mixture was stirred for 30 min. The organic layer was separated and washed with water (100 ml). The organic layer was concentrated under a vacuum (20 mbar; jacket temperature 45-55 °C) to collect the solvent to obtain 2-butylpropanedioic acid monoethyl ester **96**.⁹⁰

Yield: 59.00 g, 79 %

δ^H : 0.90 (3H, t, J 6.9, CH_3CH_2), 1.28 (3H, t, J 7.1, CH_3CH_2), 1.34 (4H, dt, J 7.3, 3.6 CH_2CH_3), 1.92 (2H, ddt, J 10.4, 7.2, 2.9 CH_2CH), 3.37 (1H, t, J 7.4, CH_2CH), 4.22 (2H, q, J 7.2, OCH_2).

7.3.50 (\pm)-2-butyl-3-hydroxypropionic acid⁹⁰ – 97

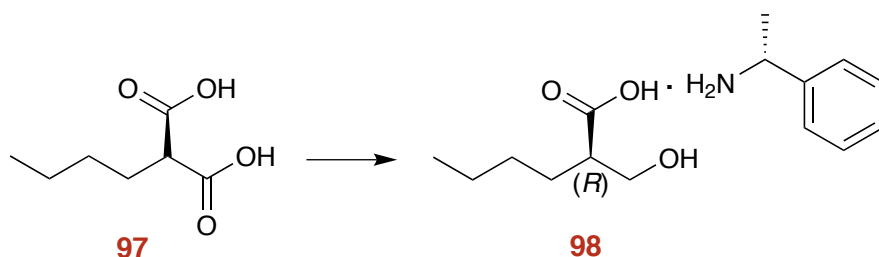


A 1-L, four-necked, round-bottomed flask, equipped with a mechanical stirrer, digital thermometer, and nitrogen inlet-outlet was charged with 2-butylpropanedioic acid monoethyl ester (65.0 g, 0.35 mol) and 2-propanol (650 ml). The solution was cooled to an internal temperature at 15-18 °C, and a 2 M solution of lithium borohydride (200 ml, 0.69 mol) in tetrahydrofuran was added over a period of 1.5 h while maintaining the internal temperature at 15-25 °C. The stirring was continued for an additional 3 h. The reaction mixture was cooled to an internal temperature of 10-13 °C and quenched by the addition of 2 N HCl (200 ml) over a period of 1 h while maintaining the internal temperature at 10-25 °C. The reaction mixture was concentrated at 35-40 °C (20 mbar) to collect a suspension (~53.96 g). This suspension was diluted with water (2.0 L) and ethyl acetate (2.5 L), and the biphasic mixture was stirred for 1 h. The organic layer was separated, and the aqueous layer was extracted with ethyl acetate (250 ml). The combined organic layers were washed with 20% aqueous solution of sodium chloride (100 ml) and concentrated under a vacuum (20 mbar) until no further solvent distilled to afford crude (\pm)-2-butyl-3-hydroxypropionic acid as a colourless liquid, which was used as such in the next step.⁹⁰

Yield: 35.00 g (68 %)

7.3.51 (*R*)-2-(Hydroxymethyl)hexanoic acid phenylethanammonium salt⁹⁰

— 98



A 1-L, four-necked, round-bottomed flask, equipped with a mechanical stirrer, digital thermometer, reflux condenser, addition funnel with nitrogen inlet-outlet, and heating mantle, was charged with (*R*) - α - methylbenzylamine (31.0 g, 0.25 mol), 2-propanol (125 ml), and ethyl acetate (100 ml). The solution was stirred and heated to an internal temperature at 60-65 °C, and a solution of (\pm)-2-butyl-3-hydroxypropionic acid (35 g, 0.24 mol) in ethyl acetate (0.2 L) was added over a period of 15 min while maintaining the internal temperature at 60-70 °C. The addition funnel was washed with ethyl acetate (15 ml) and added to the mixture. The solution was cooled to 20-25 °C over a period of 2 h, and the resulting suspension was stirred at the same temperature for an additional 5 h. The solids were collected by filtration, washed with a mixture of ethyl acetate-2-propanol (2:1 v/v) in two equal portions of 50 ml each, and dried at 50-53 °C (13-49 mbar) to afford crude (*R*)-2-butyl-3-hydroxypropionic acid (*R*)-*R*-methylbenzylammonium salt.⁹⁰

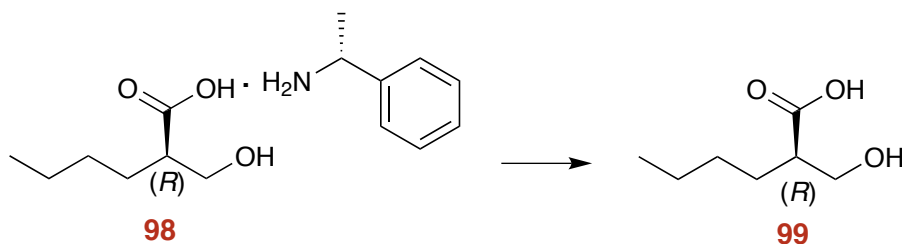
Yield: 29 g

Optical Rotation $[\alpha]_D^{29} = + 9.6$ (c 0.01 in DCM)

Melting point: 145-147 °C

δ^H : 0.91 (3H, m, CH_3CH_2), 1.32 (4H, dt, J 7.3, 3.7 CH_2CH_3), 1.44-1.55 (1H, m, CH_2CH), 2.59 (1H, qd, J 7.5, 5.0 CH_2CH), 3.76 (2H, dd, J 6.2, 3.6 $COCH_2$), 7.22 (2H, dd, J 6.2, 3.6 $OHCH_2$).

7.3.52 (*R*)-2-(Hydroxymethyl)hexanoic acid⁹⁰ — 99



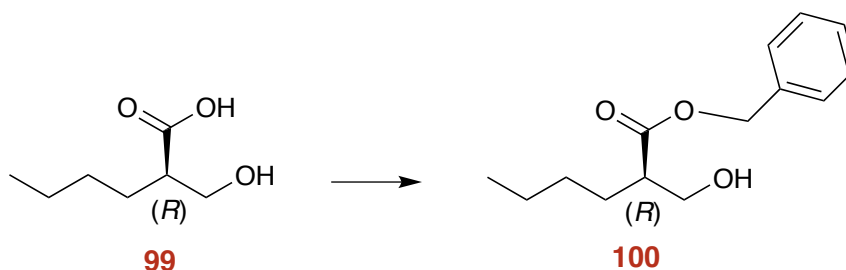
(*R*)-2-(Hydroxymethyl)hexanoic acid phenylethanammonium salt (24.00g) was dissolved in 2N HCl (100 ml) and EtoAc (125 ml), stir the solution for 10 min. The organic layer was separated and aqueous layer was extracted with EtoAc (3*50 ml) combined organic layer was washed with water and concentrated under a vacuum to get (*R*)-2-(hydroxymethyl)hexanoic acid; oil.⁹⁰

Yield: 12 g (98 %)

Optical Rotation $[\alpha]_D^{29} = + 6.4$ (c 0.01 in DCM)

δ^H : 0.88 (3H, t, *J* 7.0 CH_3CH_2), 1.27-1.36 (H, m, CH_2CH_3), 1.44-1.55 (1H, m), 1.42-1.58 (1H, m), 2.59 (1H, p, *J* 6.2), 3.71-3.82 (H, m), 7.47 (H, s).

7.3.53 Benzyl (*R*)-2-(hydroxymethyl)hexanoate⁹⁰ — 100



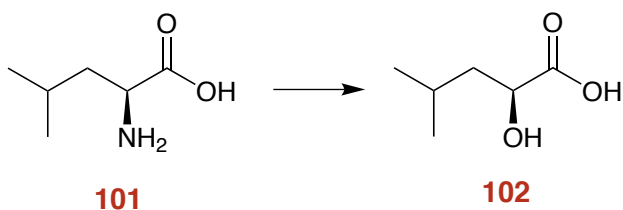
A 1-L 3-necked flask fitted with stirrer bar was charged with (*R*)-2-(hydroxymethyl)hexanoic acid (11.00 g; 0.075 mol) in methanol and water (250 and 25 ml). The 20% solution of $CsCO_3$ was added till the pH of a solution becomes pH 7, the solvent was removed by rotary evaporator (60 °C). The residue was dissolved in DMF. The benzyl bromide (13.46 g; 0.0787 mol) was added and continue the

stirring for overnight at room temperature. The reaction mixture was stirred with 50 ml brine solution and extracted with ethyl acetate. The combined organic layer was washed with water and brine, dry over MgSO_4 and solvent was removed by rotary evaporator. Column the product with hexane and ethyl acetate (4:1) obtained liquid product.

Yield: 10.80 g (62 %) ⁹⁰

δ^H : 0.86 (3H, t, J 7.0 CH_3CH_2), 1.28 (H, t, J 6.7 CH_2CH_3), 1.47-1.59 (1H, m), 1.59-1.72 (1H, m), 2.63 (1H, qd, J 7.5, 4.5), 3.69-3.82 (2H, m), 5.16 (2H, d, J 3.8), 7.28-7.41 (5H, m).

7.3.54 (S)-2-Hydroxy-4-methylpentanoic acid – 102



To a stirred solution of L-Leucine **101** (20 g, 0.076 mol,) in 2.5 N H_2SO_4 (1.25 mol, 100 mL) a solution of Sodium nitrite (15.8 g, 0.011 mol) in H_2O was added drop wise over one hour at 0 °C using ice/salt bath. Remove the salt/ice bath and stir the reaction mixture overnight at room temperature. The reaction mixture was extracted with ether (3x), and the combined organic solution washed with brine (3x), dried over magnesium sulphate, the solvent was removed under reduced pressure. The crude oily liquid product was then purified by recrystallisation using chloroform and hexane (1:4) to give D-hydroxy acid as a white precipitate. The mixture was then cooled for about 2 hour in an ice-bath, then filtered under vacuum while washing with cold hexane to give white crystals as product **102**. The crystals were then dried overnight in a vacuum desiccators.

Yield: 10.57 g, 37 %.

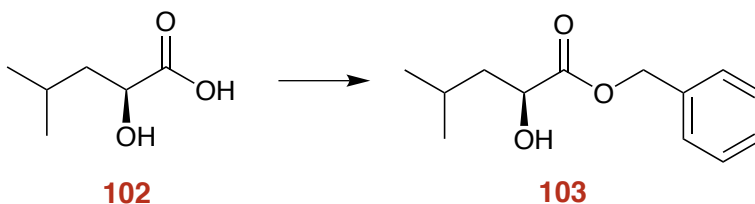
Optical Rotation $[\alpha]_D^{25} = -2.4$ (c 0.01 in DCM)

δ^H : 0.95 (6H, d, J 6.7, CH_3)

δ^C : 21.4, 23.2, 24.5, 43.2, 68.8 (C2).

V_{max}/cm^{-1} 3413 (OH), 2953, 2903, 2872, 2624, 1698 (C=O), 1267, 1228, 1136, 1076, 894, 682, 569.

7.3.55 Benzyl (S)-2-hydroxy-4-methylpentanoate — 103



To a stirred solution of **102** (7.4 g, 0.025 mol) in methanol (90 ml) and water (9 ml) a solution of 20% Cs_2CO_3 in water (50 ml) was added until pH 7.0 was attained, the solvent was then removed under reduced pressure to get a yellow oil. The residue was dissolved in DMF (60 ml) and benzyl bromide (10 g, 0.026 mol) was added. The mixture was stirred overnight at room temperature. The reaction mixture was quenched using brine and extracted with ethyl acetate and washed with water and brine, dried over magnesium sulphate and solvent was removed under reduced pressure to give pale yellow colour oil. The crude product was then purified using flash column chromatography with hexane and ethyl acetate (4:1). The product was an oil **103**.

Yield: 8.8 g, 71 %.

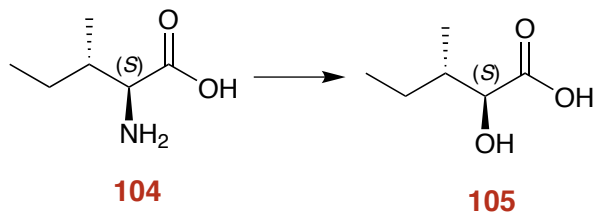
Optical Rotation $[\alpha]_D^{25} = -15.7$ (C 0.015 in DCM).

δ^H : 0.95 (3H, d, J 6.7, CH_3CH_2), 0.96 (3H, d, J 6.96, CH_3CH_2), 1.61 (2H, m, CH_2CH_2), 2.56 (1H, b s, CH), 4.26 (1H, dd, J 8.0, 5.3, OH), 5.2 (2H, b s, OCH₂), 7.38 (5H, m, ArH)

δ^C : 21.5, 23.2, 24.3, 43.3, 67.2, 69.1, 128.3, 128.4, 128.5, 128.6, 136.2, 175.7 (C=O).

V_{max}/cm^{-1} 3470 (OH), 2955, 1730 (C=O), 1455, 1194, 1136, 1082, 743, 695.

7.3.56 (2S,3S)-2-Hydroxy-3-methylpentanoic acid — 105



To a stirred solution of L-Isoleucine **104** (20 g, 0.076 mol) in 2.5 N H₂SO₄ (50 ml, 1.25 mol) a solution of sodium nitrite (15.8 g, 0.011 mol) in water (80 ml) was added drop wise for 1h at 0 °C. The reaction was allowed to stir overnight at room temperature. The reaction mixture was then extracted with ether, washed with brine and dried over magnesium sulphate. and The solvent was removed in vacuo. The oily liquid crude product purified by re-crystallisation from chloroform/hexane to give white precipitate. **105**. The crystals were then dried overnight in a vacuum.

Yield: 7.7 g, 38 %.

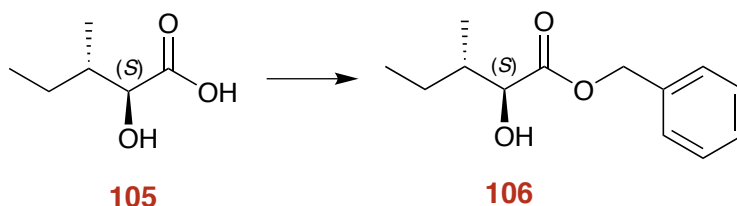
Optical Rotation $[\alpha]_D^{24} = +25.8$ (c 0.012 in DCM)

δ^H : 0.94 (3H, t, *J* 7.3, CH₃CH₂), 1.05 (3H, d, *J* 6.9 CH₃CH₂), 1.28 (2H, m, CH₂CH₂), 1.92 (1H, m, CHCH₃) and 4.20 (1H, d, *J* 3.7, CHOH)

δ^C : 11.7, 15.3, 23.6, 38.9, 74.6, 179.1

V_{max}/cm^{-1} 3459 (OH), 2963, 2922, 2877, 1713 (C=O), 1460, 1234, 1112, 1015, 892,744, 657, 613.

7.3.57 Benzyl (2S,3S)-2-hydroxy-3-methylpentanoate — 106



Quantities:

(2S,3S)-2-hydroxy-3-methylpentanoic acid **105**, (7.40 g, 0.025 mol)

Methanol, (90 ml)

Water, (9 ml)

Cs₂CO₃ in water (20% solution), (50 ml)

DMF, (75 ml)

Benzyl bromide (10 g, 0.026 mol)

The experimental procedure was as described for the preparation of compound **36** to give a white solid of **103**.

Yield: 11.92 g, 96 %

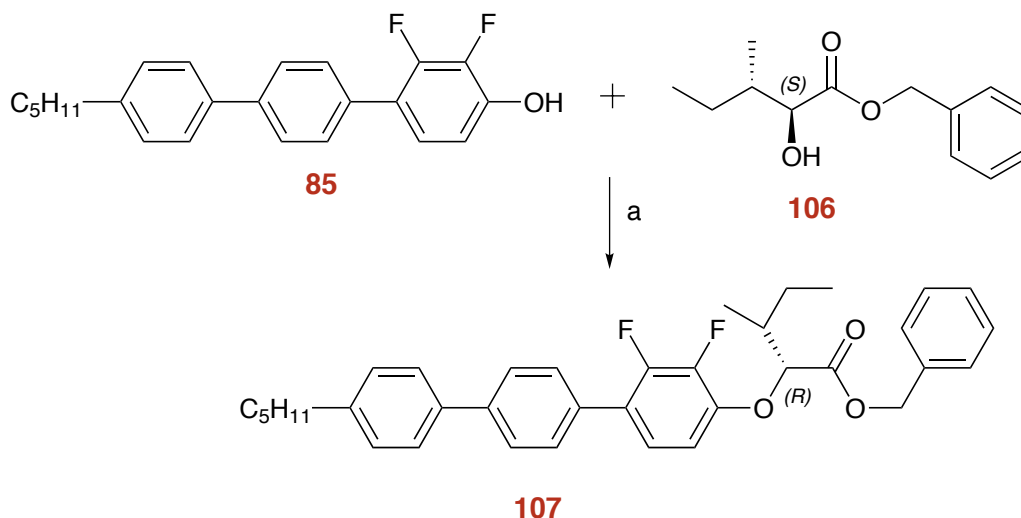
Optical Rotation $[\alpha]_D^{23} = -2.0$ (c 0.013 in DCM)

δ^H : 0.78 (3H, t, *J* 2.3, CH₃CH₂), 0.9 (3H, d, CH₃CH), 1.1-1.32 (2H, m, CH₂CH₃), 1.76 (1H, m, CHCH₃), 3.0 (1H, s), 4.4 (1H, d, *J* 3.8 CHOH), 5.13 (2H, q, *J* 12.0, CHCH₃) and 7.2 (5H, m, ArH).

δ^C : 174.7, 135.1, 128.4, 74.7, 67.0, 60.3, 39.0, 23.5, 15.3, 11.6

V_{max}/cm^{-1} : 3503.43(O-H), 2961.83, 1727.61, 1455.36, 1210.98, 1132.90, 747.81, 695.54

7.3.58 Benzyl (2*R*,3*S*)-2-((2,3-difluoro-4''-pentyl-[1,1':4', 1''-terphenyl]-4-yl)-oxy)-3-methylpentanoate — 107



A solution of DEAD (1.6g, 0.013mol) (neat) was added drop wise to a solution of PPh_3 (3.3 g, 0.013 mol), **106** (2.8 g, 0.13 mol) and **85** (3.0 g, 0.085 mol) in THF (40 ml). The mixture was stirred at room temperature overnight. TLC was used to check for the completion of the reaction, 0.48 g of DEAD and 0.84 g of the **106** were added to the mixture, the reaction was stirred overnight. The solvent was removed in vacuo to afford a brown viscous mixture. The crude product was purified by flash column chromatography using ethyl acetate in hexane (3

Yield: 1.87 g, 40 %

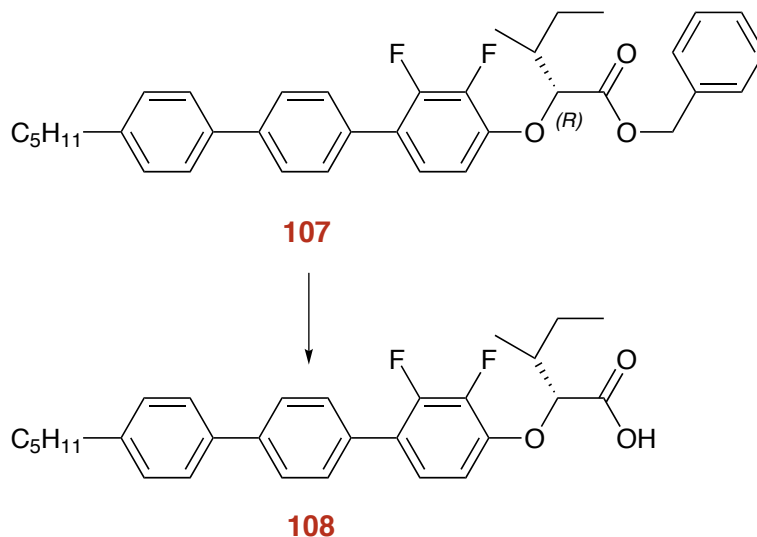
Optical Rotation $[\alpha]_D^{22} = + 26$ (c 0.011 in DCM)

δ^H : 0.84 (3H, t, J 6.7, CH_3CH_2), 0.87 (3H, t, J 7.6, CH_2CH_3), 0.98 (3H, d, J 6.7, CH_3CH), 1.30 (5H, m, CH_2CH_2), 1.55 (3H, m, CH_2CH_2), 2.56 (2H, d t, J 7.5, CH_2 Ar), 4.58 (1H, d, J 4.1 H), 5.10 (1H, d, J 12, ArOCH), 5.16 (1H, d, J 1, $\text{textit{CH}_2\text{Ar}}$), 6.94 (1H, dt, J 8.4, 2.0), 7.23 (7H, m, ArH) and 7.51 (2H, d, J 8.2, ArH)

δ^C : 174.7, 135.1, 128.4, 74.7, 67.0, 60.3, 39.0, 23.5, 15.3, 11.6

$V_{\text{max}}/\text{cm}^{-1}$: 2955, 2864, 1737 (C=O), 1494, 1279, 1192, 1121, 1067, 795, 747, 697

7.3.59 (2*R*,3*S*)-2-((2,3-Difluoro-4''-pentyl-[1,1':4',1''-terphenyl]-4-yl)oxy) -3-methylpentanoic acid — 108



Quantities:

Benzyl (2*R*,3*S*)-2-((2,3-difluoro-4''-pentyl-[1,1':4',1''-terphenyl]-4-yl)oxy)-3-methylpentanoate **107**, (1.40 g, 0.0056 mol)

Pd/C, (1.00 g)

EtOAc, (100 ml)

The experimental procedure was as described for the preparation of compound **46** to give a white solid (2*R*,3*S*)-2-((2,3-difluoro-4''-pentyl-[1,1':4',1''-terphenyl]-4-yl)oxy) -3-methylpentanoic acid **108**.

Yield: 0.86 g, 73 %

Optical Rotation $[\alpha]_D^{23} = + 8.16$ (c 0.025 in CHCl₃)

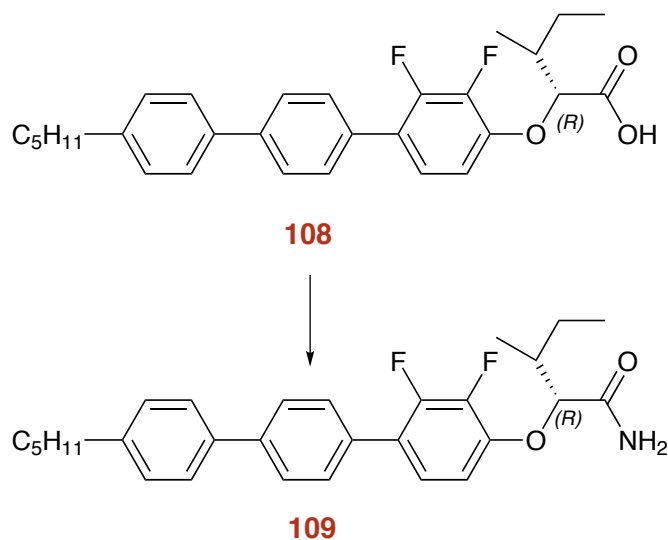
V_{max}/cm^{-1} : 2925 (OH), 2858, 1700 (C=O), 1493, 1469, 1284, 1065, 793. δ c 11.7, 14, 22.5, 25.8, 31.1, 35.5, 38.3, 126.8, 128.9

δ^H : 0.95 (3H, d, J 6.7, CH₃CH₂), 0.96 (3H, t, J 6.96, CH₂CH₃), 1.54 - 1.65 (2H, m, CH₃CH₂), 2.5 (H, bs), 4.26 (1H, dd, J 8.0, 5.3 OHCH), 5 - 2 (2H, bs, CH₂ O) and 7.74 - 7.72 (5H, m, Ph)

δ^C : 11.71, 22.5, 31.2, 31.6, 35.6, 38.3, 126.9, 127.1, 128.9, 129, 137.8, 140.6 and 142.4

δ^F : -140.5, -156.4 (dd, J 13.8; 6.2).

7.3.60 (2*R*,3*S*)-2-((2,3-Difluoro-4''-pentyl-[1,1':4',1''-terphenyl]-4-yl)oxy)-3-methylpentanamide – 109



The carboxylic acid **124** (1.07 g, 0.0011 mol) was initially converted to an acid chloride by reacting with oxalyl chloride (0.2 g, 0.017 mol), DCM (5.3 ml) and DMF (7 ml) catalyst for 3 h under a nitrogen atmosphere. The excess oxalyl chloride and solvent were removed in-vacuo. The acid chloride residue was then dissolved in dry THF (100 ml) and added to an aqueous solution of ammonia (20 ml) with stirring. After 30 min, water (90 mL) was added and the mixture stirred continuously (gave white precipitates) for 2 days at room temperature. The product was then filtered under vacuum to afford white crystals as product. These were then dried overnight in a desiccator connected to an oil pump.

Yield: 0.57 g, 100 %

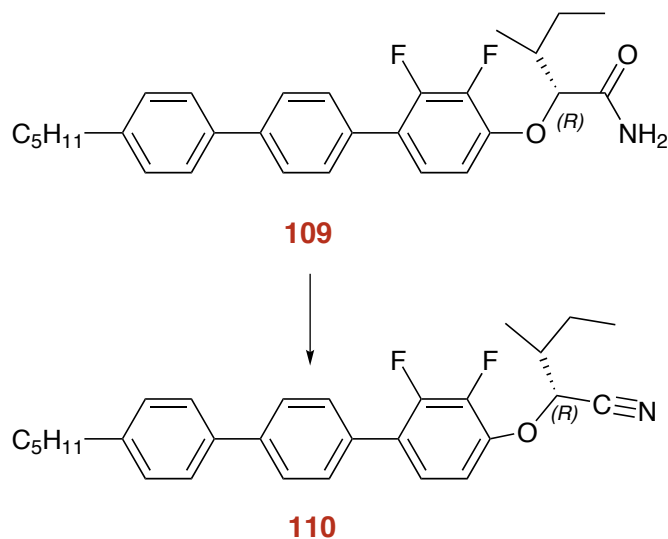
V_{max}/cm^{-1} : 3359 (N-H), 3160, 2926, 1659 (C=O), 1493, 1289 (C-N), 1059, 795.

δ^H : 0.84 (3H, t, J 6.7, CH_3CH_2), 0.87 (3H, t, J 7.6, CH_2CH_3), 0.98 (3H, d, J 6.7, CH_3CH), 1.22-1.37 (5H, m, CH_2CH_2), 1.48-1.61 (3H, m, CH_2CH_2), 1.98-2.08 (1H, m), 2.56 (1H, t, J 7.5, CH_2Ar), 4.58 (1H, d, J 4.1), 5.10 (1H, d, J 12, $OCHAr$), 5.16 (1H, d, J 1.0, ArH), 6.56 (1H, m, ArH) 6.94 (1H, dt, J 8.4, 2.0, ArH), 7.15-7.28 (7H, m, ArH) and 7.44-7.57 (2H, d, J 8.2, ArH)

δ^C : 13.8, 22.5, 25.9, 31.6, 35.6, 38.2, 84, 127.1, 128.9.

δ^F : -140.2, -157.

7.3.61 (2*R*,3*S*)-2-((2,3-Difluoro-4''-pentyl-[1,1':4',1''-terphenyl]-4-yl)oxy)-3-methylpentanenitrile – 110



Quantities:

POCl_3 , (1.53 g, 0.010 mol)

DMF, (25 ml)

(2*R*,3*S*)-2-((2,3-Difluoro-4''-pentyl-[1,1':4',1''-terphenyl]-4-yl)oxy)-3-methylpentanamide **109**, (0.5 g, 0.001 mol)

The experimental procedure was as described for the preparation of compound **36** to give a white solid of **110**.

Yield: 180 mg, 38 %

Optical Rotation $[\alpha]_D^{25} = + 21.6$ (c 1.0 in CHCl_3)

V_{max}/cm^{-1} : 3441, 1924, 1491, 1471, 1470, 1047, 800

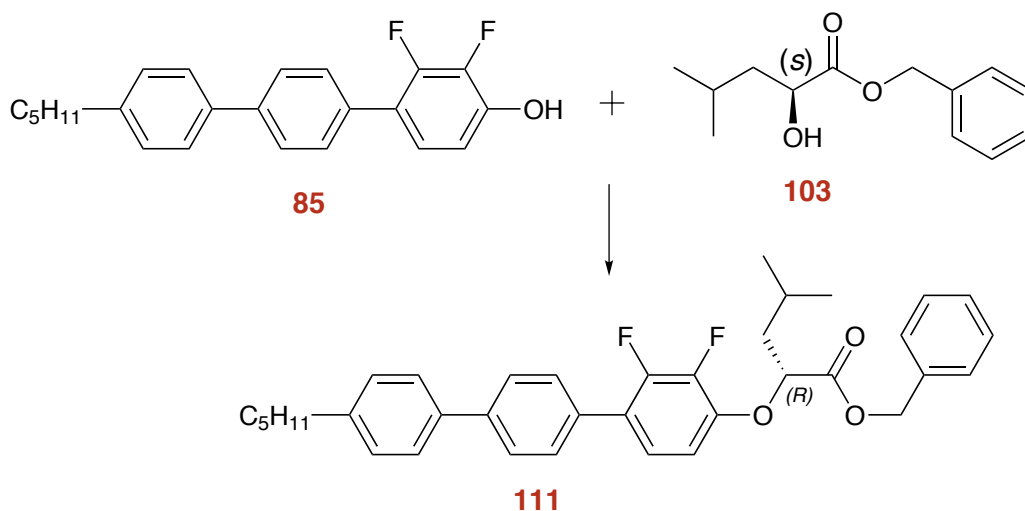
δ^H : 0.90 (3H, t, J 6.7, CH_3CH_2), 1.04 (3H, t, J 7.6, CH_2CH_3), 1.3 (3H, d, J 6.7, CH_3CH), 1.22-1.37 (H, m, CH_2CH_2), 1.48-1.61 (1H, m, CH_2CH_2), 2.56 (2H, t, J

7.5), 4.58 (1H, t, J 7.1), 5.10 (1H, d, J 12, $OCHAr$), 5.16 (1H, d, J 1.0, ArH), 6.56 (1H, m, ArH) 6.94 (1H, dt, J 8.4, 2.0, ArH), 7.15-7.28 (7H, m, ArH) and 7.44-7.57 (2H, d, J 8.2, ArH)

δ^C : 11.3, 14.6, 22.6, 22.7, 31.2, 31.5, 35.6, 38.8, 113.2, 116.7, 124, 126.9, 127.2, 128.9, 129.1

δ^F : -155.2 (dd, J 13.8; 6.9), -139.7 (dd, J 13.8; 6.9).

7.3.62 Benzyl (*R*)-2-((2,3-difluoro-4''-pentyl-[1,1':4',1''-terphenyl]-4-yl)oxy)-4-methylpentanoate — **111**



Quantities:

DEAD, (2.2 g, 0.013 mol)

PPh_3 , (3.3 g, 0.013 mol)

85, (2.8 g, 0.013 mol)

103, (3.0 g, 0.008 mol)

THF, (40 ml)

The experimental procedure was as described for the preparation of compound **107** to give a white solid of **111**.

Yield: 4.1 g, 87 %

Optical Rotation $[\alpha]_D^{25} = + 21.6$ (c 1.0 in CHCl_3)

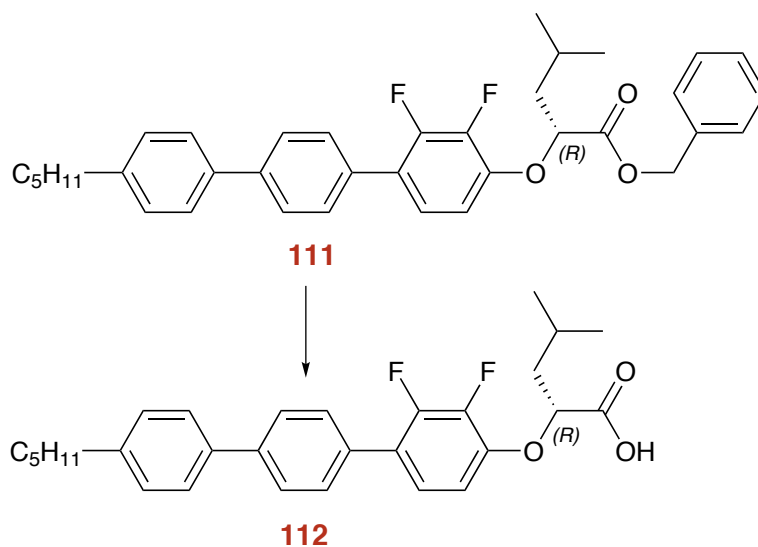
$V_{\text{max}}/\text{cm}^{-1}$ 2950, 2860, 1736 (C=O), 1471, 1269, 1192, 1096, 797, 697.

δ^H : 0.91 (3H, t, J 6.7, CH_3CH_2), 0.97 (3H, t, J 7.6, CH_2CH_3), 0.98 (3H, d, J 6.7, CH_3CH), 1.30 (5H, m, CH_2CH_2), 1.55 (3H, m, CH_2CH_2), 2.56 (2H, d t, J 7.5, CH_2 Ar), 4.58 (1H, d, J 4.1 H), 5.10 (1H, d, J 12, ArOCH), 5.16 (1H, d, J 1, CH_2Ar), 6.94 (1H, dt, J 8.4, 2.0), 7.23 (7H, m, ArH) and 7.51 (2H, d, J 8.2, ArH)

δ^C : 174.7, 135.1, 128.4, 74.7, 67.0, 60.3, 39.0, 23.5, 15.3, 11.6

$V_{\text{max}}/\text{cm}^{-1}$: 2955, 2864, 1737 (C=O), 1494, 1279, 1192, 1121, 1067, 795, 747, 697

7.3.63 (R)-2-((2,3-Difluoro-4''-pentyl-[1,1':4',1''-terphenyl]-4-yl)oxy)-4-methylpentanoic acid — 112



Quantities:

Benzyl (R)-2-((2,3-difluoro-4''-pentyl-[1,1':4',1''-terphenyl]-4-yl)oxy)-4-methylpentanoate — **111**, (3.80 g, 0.068 mol)

Pd/C, (2.00 g)

THF, (100 ml)

The experimental procedure was as described for the preparation of compound

46 to give a white solid (*R*)-2-((2,3-difluoro-4''-pentyl-[1,1':4',1''-terphenyl]-4-yl)-oxy)-4-methylpentanoic acid — **112**.

Yield: 2.25 g, 70 %

Optical Rotation $[\alpha]_D^{24} = +20.1$ (c 1.0 in CHCl_3)

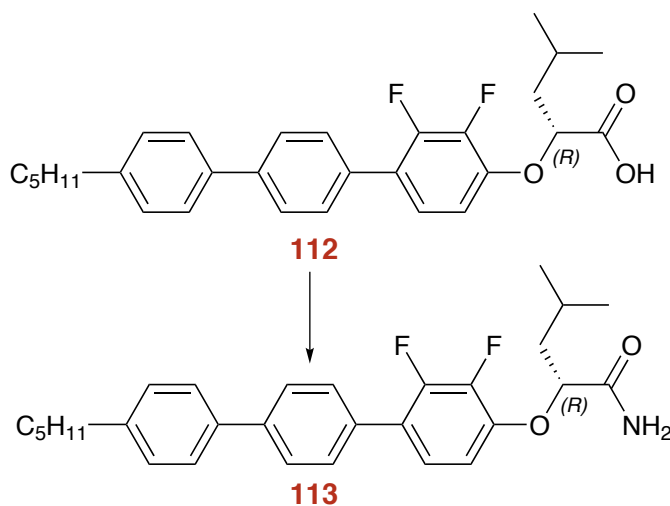
V_{max}/cm^{-1} : 2923 (OH), 1702 (C=O), 1495, 1469, 1292, 1088, 895.

δ^H : 0.91 (3H, t, J 7.0, CH_3CH_2), 0.98 (3H, t, J 7.4, CH_3CH_2), 1.14 (3H, d, J 6.7, CH_3CH), 1.31-1.40 (4H, m, CH_2CH_2), 1.61-1.71 (2H, m, CH_2CH_2), 2.09-2.19 (1H, m), 2.65 (2H, t, J 7.7, H), 4.71 (1H, m), 6.77 (1H, t, J 7.8), 7.12 (1H, t, J 7.6 ArH), 7.27 (2H, d, J 8.1, ArH), 7.54 (4H, m, ArH) and 7.65 (2H, d, J 8.2, ArH)

δ^C : 11.80, 13.90, 14.0, 22.6, 31.2, 31.2, 31.6, 35.6, 38.2, 84.1, 126.9, 127.2, 128.9, 129.0 (d, J 3.1) and 142.5

δ^F : -140.4 (d, 13.8) , -186.4 (d, J 16.1).

7.3.64 (*R*)-2-((2,3-Difluoro-4''-pentyl-[1,1':4',1''-terphenyl]-4-yl)oxy)-4-methylpentanamide — **113**



Quantities:

112, (1.82 g, 0.039 mol)

Oxalyl chloride , (0.6 ml, 0.0697 mol)

DCM, (22.0 ml)

THF, (44.0 ml)

Ammonia (Aq), (4.4 ml)

DMF, (3.0 ml)

The experimental procedure was as described for the preparation of compound **109** to give a white solid (*R*)-2-((2,3-difluoro-4''-pentyl-[1,1':4',1''-terphenyl]-4-yl)-oxy)-4-methylpentanamide — **113**.

Yield: 1.79 g, 99 %

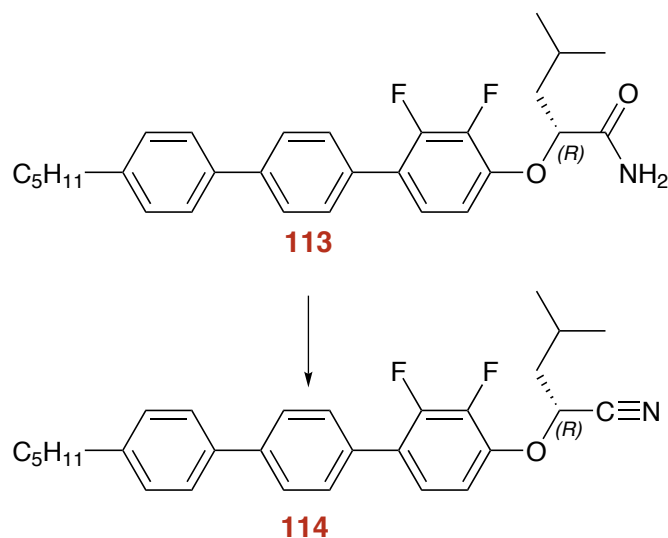
V_{max}/cm^{-1} : 3359 (N-H), 3183, 2926, 1659 (C=O), 1583, 1492, 1288, 1072, 747.

δ^H : 0.90 (3H, t, J 7.1, CH_3CH_2), 1.04 (3H, d, J 2.3, CH_3CH_2), 1.06 (3H, d, J 2.3, CH_3CH), 1.30-1.40 (10H, m, CH_2CH_2), 1.91-2.00 (1H, m, CH_2CH_2), 2.01-2.18 (1H, m), 2.65 (2H, t, J 7.1, H), 4.88 (1H, t, J 7.3), 7.04 (1H, t, J 8.2), 7.22 (1H, m), 7.27 (2H, d, J 8.0, ArH), 7.52-7.59 (4H, m, ArH) and 7.67 (2H, d, J 8.2, ArH)

δ^C : 14.0, 22.6, 23.1, 24.7, 31.2, 31.6, 35.6, 42.0, 82.0, 110.6, 126.9, 127.2, 128.9, 129.0, 137.8, 140.8 and 142.5.

δ^F : -140.2, -157.1.

7.3.65 (*R*)-2-((2,3-Difluoro-4''-pentyl-[1,1':4',1''-terphenyl]-4-yl)oxy)-4-methylpentanenitrile — **114**



Quantities:

POCl₃, (5.06 g, 0.33 mol)

DMF, (200 ml)

(*R*)-2-((2,3-difluoro-4''-pentyl-[1,1':4',1''-terphenyl]-4-yl)oxy)-4-methylpentanamide
— **113**, (1.53 g, 0.033 mol)

The experimental procedure was as described for the preparation of compound **36** to give a white solid of **114**.

Yield: 0.34 g, 39 %

Optical Rotation $[\alpha]_D^{23} = + 107.6$ (c 1.0 in CHCl₃)

V_{max}/cm^{-1} : 3434, 2930, 1632, 1495, 1296, 1077 (C=O), 800

δ^H : 0.92 (3H, t, *J* 6.9, CH₃CH₂), 1.00 (3H, t, *J* 7.4, CH₃CH₂), 1.04 (3H, d, *J* 6.7, CH₃CH), 1.95-2.22 (2H, m, CH₂CH₂), 1.65 (2H, t, *J* 7.5 CH₂CH₂), 4.78 (1H, m), 6.98 (1H, t, *J* 7.6), 7.13 (1H, t, *J* 7.4 ArH), 7.27 (2H, d, *J* 6.9, ArH), 7.52-7.57 (4H, m, ArH) and 7.65 (2H, d, *J* 8.3, ArH)

δ^C : 14.0, 18.4, 22.0, 22.4, 22.5, 24.4, 31.2, 31.5, 35.6, 42.1, 50.8, 58.4, 67.9, 113.3, 124, 126.9, 127.2, 128.9, 129.1 (J 11.5) and 142.5

δ^F : -155.1, -139.7 (dd, *J* 13.9; 6.9).

8 Bibliography

- [1] S. T. Lagerwall, *Ferroelectric and Antiferroelectric Liquid Crystals*, Wiley-VCH Verlag GmbH, Weinheim, Germany, 1999.
- [2] D. Demus, J. W. Goodby, G. W. Gray, H. W. Spiess and V. Vill, *Handbook of Liquid Crystals*, Wiley-VCH, 1998.
- [3] O. Z. Lehmann, *Z. Phys. Chem. (Leipzig)*, 1889, **4**, 462.
- [4] M. Friedel, *Annales de Physique*, 1922, **18**, 273–474.
- [5] G. W. Gray, K. J. Harrison and J. A. Nash, *Electron. Lett.*, 1973, **9**, 130.
- [6] P. Kirsch and M. Bremer, *Angewandte Chemie*, 2000, **39**, 4216–4235.
- [7] P. J. Collins and J. S. Patel (Eds.), *Handbook of Liquid Crystal Research*, Oxford University Press, New York, 1997.
- [8] D. Walba, *Science*, 1995, **270**, 250–251.
- [9] J. A. Castellano, *Liquid Gold: The Story of Liquid Crystal Displays and the Creation of an Industry*, World Scientific Publishing Co. Pte. Ltd, Singapore, 2005.
- [10] W. Schadt, M.; Helfrich, *Appl. Phys. Lett.*, 1971, **18**, 127–128.
- [11] Q. Cui, C. M. Huntley and R. P. Lemieux, *J. Mater. Chem.*, 2009, **19**, 5188.
- [12] T. Scheffer, *Annu. Rev. Mater. Sci.*, 1997, **27**, 555–583.
- [13] *Twisted Nematic (TN) mode*, <http://personal.kent.edu/~mgu/LCD/tn.htm>, accessed 09/11/2014.
- [14] M. F. Reinitzer, *Monatsh. Chem*, 1888, **9**, 421–441.
- [15] P. J. Collings, *Am. J. Phys.*, 1998, **66**, 551.
- [16] L. Gattermann and A. Ritschke, *Ber. Dtsch. Chem. Ges.*, 1890, **23**, 1738–1750.
- [17] W. Heintz, *J. Prakt. Chem*, 1855, **66**, 1–51.
- [18] J. W. Goodby, *J. Mater. Chem.*, 1991, **1**, 307.
- [19] V. Jayalakshmi, T. Wood, R. Basu, J. Du, T. Blackburn, C. Rosenblatt, C. M. Crudden and R. P. Lemieux, *J. Mater. Chem.*, 2012, **22**, 15255.
- [20] P. G. de Gennes, *Physics of Liquid Crystals*, International Series of Monographs on Physics, Oxford, 1976.
- [21] I. Dierking, *Textures of liquid crystals*, Wiley-VCH Verlag GmbH, 2003, p. 33.
- [22] M. Hird and P. J. Collings, *Introduction to Liquid Crystals*, Taylor & Francis, London, 1997.

- [23] J. W. Goodby, V. Görtz, S. J. Cowling, G. Mackenzie, P. Martin, D. Plusquellec, T. Benvegnu, P. Boullanger, D. Lafont, Y. Queneau, S. Chambert and J. Fitremann, *Chem. Soc. Rev.*, 2007, **36**, 1971–2032.
- [24] *Liquid Crystal Textures*, <https://bly.colorado.edu/lcphysics/textures/>, accessed 09/11/2014.
- [25] C. K. Lai, Y.-C. Ke, J.-C. S. Chien-Shen and W.-R. Li, *Liq. Cryst.*, 2002, **29**, 915–920.
- [26] H. Wang, Z. Lu, S. J. Lord, K. a. Willets, J. a. Bertke, S. D. Bunge, W. Moerner and R. J. Twieg, *Tetrahedron*, 2007, **63**, 103–114.
- [27] H. Wang, Z. Lu, S. J. Lord, W. E. Moerner and R. J. Twieg, *Tetrahedron Lett.*, 2007, **48**, 3471–3474.
- [28] D. A. PRICE and F.P., *J. Phys. Colloques*, 1975, **36**, 133–136.
- [29] B. Pansu, E. Grelet, M. Li and H. Nguyen, *Phys. Rev. Lett.*, 2000, **62**, 658–65.
- [30] J. W. Goodby and M. A. Waugh, *Nature*, 1989, **337**, 449–452.
- [31] Z. Kutnjak, C. W. Garland, J. Loren and J. Collings, *Phys. Rev. Lett.*, 1995, **74**, 4859–4862.
- [32] D. Gennes, *Phys. Rev. A*, 1987, **35**, 4419–4423.
- [33] P. Cladis, *Phys. Rev. Lett.*, 1984, **52**, 532–545.
- [34] A. Yoshizawa, *RSC Adv.*, 2013, **3**, 25475.
- [35] I. Dierking, *Symmetry*, 2014, **6**, 444–472.
- [36] M. D. Wand, R. Vohra, D. M. Walba, N. A. Clark and R. Shao, *Mol. Cryst. Liq. Cryst.*, 1991, **202**, 183–192.
- [37] N. A. Clark and S. T. Lagerwall, *Appl. Phys. Lett.*, 1980, **36**, 899–901.
- [38] Q. Cui and R. P. Lemieux, *Liq. Cryst.*, 2013, **40**, 1609–1618.
- [39] K. Siemensmeyer and H. Stegemeyer, *Chem. Phys. Lett.*, 1988, **148**, 409–412.
- [40] F. Walba, D. M.; Slater, S. C.; Thurmes, W. N.; Clark, N. A.; Handschy, M. A.; Supon, *J. Am. Chem. Soc.*, 1986, **108**, 5210–5221.
- [41] G. W. Gray, M. Hird, D. Lacey and K. J. Toyne, *Mol. Cryst. Liq. Cryst.*, 1989, **172**, 165–189.
- [42] L. K. M. Chan, G. W. Gray, D. Lacey, R. M. Scrowston, I. G. Shenouda and K. J. Toyne, *Mol. Cryst. Liq. Cryst.*, 1989, **172**, 125–146.
- [43] M. Hird, *Chem. Soc. Rev.*, 2007, **36**, 2070.

- [44] M. Hird, K. J. Toyne and G. W. Gray, *Liq. Cryst.*, 1994, **16**, 625–641.
- [45] G. W. Gray, M. Hird and K. J. Toyne, *Mol. Cryst. Liq. Cryst.*, 1991, **204**, 43–64.
- [46] S. M. Kelly, *Liq. Cryst.*, 1996, **20**, 493–515.
- [47] D. Coates, *Liq. Cryst.*, 1987, **2**, 63–71.
- [48] D. Coates, *Liq. Cryst.*, 1987, **2**, 423–428.
- [49] R. G. Solladié, G. and Zimmermann, *Angew. Chem. Int. Ed. Engl.*, 1984, **23**, 348–362.
- [50] T. Ikeda, *J. Mater. Chem.*, 2003, **13**, 2037–2057.
- [51] N. Tamaoki, *Adv. Mater. (Weinheim, Ger.)*, 2001, **13**, 1135–1147.
- [52] T. I. Kanazawa and A., *Molecular Switches*, B. L. Feringa (Ed.), Wiley-VCH, Weinheim, 2001, pp. 363–397.
- [53] G. P. e. Spada and G.P., *Enantiomer*, 2001, 2–3.
- [54] G. P. S. Proni and G., *Enantiomer*, 1998, **3**, 301–314.
- [55] M. Goh, J. Park, Y. Han, S. Ahn and K. Akagi, *J. Mater. Chem.*, 2012, **22**, 25011.
- [56] R. P. Lemieux, *Chem. Soc. Rev.*, 2007, **36**, 2033–2045.
- [57] C. Lazar, K. Yang, M. a. Glaser, M. D. Wand and R. P. Lemieux, *J. Mater. Chem.*, 2002, **12**, 586–592.
- [58] M. P. Thompson and R. P. Lemieux, *J. Mater. Chem.*, 2007, **17**, 5068.
- [59] K. M. Wand, M D; Thurmes, W N; Vohra, R T; More, 4th Int Display workshop, Nagoya, 1997, pp. 89–92.
- [60] J. S. Sei'Ichi Arakawa, Kei'Ichi Nito, *Mol. Cryst. Liq. Cryst.*, 1991, **204**, 15–25.
- [61] M. Nohira, Hiroyuki, Nohira, *Senryo to Yakuhin*, 1993, **38**, 258–268.
- [62] J. U. Michael D. Wand, William N. Thurmes, Rohini T. Vohra, Kundalika M More, Atsushi Yoshizawa, Toshihiro Hirai, *Mol. Cryst. Liq. Cryst.*, 1995, **263**, 217–222.
- [63] T. H. Atsushi, Yoshizawa, N Ise, Tetsuo Kusumoto, Yoichi Takanishi, Hideo Takezoe, *Mol. Cryst. Liq. Cryst.*, 2001, **364**, 271–277.
- [64] M. K. M. Takeda, M.T. Kitazume, T. Yymazaki, *J. Mater. Sci.*, 1995, **38**, 5199–5209.
- [65] R. Eelkema and B. L. Feringa, *Org. Biomol. Chem.*, 2006, **4**, 3729–45.
- [66] M. Goh, J. Park, Y. Han, S. Ahn and K. Akagi, *J. Mater. Chem.*, 2012, **22**,

25011.

- [67] E. P. Pozhidaev, S. I. Torgova, V. M. Molkin, M. V. Minchenko, V. V. Vashchenko, a. I. Krivoshey and a. Strigazzi, *Mol. Cryst. Liq. Cryst.*, 2009, **509**, 300/[1042]–308/[1050].
- [68] Y. Aoki, K. Matsushima, T. Taroura, T. Hirose and H. Nohira, *Mol. Cryst. Liq. Cryst.*, 2003, **398**, 189–193.
- [69] K. Watanabe, I. Osaka, S. Yorozya and K. Akagi, *Chem. Mater.*, 2012, **24**, 1011–1024.
- [70] J. Yoshida, H. Sato, A. Yamagishi and N. Hoshino, *J. Am. Chem. Soc.*, 2005, **127**, 8453–8456.
- [71] H. Stegemeyer and K.-J. Mainusch, *Chem. Phys. Lett.*, 1970, **6**, 5–6.
- [72] R. Eelkema and B. L. Feringa, *Org. Biomol. Chem.*, 2006, **4**, 3729–45.
- [73] N. Katsonis, E. Lacaze and A. Ferrarini, *J. Mater. Chem.*, 2012, **22**, 7088.
- [74] K. J. T. L. K. M. Chan, G. W. Gray, D. Lacey, R. M. Scrowston, I. G. Shenouda, *Mol. Cryst. Liq. Cryst.*, 1989, **172**, year.
- [75] V. V. Dietrich Demus, John W. Goodby, George W. Gray, Hans W. Spiess, *Handbook of Liquid Crystals, Low Molecular Weight Liquid Crystals II*, John Wiley & Sons, 2011, p. 579.
- [76] Y. Shirota, *J. Mater. Chem.*, 2000, **10**, 1–25.
- [77] Q. Pei and Y. Yang, *Chem. Mater.*, 1995, **7**, 1568–1575.
- [78] W. Huang, W.-L. Yu, H. Meng, J. Pei and S. F. Y. Li, *Chem. Mater.*, 1998, **10**, 3340–3345.
- [79] M. Hird and K. J. Toyne, *Mol. Cryst. Liq. Cryst.*, 1998, **323**, 1–67.
- [80] S. Misaki, S. Takamatsu, M. Suefuji, T. Mitote and M. Matsumura, *Mol. Cryst. Liq. Cryst.*, 1981, **66**, 123–132.
- [81] V. V. Titov, T. I. Zverkova, E. I. Kovshev, Y. N. Fialkov, S. V. Shelazhenko and L. M. Yaguposki, *Mol. Cryst. Liq. Cryst.*, 1978, **47**, 1–5.
- [82] K. Dimitrowa, J. Hauschild, H. Zaszke and H. Schubert, *Journal für Praktische Chemie*, 1980, **322**, 933–944.
- [83] R. Cai and E. T. Samulski, *Liq. Cryst.*, 1991, **9**, 617–634.
- [84] L. A. Karamysheva, E. I. Kovshev, A. I. Pavluchenko, K. V. Roitman, V. V. Titov, S. I. Torgova and M. F. Grebenkin, *Mol. Cryst. Liq. Cryst.*, 1981, **67**, 241–251.
- [85] D. O'Hagan, *Chem. Soc. Rev.*, 2008, **37**, 308–19.

- [86] Z. N. Kayani, R. A. Lewis and S. Naseem, *J. Mol. Liq.*, 2013, **180**, 74–88.
- [87] Z. N. Kayani, R. A. Lewis and S. Naseem, *J. Mol. Liq.*, 2012, **175**, 72–84.
- [88] Z. N. Kayani, R. A. Lewis and S. Naseem, *J. Mol. Liq.*, 2012, **170**, 11–19.
- [89] J. S. Gasowska, S. J. Cowling, M. C. R. Cockett, M. Hird, R. A. Lewis, E. P. Raynes and J. W. Goodby, *J. Mater. Chem.*, 2010, **20**, 299.
- [90] B. Hu, M. Prashad, D. Har, K. Prasad, O. Repic and T. J. Blacklock, *Org. Process Res. Dev.*, 2007, **11**, 90–93.
- [91] N. Miyaura, K. Yamada, H. Suginome and A. Suzuki, *Am. J. Org. Chem.*, 1985, 972–980.
- [92] M. Moreno-man, *Am. J. Org. Chem.*, 1996, 2346–2351.
- [93] N. Iranpoor, H. Firouzabadi and D. Khalili, *Org. Biomol. Chem.*, 2010, **8**, 4436–43.
- [94] O. Mitsunobu, M. Yamada and T. Mukaiyama, *Bull. Chem. Soc. Jpn.*, 1967, **40**, 935–939.
- [95] O. Mitsunobu, M. Yamada, O. Y. O. Mitsunobu and O. Chemistry, *Bull. Chem. Soc. Jpn.*, 1967, **40**, 2380–2382.
- [96] J. Kirchhoff, *PhD thesis*, The Florida State University, 2010.
- [97] D. Podolsky, O. Banji and P. Rudquist, *Liq. Cryst.*, 2008, **35**, 789–791.
- [98] A. K. George, C. Carboni, W. M. Zoghaib and D. M. Potukuchi, *World J. Condens. Matter Phys.*, 2012, **2012**, 75–79.
- [99] D. Demus, J. W. Goodby, G. W. Gray, H. W. Spiess and V. Vill, *Handbook of Liquid Crystals*, Wiley-VCH, 1998.
- [100] R. B. Meyer, *Mol. Cryst. Liq. Cryst.*, 1977, **40**, 1977.
- [101] K. F. T. Inukai, S. Saitoh, H. Inoue, K. Miyazawa, K. Terashima, *Mol. Cryst. Liq. Cryst.*, 1989, **141**, 251.
- [102] T. I. K. Terashima, M. Ichihashi, M. Kikuchi, K. Furukawa, *Mol. Cryst. Liq. Cryst.*, 1986, **141**, 237–244.
- [103] A. H.-s. G. Which, D. T. Chin, S. A. Goff, T. Webstern, T. Smithn and A. L. Goldberg, *J. Biol. Chem.*, 1988, **263**, 11718–11728.
- [104] J. Brock and D. Finotello, *Experimental Study of Physical Properties*, Cambridge University Press, 1st edn, 2000, p. 483.
- [105] M. K. N. Kasai, *X-Ray Diffraction by Macromolecules*, Springer Series in Chemical Physics, 2005.
- [106] K. Hiraoka, Y. Uematsu, P. Stein and H. Finkelmann, *Macromol. Chem.*

Phys., 2002, **203**, 2205–2210.

- [107] I. W. Hamley, *Introduction to Soft Matter – Revised Edition*, Wiley-Blackwell, Revised Ed edn, 2007, p. 342.
- [108] A. de Vries, *J. Mol. Liq.*, 1986, **31**, 193–202.
- [109] C. Keith, A. Lehmann, U. Baumeister, M. Prehm and C. Tschierske, *Soft Matter*, 2010, **6**, 1704–1721.
- [110] O. Francescangeli, *Phys. Rev. E*, 1997, **55**, 481–487.
- [111] J. K. Tamon Okano, Nobuyuki Harada, *Bull. Chem. Soc. Jpn.*, 1994, **67**, 2329–2332.
- [112] C. C. Dman, B. H. M. Mahoney, Caroline AColquhoun, D. O and G. C. Robinson, *Adv. Mater. (Weinheim, Ger.)*, 1990, **2**, 139–141.
- [113] W. Weissflog, U. Baumeister, M.-G. Tamba, G. Pelzl, H. Kresse, R. Friedemann, G. Hempel, R. Kurz, M. Roos, K. Merzweiler, A. Jákli, C. Zhang, N. Diorio, R. Stannarius, A. Eremin and U. Kornek, *Soft Matter*, 2012, **8**, 2671–2685.
- [114] T. N. Ahipa, V. Kumar, D. S. Shankar Rao, S. K. Prasad and A. V. Adhikari, *Cryst.Eng.Comm.*, 2014, **16**, 5573–5582.
- [115] J. C. W. Tseng, R. Rondla, P. Y. S. Su and I. J. B. Lin, *RSC Adv.*, 2013, **3**, 25151–25158.
- [116] H. R. Powell, *Annu. Rep. Prog. Chem., Sect. C: Phys. Chem.*, 2013, **109**, 240–265.
- [117] K. Kaznacheev and T. Hegmann, *Phys. Chem. Chem. Phys.*, 2007, **9**, 1705–12.
- [118] N. M. O’Boyle, M. Banck, C. a. James, C. Morley, T. Vandermeersch and G. R. Hutchison, *J. Cheminf.*, 2011, **3**, 33–47.
- [119] N. Frank, *Comput Mol Sci*, 2012, **2**, 73–78.
- [120] J. Perdew, K. Burke and M. Ernzerhof, *Phys. Rev. Lett.*, 1996, **77**, 3865–3868.
- [121] M. J. F. P. J. Stephens, F. J. Devlin, C. F. Chabalowski, *J.Phys.Chem.*, 1994, **98**, 11623–11627.
- [122] A. N. Shaw, R. Tedesco, R. Bambal, D. Chai, N. O. Concha, M. G. Darcy, D. Dhanak, K. J. Duffy, D. M. Fitch, A. Gates, V. K. Johnston, R. M. Keenan, J. Lin-Goerke, N. Liu, R. T. Sarisky, K. J. Wiggall and M. N. Zimmerman, *Bioorg. Med. Chem. Lett.*, 2009, **19**, 4350–3.

- [123] K. J. T. G. W. Gray, M. Hird, *Mol. Cryst. Liq. Cryst.*, 1991, **195**, 221–237.
- [124] M. F. Prodanov, O. V. Vashchenko and V. V. Vashchenko, *Tetrahedron Lett.*, 2014, **55**, 275–278.
- [125] W.-J. Hu, X.-L. Zhao, M.-L. Ma, F. Guo, X.-Q. Mi, B. Jiang and K. Wen, *Eur. J. Org. Chem.*, 2012, **2012**, 1448–1454.
- [126] S. M. Allin, W. R. Barton, W. Russell Bowman, E. Bridge (née Mann), M. R. Elsegood, T. McInally and V. McKee, *Tetrahedron*, 2008, **64**, 7745–7758.
- [127] G. W. Gray, M. Hird, D. Lacey and K. J. Toyne, *J. Chem. Soc. Perkin Trans.*, 1989, **9**, 3041–2053.
- [128] A. Chołuj, P. Kula, R. Dąbrowski, M. Tykarska and L. Jaroszewicz, *J. Mater. Chem. C*, 2014, **2**, 891–900.
- [129] J. W. Goodby, M. Hird, J. C. Jones, R. A. Lewis, I. C. Sage and K. J. Toyne, *Ferroelectrics*, 2000, **243**, 19–26.
- [130] J. Yao, H. Liu, T. Zhou, H. Chen, Z. Miao, C. Sheng and W. Zhang, *Eur. J. Med. Chem.*, 2012, **50**, 196–208.
- [131] C. Yelamaggad, M. Mathews, U. S. Hiremath, D. Shankar Rao and S. Krishna Prasad, *Tetrahedron Lett.*, 2005, **46**, 2623–2626.